THE INFLUENCE OF PACKING STRUCTURE ON SEISMIC WAVE VELOCITIES IN SEDIMENTS

by

Peter John Schultheiss, B.Tech. (Bradford)

Thesis submitted to the University of Wales
for the degree of Doctor of Philosophy

1982

Declaration in accordance with regulations 11 and 18 for the Degree of Philosophiae Doctor

I declare that the contents of this thesis submitted for the Degree of Philosophiae Doctor are the result of my own investigation. This work has not already been accepted in substance for any degree and is not being currently submitted in candidature for any degree.

All other works referred to in this thesis have been acknowledged.

Candidate

Director of Studies

SUMMARY

Piezo-electric shear wave transducers have been developed and used in a range of unconsolidated sediments under varying effective stress conditions. A new self-monitoring technique has provided information on transmitter response. Their incorporation in oedometer and triaxial cells, together with compressional wave transducers have enabled the velocity of shear and compressional waves (V_s and V_p) to be monitored during soil mechanics tests. Installation of these transducers into a variable porosity cell has also enabled the relationship between V_p, V_s and porosity to be defined for sands at low effective stresses. V_s has been measured in surficial sediments in situ using specially developed probes.

In the porosity cell V_s varied between 17 m/s and 120 m/s depending on porosity, grain shape and size distribution. The effective stress-V_s profile for different sediment types has been defined in the oedometer cell with small decreases in V_s occurring after each incremental load for a low permeability clay. Computed static and dynamic moduli exhibit a considerable difference in both magnitude and as a function of stress. This is attributed to differences in drainage conditions. Continuous measurements of V_s and V_p during cyclic loading tests on sand have clearly defined the behaviour around liquefaction. V_s varied between 0 and 300 m/s in this test and the V_p/V_s ratio enabled the sample liquefaction process to be analysed, concluding that only a small part of the sample had probably failed.

In-situ measurements of V_s varied between 27 m/s and 120 m/s without any apparent correlation with electrical formation factor, V_p or sediment type.

It has been postulated that the second, slower, bulk compressional

wave, predicted by theory but rarely observed might be more appropriate for calculating soil moduli. Observation of received waveforms in the triaxial cell has tentatively identified what may be this slower compressional wave.

ACKNOWLEDGMENTS

During the course of this study I have benefited from practical help and discussions with a number of people. In particular I would like to express my appreciation to the following individuals. D. Shirley and L Hampton provided the initial facilities and guidance at the Applied Research Laboratories, Austin, Texas, for the work on shear wave transducers. I am deeply indebted to D. Taylor Smith at the Marine Science Laboratories, UCNW, for his experienced help and sound guidance throughout this project under a NERC Contract (No. F60/A1/30) with the Engineering Geology Unit at the Institute of Geological Sciences. I am extremely grateful to P. Jackson and R. Baria (IGS) for many informative disucssions as well as their collaboration with the combined geophysical probes. Other beneficial discussions occurred with colleagues at UCNW J. Bennell, F. Hamdi, A. Davis and F. Dewes (who drafted some of the illustrations); R. Cratchley and D. McCann (IGS) and P. Strachan (Newcastle). The crew of the R.V. 'Prince Madog' are thanked for their help during the in-situ measurements.

This project was started with the help of an award from the Science Research Council (research studentship, B74/4373) under the direction of S. Freeth, at Swansea University, whom I wish to thank for his continual support, encouragement and criticism throughout this work. I also wish to thank Professor Ager for the use of facilities of the geology department during this stage.

CONTENTS

LIST OF FIGURES

5.1 Grain size distributions for the samples tested in the oedometer cell.

5.2 Stress-strain consolidation plots for the samples tested in the oedometer cell.

5.3 Stress-V_s consolidation plots. Power equations $P = KV_s^n + C$ are fitted to the final compression curve.

5.4 Strain-V_s consolidation plot for potter's clay.

5.5 The yielding and locking behaviour of a sand in confined compression.

5.6 Stress strain consolidation plot for a silt preconsolidated to 108 kPa.

5.7 V_s and V_p versus stress for the preconsolidated silt sample.

5.8 Static and dynamic moduli versus stress for the preconsolidated silt sample.

6.1 V_s versus effective stress for a medium sand in the small triaxial cell

6.2 Deviator stress and V_s versus strain for a medium sand in the small triaxial cell.

6.3 Received shear wave signals through sand in the small triaxial cell at different effective stress levels.

7.1 Shear wave signals recorded during a cyclic loading test on sand.

7.2 Received shear wave signals during cyclic loading tests on sand illustrating the liquefaction at X.

7.3 Shear and compressional waves during cyclic loading on sand.

7.4 Stress, strain and shear wave data during cyclic loading of sand.

7.5 Stress, strain and compressional wave data during cyclic loading on san

8.1 Site location map for RV Prince Madog cruise, December 1979.

9.1 A received signal through a saturated sand showing the possible existence of three types of body waves: (a) complete signal (b) 'liquid wave', (c) 'frame wave', (d) shear wave.

LIST OF TABLES

SYMBOL NOMENCLATURE

C - constant

D - primary static constrained modulus, transducer displacement

D_1 - initial loading modulus

D_m - grain sorting coefficient

D_r - final relaxation modulus

d - transducer separation

d_{31} - piezoelectric constant

E - Young's modulus

e - void ratio

FF - formation factor

f - frequency

G - shear modulus

H - transfer function

K - bulk modulus; constant

K_f - sediment frame bulk modulus

K_m - mineral bulk modulus

K_w - water bulk modulus

K_p - kurtosis

L - Lame's constant

n - fractional porosity

n' - frequency exponent

n_r - relative porosity

P,Q,R,- Biot's coefficients

P - compacting pressure

P_0 - initial axial stress

P_p - preconsolidation pressure

R_{50} - mean grain roundness

r^2 - correlation coefficient

SL - spreading loss

T - transducer thickness

u - pore pressure

V - voltage

V_f - compressional wave velocity of a fluid

V_p - compressional wave velocity

$^{l}V_p$ - 'liquid wave' velocity

$^{f}V_p$ - 'frame wave' velocity

V_s - shear wave velocity; volume of solids

V_t - total volume

V_v - volume of voids

VR - velocity ratio

α - attenuation coefficient

β - bulk compressibility

β_f - bulk compressibility of the sediment frame

$\beta_{m,w}$ - mineral, water bulk compressibility

β_p - coupled pore compressibility

ν - Poisson's ratio

ρ - bulk density

ρ_m - mineral density

σ - total stress

σ' - effective stress

1. INTRODUCTION

1.1 Background

Wave motion is the propagation of a periodic disturbance carrying energy; it is this transfer of energy from one place to another that find such a multitude of applications. As a tool for scientific investigation it must be virtually unrivalled in its versatility, from revealing the detailed atomic structure of crystals, proteins and nucleic acids to unravelling the mysteries of the earth's inner structure and indeed the universe itself.

Material properties of any media through which a wave motion propagates dictates many of the characteristics of such a wave. By measuring the effects the media has on a wave as it is transmitted through or reflected from its surface some of the material properties can be deduced.

Within the field of geology, seismologists have used the propagation of elastic waves to study both surface and deep structural properties of the earth. The basis of the techniques rely on arrival times of elastic waves, generated by mechanical or explosive shocks reflected from and refracted through geological boundaries. It is known that in sediments direct relationships exist between physical properties and acoustic characteristics. Mass physical properties, such as, bulk density, porosity, grain size, grading and grain shape that affect the engineering properties of sediments are termed geotechnical parameters. From a knowledge of compressional wave speed, reflectivity and attenuation, it is possible to predict approximately the porosity and mean grain size of a sediment. However, the relationship between these geotechnical parameters and the more important shear strength is not unique, hence compressional wave measurements on

their own are of little practical use to an engineer.

1.2 Shear Wave Propagation

1.2.1 Shear waves in sediments

A shear wave is the propagation of energy in which the particle displacement or vibration is in a plane normal to the direction in which the wave is travelling. For a media to transmit a shear wave it must exhibit a finite shear modulus.

Propagation of shear waves is easily measured in rocks and other solid materials, but in unconsolidated sediments shear waves have proved comparatively difficult to measure because of their low velocities and rapid attenuation. In many offshore engineering projects the foundation sediments are a consequence of location rather than choice. The physical nature of many sediments creates engineering difficulties that are also responsible for the difficult evaluation of shear wave characteristics. Measurements of both shear and compressional wave speed also allows the sediments' elastic moduli to be calculated.

From a more general standpoint, in the field of non-destructive analysis of sediments, shear wave propagation and its characteristics may have distinct advantages. Other analysis techniques, such as acoustic transmission and reflection, electrical resistivity, and nuclear methods, generally relate more closely to the pore phase and its contents than they do to the solid phase. However, as shear waves cannot be accommodated in the fluid-filled pore space of a sediment, their propagation characteristics are primarily controlled by the solid phase and its structure. Shear waves must travel through the individual grains, which make up the soil skeleton, and across the grain-to-grain contacts. It is at these contacts that the pore fluid will have its

greatest effect on the propagation characteristics of shear waves.

It is generally accepted that nearly all marine sediments exhibit enough rigidity (via frictional forces at grain-to-grain contacts in sands and via electrochemical forces in clays, or a combination of both) to transmit shear waves.

As materials, sediments are multiphase media, characterised by the mineral and fluid characteristics and the relative amounts of each constituent. In this way even a simple two-phase sediment, such as a pure quartz saturated sand must be considered as a range of materials. The material changes as the relative amounts of each phase changes. It is not uncommon even for a saturated sand to exhibit porosity ranges of up to 10% (i.e. a stable structure could exist given the same sand grains with porosities of anywhere between 35% and 45%). In this study the corresponding changes in acoustic properties, reflecting the variation in material properties, with changing sand structure has been recorded illustrating the large differences that can occur.

In order to increase our understanding of the acoustic and mechanical properties of sediments, it is necessary to establish a reliable technique for generating and measuring shear waves in these materials. This must be followed by the collection of data in many different sediments under varying conditions as that has been collected for compressional waves (see Chapter 2.3.2). Although explosive and mechanical sources find some application in the field for transmitting shear waves in soils, they have no practical use in any small scale in situ or laboratory investigation. Ideally, for this type of work, a small piezo-electric transducer is required, capable of transmitting and receiving shear waves even in soil with very low shear moduli. A transducer of this kind would be similar to that commonly used for measuring compressional waves in sediments. It would have the advantages of reproducing electrical wave forms as well as enabling frequency pulse length to be controlled.

1.2.2 Land shear wave systems

A shear wave velocity measuring system consists of a source, a sensor and an appropriate timing mechanism. Several types of sources have been used for shear wave surveys in engineering seismology. The plank and sledge-hammer is probably the most popular surface source. By either using the plank lying on the ground and weighted down with a vehicle (e.g. Viksne, 1976) or with the plank driven vertically into the ground (e.g. Davis and Schultheiss, 1980) polarized shear waves are generated by a horizontal impact with the hammer. These techniques allow surface refraction surveys or down-hole measurements to be made. For a more detailed look at layer velocities cross-hole techniques can be employed. Stokoe and Woods (1972) use an impulse rod to generate vertically-polarized shear waves from the bottom of a hole. Miller et al., (1975) use an anchoring technique to generate vertically polarized shear waves at any position in the hole. Explosive sources have also been reported to generate recognisable shear waves in boreholes (Kitsunezaki, 1971; Viksne, 1976). Continuous vibration techniques using electro-dynamic or mechanical vibrators (Jones, 1958) can be employed to measure surface waves which can then be used to esimate shear wave velocities.

Sensors used in S- wave surveys are typically the same as those used in P-wave surveys. Special attention has to be paid to the orientation and it is preferable to use three component geophones (two horizontal and one vertical component). Another important feature of shear wave detection is the coupling between the sensor and the ground. Shear waves do not travel through fluids, therefore sensors have to be rigidly clamped to the borehole or firmly embedded in the surface.

1.2.3 Offshore shear wave systems

Techniques for measuring shear wave velocities on the sea bed are scarce. Bucker et al., (1964) and Hamilton et al., (1970) obtained shear wave velocities from measured Stoneley waves on the sea floor. Schwarz and Conwell (1974) developed a sea-floor electromagnetic hammer which generated detectable waves up to 300 metres from the source. Stokoe et al., (1978) describe the development of a bottom hole device to measure shear waves in the offshore environment. It incorporates a mechanical tensional source and piezo-electric ceramics as receivers. Apart from these few instances shear wave measurements in offshore sediments are rarely made due to lack of versatile and reliable techniques.

1.2.4 Laboratory shear wave systems

In the laboratory, resonant column tests are the most commonly used to determine the shear wave characteristics of soils. Hardin and Music (1965) describe how this technique can be adapted and used during the tri-axial test, the shear wave velocity being a function of the resonant frequency and length of the sample. An important advantage of the technique is that it allows damping characteristics to be investigated with changes in the shear strain amplitude. Celikkol and Vogel (1973) designed a shear wave probe system which transferred the oscillations of a piezo-electric ceramic crystal disc coupled to a back-up mass to an aluminium probe. They concluded that the system was only suitable for soils with an intermediate range of water contents. They did not detect shear waves in saturated sediments. Stephenson (1978) used ultrasonic transducers to measure both P and S wave velocities in soils to calculate dynamic moduli. However, a close inspection of the waveforms reveals that the onset of the S wave arrival is particularly difficult to ascertain

with any reasonable degree of certainty. It is thought likely that these transducers are not suitable to measure shear wave parameters in sediments because of their relatively low compliances and small shearing motions.

Shirley and Hampton (1978) describe the design of a shear wave transducer system capable of measuring shear wave velocities in saturated high porosity laboratory sediments. These transducers are based on the piezo-electric ceramic bender element which is described in a later section. The advantages of the basic transducer, conceived and first used by Shirley, are so strong that this type of transducer system is the only one to have been investigated and developed during this study.

1.3 Objectives of the Study

It is readily apparent from both the literature and theory of wave propagation through sediments that shear wave information is of fundamental importance yet little data has so far been collected. Although many studies have been made using compressional waves propagating in a host of different sediment types, both in the laboratory and in situ, the overall data indicate that useful correlations can only be obtained empirically and their use in terms of predicting geotechnical properties are obviously limited.

The main aims of this study were as follows:-

1. To develop a versatile shear wave measuring system, capable of measuring velocities in a wide range of saturated unconsolidated sediments. Development of shear wave transducers suitable for this application is described in Chapter 3.1.
2. To install these transducers in a variety of laboratory test cells and to investigate the behaviour of shear waves in different sediment types under various stress and packing conditions. Installation of transducers in laboratory cells is described in Chapter 3.2 and

and some preliminary results from porosity cells, an oedometer cell and triaxial cells are presented in Chapters 4, 5, 6 and 7.

3. To design and build probes suitable for measuring the shear wave velocities of surficial marine sediments in situ. Design and construction of these probes is described in Chapter 3.3 and a limited amount of data from cruises is presented and discussed in Chapter 8.

Techniques for measuring compressional wave velocity and electrical resistivity in a variety of laboratory test cells and in-situ probes have already been developed at the Marine Science Laboratories, UCNW (McCann, 1972; Simpkin, 1975; Jackson, 1975, 1978). With a capability of measuring shear wave velocities in the laboratory and in situ, these previous developments would be suitably complemented providing a more complete geophysical characterisation of the sediments. The regular inclusion of shear wave information in the list of physical properties will provide the basis for further fundamental investigations into the acoustic properties of sediments and its relation to geotechnical parameters to be made in the future and hence increase our understanding of the behaviour of these materials as man with his technology continues to make more use of the sedimentary continental shelves and ocean beds.

2. EXPERIMENTAL AND THEORETICAL BACKGROUND

2.1 Wave Propagation

Transfer of energy between two points, in the form of elastic stress waves, is governed by Hookes Law. This states that, within certain limits, the strain produced in an elastic solid is linearly proportional to the applied stress.

The proportionality between stress and strain breaks down at a given strain level which is dependent on the material. It transpires that for saturated sediments this strain level is exceedingly low. After this limit has been exceeded the response is no longer truly elastic.

Mathematical expression of Hookes Law, in its most generalised form, requires 36 independent elastic constants. In an isotropic elastic solid, the number of independent variables needed to fully describe the elastic nature of the media is only two. Lame's constants L and G (G is commonly known as the shear or rigidity modulus) are those most frequently used. Others frequently used are Young's modulus, E, Poissons ratio, ν, and the bulk modulus, K. These constants can all be expressed as simple functions of Lames constants L and G.

When the stress-strain relations of Hookes Law are written in terms of L and G and these relations are used with the wave equation, propagation of two independent waves is indicated. The speed of propagation being governed by the elastic constants and the bulk density ρ. Longitudinal waves propagate at a speed given by

$$V_p = \left(\frac{L + 2G}{\rho} \right)^{\frac{1}{2}} \tag{2.1}$$

and shear waves propagate at a speed given by

$$V_s = \left(\frac{G}{\rho} \right)^{\frac{1}{2}} \tag{2.2}$$

The bulk modulus K is given by

$$K = L + \frac{2}{3} G \tag{2.3}$$

substituting this in equation (1) yields V_p in terms of K and G

$$V_p = \left(\frac{K + \frac{4}{3} G}{\rho} \right)^{\frac{1}{2}} \tag{2.4}$$

which is how V_p is most frequently expressed. When the shear modulus (G) is zero, the medium is a fluid and only a longitudinal wave will propagate with a velocity V_f given by:

$$V_f = \left(\frac{K}{\rho}\right)^{\frac{1}{2}} = \left(\frac{1}{\beta\rho}\right)^{\frac{1}{2}} \qquad (2.5)$$

where β, the bulk compressibility of the media, is the reciprocal of the bulk modulus.

For completeness, useful relations between the various elastic constants are given in equations 2.6 and 2.7

$$E = \frac{G(3L + 2G)}{L + G} \qquad (2.6)$$

$$\nu = \frac{L}{2(L + G)} \qquad (2.7)$$

It should be noted that when G = 0 (as in a fluid) and K = L (from equation 2.3) the compressional wave speed in a fluid is also given by:

$$V_f = \left(\frac{L}{\rho}\right)^{\frac{1}{2}} \qquad (2.8)$$

By re-arrangement of the above equations all the elastic moduli may be expressed in terms of compressional wave speed, shear wave speed and bulk density.

from equation (2.2)

$$G = V_s^2 \rho \tag{2.9}$$

from equations (2.4) and (2.2)

$$K = \rho (V_p^2 - \frac{4}{3} V_s^2) \tag{2.10}$$

from equations (2.3), (2.7), (2.9) and (2.10)

$$\nu = \frac{(V_p/V_s)^2 - 2}{2(V_p/V_s)^2 - 1} \tag{2.11}$$

2.2 Acoustic Properties of Suspensions

Marine sediments are a diverse range of materials varying from de-floculated suspensions at one end of the spectrum, to porous solids at the other. Although this study is primarily concerned with a range of sediments in the middle of this spectrum, it is instructive to relate their physical and acoustic properties to the overall range of materials.

Equations 2.1 - 2.11 apply to homogeneous, isotropic elastic media; in particular, equation (2.5) applies to a fluid. Suspensions of solid particles in liquids are fluid (i.e. have no shear strength) as long as the individual grains do not interact with one another (either by contact, or electrochemical forces). The suspension system therefore has a zero shear modulus and equations (2.5) and (2.8) are applicable.

Wood (1930) originally developed an equation to relate sound speed to suspensions. Wood's equation for velocity replaces bulk density and compressibility by component terms for the water and mineral fractions.

Each component contributing to the bulk compressibility and bulk density of the suspension in proportion to its volume concentration in the suspension. ρ and β become

$$\rho = n\rho_w + (1 - n)\rho_m \tag{2.12}$$

$$\beta = n\beta_w + (1 - n)\beta_m \tag{2.13}$$

where

ρ_m = mineral density

β_m = mineral compressibility

ρ_w = water density

β_w = water compressibility

n = fractional porosity

Substituting equations (2 12) and (2.13) into equation (2.5), the velocity of sound in a suspension becomes

$$V_f = \left(\frac{1}{(n\beta_w + [1 - n]\beta_m)\ (n\rho_w + [1 - n]\rho_m)} \right)^{\frac{1}{2}} \tag{2.14}$$

Equation (2.14) is known as Wood's emulsion equation; an important feature of which is that it predicts that the sound speed can be lower in dilute suspensions than in the individual water or mineral component. Early laboratory measurements on low concentration suspensions of kaolinite made by Urick (1947, 1948; Urick et al., 1949), demonstrated the validity of Wood's equation in these suspensions. In situ measurements, using transducers inserted by divers, described by Hamilton (1956), recorded sediment velocities three per cent lower in high porosity muds than in the overlying water. This phenomena agreed with Wood's equation. However, in all but very high porosity sediments, the velocity was found to be

higher than Wood predicted. It therefore provides a lower limit for most sediment data rather than describing it.

2.3 Propagation of Elastic Waves in Saturated Sediments

2.3.1 Theory

Biot has developed a comprehensive theory for the static and dynamic response of porous materials consisting of a frame which is macroscopically homogeneous and elastic, containing compressible fluid in the pore spaces (Biot, 1941, 1956, 1962a, b). In these various papers, Biot discusses the full range of systems in which the fluid occupying the pore spaces does or does not move with the solids upon the application of a small stress, such as that from a sound wave.

In the absence of boundaries, Biot's theory predicts that three types of body waves are possible in a fluid-saturated porous medium. These are two dilatational waves and one shear wave. One dilatational wave travels through the fluid, and both the shear wave and the second dilatational wave travel through the solid frame. In a solid elastic media there is no distinction between fluid matrix and frame, therefore, the second dilatational wave would not be found. In the two phase sediment this wave is predicted to be highly attenuated in the nature of a diffusion process as it propagates through the sediment skeleton. The dilatationalwave usually measured is the more normal compressional wave in a porous material and is transmitted essentially through and governed by the fluid phase. This wave travels with the highest velocity and as a result of the vibrating elastic structure of the solid constituent, travels faster than in the fluid alone. Viscous coupling between the fluid and solid constituents means that none of these waves are entirely independent; however, the shear wave is probably least influenced by pore fluid coupling (Nacci et al. 1974).

Taylor Smith (1974) analysed Biot's equation and compared it with normal elastic theory. To confirm or otherwise the validity of his approximation, measurements of bulk moduli are needed to compare with the computed values. To do this values of the rigidity modulus are required which of course necessitates shear wave velocity measurements. Biot's equation for the compressional wave velocity, where little relative motion exists between solid and fluid components, includes a coupled pore compressibility term, β_p, which takes into account the low permeability in clay sediments and a total bulk compressibility of the sediment frame or skeleton, β_f, where

$$\beta_f = n\beta_p + \beta_m \tag{2.15}$$

where β_m is the bulk compressibility of the solid particles. The compressional wave velocity (from Taylor Smith, 1974) will be given by

$$V_p^2 = (P + 2Q + R)/\rho \tag{2.16}$$

where P, Q and R are the Biot coefficients.

$$P = \frac{(n-1)^2\beta_p + (n-1)\beta_m + \beta_w}{\beta_f(\beta_w - \beta_m) + \beta_p\beta_m} + \frac{4G}{3} \tag{2.17}$$

$$Q = \frac{-n([n-1]\beta_p + \beta_m)}{\beta_f(\beta_w - \beta_m) + \beta_p\beta_m} \tag{2.18}$$

$$R = \frac{n\beta_f}{\beta_f(\beta_w - \beta_m) + \beta_p\beta_m} \tag{2.19}$$

Hamdi and Taylor Smith (1981) point out that a slight controversy exists about the choice of the frame compressibility β_f. Bishop and Hight (1977) state that it denotes the compressibility of the soil when measured in a test with drainage to constant pore pressure. Hamdi (1981) concluded that it is best measured by the reciprocal of the slope of the unloading curve in a drained consolidation test. In this way, β_p and β_f decrease as the effective stress is increased and the porosity decreases.

An alternative approach is again to use the well known elastic theory for homogeneous, isotropic media, using elastic moduli obtained from component parts of the system except without using a coupled pore compressibility term. This is much the same as Wood's approach for dealing with suspensions, except a simple aggregate modification of component moduli is no longer applicable.

Wood's theoretical formulation of compressional wave velocity does not account for any interaction between the individual solid particles in the two phase media. It is, therefore, restricted in application to true suspensions. In the majority of real sediments, interaction between grains, either frictional or electrochemical does exist providing the system with some rigidity. This rigidity is provided solely by the solid framework (although it is influenced by the fluid matrix) and the framework is considered to be elastic. In Wood's formulation of system compressibility he used an aggregate value derived from the component compressibilities of the mineral and fluid constituents. For a model where the grains do interact, a third component due entirely to the resulting framework or skeleton or mineral grains, must be included.

Gassman (1951) has used this frame component concept in his formulation of a 'closed system', in which the pore fluid does not move significantly relative to the mineral frame. Hookean elastic equations are considered applicable in studying wave velocities, but not for energy damping. Of

particular interest is Gassman's equation for deriving a system bulk modulus for the porous medium, as used by Hamilton (1971a)

$$K = K_m\left(\frac{K_f + Q'}{K_m + Q'}\right) \tag{2.20}$$

$$\text{where } Q' = \frac{K_w(K_m - K_f)}{n\,(K_m - K_w)} \tag{2.21}$$

K = system bulk modulus

K_m = mineral bulk modulus

K_w = pore fluid bulk modulus (usually water)

n = fractional porosity

The system bulk modulus is greater in equation (2.15) than that calculated from volumetric considerations. When the frame bulk modulus is zero (i.e. true suspension conditions), equation (2.15) reduces to Wood's equation, (2.14). Also, when n = 0 (i.e. 100% mineral solid)

$$K = K_f = K_m \tag{2.22}$$

and when n = 1 (i.e. 100% fluid)

$$K = K_w \tag{2.23}$$

The model is theoretically accurate at both extremes of porosity and complies with the proven Wood's equation only when the suspension condition exists. Assuming K_f to be finite, then the bulk modulus, K, from equation (2.15) is greater than that calculated from only volumetric considerations.

Solving equation (2.15) for K_f, it becomes

$$K_f = \frac{nK\,K_m\,(K_m - K_w) + K_m\,K_w\,(K - K_m)}{n\,K_m\,(K_m - K_w) + K_w\,(K - K_m)} \qquad (2.24)$$

2.3.2 Compressional Wave Data

A large amount of data has been published on the physical/compressional wave interrelationships of saturated sediments (e.g. Hunter, et al., 1967; Morgan, 1969; Buchan et al., 1972; Anderson, R.S., 1974; Akal, 1972; and Hamilton, 1970, 1972, 1976). Expense, practical difficulties and lack of control over in situ sediments, have resulted in many measurements being performed on artificially sedimented material in the laboratory (Busby and Richardson, 1957; Shumway, 1960; Nolle et al., 1963; Hampton, 1967). McCann and McCann (1969) have used published results to study attenuation mechanisms. Acoustic measurements on retrieved core samples have been made (e.g. Hamilton, 1963; Buchan, et al., 1967. Schreiber, 1968; Horn et al., 1968; and McCann, 1972). Measurements during coring, giving in situ profiles, have been made by Shirley and Anderson (1973, 1975c).

Several generalizations can be made from the results of the above workers. Compressional wave velocity, over a wide frequency range, correlates more consistently with parameters such as the bulk density, porosity and void ratio than with other geotechnical parameters. Graphic mean diameter also shows a correlation with velocity from natural sediments, but this can be attributed to the density as bulk density and grain size are also related in situ (see Chapter 4.3). Attenuation of compressional waves in saturated sediments has been the topic of much discussion but as the mechanisms are not central to this study they will be mentioned only

briefly. Three mechanisms are identified; these are, scattering, viscous losses (caused by relative motion between the solid grains and the liquid matrix) and frictional losses at grain-to-grain contacts. Stoll and Bryan (1970) suggest that internal friction is the dominant attenuation mechanism over a wide frequency range (10 Hz to about 1 MHz) for fine sediments. In the closed system, as used by Hamilton (1972), no relative motion between solid and fluid phases occur, attenuation is entirely attributed to internal friction and is proportional to frequency. Hence when sediment acoustic attenuation is expressed in a generalised form

$$\alpha = kf^{n'} \tag{2.25}$$

where α = attenuation coefficient

k = constant coefficient

f = frequency

n' = exponent

then $n' = 1$. The exponent may vary for limited frequency ranges (Hampton, 1967; Stoll and Bryan, 1970; Taylor Smith, 1974), but the overall variation is approximately linear as noted by Hamilton (1972).

Despite variable bulk density for any given sediment being an important material property for soil engineers and geophysicists, little information is available on the variation of acoustic properties with changes in sediment structure under ambient conditions. Laughton (1957) and Brandt (1960) studied the variations that occur when high external loading causes porosity changes. Under ambient conditions sound speed and electrical formation factor are both very sensitive to variations in packing (Taylor Smith, 1975).

Hamilton (1971b) suggested methods of predicting compressional wave velocity <u>in situ</u> from laboratory measurements. Sound speed variations,

in unconsolidated marine sediments, with temperature and pressure are very similar to that found in sea-water. Using the ratio of laboratory sediment velocity to laboratory water velocity and multiplying it by the in situ water velocity, a predicted in situ ratio can be obtained.

Compressional wave velocities for saturated marine sediments from all sources exhibit velocities above those predicted by Wood's suspension equation (except for very high porosity muds). A finite rigidity within the sediment, caused by the structural frame, is generally the accepted explanation of the departure from Wood's equation (which, modelled on a true suspension, does not exhibit rigidity). Shumway (1960), amongst others, empirically modified the equation to include a rigidity term so that the discrepancy, between experimental and theoretical values, was reduced to a minimum. Using Gassman's (1951) theory, Hamilton (1970) included a rigidity term so that the system bulk modulus included a frame component and shear wave velocities could be utilised.

Hamilton (1971a, b; Hamilton et al., 1970) discusses appropriate elastic and visco-elastic models for saturated sediments, concluding that for small stresses (such as those of a sound wave) elastic equations can be used, but a linear visco-elastic model should be used to account for wave attenuation. Differences between acoustic and mechanical loading of sediments, in relation to elastic theory and its limitations, are discussed by Taylor Smith (1974). Elastic constants can be derived from a knowledge of bulk density, compressional and shear wave velocities, the latter being the most difficult to ascertain with confidence in sediments. The value of seismic techniques for dynamic testing in marine sediments is reviewed by Feldhausen and Silver (1971). The need for information on both shear and compressional waves in sediments for geoacoustic modelling of the sea floor is illustrated by Hamilton (1974).

2.3.3 Shear Wave Data

2.3.3.1 General Background

As the propagation of shear waves in sediments and the application of techniques for such measurements is central to this study it is appropriate to briefly review previous and current techniques and data. As a generality the paucity of shear wave data compared to compressional wave data in sediments can be accounted for by the lack of reliable techniques for propagating, receiving and analysing shear waves. Sources and receivers in sediments which are rich in shear wave characteristics and where the compressional wave pulse does not mask the slower and more highly attenuated shear wave pulse have proved to be problematic. Consequently, the relative simplicity of producing and receiving compressional waves has probably detracted attention from the shear wave problem. Nevertheless, as vast amounts of compressional wave data has now been collected and as geophysical modelling of sediments becomes more sophisticated, the necessity of shear wave data to complete these models has resulted in a substantial amount of recent effort being made into providing the required techniques.

2.3.3.2 Resonant Column Techniques

In resonant frequency tests solid or hollow cylindrical soil specimens are forced to vibrate at low frequencies in either a longitudinal or torsional mode. The longitudinal mode is used to measure Young's modulus, E, and the torsional mode is used to measure the shear modulus, G. A variable frequency oscillator is used to excite the specimen and the resultant amplitude of vibration is measured as a function of frequency. The resonant frequency, as defined by the response curve is used with the length of the sample to calculate the appropriate modulus. A comprehensive

account of obtaining the moduli and damping of soils using the resonant column method is provided by Hardin and Music (1965) and Drnevich et al. (1978). The damping characteristics of the soil are obtained from the response curve when the specimen is allowed to decay from its driven resonance. Hardin and Drnevich (1972a, b) provide a full account of the background, theory and data for cohesive and non-cohesive soils.

Apart from providing an excellent laboratory technique for the determination of the shear moduli of both cohesive and non-cohesive soils it has several advantages over other systems. The main attribute of the resonant column device is that it allows the effects of strain amplitude on shear moduli to be investigated. Hardin and Drnevich (1972a, b) have shown that the relationship between shear modulus and strain is non-linear and that beyond a threshold strain the modulus decreases with increasing strain which has been modelled with a hyperbolic curve. When used within a triaxial cell (which is the normal situation) the resonant column test permits both confining pressures and axial loads to be applied which allow simulation of in-situ conditions to be made as well as providing a versatile apparatus for fundamental studies. Confining stress have the largest influence on shear moduli but the time of application must also be considered. Anderson and Stokoe (1978) have demonstrated that the shear moduli of sands, silts and clays can all increase significantly with time of confinement at a constant confining pressure. Hardin and Drnevich (1972b) concluded that a maximum shear modulus, G max, can be determined by extrapolation of a strain amplitude-shear modulus curve to zero strain. However, for practical purposes a value of shear modulus using a strain amplitude of 0.0025% or less can be taken as equal to G max.

Despite the numerous advantages of the triaxial resonant column system it is not easily accommodated in many other types of laboratory tests which may usefully wish to monitor shear moduli, nor does it render itself to

installation on in-situ equipment.

2.3.3.3 In-situ onshore techniques

The necessity to characterise dynamic responses of soils has arisen because of the problems associated with the stability of soils subjected to earthquakes and machine vibrations. Shear moduli is the most important parameter to these studies and consequently some considerable effort has been expended to devise and develop suitable techniques for its in-situ evaluation. Techniques employed can be classed into two groups: continuous and transient methods.

Continuous methods described by Jones (1958) involve the generation of surface Rayleigh waves using a controlled energy source, commonly a counter-rotating mass or electromagnetic vibrator producing vertical vibrations. Phase relationships and hence wavelengths are ascertained using a portable geophone as the vibrator which is operated at several frequencies. From a plot of number of wavelengths versus distance the velocity of the surface Rayleigh waves V_R, is calculated. Shear wave velocities, V_s, can be calculated from elastic theory assuming a Poisson's ratio, or assumed to be equal (V_R and V_s differ by a maximum of only a few per cent in soils). It is considered that the shear modulus derived using this technique is an average value for an effective depth of one-half wavelength. According to Ballard and Mclean (1975) good agreement has been found to exist between these surface vibratory tests and other techniques. The main disadvantages of these techniques are that they do not provide accurate shear velocity-depth profiles and for practical purposes the availability of large vibrators limits the depth of penetration to less than 30 meters.

Surface shear wave refraction techniques offer a simple and inexpensive technique for preliminary site investigation. The method is similar to that used for the more normal compressional wave refraction survey except

the source and receivers are rich and sensitive, respectively, to horizontally polarised shear waves. Sources consist of weighted planks as used by Viskne (1976) or wooden stakes driven into the ground as used by Davis and Schultheiss (1980). Horizontal impacts from a sledgehammer provide the horizontal ground shearing motion. Assuming that identifiable shear wave arrivals can be recognised the interpretation is the same as for compressional waves. The depth of penetration is limited with this technique because the high attenuation of shear waves makes signal detection difficult over 100 metres in distance Improvements in shear wave geophones and their ground coupling as well as developments in signal processing techniques could improve the range of detection and hence the effective depth surveyed.

Techniques using boreholes are the most widely used for determining shear wave velocities and hence the shear moduli of onshore soils. Two systems have been well reported: crosshole and downhole methods.

The crosshole method (Stokoe and Woods, 1972) consists of using two or more boreholes with a seismic source in one and multi-axis (three component) geophones in the other borehole or boreholes placed at known elevations. Shear waves can often be difficult to positively identify and some considerable care must be exercised when interpreting the seismic records. It is imperative to use sources which are rich in shear energy (preferably polarised in which the impulse direction is reversible) and repeatable (for stacking purposes) (Davis and Schultheiss, 1980) if good records are to be obtained. For crosshole surveys it is normal to provide a vertical impulse at the bottom of an advancing hole providing horizontally propagating vertically polarised shear waves. This is accomplished using rods and a surface hammer or by using the standard penetration test as a repeatable reversible impulse source (Stokoe and Abdel-razzak, 1975) which has the advantage of providing strength profiles to supplement the data.

Other downhole sources have been designed, one of which provides horizontally polarised shear waves. It consists of a tube or vane imbedded in the base of a borehole, a torsional impulse is applied through the rods and is converted to shear energy in the soil (Hoar and Stokoe, 1978). A system which can be used in a previously drilled hole, therefore, eliminating the need to drill out to different depths is described by Statton et al. (1978) which involves using a hammer device which can be hydraulically clamped to the sides of the hole and produces reversible vertical impulses. Miller et al. (1975) report on a similar device capable of providing large shear strains in the soil mass. Explosive sources can also be used to generate shear waves in boreholes but McLamore et al. (1978) in a comparison of both mechanical and explosive sources used in crosshole testing conclude that mechanical sources provide more identifiable shear wave arrivals whereas P-wave arrivals are more readily identifiable from explosive sources. By using accurately measured holes at close separations the crosshole technique is a versatile technique which fits into site survey programmes and can generally provide accurate shear wave velocity-depth profiles.

The downhole method involves using a seismic source at the ground surface next to a borehole with one or more geophones clamped at variable known depths. In this technique the source is usually a partially buried stake or plank which is struck horizontally with a sledge hammer producing vertically propagating horizontally polarised shear waves (Wilson et al., 1978; Davis and Schultheiss, 1980). This source is obviously easily repeated and reversed. By using two geophones time differences of arrival can provide interval velocities to compile a velocity-depth profile. This technique has the significant advantage over crosshole testing of only requiring a single borehole.

It can be seen from the above brief literature review that on-shore shear wave techniques, although still not extensively used, have become established

over the past ten years as soil mechanics methods have demanded accurate in-situ data. However, this is not the case for offshore techniques.

2.3.3.4 Offshore Techniques

It can be seen from the previous section that shear wave generating and receiving techniques used on land cannot easily be adapted for sea floor use. Various attempts, however, have been made to measure the in-situ shear wave velocities of the sea bottom sediments. Dynamic loading of sediments can occur from wind and waves as well as from earthquakes and machine vibration, hence the need to characterise sediment dynamic response becomes more important as more technological uses are made of the sea floor, especially in seismically active areas.

Davies (1965) and Hamilton et al. (1970) have made measurements of Stoneley wave velocities in the Indian Ocean and off San Diego, California, respectively using explosive detonators as sources and an array of receivers on the sediment surface. Hamilton (1970) used a submersible as well as divers to place the equipment on the sea floor. These techniques enable V_s to be computed from the surface Stoneley wave using elastic equations or by using complex Lame constants for a visco-elastic water sediment interface (Bucker et al., 1964). Bucker et al. (1964) found that the ratio of Stoneley wave velocities to shear wave velocities computed in this way are insensitive to moderate changes in sediment densities and compressional wave velocities and is approximately 0.87. Davies (1965) reported values of shear wave velocity at the sediment surface on the deep sea floor of 50 $msec^{-1}$ and Hamilton et al. (1970) report values ranging from 88 $msec^{-1}$ for a clayey silt to 197 $msec^{-1}$ for sand in water depths from 20 to 986 meters.

Stokoe et al., (1978) have presented the concept and design studies of a shear wave velocity borehole logging tool. The measurements would

be made at the bottom of an advancing borehole in the same way as other wire-line logging tools are commonly used. This device consists of torsional source which produces vertically propagated horizontally polarised shear wave which are detected using piezo-electric ceramic transducers which are mounted in guide rods which are advance beyond the bottom of the hole. The author is unaware of any further development of this device but if it proves successful and reliable it would be a most valuable addition to the suite of geophysical tools used in the borehole logging industry.

Schwarz and Conwell (1974) developed and used successfully on the seafloor in 300 meters of water a refraction technique for measuring shear wave velocities. The source consisted of a heavy (170 lb) iron slug acting as an electromagnetic hammer against the end plates of a tube. Two solenoids at either end of the tube, driven by discharges from a capacitor bank, enabled repeatable and reversible shots to be fired. An array of horizontal geophones on gimbals extending over a 300 meter line were used as receivers. Results showed shear wave velocities increasing from 38 $msec^{-1}$ at the surface to 345 $msec^{-1}$ at a calculated depth of 90 meters. Although the source is large and the array of bottom geophones not easy to handle it would seem that this technique is the only one tested at present which can provide data over such large distances and hence probably most representative of gross in-situ conditions To increase the range and hence the depths of penetration either more sensitive geophones or their couplings must be developed or larger and more efficient shear wave sources must be used. Developments along these lines are currently taking place at UCNW and at the Institute of Oceanographic Sciences (Wormley),(Whitmarsh and Lilwall,1982)

2.3.3.5 Laboratory Pulse Techniques

Whilst the direct transmission of pulsed waves has provided a technique for the study of compressional waves in unconsolidated sediments similar techniques for shear waves at low confining pressures have until recently been non-existent. Laughton (1957) using Y-cut quartz crystals in a confined compression test, found that shear waves could only be detected in ocean bottom sediments at very high compaction pressures (49 MPa). At these high pressures the lowest calculated value was 1140 $msec^{-1}$. It is obvious that below these pressures shear waves with much lower velocities do exist but this type of measuring system is far too insensitive for their detection. It is interesting to note that considerable compressional and shear wave velocity anisotropy was recorded for deep sea clays and terriginous muds. For example in a red clay the following mean values are quoted for a maximum pressure of 1333 MPa:

	$msec^{-1}$
$^{h}V_{sh}$	1370
$^{h}V_{sv}$	1140
$^{v}V_{sh}$	1110
$^{v}V_{pv}$	1610
$^{v}V_{ph}$	2170

$^{a}V_{bc}$ is the wave velocity where:

a is the direction of propagation (h - horizontal, v - vertical)

b is the wave type (p - compressional, s - shear)

c is the particle vibration direction (h - horizontal, v - vertical).

It can be clearly seen from thesedata that sediments of this type (especially at high pressures) cannot be considered to be isotropic but may only be considered as transversely isotropic.

Stephenson (1978) has reported measuring shear wave velocities in a remoulded silty clay compacted to various void ratios and values of water contents. The transmitting and receiving transducers were piezo-electric radial expanders with a resonant frequency of 90 kHz. Although the raw shear wave velocities are not given it is possible to calculate these velocities from the smoothed graphs of shear modulus (G) versus void ratio. At the highest void ratio on the graph 0.65 the value for G is 500 MPa. Using a degree of saturation of 85% as indicated the bulk density is approximately 2000 kg m^{-3}. This means that the shear wave velocity is 500 $msec^{-1}$. At a void ratio of 0.35 the shear wave velocity is over 1000 $msec^{-1}$. For this type of material under no confining stress these velocities are extremely high and do not compare with the much much lower values provided by Hardin and Black(1968). It is difficult to see how the differences can be explained except by assuming the shear wave values to be incorrectly interpreted from the records. An examination of an example wave trace given by Stephenson (1978) in Fig. 3, p. 188, reveals a complex waveform which is difficult to interpret (especially in the time domain) from the information given. In the light of the author's own experience it seems that shear waves with a frequency around 90 kHz under no confining pressure would be attenuated so rapidly as to make their identification extremely difficult.

Celikkol and Vogel (1973) describe the design of shear wave transducers using piezo-electric transducers mounted at the top of aluminium probes. The probes inserted into the sediment provides a shearing motion which is transferred to the sediment and received by the second probe in a reciprocal manner. Shear wave velocities in a fine sand and a sand-silt-clay are

reported for water contents between 5.7 and 34.6 per cent. Shear wave velocities were generally found to increase with decreasing water content; values lying between 198 and 384 msec^{-1}. However, it was concluded that the system could not measure shear wave velocities in soils with a water content greater than 50 per cent even with the probe separation that was used of only 7 mm.

The most significant developments in laboratory pulse techniques for measuring shear wave characteristics, in all types of unconsolidated sediments and at low confining pressures, have been made by Shirley and others at the Applied Research Laboratories, Austin, Texas, since 1975. Published papers and internal reports document the transducer development and data obtained. Shirley and Anderson (1975a) describe initial developments in transducer design including the use of piezo-electric bender elements as shear wave transducers. This type of piezo-electric element proved to be most successful and its operation is described in detail in Chapter 3. Shirley and Anderson (1975b) and Shirley and Hampton (1978) describe measurements of shear wave velocities in high porosity kaolinite clay as low as 2 msec^{-1} with an attenuation of 520 dB m^{-1}. Further reports, Shirley (1977), Shirley and Bell (1978), Shirley et al. (1979) have concentrated on developing transducers to measure shear wave velocity profiles during coring in the same way as compressional wave profiles are obtained (Shirley and Anderson, 1975c). Horn (1980) used composite piezo-electric benders as shear wave transducers to measure shear wave velocities in saturated laboratory sands. This work is discussed in more detail in Chapter 3. The above references of Shirley and others are referred to elsewhere in this report as the concept of using ceramic bender elements for a diverse range of shear wave applications is presented, results obtained and discussed.

2.4 Sediment Structure and Fabric

2.4.1 Packing structure of sands

Sands are composed of solid grains of varying shapes, sizes and surface textures. The bulk properties, of the sand body, are controlled by the arrangement or geometrical configuration of all these grains. To completely describe such an assembly would be an impossible task since every grain would need to have its co-ordinates, shape and orientation in space quantified. Each grain would then need to be characterised by its interaction with its neighbours, type of contact and so on. A description of this type can only readily be applied to granular materials consisting of symmetrical shapes with systematic arrangements. An understanding of packing characteristics is important in other disciplines apart from the soil sciences (e.g. ceramics and crystallography), and so has received much attention. A complete analysis of regular packing in spheres has been written by Graton and Fraser (1935).

Systematic packing of uniform spheres produces four essentially different structures (cubic, orthorhomic, tetragonal and rhombohedral). Each system is characterised by its type of packing, which is reflected by the number of contacts a typical sphere makes with its neighbours (co-ordination number). Most tightly packed is the rhombohedral structure, that has a co-ordination number of 12.

Relative volumes occupied by the solid spheres and the interstices or voids are given by porosity (n) or void ratio (e) which are easily calculated for systematic arrangements of spheres. Fractional porosity (n) is given by

$$n = \frac{V_v}{V_t} \qquad (2.26)$$

where V_v = volume of voids

V_t = total volume

Void Ratio (e) is given by

$$e = \frac{V_v}{V_s} \tag{2.27}$$

where V_s = volume of solids

Porosity and void ratio are related by

$$e = \frac{n}{1-n} \quad \text{or} \quad n = \frac{e}{1+e} \tag{2.28}$$

Porosities for systematically arranged structures of uniform spheres range from 0.4764 to 0.2595 for cubic and rhombohedral packing respectively. Further regular structures can be composed by inserting secondary, tertiary, quaternary spheres into the interstices of the structure, reducing the porosity of the structure at each stage. These models, although extremely valuable in crystallography, are inadequate for a complete description of granular materials. Variations in particle size and shape make models based on spheres and their regular packing structures, extremely limited. In real granular systems the co-ordination number of any grain depends on its position within the overall structure as well as its size shape and orientation. A sand is more accurately described as a random granular assemblage of irregularly-shaped particles (to distinguish the deviation from systematic packing structures). However, the bulk properties, such as porosity, can still be used as an overall measure of packing structure. It must be stressed that using porosity as an overall measure is statistical by nature and gross heterogeneities remain unquantified.

Variable structure, measured by changes in porosity, is an important characteristic of granular materials and, as such, its limiting values are worth considering. Limiting values can be expressed as maximum and minimum density, void ratio or porosity. In this study porosity has been used to quantify structural differences, although in engineering practice density is more commonly used. Limiting values of porosity are controlled by the inherent factors of a sand: size, size grading, shape and shape grading. The range of possible porosities, for any given sample, will, therefore, vary according to its bulk grain characteristics. In this way, it is possible to have two sands with identical porosities, but one is very loose (close to its maximum porosity) and the other tightly compacted (close to its minimum porosity). Porosity, as can be seen by this example, does not describe packing in all its aspects. Kolbuszewski (1948) considered that relative porosity (n_r) gave a better assessment of packing than fractional porosity. Relative porosity is given by

$$n_r = \frac{n_{max} - n}{n_{max} - n_{min}} \times 100\% \qquad (2.29)$$

where n_{max} = maximum porosity

n_{min} = minimum porosity

n = actual porosity

Relative porosity is measured in per cent: $n_r = 0\%$ is the loosest state, $n_r = 100\%$ is the most compact state. A complete evaluation of measurements, influencing parameters, accuracy and engineering uses of relative density measurements (which is comparable with relative porosity) is given in a collection of papers edited by Selig and Ladd (1973).

Experimentally determined limiting porosities depend on the technique used. In this study a simple technique was used where the sand was allowed to free-fall from a funnel into a large (one litre) measuring cylinder.

Both the height of fall and the rate of pouring influence the resulting porosity. Increasing height and decreasing rate both reduce the final volume occupied in the measuring cylinder, and hence the porosity, of a given weight of sand. However, there is a limiting height, above which the porosity remains constantly low and similarly a limiting rate of pouring, below which the porosity is constant. These limiting values of height and rate depend on the sand being tested. Larger grain sizes require greater heights of fall and slower rates of pouring.

Apart from porosity, which provides only an overall picture of the relative proportion of mineral and fluid constituents, grain characteristics must be defined. Quantitative analysis of the particulate mineral phase can be obtained from grain size measurements. Sand grains are not spherical hence a single parameter does not uniquely define its size, it can only provide a 'size' as measured by a given technique. A single parameter sizing of a sand grain can be its maximum dimension, minimum dimension, volume, surface area, equivalent sphere diameter (determining from settling velocities and Stokes Law). The most common technique for sand size particles is to group them into size intervals according to a sieve mesh size through which they will not pass after a certain vibration period. Folk and Ward (1957) describe the subsequent parameters which are used to describe a size distribution where D_n is the grain diameter in phi units at the nth percentile.

Mean grain size (D_M) is a measure of the overall average grain size and is given by

$$D_M = \frac{D_{16} + D_{50} + D_{64}}{3} \qquad (2.30)$$

Sorting (S_p) is a standard deviation measure of the grain sizes in a sample and is given by

$$S_p = \frac{(D_{84} - D_{16})}{4} + \frac{(D_{95} - D_5)}{6.6} \qquad (2.31)$$

Skewness (Sk_p) is a measure of the deviation from normality of a grain-size distribution and is given by

$$Sk_p = \frac{(D_{84} + D_{16} - 2D_{50})}{2(D_{84} - D_{16})} + \frac{(D_{95} + D_5 - 2D_{50})}{2(D_{95} - D_5)} \qquad (2.32)$$

A symmetrical curve has a Sk_p value of zero; positive values indicate that the curve has a tail in the smaller grains, whereas negative values indicate that the curve has a tail in the larger grains.

Kurtosis (K_p) is a measure of the degree of peakedness, that is, the ratio between the spread of the grain diameters in the tails and the spread of the grain diameters in the central portion of the distribution, and is given by

$$K_p = \frac{D_{95} - D_5}{2.44(D_{75} - D_{25})} \qquad (2.33)$$

Quantitative description of grain size and grading is, to some extent, arbitrary. When used for potential correlation with other parameters (in this case acoustic), different methods of quantifying the data may prove more valuable than those above. The number and type of samples tested in this study does not justify a rigorous examination of different quantitative descriptors. However, with the accumulation of more data under the same controlled conditions, an analysis of numerical measures of grain size and grading could be of value. For example, a quantitative measurement that uses all the grain size data to describe the grading characteristics has been devised by Sharp and Pow-Foong Fan (1963).

Particle shape is a difficult grain parameter to quantify. However,

for its limited application in this study a visual method has been used that qualifies the differences between samples. Particle shape is usually sub-divided into the two more distinctive parameters of roundness and sphericity. Roundness is a measure of the sharpness of the particle edges, whereas sphericity is a measure of the degree to which shape of the particle approaches that of a sphere. It is possible to have grains that are well-rounded, but with a low degree of sphericity and grains that are almost spherical but very angular. To assess the shapes of the sands tested the grains were compared with visual estimation charts. Pettijohn (1957) defined five roundness grades: (1) angular, (2) subangular, (3) subrounded, (4) rounded and (5) well-rounded. Images for estimating two-dimensional sphericity have been drawn by Rittenhouse (1943). The visual estimation charts used were those reproduced by Chilingarian and Wolf (1975, pp. 15-16).

2.4.2 Clay fabric

In this study clay 'fabric' or 'structure' is relevant only to a few measurements (clays have been used in the oedometer cell and acoustic velocities measured in situ). The terms fabric and structure refer to the orientation and distribution of particles within the sediment and to the forces between adjacent particles. It is relevant to mention briefly the nature of clay fabrics so that the important differences that exist between cohesive and non-cohesive sediments are appreciated when the measured physical and acoustic properties are examined.

The difference between sand sized (2000-63μm) and clay sized (<2μm) particles has a profound effect on their mass properties (silts, 63-2μm, exhibit a range of intermediate properties as might be expected). Another major difference between sands (including most silts) and clays is their

particle shapes. Generally sands tend to be equidimensional whereas clay particles are most commonly plate-shaped.

Net negative charges are carried by soil particles primarily through isomorph substitution (substitution of an atom in the crystal lattice by another, possibly with a different valency state). Lambe and Whitman (1979) present a clear discussion of this and other phenomena relating to the nature of soils and their individual particles. Electrical charge on a particle is not uniformly distributed over its surface, hence a charge distribution is set up which influences the way in which the particles interact. Also the magnitude of the electrical charge is related to the surface area, therefore, the effect of the electrical charge will be strongly related to ratio of surface area to volume. Between sand and clay size particles this can vary by 10^7. It can be seen that the influence of the electrical charge on clay particles will be much greater than on sand sized particles; in fact, it dominates the behaviour of clays.

The effect of this net electrical charge when the particle is in water is to attract oppositely charged ions to its surface to achieve neutrality which in turn attracts water because of its polar nature. In this way the particles are surrounded by a layer of adsorbed water (the thickness of which depends on the mineralogy) which in terms of the overall sediment properties can not necessarily be considered to be part of the 'free' fluid phase. The distribution of charge on fine-grained particles and the resulting attractive and repulsive forces, have a great influence on their mass arrangement. In this way fine-grained particles which have formed by natural sedimentation can have open flocculated structures (this depends on the ion concentration in the water) which if remoulded may form relatively closed dispersed structures.

It can be seen from the above brief discussion that clay fabrics can be very different depending on a multitude of factors and that they are

always substantially different from sediment structures composed of sand sized particles. These differences result only indirectly from the large change in particle size. Both the geotechnical and acoustic properties are inevitably closely linked to the parameters which describe the sediment fabric.

3. EQUIPMENT DEVELOPMENT

3.1 Shear Wave Transducers

3.1.1 Design Considerations

Two requirements exist for shear wave measurements to be successfully implemented:

(a) The shear transducers must generate and detect a shearing motion within the medium.

(b) The received signal (assuming a pulse technique is used) should be of such a quality that either its signature and preferably its onset can be clearly identified in order that timing measurements can be performed.

In saturated unconsolidated sediments both these requirements are far more difficult to achieve than in hard rocks. The following generalised saturated sediment characteristics serve to illustrate the problems encountered when designing shear transducers for use in these types of materials.

(1) They have high compliances: shear moduli in the range 10^4 - $10^8 N/m^2$. It is essential that the transducer stiffness is as close to that of the sediment to minimize the impedance mismatch.

(2) High attenuation co efficients exist for shear waves which increase rapidly with increasing frequency. Transducers which operate at

relatively low frequencies are, therefore, required if transmission is to take place over long path lengths.

(3) Compressional waves travel at velocities around 1600/sec and are less highly attenuated than shear waves. If these form a significant component of the received signal then they can easily obscure the later arriving shear wave.

Apart from these three sediment characteristics which have to be considered when satisfying the requirements (a) and (b), the physical limitations of the system have to be catered for. For the purposes of this work, shear wave systems for use in laboratory cells as well as in situ needed to be designed. It is necessary, therefore, to have a compact transducer design enabling it to be incorporated into small cells such as the standard oedometer.

3.1.2 The bender element

Piezo-electric materials when strained produce a voltage difference across opposing faces. The inverse also occurs i.e. electric fields cause alterations in the size of the material. Exactly how the electric field and strains are related depends on the material properties and its physical dimensions. Ceramic piezo-electric materials are commonly manufactured from lead zirconate and lead titanate (PZT). These are polycrystalline ceramics which obtain their piezo-electric characteristics after they have been polarized in a d.c. electric field during cooling. Piezo-electric ceramics can be fabricated into a widerrange of shapes and sizes than would be possible to achieve with single crystals.

Piezo-electric ceramic crystals have been used very successfully for generating and receiving compressional waves in sediments when they operate in their thickness mode. A piezo-electric ceramic can be used to generate

shear waves, in a solid material, when the direction of polarization and electrode surfaces are arranged as illustrated in Figure 3.1. If an electric field is applied to the piezo-electric ceramic, perpendicular to its direction of electrical polarization, then the ceramic will experience a shear deformation as shown by the broken line. When the electric field is reversed, so also is the deformation. In this manner, with the application of an alternating electric field, a shear wave will propagate normally to the face experiencing the transverse motion when this is in contact with a solid medium.

Attenuation of shear energy, resulting from the granular nature of soils, is very high and increases rapidly with increasing frequency. Therefore, a transducer suitable for generating, transmitting and receiving shear waves in sediments should have a low operating frequency (probably less than 5 kHz). The resonant frequency of a transducer, of the type shown in Figure 3.1, is a function of its stiffness, because when an alternating electric field is applied, it acts as a vibrating bar. If used in conjunction with a sediment, there would be a large mismatch of characteristic impedance between such an element and the sediment. This is a result of the large difference in the compliance of the two media (i.e. the element exhibits a small movement with a large applied force, whereas a sediment exhibits a large movement with the application of a small applied force). Hence, only a very small portion of the mechanical motion of the ceramic element would be transferred into the sediment. Shear moduli in sediments, especially saturated marine sediments, are very small in comparison with crystalline solids, and this type of transducer which is similar to a Y-cut quartz crystal is not suitable for unconsolidated sediments at low confining pressure as demonstrated by Laughton (1957).

PZT bender or 'bimorph' (Vernitron trade name) elements are composite

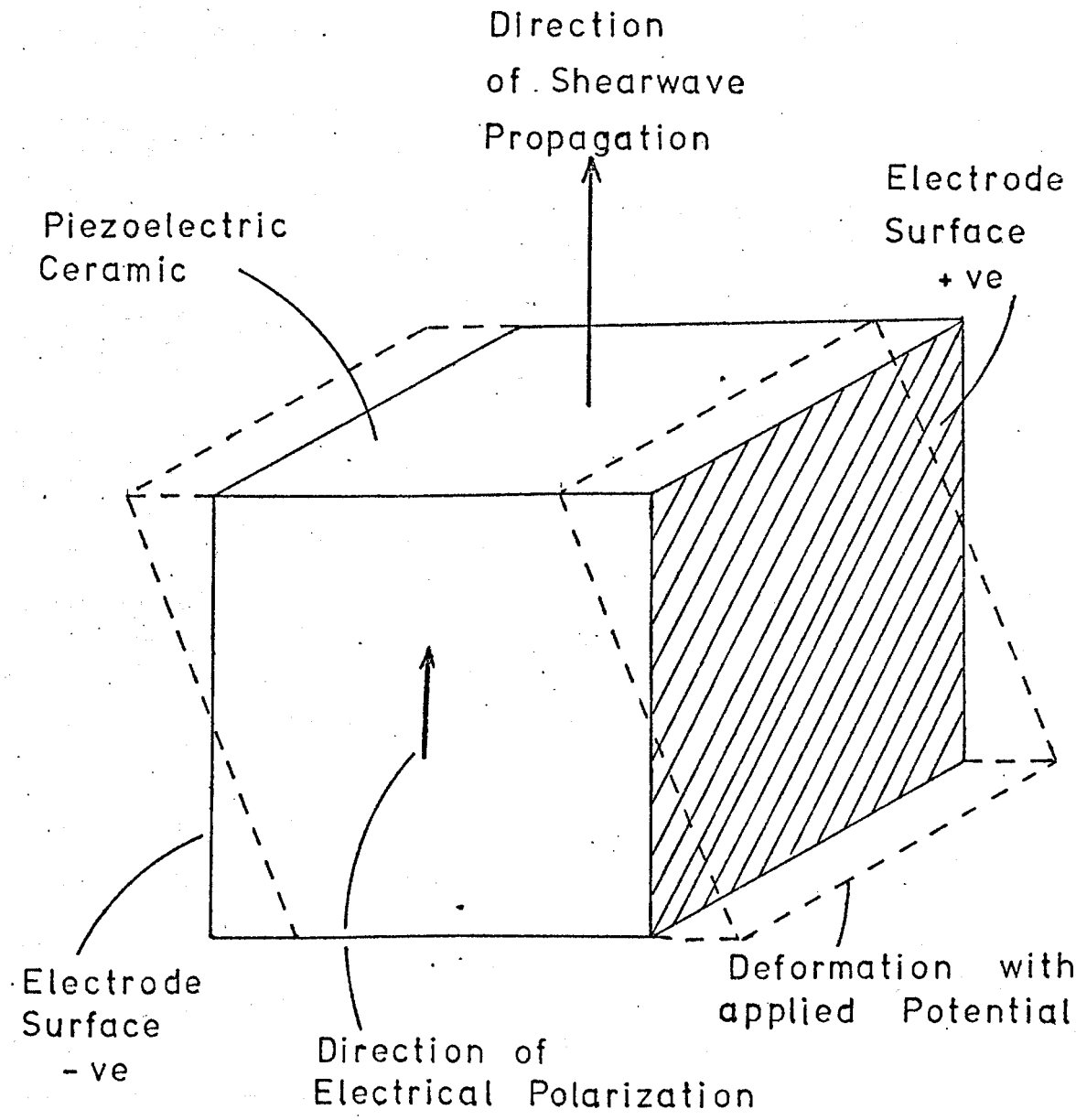

FIGURE 3.1 Principle of Shear Wave Transducer

sheets consisting of two piezo-electric transverse expander plates bonded together face-to-face so that an applied voltage across the plates causes it to bend as illustrated in Figure 3.2a. The bending motion arises because one plate expands at right angles to the polarization direction while the other one contracts. This motion is analogous to the action of a bimetallic strip. Electrical connections to the bimorph are arranged depending on the polarization direction of the two plates (see Figure 3.2b). A series connected element develops twice the voltage of a parallel connected element but provides only half the displacement of the parallel element for the same applied voltage. Figure 3.2a shows the deformation of a bender element operating without any constraints in air. In practice, the performance of a bender element is greatly influenced by the manner in which it is mounted and driven.

The maximum displacement of a parallel bender element at each end in free air is given by (Shirley and Anderson, 1975)

$$D = 1.5\, d_{31} \frac{L^2 V}{T^2}$$

where L = length

T = thickness

V = applied voltage

d_{31} = piezo-electric constant

Therefore, for a typical element used in these studies (L = 30 mm, T = 0.5 mm) the displacement is 3.1×10^{-4} mm/v. For elements loaded by mounting constraints these displacements will, of course, be different and for cantilever mounts it will be double at the free end. It is these relatively large displacements for small applied voltages coupled with the low resonant frequencies that make bender elements suitable as shear wave transducers for sediments under low confining pressures.

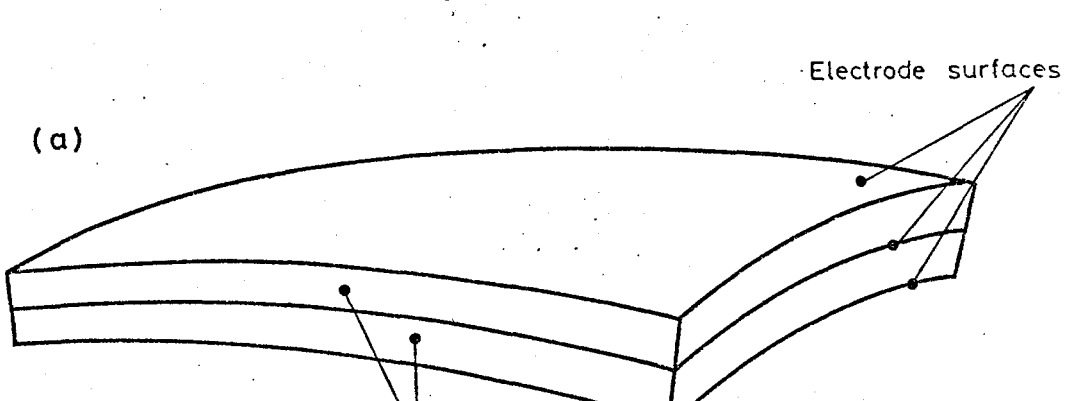

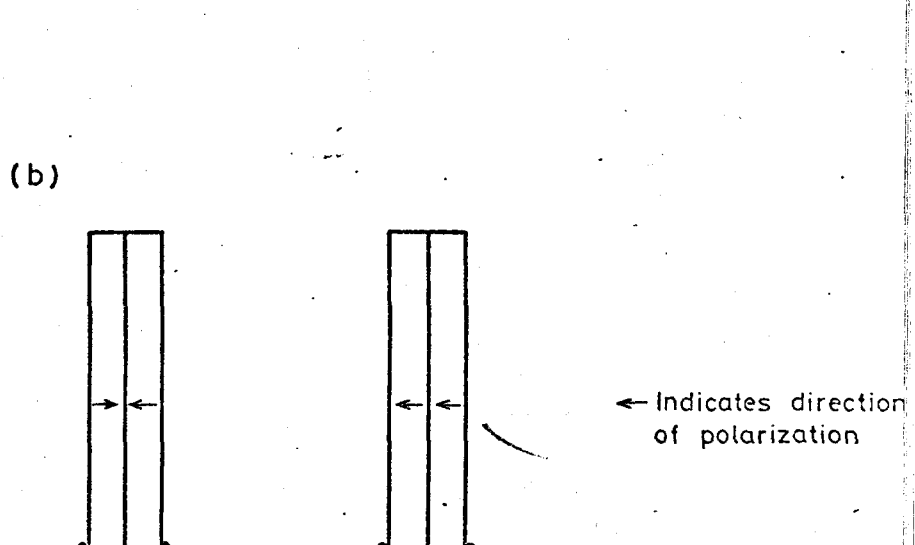

FIGURE 3.2 'Bimorph' bender element; (a) the free bending motion, (b) the electrical connections.

3.1.3 Bender elements as shear transducers

A ceramic bender can come closer to meeting the design requirements, needed for shear wave transducers in sediments, than other piezo-electric elements. Bender elements can be made in thin sheets (typically 0.5 mm) with low resonant frequencies and relatively high compliances in a small size. The basic concept of using this type of element as a shear wave transducer is shown in Figure 3.3. Here a parallel connected element mounted in a cantilever mode is subjected to a driving voltage which results in a transverse bending motion. This creates shear stresses in the surrounding media which may propagate as shear waves in the direction as shown. A bender element may also be used as a shear wave receiver because of its reciprocal behaviour. A parallel connected element is used as the transmitter and a series connected element as the receiver because of its greater voltage sensitivity to strain displacements.

Shirley,working at the Applied Research Laboratories, had the original concept of using bender elements as shear wave transducers. Shirley and Hampton (1978) describe the design of a multi-element transducer and using this they obtained measurements in high porosity sediments. Velocities as low as 2m/sec were reported and attenuations as high as 520 dB/m. These transducers consisted of a stack of bender elements separated by layers of highly-compliant material. With these transducers only the front face of the stacked array was designed to be in contact with the sediment. A large radiating face is, therefore, necessary to provide an adequate coupling to the sediment.

The large mechanical motion and low resonant frequency of such a ceramic bimorph, makes it more suitable for generating shear waves in highly compliant, unconsolidated sediments than the transducer shown in Figure 3.1. A full discussion of the theory behind the development of the bimorph

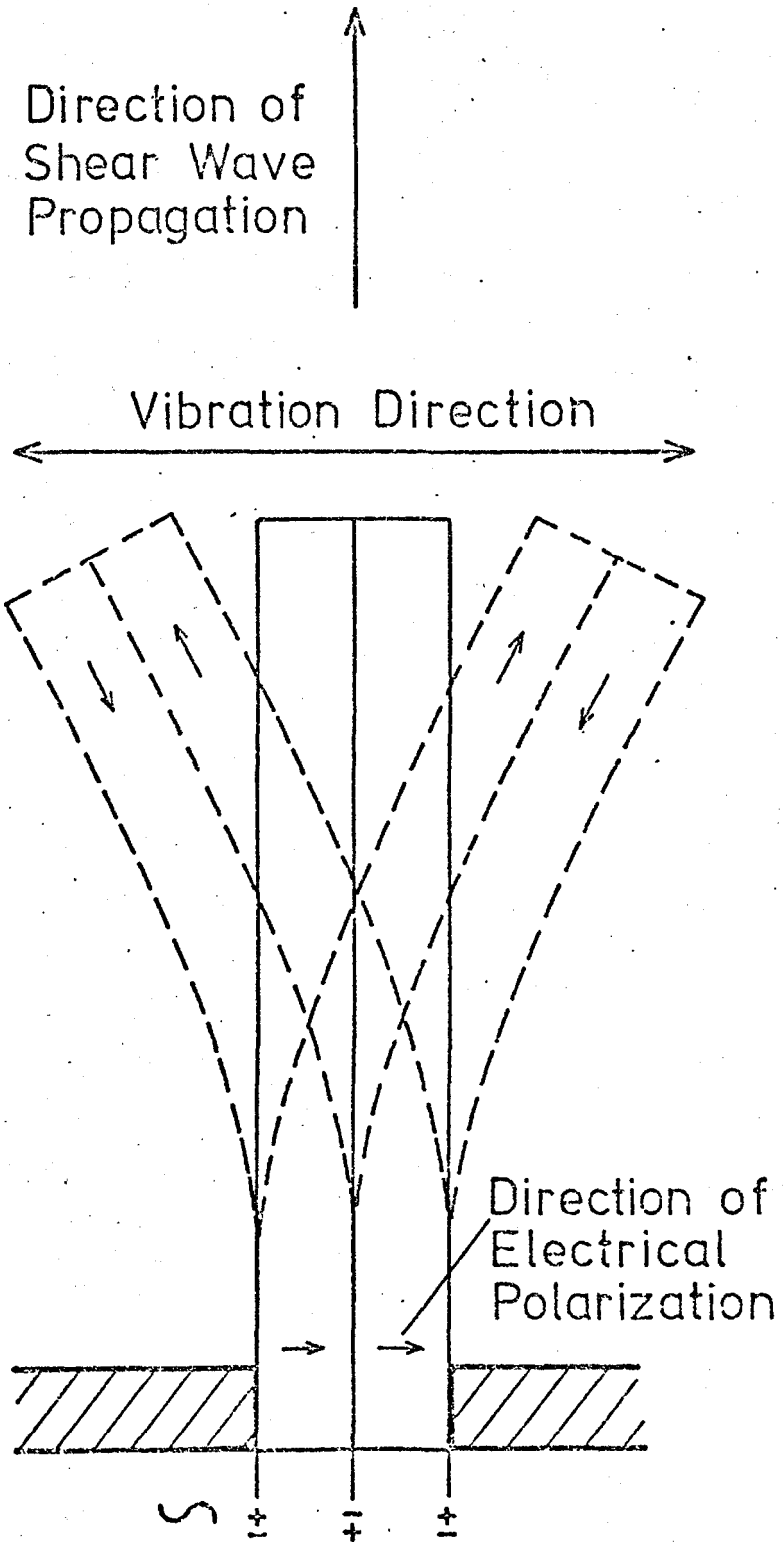

FIGURE 3.3 Schematic operation of a bender element in a cantilever mode

element is given by Shirley and Anderson (1975b). To increase the area of the radiating surface an array of identical bimorph elements in parallel, separated by a layer of highly compliant 'corprene', is used. Figure 3.4 shows this configuration after construction.

Other types of shear wave transducers have been designed using bender elements, one in particular which is similar to designs tested during this work is described by Shirley (1978).

It is interesting at this stage in the discussion to quote Ballard and McLean (1975):

> "The most desirable seismic source is one which inputs repeatable amounts of energy into the soil, may be adjusted to various energy levels, has provisions for consistent coupling with the soil medium, is capable of generating oriented waves, has provision for frequency control, and is preferably non-explosive."

Bender elements may come very close to meeting these requirements for small-scale applications.

3.1.4 Transmitter monitoring

A pulse technique is commonly used to measure seismic velocities both *in situ* and in the laboratory. In the case where piezo-electric ceramics are used as transmitters, electrical impulses are used to generate stress transients that propagate as seismic waves. Ordinarily, the onsets of received pulses are identified and timed to compute the required velocity in a given material. If other information is required from the energy pulse i.e. attenuation data, then the appropriate data is obtained by comparing the frequency spectra of a given pulse at two or more receivers situated at different distances from the source. In this way, the wave-form received at the nearest receiver can then be considered as the source signal. The real source signal is unknown and is possibly substantially

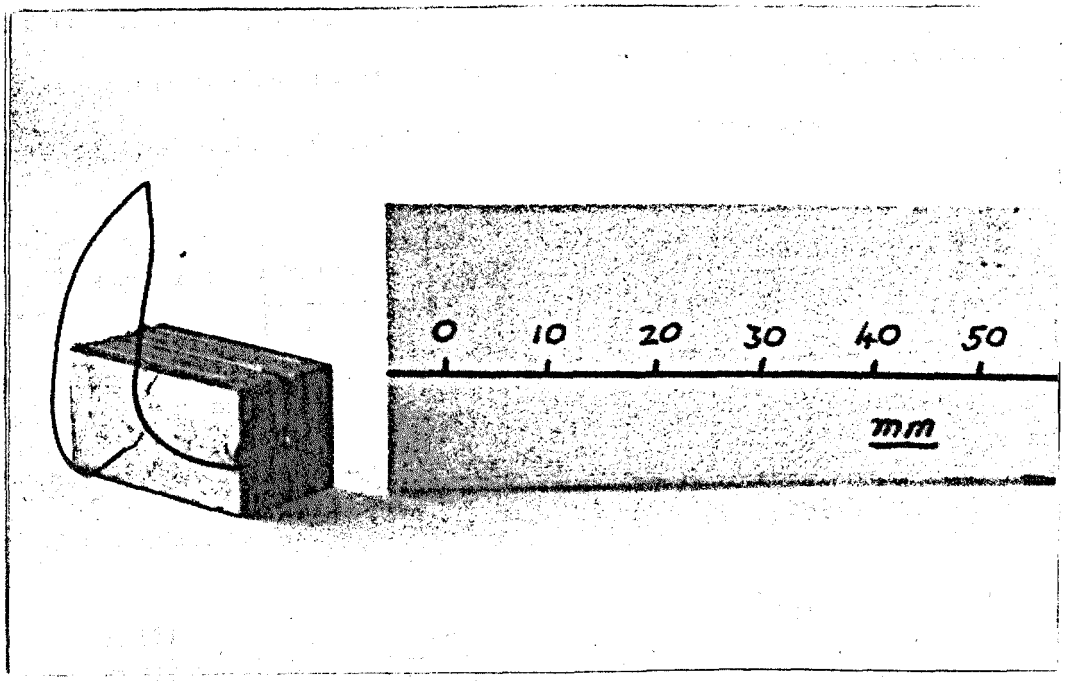

FIGURE 3.4 ARL Shear Wave Transducer constructed from bender elements

different from the electrical driving signal.

For compressional wave transducers it is possible to use water as a test media for calibrating a transmitter and then, by applying corrections for acoustic mismatches at boundaries, attenuation data can be obtained. For shear wave transducers the lack of a suitable material for calibration makes a similar procedure impossible. Consequently, attempts were made in the later stages of the transducer development programme to monitor accurately the source characteristics.

If the frequency response of the transducers within the sediments can be ascertained then it is theoretically possible to obtain the frequency response of the soil. Consider the transducer/soil system

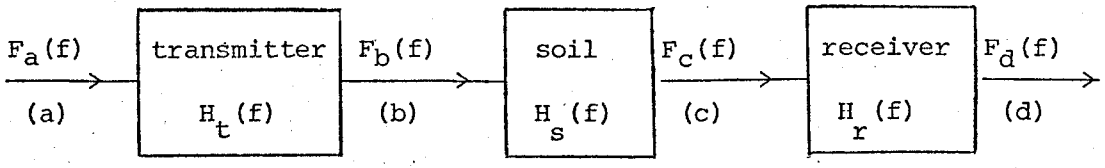

The transfer function is defined as the complex ratio of the output to the input of a system as a function of frequency. Therefore:

$$H_t(f) = \frac{F_b(f)}{F_a(f)}, \quad H_s(f) = \frac{F_c(f)}{F_b(f)}, \quad H_r(f) = \frac{F_d(f)}{F_c(f)}$$

where $H_t(f)$, $H_s(f)$ and $H_r(f)$ are the transfer functions of the transmitter, soil and receiver and $F_x(f)$ is the Fourier spectrum of the signal measured at x. In a normal experiment the electrical input signal, $F_a(f)$ would be known and the received electrical signal ($F_d(f)$. The transfer function of the whole system is given by

$$H_{tsr}(f) = \frac{F_d(f)}{F_a(f)}$$

From the above equations it can be seen that the transfer function of the soil is given by

$$H_s(f) = \frac{H_{tsr}(f)}{H_t(f)\ H_r(f)}$$

The transducer monitoring experiments described in this section are thought to enable $H_t(f)$ and $H_r(f)$ to be ascertained; $H_s(f)$ can then be obtained. Most importantly, the monitoring techniques described allow the transducer transfer functions to be ascertained under any test condition. This is necessary as the transfer function will change depending on the type of sediment and its stress state.

A 'multimorph' (Vernitron trade name) is a highly-compliant piezo-electric ceramic bender that operates on a similar principle to the 'bimorph'; it is illustrated in Figure 3.5a. In the Mk I in-situ probe a 'multimorph' element was bonded to the surface of the transmitting bender elements whereas in one of the triaxial cell transmitters and in the porosity cell transmitter a 'multimorph' was used adjacent to the bender element. These monitoring configurations are depicted in Figures 3.5b and 3.5c respectively. With these arrangements, the actual motion of the transmitter element is monitored as an output signal from the 'multimorph'. The disadvantages of this system are that it assumes the multimorph is perfectly bonded to the bimorph and that the increased mass of the transmitter does not impede its shear motion characteristics.

Another technique for monitoring a piezo-electric transmitter has also been invented during this study. It is described as a self-monitoring technique because no other mechanically independent transducer is involved. This technique of cutting and wiring the transmitter element is shown in Figure 3.6. One of the surface electrodes has two shallow cuts (deep enough to penetrate the electrode surface) running along its surface in the

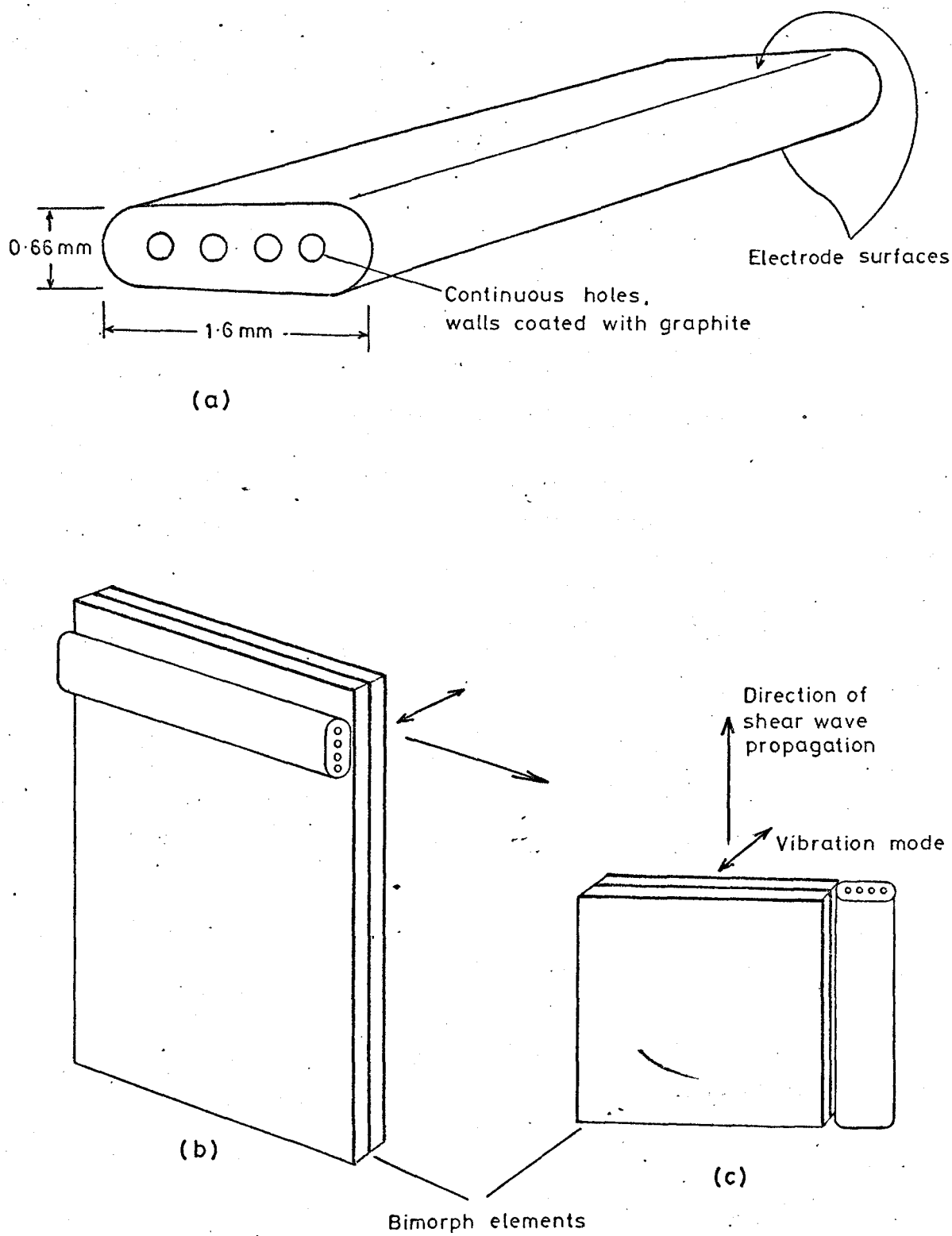

FIGURE 3.5 'Multimorph' bender element:

(a) construction,

(b) monitoring configuration as used in the in-situ probe Mk. I,

(c) as used in a triaxial cell and a porosity cell.

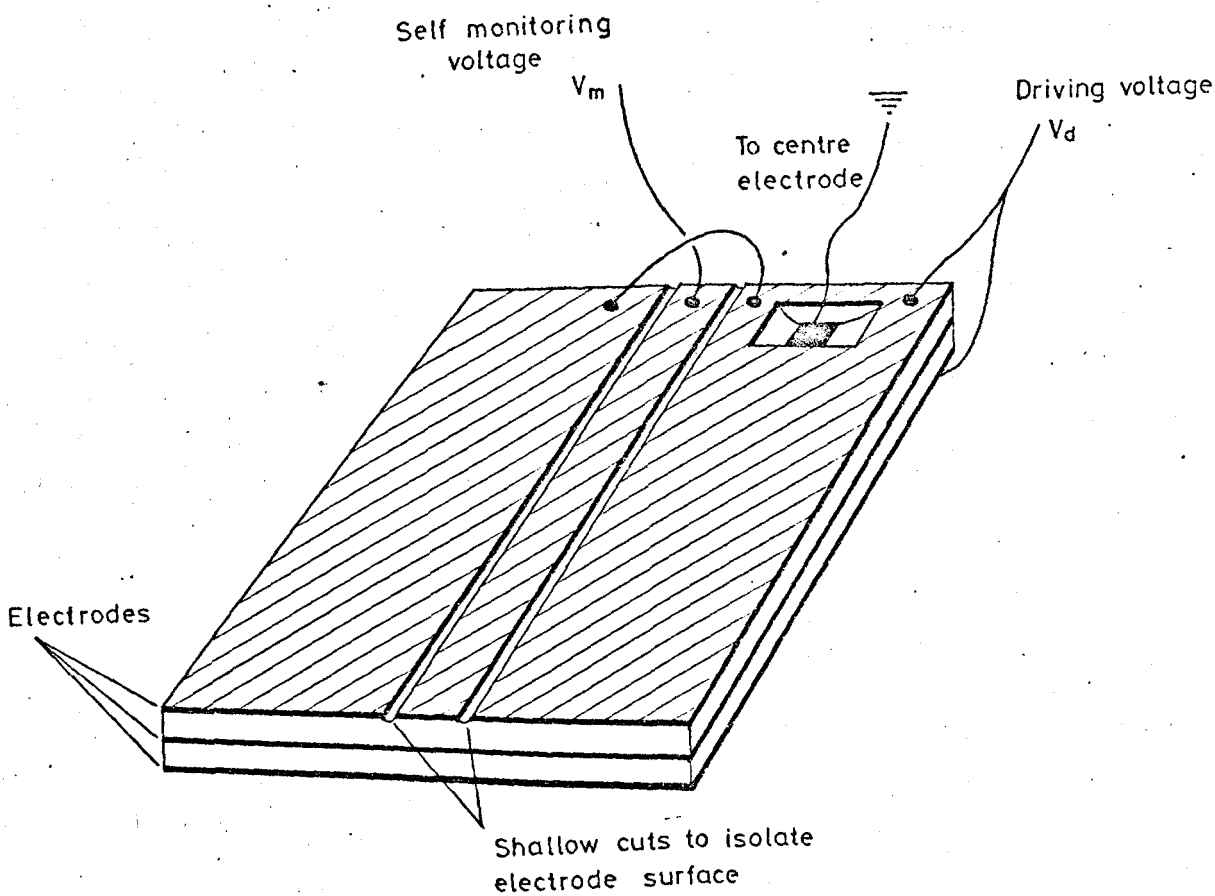

FIGURE 3.6 A parallel connected bender element with its electrodes cut and wired for a self monitoring mode of operation.

direction of shear wave propagation. With the outer two sections electrically connected this then leaves a small isolated centre section, the area of which is small in comparison with the total surface area. The electric field generated by the driving voltage (Vd) is, therefore, only slightly altered by the presence of the cuts. An electrical connection is applied to the centre electrode by cutting away part of one of the component plates revealing a small electrode area on which to solder. This delicate cutting operation and all others, including cutting the elements to size, was performed using a dentist's diamond-edged wheel in a lathe. The bender element is mounted on a horizontal table in a vertical slide; this allows freedom of movement in all three axes for the cutting operation.

When the element bends under the action of the driving voltage (Vd) another voltage is developed between the centre electrode and the thin strip electrode. This is in response to the actual movement of the element and is electrically independent of the driving voltage.

In some circumstances it may prove detrimental to have the inner electrode as the earth terminal. Normally, the outer electrodes would be earthed to improve the electrical shielding of the element. However, in most circumstances these connections can be switched depending on whether the element was being monitored or used as a transmitter with a receiver being monitored.

Figure 3.7 illustrates the use of the self-monitoring technique during the construction of an element for a triaxial endcap. A parallel bender element (18 x 18 x 0.5 mm) was cut and wired as shown in Figure 3.6. The response of this raw element (suspended in air) to a square wave driving signal is shown in Figure 3.7a. This lightly damped system, resonating at around 6kHz is different to the damped response of the raw element when buried in dry sand (Figure 3.7b). After the raw element had been encapsulated in epoxy resin (21 x 21 x 2.5 mm) the test was repeated. In air (Figure

Raw element, 18×18×0·5 mm.

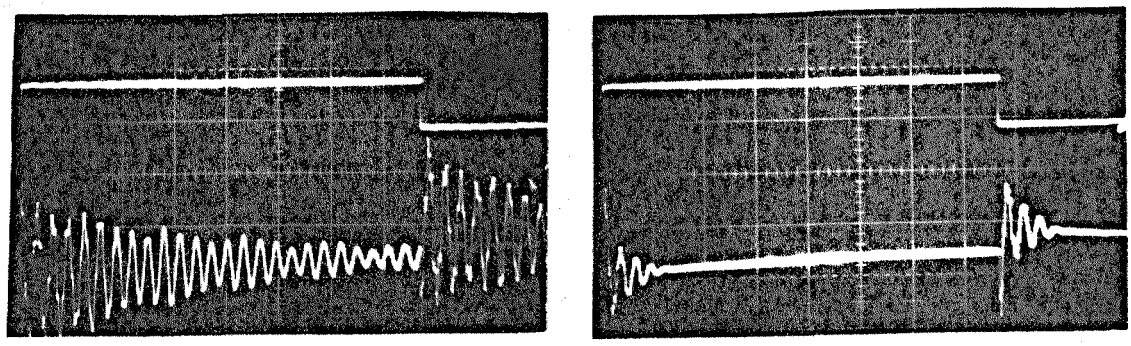

(a) In air

(b) In dry sand

Vertical scale : upper traces 5 V/div., lower traces 0·5 V/div.

Encapsulated element, 21×21×2·5 mm.

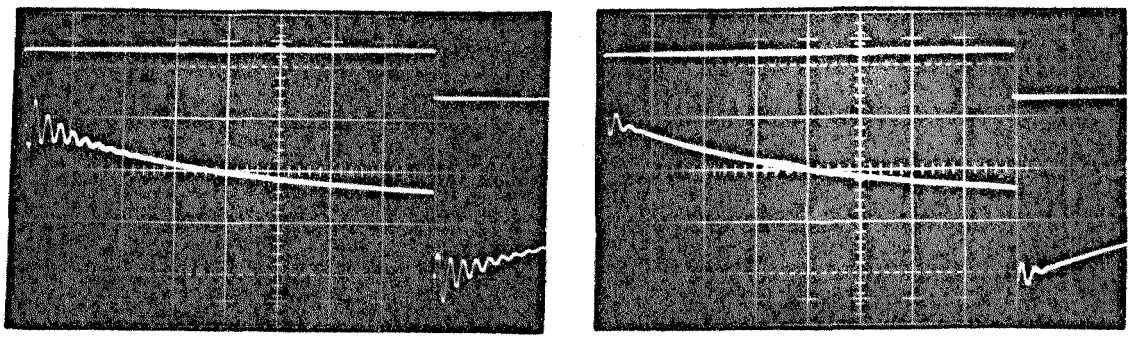

(c) In air.

(d) In dry sand.

Vertical scale : upper traces 5 V/div., lower traces 0·2 V/div.

Horizontal scale : 0·5 m.sec/div.

FIGURE 3.7 Self monitoring of a parallel bender element.

The upper traces show the square wave driving signal. The lower traces show the different responses of the element to the driving signal.

3.7c) the signal is well damped, with a higher resonant frequency 9 kHz, but it is still further damped when buried in sand (Figure 3.7d).

These self-monitoring techniques have been conceived and partially tested but not extensively used. It does appear, however, that the monitoring signal can be successfully used as the output signal in correlation studies. It can also be used as an indirect measure of sediment characteristics by observing the different damping behaviours in different sediments (see Chapter 3.3.3).

As a final point, it is interesting to note that the self-monitoring technique should work equally well on any piezo-electric element. In this way, it may prove to have an application in the compressional wave characterisation of sediments. These self-monitoring techniques have been shown to enable wave shaping to be performed using an electrical feedback system (Jackson, 1981) the signal from the monitoring transducer is compared to a reference signal and the driving voltage adjusted accordingly. In this way the shape of the received waveform can be improved for identification purposes and attenuation measurements.

3.2 Incorporating Transducers in Laboratory Test Cells

3.2.1 Introduction

Sediment characteristics which control the propagation of shear waves are probably to a greater or lesser extent responsible for the shear strength as measured by soils engineers. Therefore, the routine inclusion of shear wave velocity measurement into the suite of geophysical parameters used to characterise sediments is thought to be an important step forward. It is, however, no use determining the geophysical properties of sediments on their own and expecting them to be of any use at all to the practising

soils engineer. In the process of forwardingthe use of geophysical measurements to help predict and understand the engineering behaviour of soils under load, comparative studies of geophysical and standard engineering parameters must be undertaken. Using this philosophy, it has seemed appropriate to develop laboratory systems where both sets of parameters can be measured simultaneously. Two pieces of test apparatus are frequently used by soils engineers: the oedometer, which measures consolidation characteristics, and the triaxial cell which can measure the strength characteristics under a wide variety of test conditions. These, therefore, were the test cells chosen for the inclusion of P and S-wave transducers.

Apart from the need to understand the inter-relationships between mechanical and elastic wave properties for different sediments there is a lack of data and knowledge at the present time on the variation of elastic wave properties (especially shear wave velocities) for sediments with different geotechnical parameters. Although large differences in engineering and acoustic characteristics occur across the whole range of marine sediments, variations of structure in sand-sized sediments are smaller but still exhibit a wide range of geotechnical characteristics, primarily through porosity but also through grain size (2.0 - 0.063 mm), size distribution, grain shapes and bulk density. An understanding the the empirical correlations that exist between physical properties and stress wave propagation characteristics is important to both the engineer and geophysicist in his acquisition of geotechnical information from seismo-acoustic records. Very little reliable shear wave data was previously available to enable predictive correlations to be established or understood. It was one of the purposes of this study to produce data enabling the effects of some geotechnical parameters on the velocity of shear waves to be quantified. To do this, a range of different sands has been tested in a small vibration tank and a specially

designed 'porosity cell'.

3.2.2 ARL Vibration Tank

Small, sandwiched, ceramic, bender transducers (developed by Shirley and Anderson [1975b]) capable of transmitting and receiving shear waves in sediments with low shear moduli, were described in the previous section. This development was intended to enable shear wave measurements to be recorded *in situ*, in a manner similar to that used for compressional waves during coring. Continuous measurements of compressional wave velocity and attenuation at a fixed frequency can be made during a gravity coring operation using the profilometer developed at the Applied Research Laboratories (ARL), Austin, Texas, (Shirley and Anderson, 1975c; Anderson *et al.*, 1974; Shirley *et al.*, 1973). Two piezo-electric acoustic transducers, mounted in the cutting head, with an electronic package mounted at the top of the core barrel, measure travel times and amplitudes of pulses propagating across the diameter of the core. A profile of velocity and attenuation with depth is provided as the corer penetrates the sediment. A similar profile of shear wave parameters would greatly improve the sediment analysis if it could be obtained. The small size of the transducers is an essential component in the development, as they have to be incorporated into the cutting head of the corer. Shirley *et al.* (1979) describe a composite profilometer shear and compressional wave transducer for this purpose. However, Shirley *et al.* (1980) report that the signal to noise ratio prevented this design from functioning. A large amount of noise is generated while the corer was penetrating the sediments. Another design which uses bender elements on probes which extend in front of the cutter head were tested. Despite some unexplained phenomena some tentative shear wave data (40-100 $msec^{-1}$ in sandy mud) was

recorded before the transducers (which are particularly vulnerable) were damaged.

During the earlier stages of this development (1976) the writer had the opportunity to test the stacked piezo-electric ceramic bender array (Figure 3.4) in a vibration tank. The tank consisted of an aluminium alloy container (15.2 x 30.5 x 15.2 cm) with two compressional wave transducers mounted through the sides. A schematic representation of the tank arrangement is shown in Figure 3.8. Distances between compressional wave projector and receiver transducers were varied by moving the cylindrical aluminium transducer housings through the wall of the tank, a seal being provided by the O-rings as shown.

A variable amplitude, electromagnetic, vibrating motor was securely G-clamped to the tank so that the packing condition of the sands could be controlled.

Triple-layered, sandwiched bimorph elements described earlier were used for producing and receiving shear waves in the tank. Practical difficulties, in the use of these transducers, are substantially greater than with their compressional counterparts and need to be briefly discussed. When these shear elements were mounted in the walls of the aluminium tank (as was originally the case) in a manner similar to that used with the compressional transducers, a clearly defined shear wave was difficult to obtain. Ceramic bimorph elements, because of the nature of their oscillations, transmit compressional waves normal to the direction of shear wave propagation. When the elements were mounted in the sides of the tank, these compressional waves travelled around the tank through its walls, and were received in a reciprocal manner by the receiving transducer together with the direct shear wave of interest. Although the geometry of the system can ensure that the compressional wave path length is substantially greater than the shear

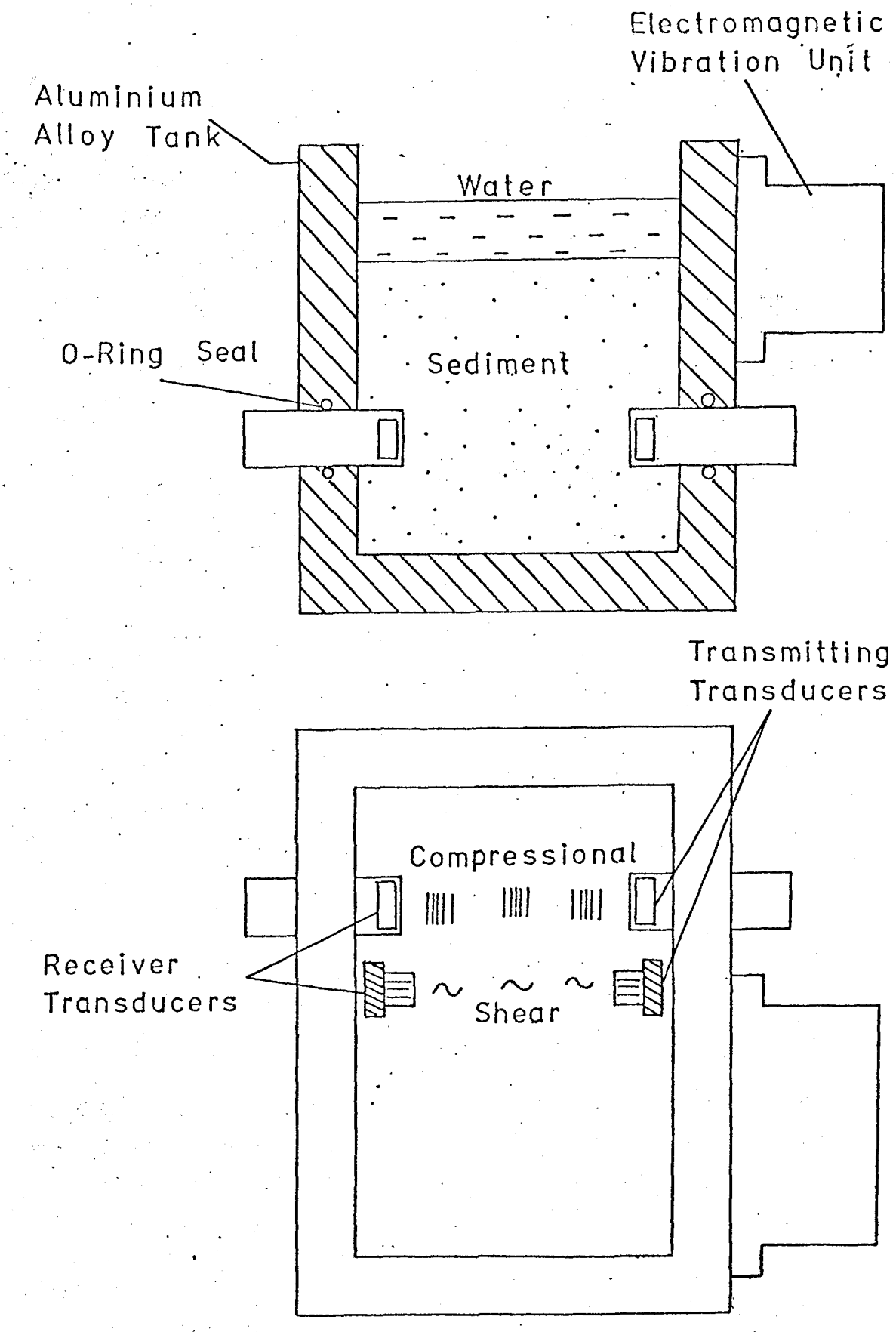

FIGURE 3.8 Schematic diagram of the ARL wave measuring tank

wave path, the low attenuation, multiple paths and greater velocities of the compressional waves make it almost inevitable that they not only interfere with the shear wave but can totally mask it. To overcome this problem, elements mounted in probes were used (Figure 3.9a) and in this way direct contact between the transducer and tank was eliminated. A framework controlling the alignment and distance between the transducers, however, had a similar effect to the tank; waves passing through the frame tended to obscure the shear wave. Total isolation was achieved by utilising an accurately machined slotted spacer, made in two identical halves, in which the probes were secured (Figure 3.9b). In this way the probes could be set in the sediment at equal depths and correctly aligned with each other without fear of disturbance even during vibration. While acoustic measurements on the wave form were being made the slotted spacers were removed leaving the probes standing free in the sediment. Using this technique suitable filtering ensured that a shear wave with a good signal to noise ratio was obtained (see Figure 4.7).

It should be noted that the shear wave transducers were mounted in the probes so that when they were inserted vertically into the sediment the vibration direction of the shear wave was also vertical. It is feasible that vertically oscillating shear waves (SV waves) will have different propagation characteristics from horizontally oscillating shear waves (SH waves). It is suggested that this may be particularly relevant in natural sediments, where a combination of grain shape factors and type of sedimentary deposition often produce a transversely anisotropic structure. In the laboratory, using artificial sands of high sphericity, such an

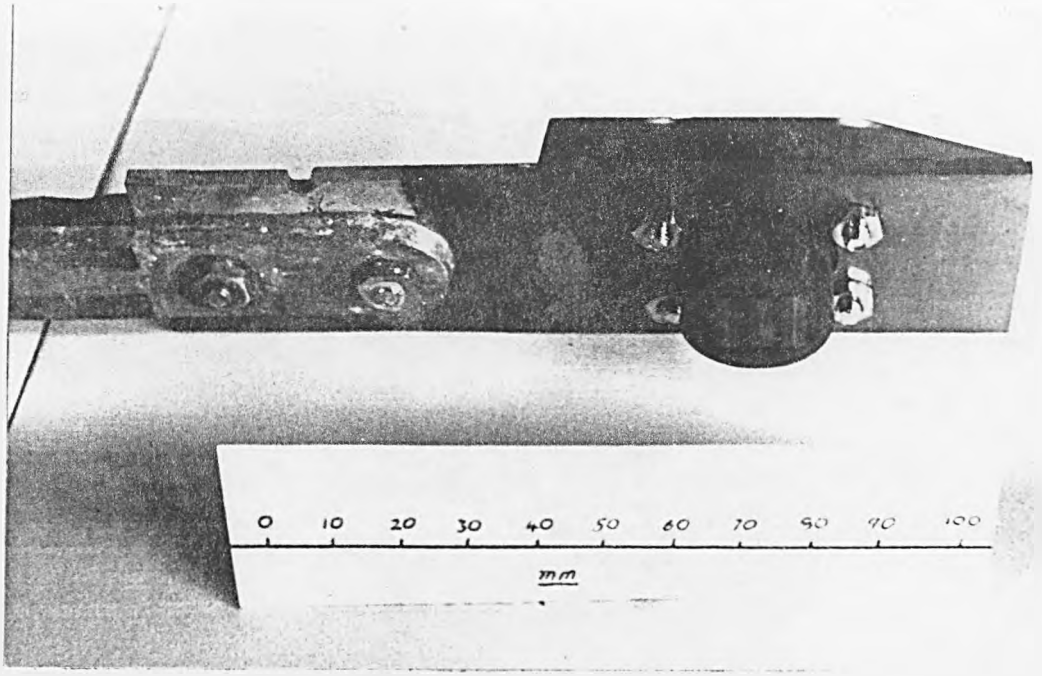

FIGURE 3.9a SANDWICHED CERAMIC BIMORPH TRANSDUCER MOUNTED IN THE END OF A SHEAR WAVE PROBE

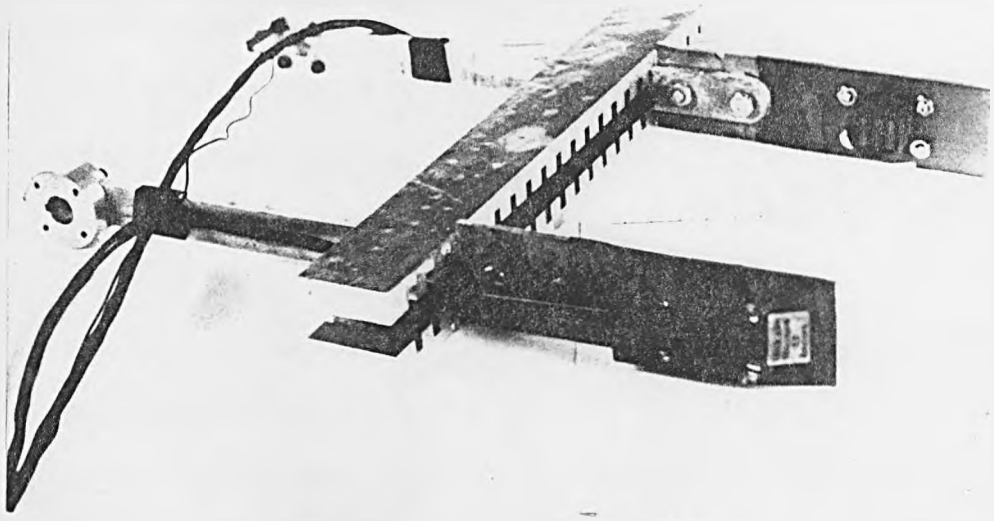

FIGURE 3.9b SHEAR WAVE PROBES SEPARATED BY THE SLOTTED SPACERS, the spacers were removed during measurements to reduce noise.

anisotropic structure is less likely to exist.

Figure 3.10 shows the system block diagram of the electronic equipment used to generate and receive both shear and compressional waves. Pulses from the projector transducer were generated in the following manner. A variable frequency oscillator (General Radio, type 1310-A) generated a continuous sine wave which was monitored by the digital Itron counter-timer (Model 650-9/R). The pulse timing generator (Scientific Atlanta Inc., series 1118B) produced a voltage pulse with a variable length and repetition rate which was fed, together with the continuous sine wave, into the transmitter signal gate (Scientific Atlanta Inc., series 1111). Opening and closing of the signal gate was controlled by the pulse timing generator so that a pulsed sine wave was generated at the gate output. This pulsed sine wave was amplified using a 3-watt pre-amp (General Radio, type 1203-B) and a wide band 10-watt power amplifier (Krohn-Hite, model DCA-10R). The projector transducer transforms this driving voltage pulse into a pulse of compressional or shear wave energy (depending on the transducer type) and at a frequency, pulse length and repetition rate set by the oscillator and pulse timing generator.

A signal was received by a similar transducer after the pulse had traversed the sediment between the two transducers. This signal is transformed from a mechanical stress to an analog electrical signal by the reciprocal action of the piezo-electric ceramic receiver. The time taken for the pulse to traverse the sediment depends on the characteristic speed of propagation for the type of wave in the particular sediment as well as the separation between the two transducers. Received signal level will be less than the input level because of several factors, predominantly those of acoustic impedance mismatching between the transducers and the sediment, spreading losses and attenuation. The signal was

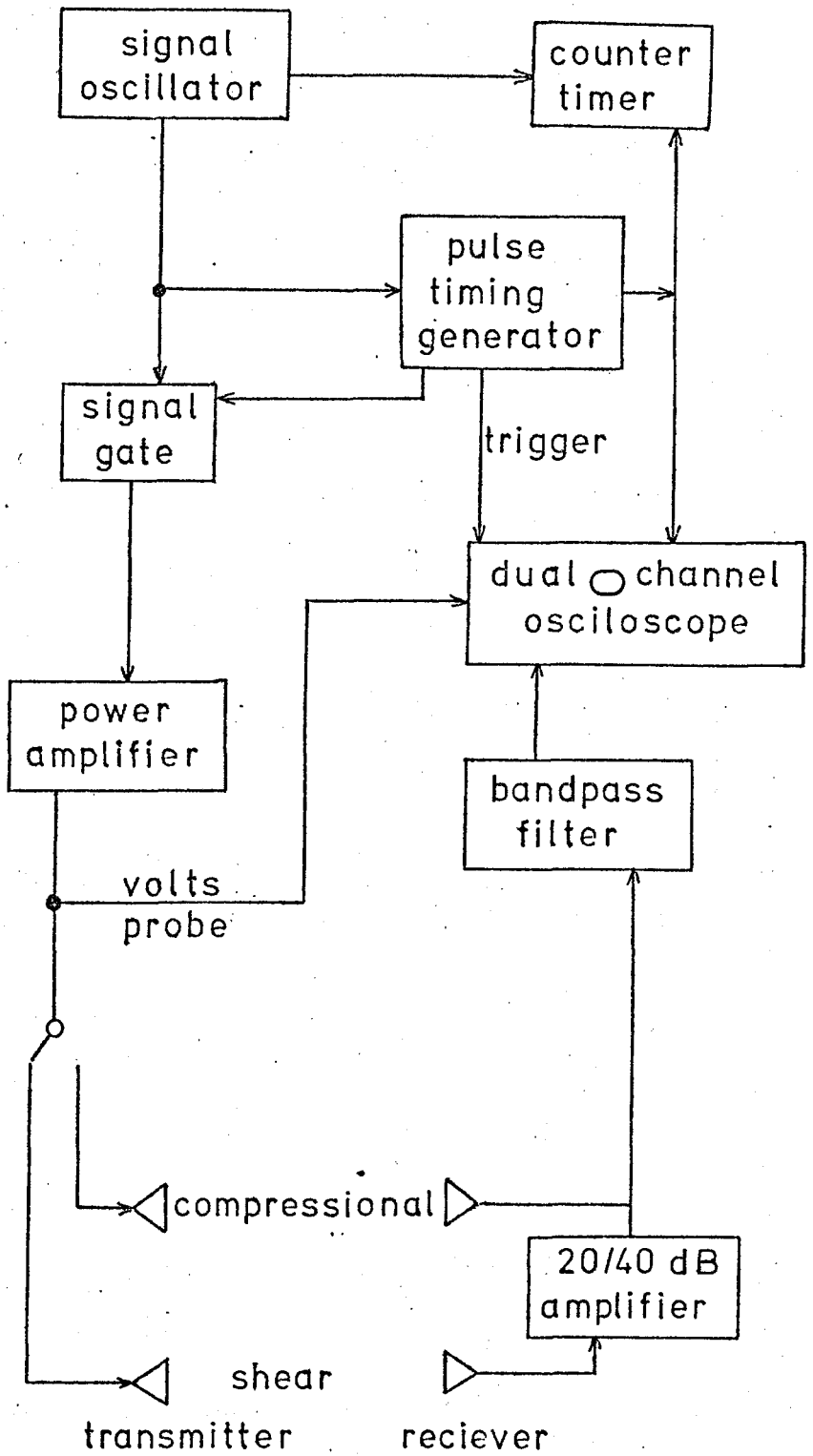

FIGURE 3.10 Electronic System block diagram for the compressional and shear wave measurements in the ARL tank

amplified using a 20/40 dB amplifier before it was "band-pass" filtered (Krohn-Hite, model 3100R). In the case of the shear wave measurements another 20/40 dB amplifier was incorporated after the filter, for use when the signal level was still very low. A dual channel oscilloscope (Tektronix type RM561A) monitored the resultant signal and allowed quantitative measurements to be made on the pulse.

Attenuation calculations were made from voltage readings taken directly from the oscilloscope, correcting for any previous amplification. Velocities of the waves through the sediments were made by measuring the time interval between transmitted and received pulses over known distances. Although these time intervals could be measured directly from the oscilloscope time base with its sweep triggered by the pulse timing generator, a more accurate technique was employed using the two channels. A variable length square pulse (produced by the pulse timing generator which started simultaneously with the start of the sinewave transit pulse through the sediment) was fed directly to the second channel of the oscilloscope. By using the near-vertical edge of this pulse as a cursor, it could be superimposed on an easily identifiable feature of the received waveform by adjusting the length of the square pulse. The period of this square pulse is the required transit time and was measured by the Itron counter/timer to an accuracy of 0.25 μs.

3.2.3 Jackson's porosity cell

Jackson (1975) built a laboratory porosity/resistivity cell in which sand samples could be deposited with a very loose packing structure (high porosity) and then compacted in known stages into a very dense packing state (low porosity) using vibration. The purpose of these experiments was to investigate the variation in formation factor (FF = resistivity of

sediments/resistivity of pore water) with changes in porosity, such that sea-bed porosities could be ascertained from in-situ resistivity measurements.

With the development of in-situ probes designed to measure P and S-wave velocities and electrical resistivity (Chapter 3.3) it seemed appropriate to extend the capability of Jackson's porosity cell to include both P and S-wave transducers as well as the resisitivity electrodes. This capability not only provides the opportunity of ascertaining in-situ conditions but allows a large range of relationships between sand structure parameters and geophysical parameters to be investigated. Previous experiments performed by the writer using the ARL vibration tank had shown that shear wave velocities changed by a factor of approximately two over the whole range of porosities for any given sample. These data have also shown some tentative correlations with grain size distributions and grain shape which needed clarification in a cell which provided better control over the packing state.

Horn (1980) using a cell based on Jackson's original design has made shear and compressional measurements in two saturated sands at varying porosities. The shear wave transducers were similar to those described and used by the author at ARL which were built by D. Shirley and based on a design that was intended to be used with only the front radiating face in contact with the sediments (Shirley and Bell, 1978). This type of transducer, in the author's experience, has proved satisfactory for laboratory measurements provided that they were completely decoupled from the sediment container. In Horn's experiments the same decoupling problem is indicated and the problem was not overcome. However, by decreasing the transducer face separation to 20.25 mm, an acceptable signal to noise ratio was obtained. The major noise results from vibrations travelling through

the cell walls.

Three major factors were particularly undesirable with Horn's experiments:

(a) The measurement of P and S-wave velocities were not made simultaneously.

(b) A transducer separation of only 20.25 mm was used in a 100-mm cell. This is likely to produce porosity irregularities especially in the travel path (only 10 or 15-grain diameter in a coarse sand) which may explain the narrow range of velocities reported.

(c) A standard laboratory sieve shaker was used which imparts violent shocks to the system, causing sand structures to alter dramatically, especially at the higher porosities.

To overcome the undesirable features described above, simultaneous measurements of P and S-wave velocity across the whole width of the cell using specially-designed transducer mountings was envisaged. These measurements, together with formation factor, would be obtained during the sand compaction on a variable amplitude vibration table which would enable the compaction rate to be accurately controlled.

This part of the project was undertaken as a collaborative effort with P. Jackson at IGS. A schematic illustration of the modified cell is shown in Figure 3.11. The perspex cell has been adapted to accommodate two perspex transducer housings which are situated either side of the sample chamber and are free to move into the cell for calibration purposes. P and S-wave transducers are mounted in the ends of the housings with constructions similar to that used in the triaxial cell (see Figure 3.16). The shear wave transducers protrude 8 mm into the sample and the parallel connected transmitter has a multimorph element mounted adjacently for monitoring purposes. 250-kHz crystals backed by silicon carbide loaded

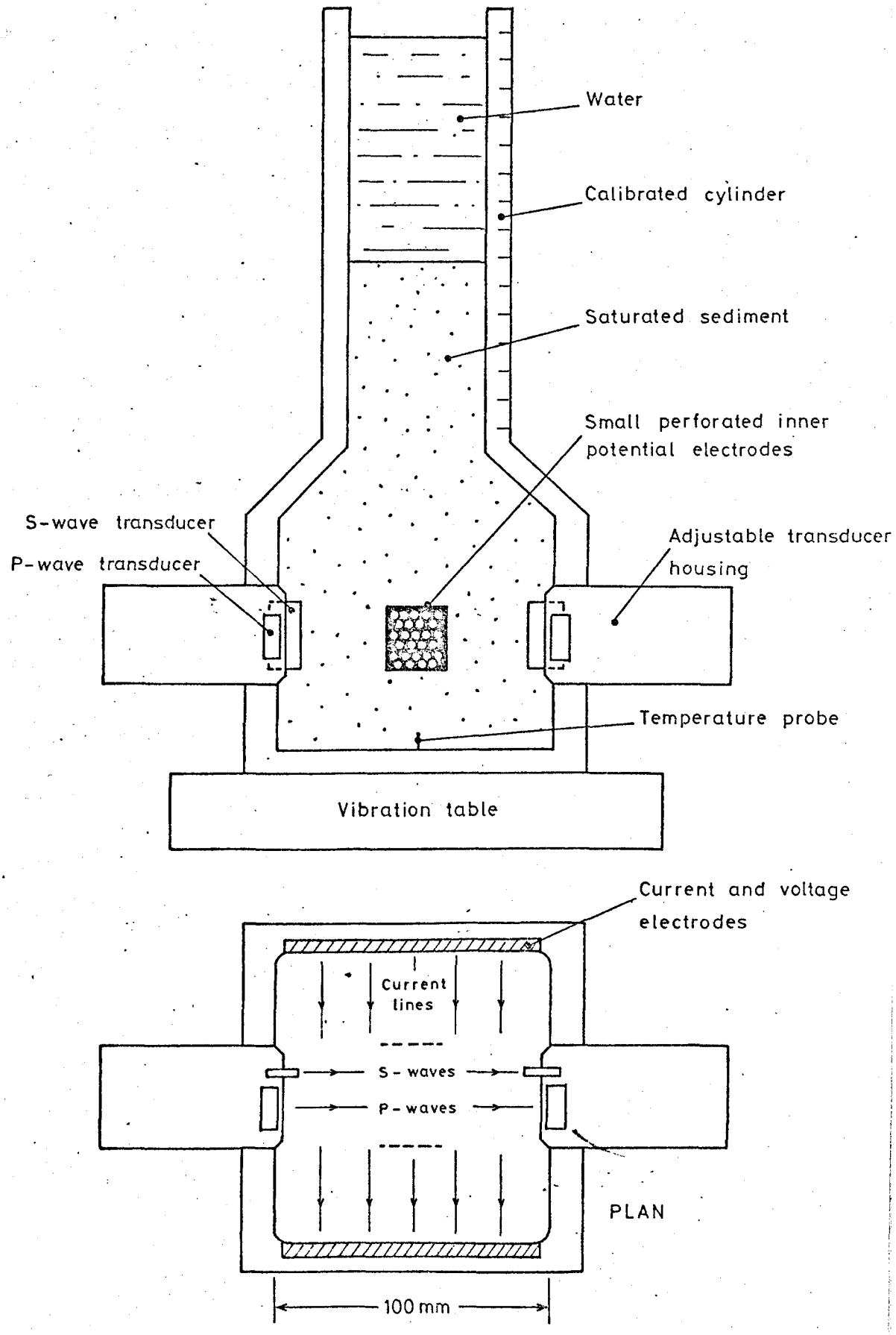

FIGURE 3.11 Schematic illustration of the modified porosity cell incorporating resistivity electrodes and P and S wave transducers.

epoxy resin were used for the P-wave transducers. A pair of small perforated potential electrodes had previously been mounted in the centre of the cell and these were monitored throughout the experiments together with the large electrodes to investigate possible inhomogeneities within the sediment structure. The electronic measuring system used was very similar to that depicted by Figure 3.19 and used in the large triaxial cell. A variable amplitude electromagnetic laboratory sieve shaker was used for the vibration table. This machine produces vertical, 50-Hz variable-amplitude oscillations with a maximum amplitude of 3 mm (with a 2.5 kg loading). There is also a facility for intermittent vibration sequences with variable duration. These controls allow the sand structure to be compacted at a very controlled rate. When the sand is loose only very low amplitude vibrations are necessary to reduce the porosity. Progressively lower porosities require increasing vibration amplitudes for further compaction. For maximum compaction, however, it has been found that it is necessary to slowly decrease the vibration amplitude to its minimum level. It has also been found that the vibration sequence has a significant effect on the shear wave velocity; this is discussed later in the light of the results obtained.

3.2.4 Oedometer

In a standard oedometer test, stress is applied to a soil specimen along its vertical axis, while strain is prevented in the horizontal directions by a sample ring (confined compression). Free drainage is permitted through one or both of the porous stones at top and bottom of the sample. Sample sizes may vary but, because of the problems associated with side friction, the thickness:diameter ratio must be minimized, usually 1:3 or 4. With sample thickness typically around 20 mm there is

little room for transducers.

The oedometer cell modified for these experiments was of the fixed-ring type holding a sample 75 mm in diameter and 19.1 mm thick. P and S-wave (compressional and shear) transducers were mounted in the porous stones as shown in Figure 3.12. The compressional wave elements are 20-mm diameter, 1-MHz elements set in epoxy resin with a quarter wavelength facing which is flush with the surface of the porous disc. Shear waves are transmitted and received using 10 x 5 x 0.5 mm bender elements which are cantilever mounted to one side of the P-wave elements. They are mounted in a slot cut in the porous stone by epoxy resin and protrude 2 mm into the sample. In the first cell to be modified, the bender element was coated in a thin layer of epoxy resin to insulate it from the sample. However, after some use, both the insulation and the element began to deteriorate physically. After testing the effects of increased epoxy resin coatings the elements were cast in resin 2.5 mm thick before being mounted as previously; this provides for a much more rugged system. Despite a decrease in signal strength for the same applied voltages, the received signal onset retained its clarity.

Figure 3.13 shows the electronic block diagram used in conjunction with the modified oedometer cell. A tone burst, tuned to the resonant frequency (1 MHz) of the crystals, was used to drive the P-wave crystal. The received signal was displayed on an oscilloscope with a delayed time base which, together with a counter timer, allowed timing measurement to be made to an accuracy of 0.05 microsecs. Time errors caused by delays were eliminated by calibrating the system using accurately-machined spacers in distilled water within the specimen cell. Shear wave signals were timed in a similar manner except the 2.5 d.c. step of a square wave was used as the transmitter excitation voltage. This has consistently been

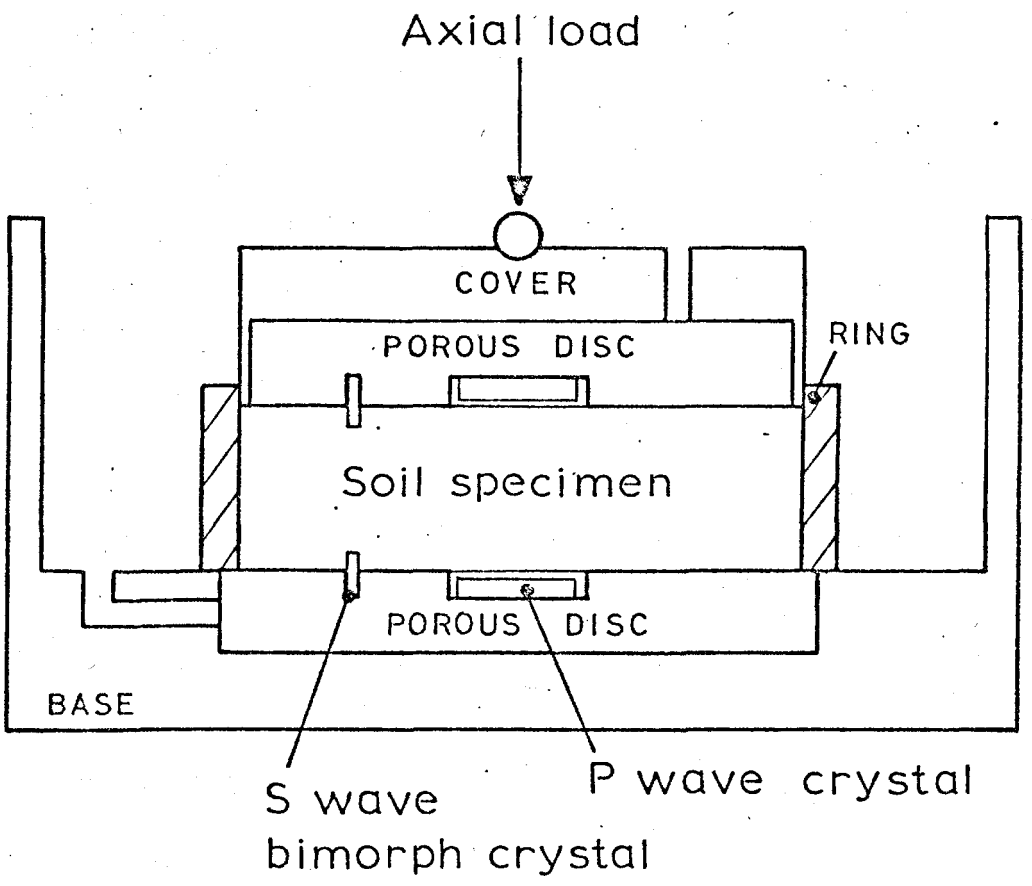

FIGURE 3.12 Standard fixed ring oedometer cell with P and S wave transducers mounted in the porous discs.

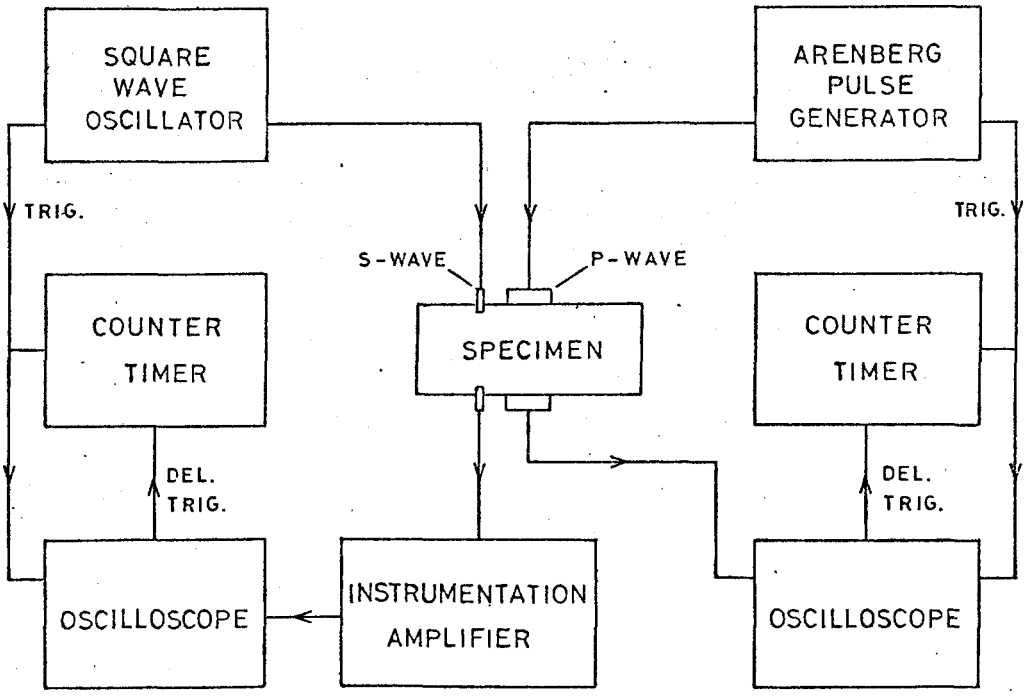

FIGURE 3.13 Block diagram of the electronics used with the modified oedometer cell.

shown to produce a sharper onset on the received signal than other driving voltage wave forms.

Calibration of S-wave transducers is substantially more difficult than for P-waves because of the lack of a suitable reference material with a known shear wave velocity. Two calibration requirements were needed: (a) ascertain the effective distance between the transducers and (b) ascertain that the received signal was a shear wave propagating through the sample being tested. For this calibration a sample of potters clay was moulded into a 250-mm-long block and left to stabilize overnight. The porous stones with S-wave transducers were then clamped to each end of the clay sample and the S-wave time interval recorded. This was performed at distance intervals on a progressively shorter sample. Finally, the sample was enclosed by the oedometer ring and placed in the cell. No significant change in the signature of the signal occurred during the procedure so it was concluded that the sample geometry precluded any interference from wave travelling in the apparatus. The intercept from a distance/time plot of this experiment ascertained that the transducer separation should be taken as the shortest distance between them (i.e. the distance between the front edges).

The short path length across the sample is the major cause of inaccuracies in the velocity measurements. For the P waves an accuracy of ± 10 m/s or ± 0.5% is obtainable whereas for the S waves a less precise onset of the wave form is the limiting factor and only a ± 5% accuracy is possible. Both these accuracies are much less than the overall changes observed during a standard test.

Sample thickness measurements were made using a dial gauge accurate to 2×10^{-3} mm. During the preconsolidation and cyclic relaxation test performed on the silt sample (described in Chapter 5) a linear variable

differential transformer (LVDT) position transducer was fitted to the oedometer. This was calibrated in a vernier jig and allowed changes in sample thickness of 5×10^{-5} mm to be detected.

3.2.5 Small triaxial cell

In a triaxial cell a soil specimen surrounded by a flexible rubber membrane is subjected to a hydraulic confining pressure as well as a vertical uniaxial stress. Using this type of cell, soils can be tested under a wide range of stress and drainage conditions. It is, therefore, particularly appropriate that P and S-wave transducers, which measure small strain, stress wave velocities, should be included in this type of apparatus which is so widely used to measure the large stress-strain characteristics of soils.

A standard triaxial cell, with a 38.1mm sample base, was modified to take a 50.8mm diameter sample, 101.6mm in height, with P and S-wave transducers mounted in the top and bottom caps. Both caps were machined from perspex, the bottom cap acted as an adapter to fit over the base pedestal as well as being the transducer housing. The top cap was a standard shape but with provisions for the transducers. Each end cap contains a centrally-mounted compressional wave element (10-mm diameter, 250 kHz) and two shear wave bender elements (15 x 15 x 9.5 mm) mounted at each side with 10 mm protruding into the sample. The constructional details of the transducer mountings are similar to those used in the 100 mm triaxial cell and are shown in Figure 3.16. Figure 3.14 shows a small triaxial cell with the modified transducer adapter/mountings installed.

Four shear wave transducers were incorporated into the first design in order that multiple travel paths might be established. However, in practice, the short path between the two transducers in one end cap meant

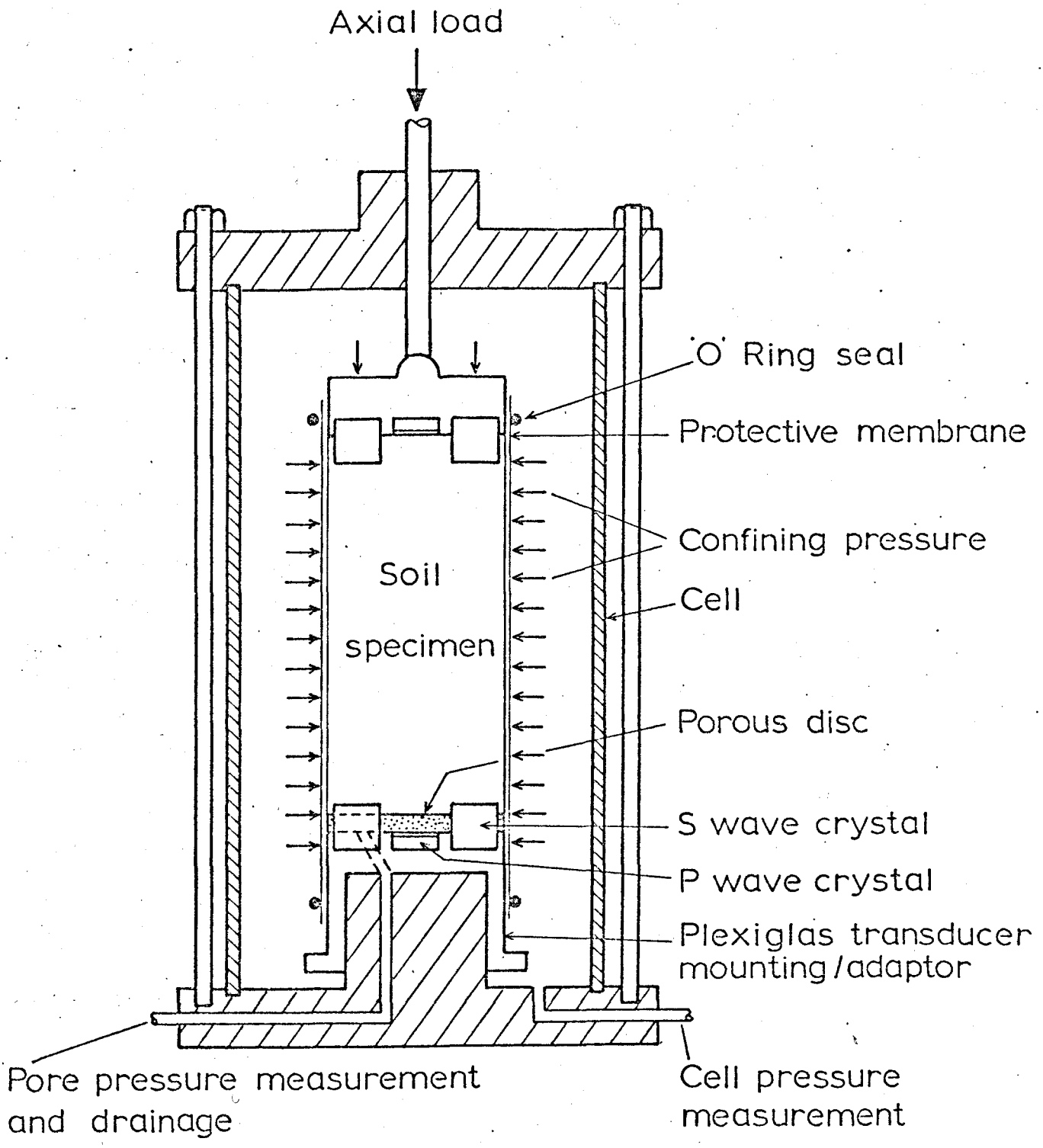

FIGURE 3.14 Standard two-inch triaxial cell with modified end caps incorporating P and S wave transducers.

that there was too much compressional wave interference from signals, both through the end cap and the sediment, for the shear wave to be recognised. Also, the difference in length between a diagonal and a normal path along the length of the sample was too small to be useful in helping either with velocity or attenuation measurements. Multiple reflection arrivals on a single receiver were sometimes extremely evident and clearly corresponded to three and five times the normal one-way travel path. Although these multiples have not been investigated further in this study, it is conceivable that the decay of these multiples may possibly be used to obtain attenuation data during testing.

As with the oedometer, the first set of shear wave transducers installed were coated with only a thin layer of epoxy resin for insulation purposes. This proved extremely susceptible to leaks and damage. Consequently, the effects of totally encapsulating the shear wave elements in a mould of epoxy resin was investigated. A mould 6-mm thick was formed around the elements used in the triaxial cell and then filled with resin. After the mould was removed leaving the shear wave elements totally encapsulated. The thickness of the encapsulant was machined away in incremental steps until only 1.75 mm remained. At each stage the performance of the system was tested in dry sand. A flat bed of sand was prepared into which the transducers were placed with a 50-mm separation. A container of sand was then slowly sprinkled over the transducers to bury the system completely. This procedure provided consistent values of shear wave velocity. In this way the signal quality and amplitude were monitored. It was found that the 6-mm thick encapsulation changed the resonant frequency of the system from 1.7 kHz without encapsulation to 4 kHz. This also reduced the received signal by 23 dB. As the thickness of the encapsulant was machined away the resonant frequency decreased and the

received signal amplitude increased until at 1.75 mm thick a resonant frequency of 2 kHz with only a 5 dB loss in signal was obtained.

Signal quality remained consistently high throughout the experiment. It is essential with the shear wave pulse technique, where only one receiver is used, to have as clear an onset as possible. Unfortunately, the frequencies used have to be relatively low because of the high attenuation characteristics which result in slow rise times. It was found in these measurements, as with nearly all the shear wave transducers tested, that a 10v d.c. step used as the driving voltage results in a clearer onset of the received signal than using a tuned 10v single cycle sine wave. This is illustrated in Figure 3.15.

3.2.6 Large triaxial cell

In 1979/80 a collaborative effort, involving P. Jackson and R. Baria from the engineering geology unit at IGS and the writer, was undertaken to design, manufacture and test specialised geophysical end caps for a large (100 mm diameter) triaxial cell. These end caps were to include transducers with the capability of simultaneously measuring P and S-wave velocities (and possibly attenuation) and electrical resistivity during a wide range of test conditions. P. Strachan at the University of Newcastle who is interested in the correlation of mechanical and geophysical properties of sediments subjected to cyclic loading, provided the impetus and the testing facilities. The writer's prime responsibility within the project was for the installation of the shear wave transducers and their associated measurements, hence, only this aspect of the project will be described in detail here, a comprehensive paper by all the participants will appear elsewhere.

Much of the development work and testing of transducer designs suitable for the above application had already been carried out for the small triaxial

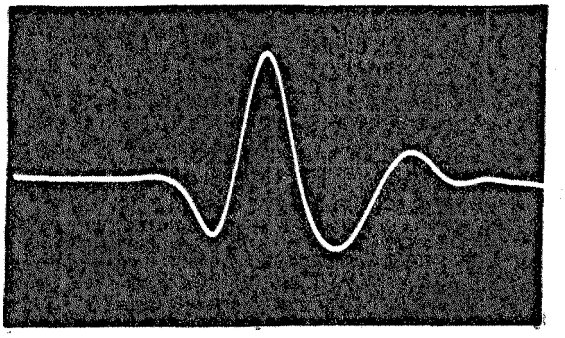

(a)

Horizontal scale 0·2 ms/div.

Transducer seperation 50 mm.

Shear wave velocity 90 m/s.

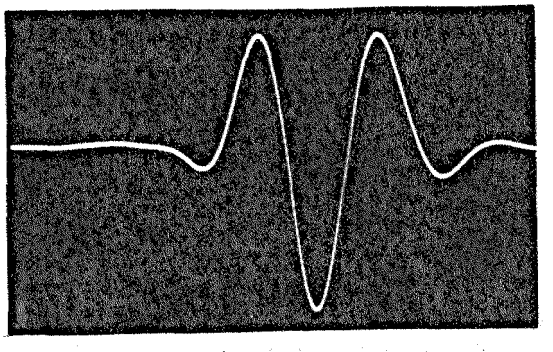

(b)

FIGURE 3.15 Received shear wave signals through dry sand using the small triaxial end caps.

(a) dc step driving voltage.

(b) Tuned single cycle sine wave driving voltage.

cell. A travel path of 200 mm as opposed to 100 mm in the small cell was the only major difference. Tests using the small triaxial transducers in a tank of sand suggested that the distance should be no problem. Consequently, the design was similar to that used in the modified small triaxial cell end caps (i.e. bender elements, cantilever mounted and encapsulated in resin). The first end cap to be made was machined as a perspex mounting/adapter which fitted onto the normal end caps. Subsequent versions were made as specially designed end caps. The constructional details of the shear wave transducer is shown in Figure 3.16 along with the details of the P-wave transducer and the resistivity electrodes. An 18 x 18 x 0.5 mm bender element has been cantilever mounted in the base. A parallel connected element, with a 'multimorph' mounted adjacently for monitoring purposes,as depicted in Figure 3.5c, was used as the transmitter and a similar sized series connected element was used as the receiver. These elements were first encapsulated in epoxy resin 2.5 mm thick before being mounted in slots cut in the end caps. The overall layout of the geophysical transducers within the end caps is shown in Figure 3.17 and their installation into the large triaxial cell is depicted in Figure 3.18. In the large cell, which was used for cyclic loading, an internal load cell was used in place of the external proving ring. This technique allows continuous monitoring as well as overcoming the problem associated with loading ram friction. A system block diagram is shown in Figure 3.19 for the complete system. Shear wave signals were recorded on a Racal tape recorder and subsequently displayed on a Medelec recording oscilloscope, a Datalab transient recorder and a Hewlett Packard mini computer. All three systems were controlled using a 40-Hz master frequency with delay triggers in order to prevent interference.

Data from tests using this equipment is presented and discussed in Chapter 7.

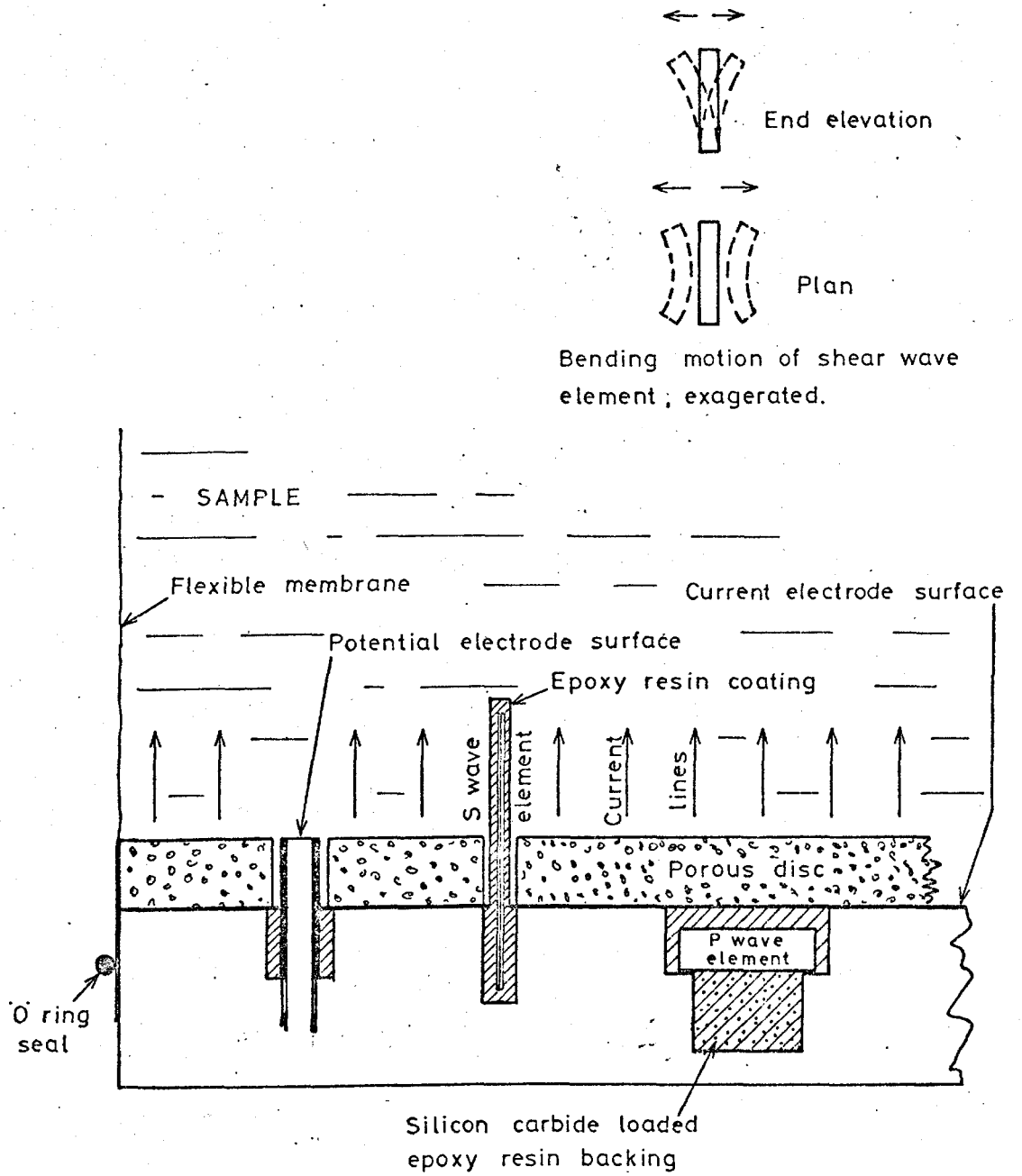

FIGURE 3.16 Schematic illustration of the constructional details used in the triaxial end caps.

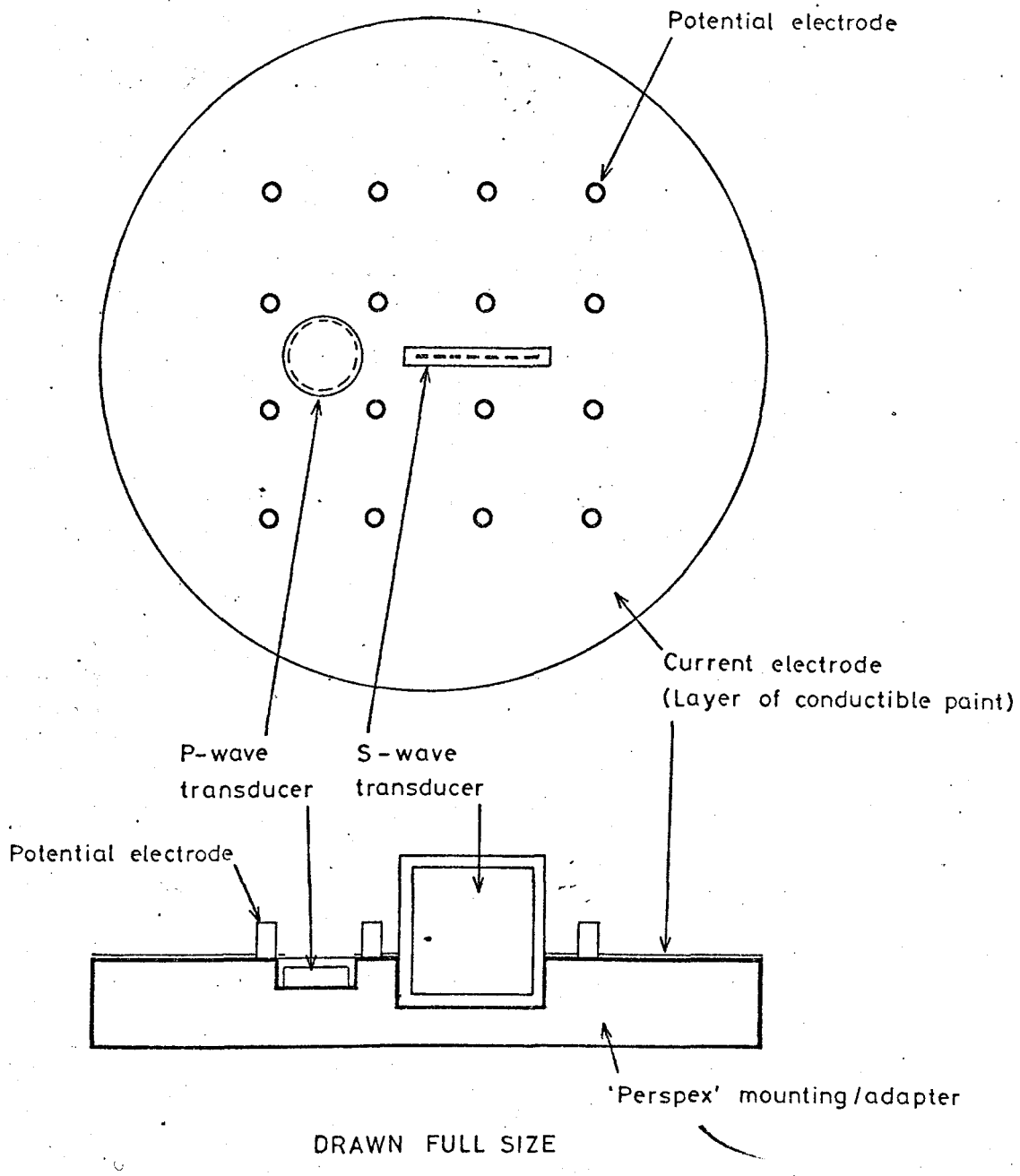

FIGURE 3.17

TRIAXIAL END CAPS INCORPORATING GEOPHYSICAL TRANSDUCERS.

P-wave and S-wave transducers together with resistivity electrodes simultaneously measure V_p, V_s and FF through the sample during testing.

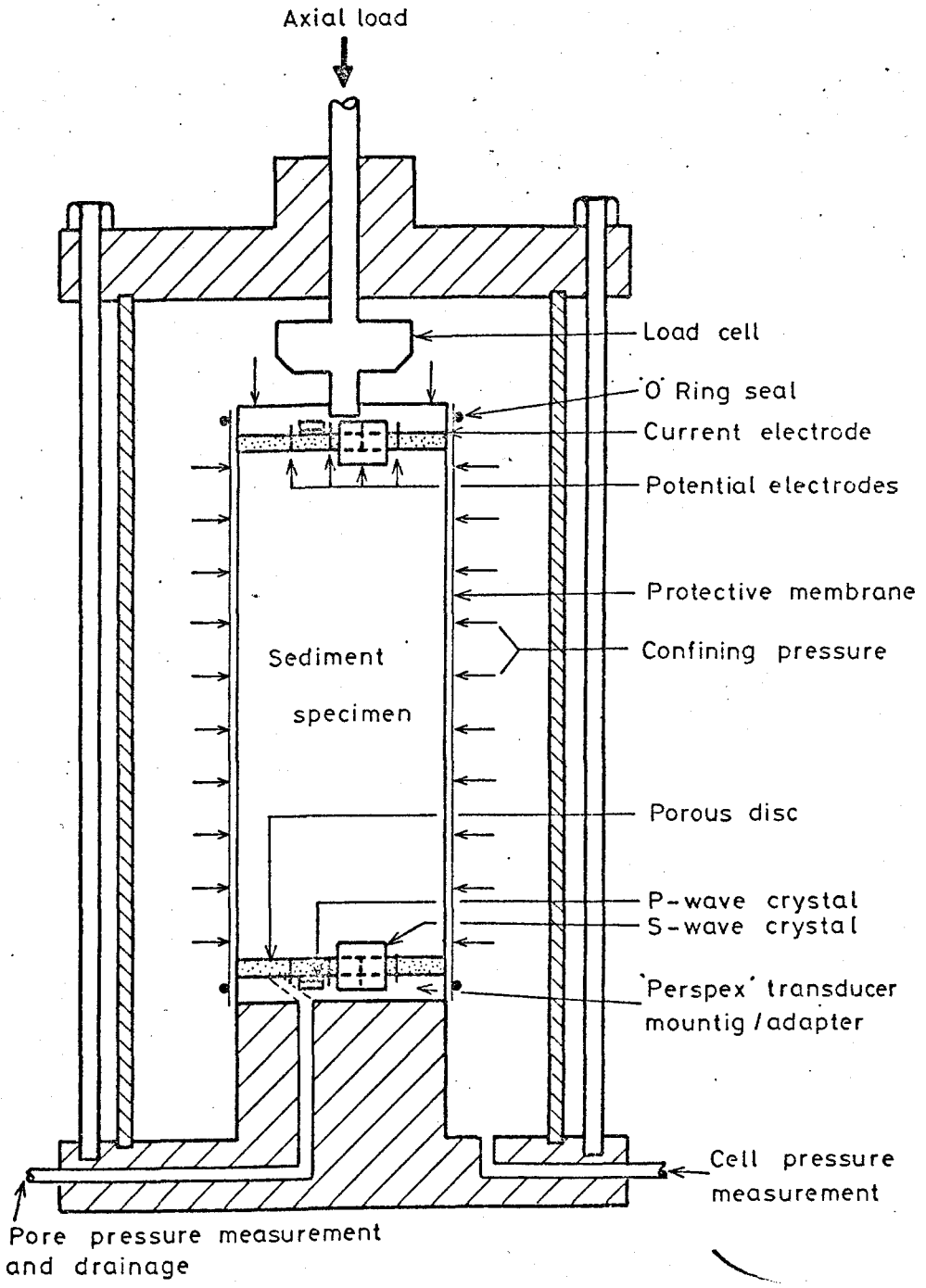

FIGURE 3.18 Standard 100 mm. triaxial cell with modified end caps incorporating P and S wave transducers and resistivity electrodes.

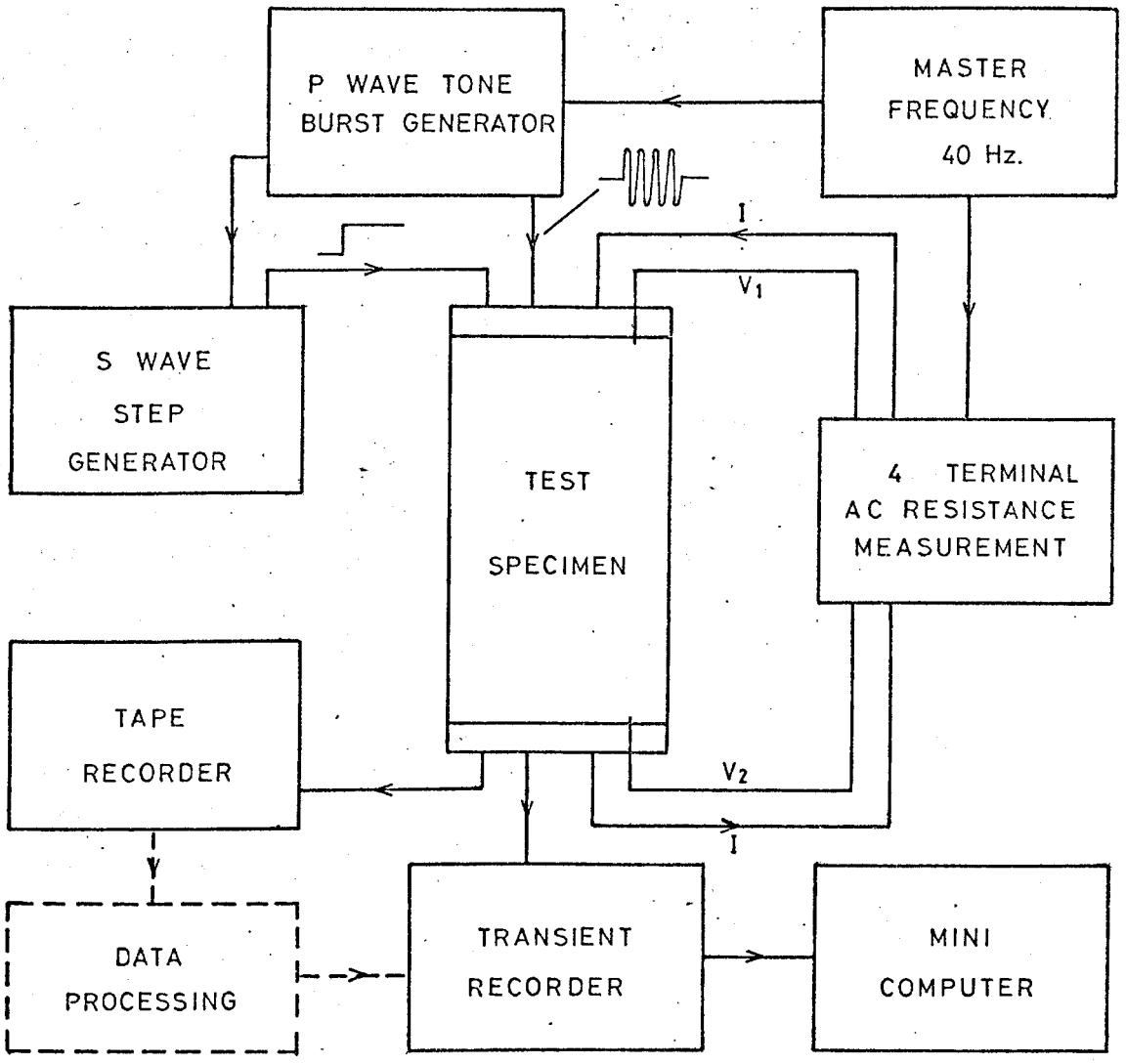

FIGURE 3.19

SYSTEM BLOCK DIAGRAM. The main input and output systems for the measurement of P and S waves and FF in a triaxial test specimen are shown for both on-line and subsequent data processing.

3.3 In-situ Shear Wave Probes

3.3.1 Introduction

The programme to develop a technique to measure shear waves in laboratory cells has two main purposes: (a) to gain further knowledge of fundamental soil properties which control both wave propagation and large strain mechanical properties; and (b) to enable in-situ shear wave measurements to be more accurately interpreted. As was outlined in the general introduction, the advantage of geophysical techniques for obtaining geotechnical information is that it has the potential for being performed on bulk material both rapidly and remotely.

With the increasing understanding of shear wave propagation in soils, it is necessary to augment the in-situ geophysical capabilities to include S-wave measurements. At the Marine Science Laboratories, geophysical probes have been built and operated which were designed to measure the in-situ geophysical characteristics of the upper layers of sea bed sediments. P-wave probes are described by Simpkin(1975) and electrical resistivity probes by Jackson (1975). More recently, these two techniques have been described and the results of two case studies discussed by Jackson et al. (1980).

It was the aim of this part of the project to design in-situ shear wave probes that would measure S-wave velocities in the top sediment layers in the same way that P-wave velocity and electrical resistivity probes had operated in the past. Finally, the intention was to produce in conjunction with P. Jackson and R. Baria at IGS a combined geophysical probe that would simultaneously provide measurents of P and S-wave velocity and electrical resistivity on the sea bed.

3.3.2 Initial tests

For the purposes of measuring in-situ shear wave velocities in near surface sediments, bender 'bimorph' elements were thought to be suitable for both transmitting and receiving over short distances. As with the laboratory systems, this was the only system tested because of the obvious advantages that it offers.

The simplest test that can be performed with bender elements to investigate their behaviour as shear wave transducers is to bury them in a container of dry sand with only their electrical connections. In this way their performance can be monitored before mountings are attached. The simple manner in which a bender element changes shape under the influence of an applied voltage causes shear stresses to be set up in all directions parallel to the plane of the element. However, it was not readily apparent which orientation of a rectangular element would produce the 'best signal'. To test for this 'best signal', two rectangular bender elements (39 x 19 mm) one parallel connected and the other series connected, were laid on a flat bed of dry sand, 76 mm apart, in a large (800 x 400 mm) container and then covered with a consistent amount of sand. This procedure proved to give consistently reproducible signals. All the different combinations of transmitter and receiver configurations in the plane of the element were tested. The effect of clampingthe elements at different positions was also investigated using a pair of modified toolmakers clamps.

By far the best configuration of the transmitter/receiver system was when both longer edges of the elements were equidistant, parallel and unrestricted by any clamps. This received signal is shown in Figure 3.20 together with the transducer configuration. The quality of the signal allows accurate velocities to be determined using a d.c. step as the driving voltage . Attenuation characteristics could be measured using a tone burst

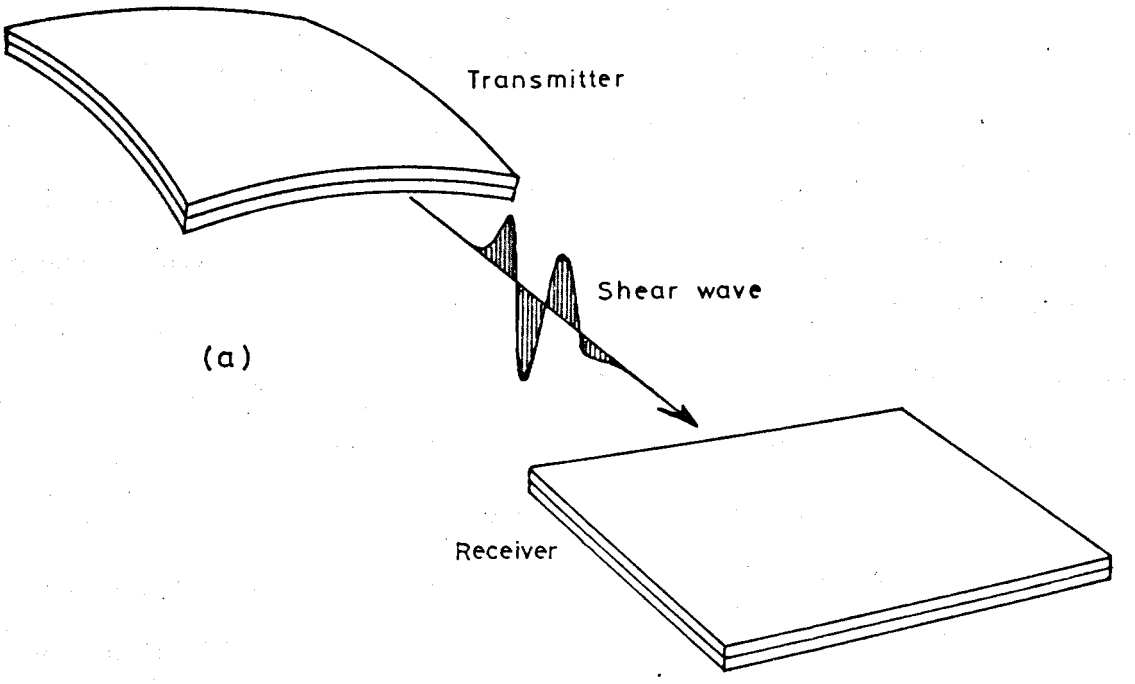

(b)

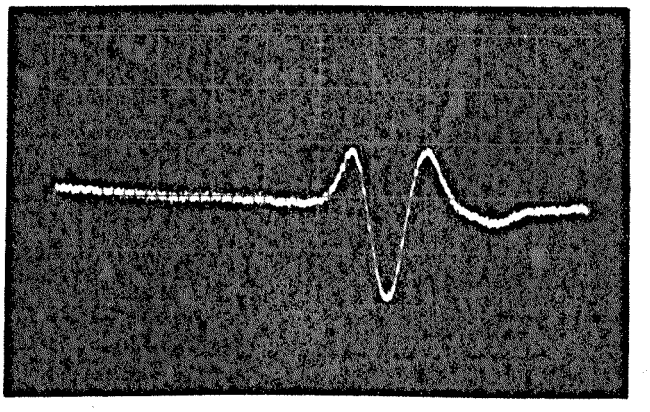

Horizontal scale 0·2 ms/div.

No filter.
Separation 76 mm.
Driving voltage 3 volts dc step.

FIGURE 3.20

(a) Configuration of rectangular bender elements which provide the best shear wave signal.

(b) The received signal.

driving signal.

Shirley (1978) working along similar lines describes a shear wave probe which uses rectangular elements with the shorter edges equidistant and parallel.It is unclear why this configuration has not proved satisfactory in these experiments. Shirley suggests that,using his configuration, maximum shear will occur at the end of the elements and will propagate along the length of the element. He argues that in the perpendicular direction the particle motions will be 180 degrees out of phase between the middle of the element and its edges, therefore, in the farfield, these motions will tend to cancel each other, with only small amounts of energy propagated in this direction. However, this does not seem to be the case in these experiments, in fact, the opposite seems to be true. The reason why the energy does not cancel out is probably due to the bending nature of the element. A normally flat bender plate tends to distort into a curved plate like the surface of a sphere. This can be considered to be composed of two component bending motions perpendicular to one another as depicted in Figure 3.21. If only one component of motion is considered (e.g. that in Figure 3.21a) then the particle motions at the end of the element and in the middle will be out of phase. But this is only a simplified case; the other component of motion as shown in Figure 3.21b should also be considered which,taken together, produces a composite motion (Figure 3.21c) in which only at the centre of the element is there an out-of-phase motion. The relative sensitivity of the element in any configuration is still, however, not fully understood and further experiments using different size and shape elements are required to resolve the difficulties and aid future shear wave transducer designs.

It is appropriate to note here that a non-linear phenomenon has been observed which occurs when using these types of shear wave transducers.

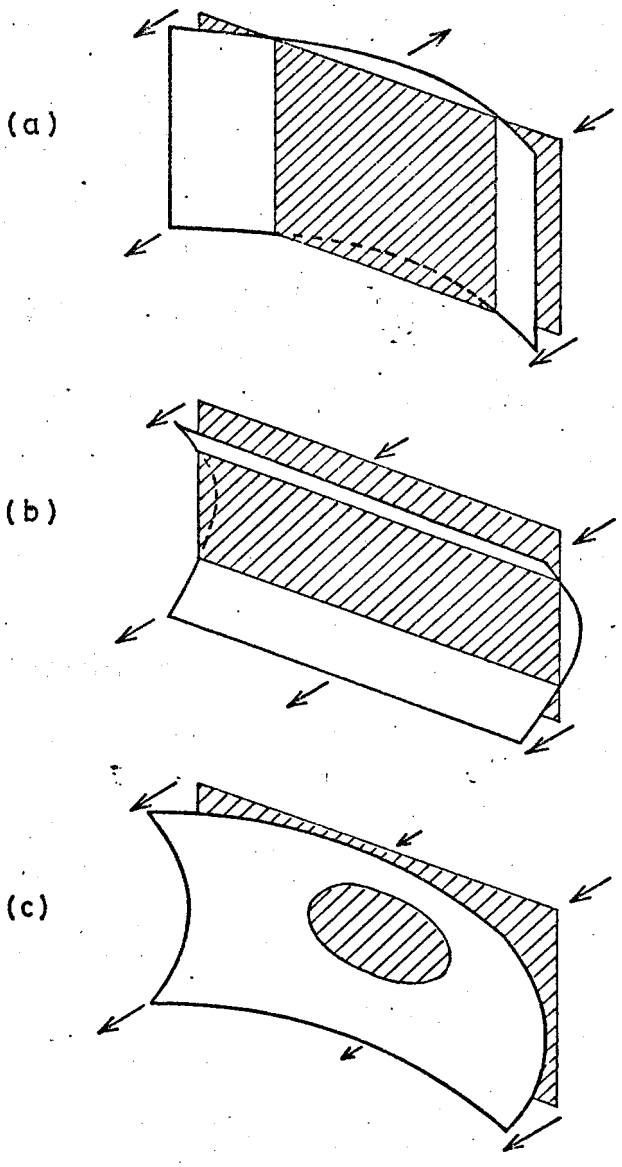

FIGURE 3.21

(a) & (b) The component bending motions of a rectangular bimorph element.

(c) The composite motion showing the formation of a spherical surface.

The arrows depict the direction of particle motion in the surrounding medium.

The ratio of input voltage to the transmitter and output voltage from the receiver has been found to be constant only up to a given threshold point at which stage not only does the received signal amplitude decrease but the signal quality is grossly degraded. This threshold voltage has been found to depend on the transducer size, the mounting characteristics, the sediment type and the environmental conditions. It has been observed in some instances (large elements in loose dry sand) to be as low as three or four volts. The explanation of this phenomenon is simple, the transmitter at a given amount of strain starts to decouple from the sediment; at an advanced stage this can be considered as local liquifaction around the transducer. The important implication arising from this is that because of the maximum energy input level there is a corresponding maximum transmit distance for detection using this system which also depends on a multitude of other factors. However, with ambient laboratory noise levels and receiving sensitivities of approximately 0.5 mV, transit distances greater than 200 mm in dry sands become problematic. Fortunately, this does not mean that the transducers cannot be used over greater distances using different techniques. Simple signal processing using a stacking program (Jackson et al. 1981) can eliminate noise and has been successfully used over larger distances. Another technique which showed some success involved using a single shot technique of a larger input voltage; the measurements are made using a transient recorder. Another processing technique which showed a significant amount of promise was that of cross-correlation. Experiments using this technique are continuing at UCNW.

Several probes were constructed using a technique similar to that used by Shirley (1978) i.e. mounting elements on this probes using various potting compounds. One of the better designs is shown in Figure 3.22; the bender element is backed with a rubber compound and mounted on an aluminium

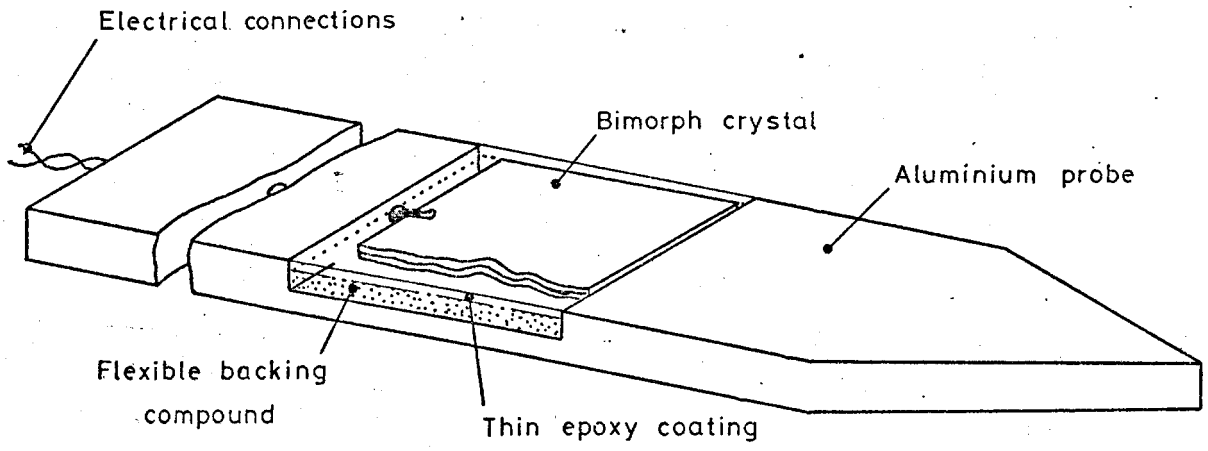

FIGURE 3.22

Schematic diagram of an early shear wave probe design.

probe. The transmitting face is protected by a thin coating of epoxy resin. Although this design produced shear waves, the sensitivities and signal quality was significantly worse than that obtained using raw elements or with the mountings described below.

3.3.3 In-situ Probe Mk I

Experience from the initial testing programme and from early designs suggested that to maximize the sensitivity the bender element should be as free to move as possible and preferably have both faces in contact with the sediment. The other primary design criteria for an in-situ probe are that it is waterproof and as rugged as possible.

Figure 3.23 illustrates the Mk I probe design. The bender element is allowed to move as freely as possible by only clamping it at one point. It is protected by a stainless steel housing whilst still enabling the transfer of particle motion from both faces of the element. A semi-flexible urethane compound, 'scotchcast', provides the waterproofing as well as affording some mechanical protection. The transducer housing is mounted at the end of a steel tube, via a plastic connection, which provides the pathway for the electrical connections.

Tests in the laboratory indicated that the mechanical ruggedness of the system was probably sufficient for softer sediments, muds and silty clays, but may not be suitable in sands if forces other than vertical ones were applied. Initial in-situ tests with this design were intended, therefore, to be limited to the softer sediment types.

A calibration of the Mk I probes was performed in a small tank of dry sand. The received signal at a series of separation distances is reproduced in Figure 3.24 for both a single cycle sine wave and a d.c. step driving signal. Signal quality is considered to be very good, especially up to

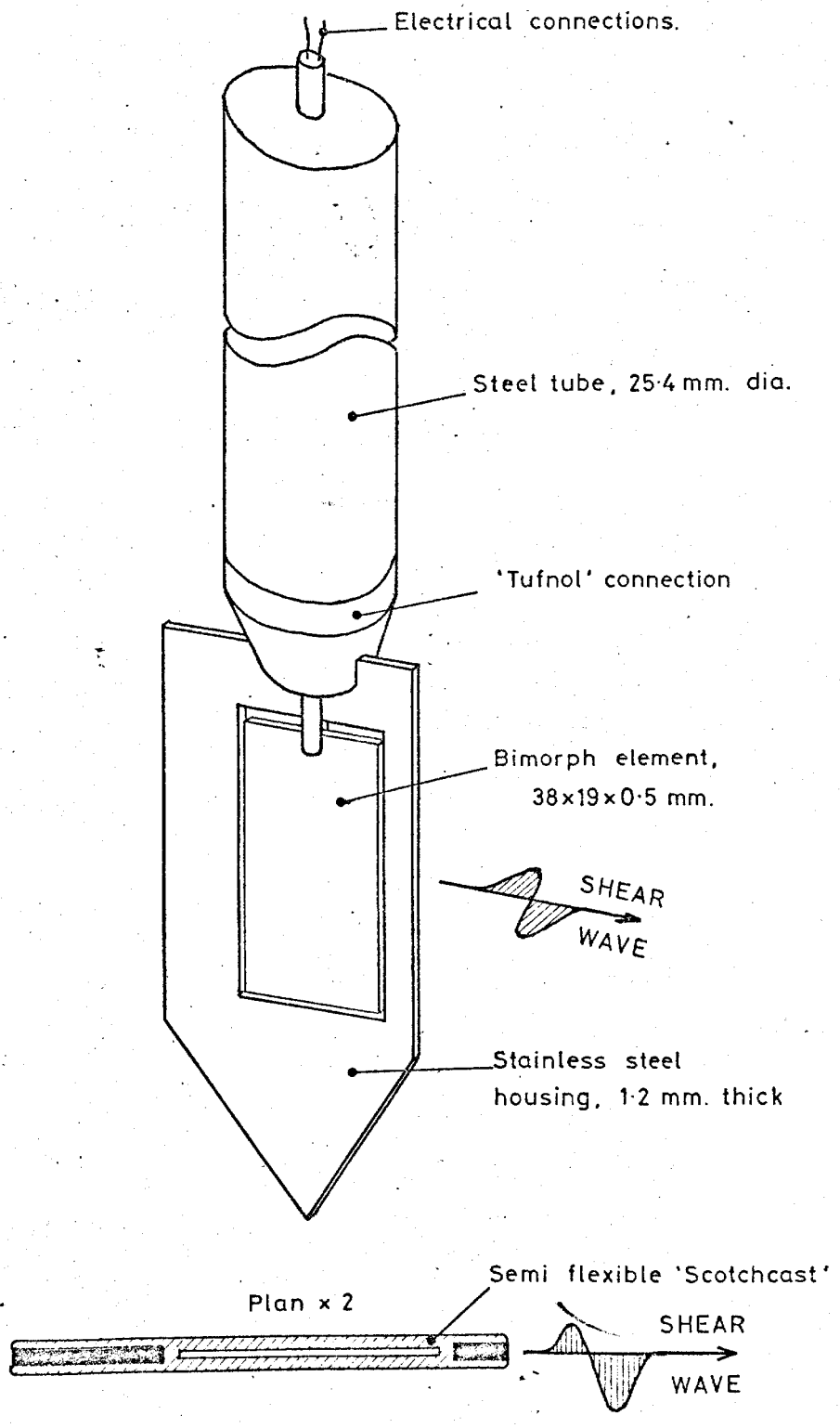

FIGURE 3.23

Mk. I In-situ Shear Wave Probe, showing the constructional details before being coated in 'Sotchcast'.

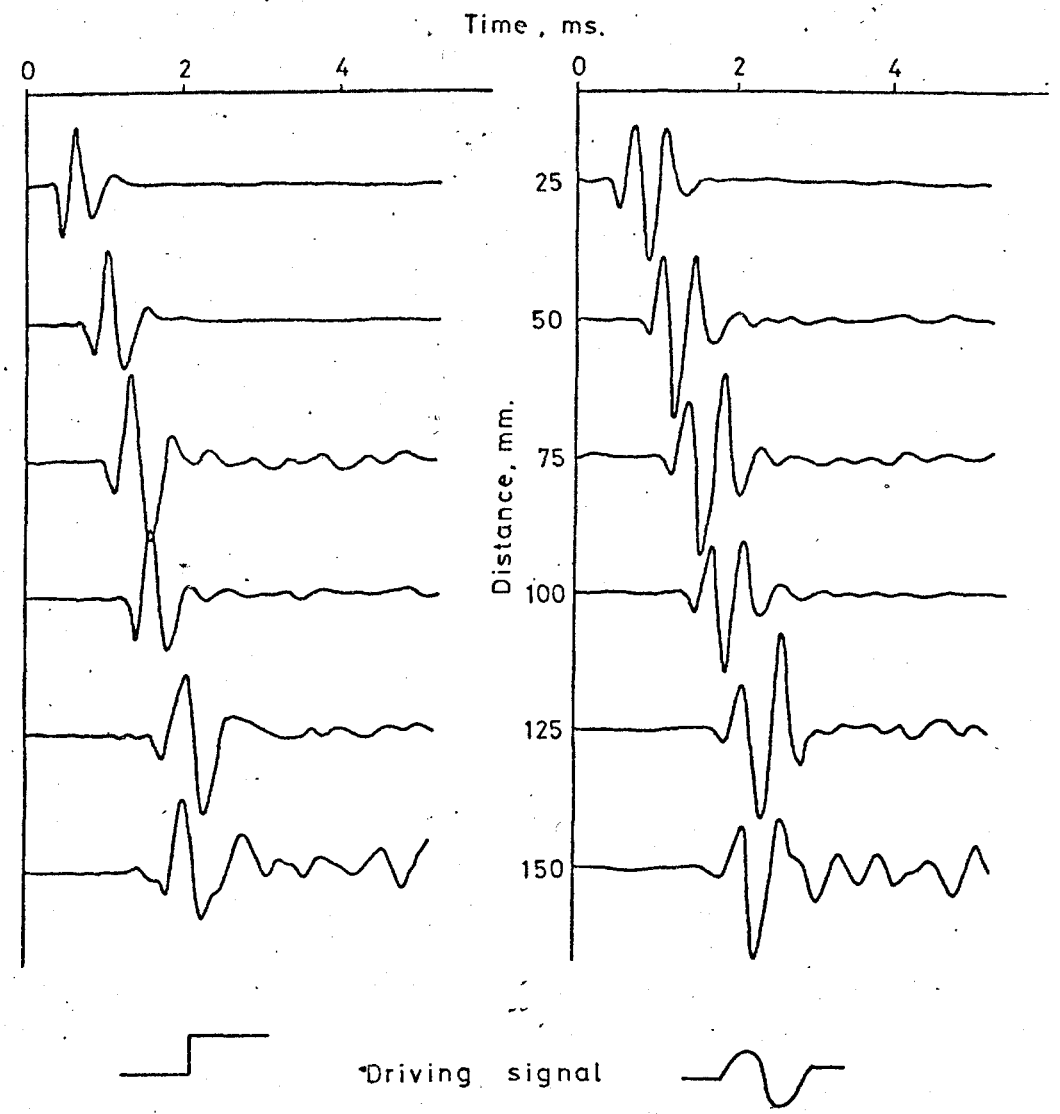

FIGURE 3.24

Unfiltered received wave forms using the Mk.I in-situ probes in dry sand.

100 mm separation, thereafter the shear wave signal onset becomes less clear; this could be due to the relatively small test tank used. The d.c. step driving signal provides, in most cases, a marginally clearer onset than the sine wave as well as producing a shorter pulse.

It was on the Mk I probe that the idea of monitoring the actual response of the transmitter to the driving wave form was first tested. A 'multimorph' element was rigidly bonded to one face of the transmitter as shown in Figure 3.5b before the 'scotchcast' was applied. It was considered that because the ratio of masses between the 'bimorph' and 'multimorph' was large (10:1) the behaviour of the 'bimorph' would be only slightly affected by the 'multimorph's' presence. However, it was considered that because the 'multimorph' was rigidly bonded to the 'bimorph' it would respond faithfully to its vibrations. In Figure 3.25 five oscillographs are shown illustrating the transmitter response in different media. Damping increases roughly as the test media increases in density, as would be expected. It is interesting to note that in the sands the response at the resonant frequency is nearly perfect. The transmitter is behaving as a highly-damped, low Q system. The damping is not simply a function of the media's density as the wet sand, although being more dense than the dry sand, exhibits a lower damping factor. Differences in damping as shown using this technique could, therefore, be used as another means of discriminating between sediment types. It is also possible, although no other experiment work has been performed, that the transmitter damping observed using this technique may be closely related to the shear wave attenuation.

In December 1979, the Mk I probe was successfully used in situ from R.V. Prince Madog. The probes were attached to a wooden 'sledge' designed by P. Jackson to make resistivity profiles whilst underway. However, with the probes inserted the sledge had to remain static on the sea bed. Modifications to this sledge enabled P-wave transducers and the S-wave transducers to be

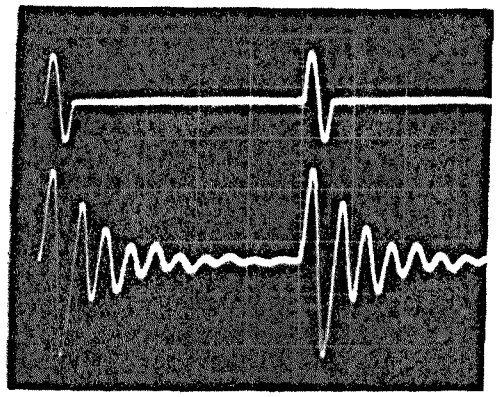

Air

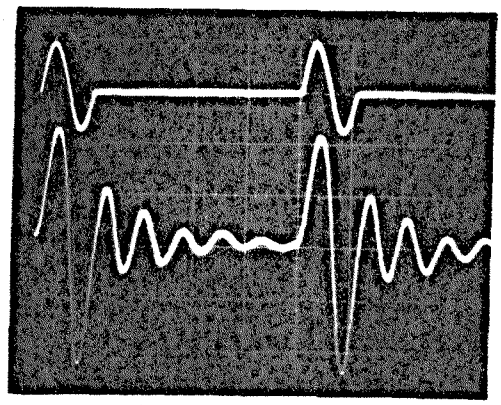

Water

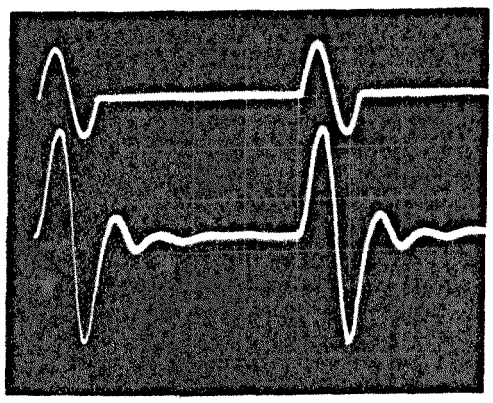

Mud

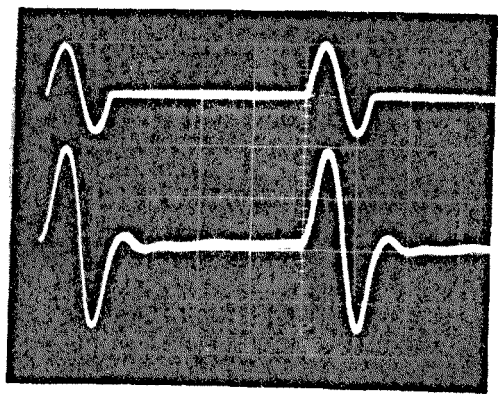

Wet sand

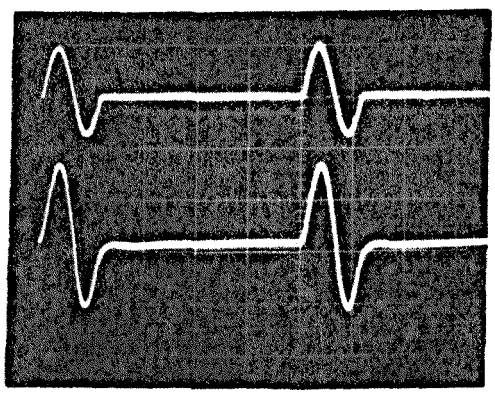

Dry sand

Horizontal scale =
0·5 ms/div.

FIGURE 3.25

Mk. I in-situ probe transmitter response in different media. The upper trace is the 'bimorph' driving signal and the lower trace the 'multimorph' monitoring response.

installed. By also incorporating a larger wooden outrigger frame (to protect the combined probe from being turned over) measurements at sites around the North Anglesey coast and in Holyhead harbour were obtained. Data from this cruise is presented and discussed in Chapter 8.

Despite the success of these Mk I probes in obtaining some in-situ data they had several problems:

(a) They were not sufficiently rugged for continual use from a ship. This lack of ruggedness was known beforehand but as an experimental probe it was decided that if handled with care it might work in soft sediments. It did; subsequently, it worked in harder sediments but on two stations the probes were bent on retrieval, but still working! However, the severest damage occurred when the tip of one of the shear wave probes accidently took the weight of the wooden frame (and lead weights) on deck, rendering it useless. This rough shipboard handling is to be expected and Mk II had to include more rugged design features.

(b) The shear wave travel path was limited to only a few centimetres. This is because of noise, both electrical and mechanical, and because of the inherent difficulties of using a pulse technique where there is a low maximum driving voltage. Other measurement and signal processing techniques (cross correlation using binary noise and signal stacking) were experimented with suggesting that further separations will be possible with the aid of such techniques.

(c) Another difficulty encountered in Red Wharf Bay was the sediment variability. Good samples were taken at each station but on several occasions the material which was found adhering to the probes on retrieval was not the same as the sediment

sampled by the grab. It is imperative, therefore, to include a sampling device on the probe so that more accurate data can be obtained.

3.3.4 In-situ Probe Mk II

The limitations of the Mk I design, discussed at the end of the last chapter, provided the design foundations for the Mk II probe illustrated in Figure 3.26. Essentially, the difference between this probe and the Mk I version is the large diameter stainless steel tube which provides a greatly improved degree of ruggedness, the transducer is mounted on the side rather than beneath. Should hard impenetrable sediment, rock or, indeed, the deck be encountered, the transducer is afforded ample protection. This tube can also act as a sampling barrel. A bevelled edge has been cut but no material-retaining device has yet been fitted. Consequently, on the May 1980 R.V. *Prince Madog* cruise in Carmarthen Bay, where these probes were tested, only a few soft sediment samples were recovered in the core tube.

A new wooden frame was constructed by IGS to accommodate the new shear wave probes, the P-wave probes and the electrical resistivity probes. Figure 3.27 shows a schematic diagram of the combined probe. A short core tube with core catcher was placed in the centre of the probe to enable more accurate sampling to be achieved.

Due to a foreshortened timetable, laboratory testing of these Mk II probes has not been possible. However, the ruggedness of the design has been shown by a lack of damage on the May 1980 cruise. The full potential of these probes was not, however, fully investigated as the signal processing equipment, Hewlett Packard correlator and noise generator, were unavailable for this cruise. An online signal stacking program using the HP mini-computer

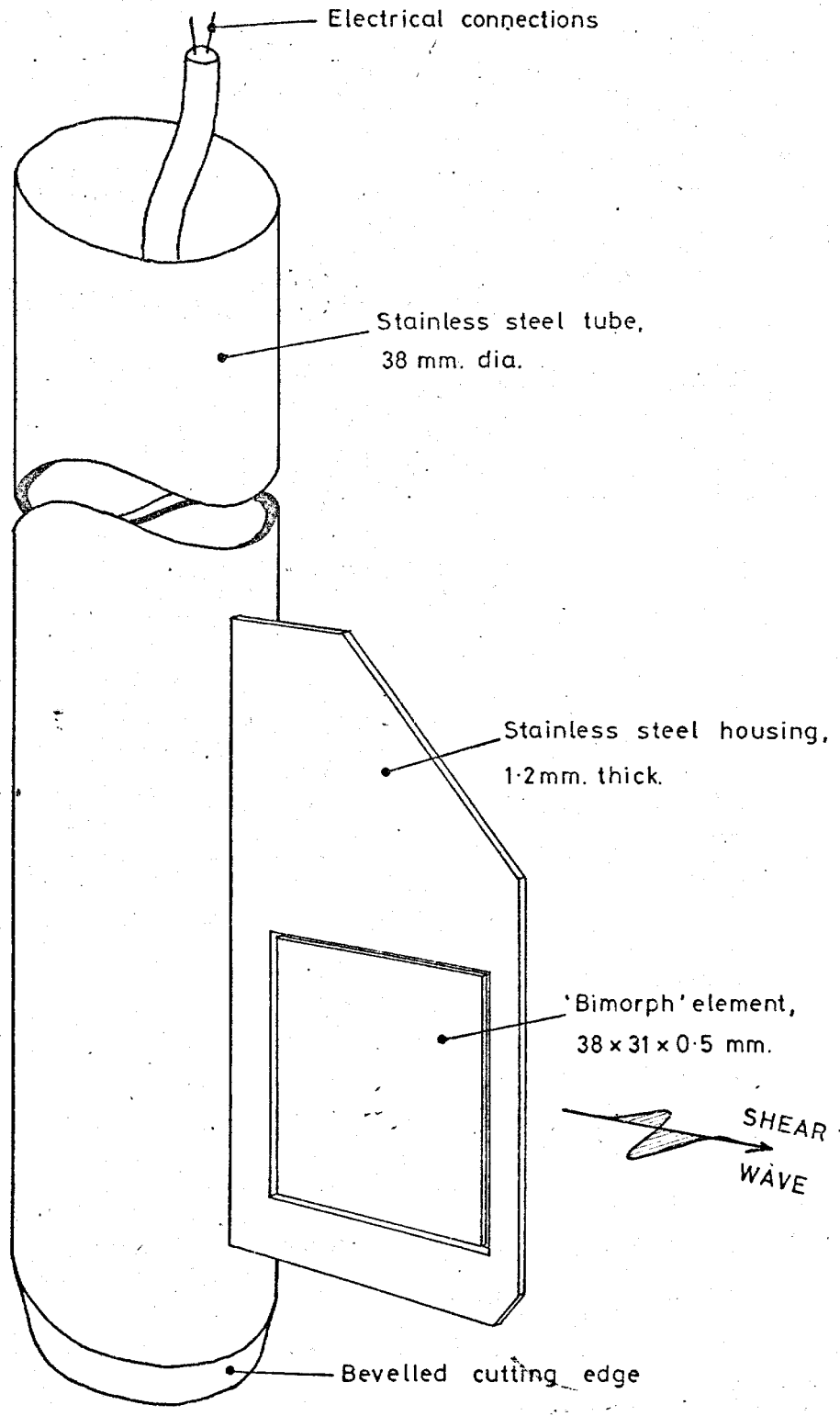

FIGURE 3.26

Mk. II in-situ shear wave probe, showing the constructional details before being coated in 'Scotchcast'.

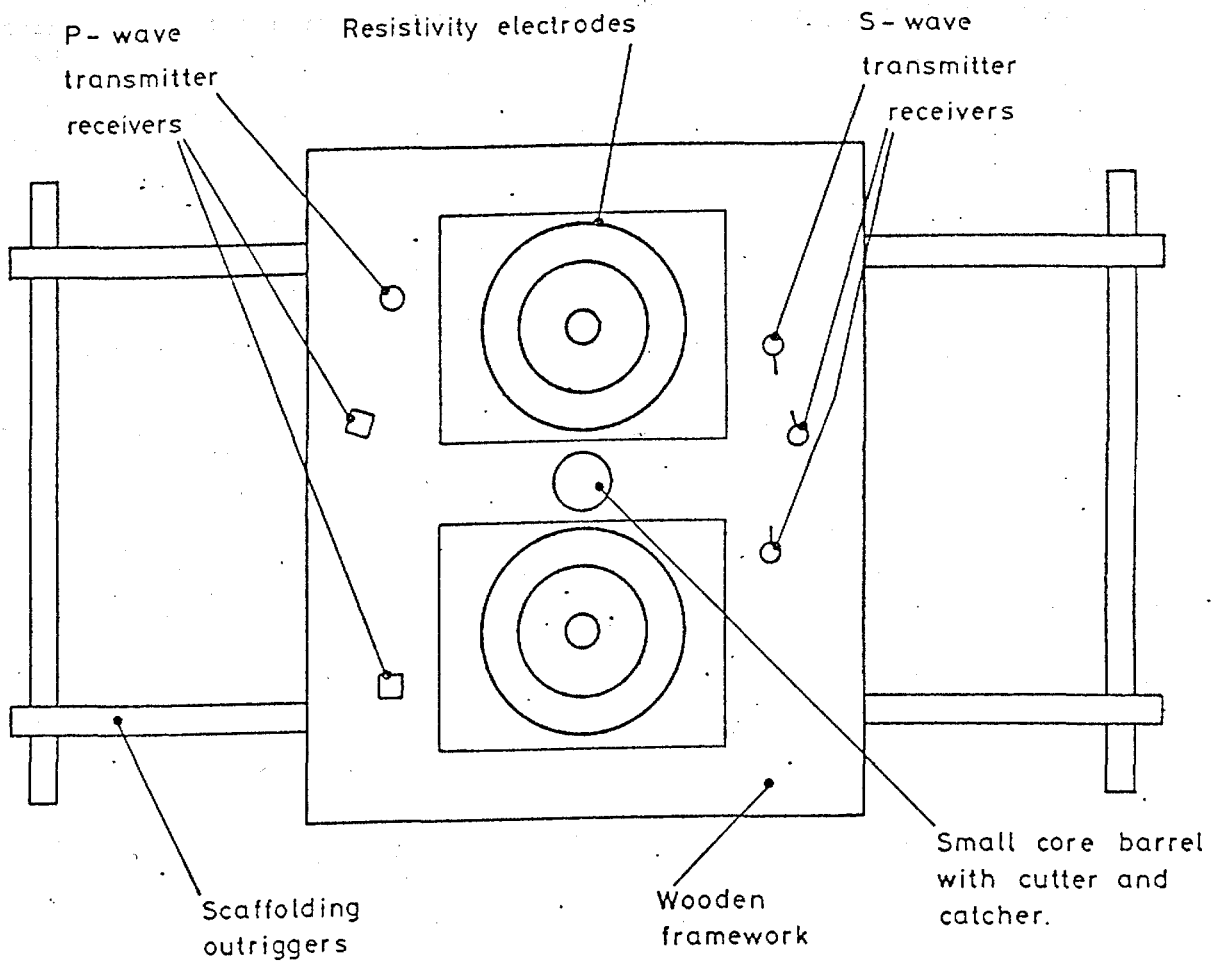

FIGURE 327

Schematic layout of the combined in-situ geophysical probe.

was successfully implemented at the end of the first leg but this development was halted before it had been used due to the unavailability of the computer for the final leg. Despite this, a limited amount of data was obtained using the normal pulse technique and this is presented in Chapter 8.

4. VARIABLE POROSITY TESTS WITH SANDS

4.1 Initial Experiments at ARL

4.1.1 Introduction

The purpose of the ARL experiment was to perform a limited study on a few sands to ascertain whether or not shear wave parameters could be reliably measured at different packing states using the new transducers. Three different sands were split and mixed for testing purposes producing six samples. They were chosen for their availability rather than for any other reason. Due to the preliminary nature and time constraints on this part of the programme the sediment vibration tank was not designed specifically for the purpose of these experiments. The limitations imposed by this factor will become clear later.

4.1.2 Sediment Description

Three sands were used for the evaluation of wave propagation characteristics in the ARL tank. The first sand was a coarse river-bed sand with a wide distribution of grain sizes. A modal analysis of 100 grains in a thin section gave the following result: quartz 58, feldspar 24, calcite 7, chert 6 and rock fragments 6. This river-bed sand was split to produce two sands with different size characteristics for testing; a coarse fraction with grain sizes ranging from 1.0 - 2.0 mm (A) and the remaining fraction with sizes ranging from 0.1 - 1.0 mm (B). The second sand was an angular, pure quartz medium-fine, white, beach sand from Panama City, Florida, with a narrow distribution of sizes, 0.2 - 0.5 mm (C). A fine, rounded, sandblasting sand, composed of pure quartz, was the third sediment used (D) with grain sizes in the range 0.06 - 0.3 mm. Two further

samples were prepared by mixing sands (A) and (D) with sand (B) to provide samples with wider grain size distributions. Six samples were, therefore, finally tested: A, B, C, D, $B_{60}A_{40}$ and $B_{60}D_{40}$. The subscripts are per cent by weight of the component sands. Cumulative grain size distributions for all the sands are plotted in Figure 4.1 where sieves with ½ ϕ intervals were used.

To obtain a quantitative description of each sand, statistical measures from the grain size analyses have been calculated. The measures used are those from Folk and Ward (1957).

In Table 4.1 the statistical measures defined previously are presented for each of the six sands.

SAND	D_M	S_p	Sk_p	K_p
A	-0.353	-0.195	0.184	1.359
B	1.277	-0.756	0.150	0.790
C	1.603	-0.234	-0.367	1.583
D	2.632	-0.283	-0.356	1.270
$B_{60}A_{40}$	0.631	-1.018	-0.285	0.707
$B_{60}D_{40}$	1.809	-0.877	0.301	0.749

TABLE 4.1 - STATISTICAL MEASURES FROM THE GRAIN SIZE ANALYSES OF THE SANDS TESTED IN THE ARL TANK

Using a binocular microscope, a sample of 100 grains from each sand was compared with the visual estimation charts and assigned a sphericity and roundness class. Sphericity in all the sands is described as nearly spherical, lying between 0.70 and 0.95. No substantial differences occurred between each sand. Roundness values, however, were variable. Percentages of each class found in the sands

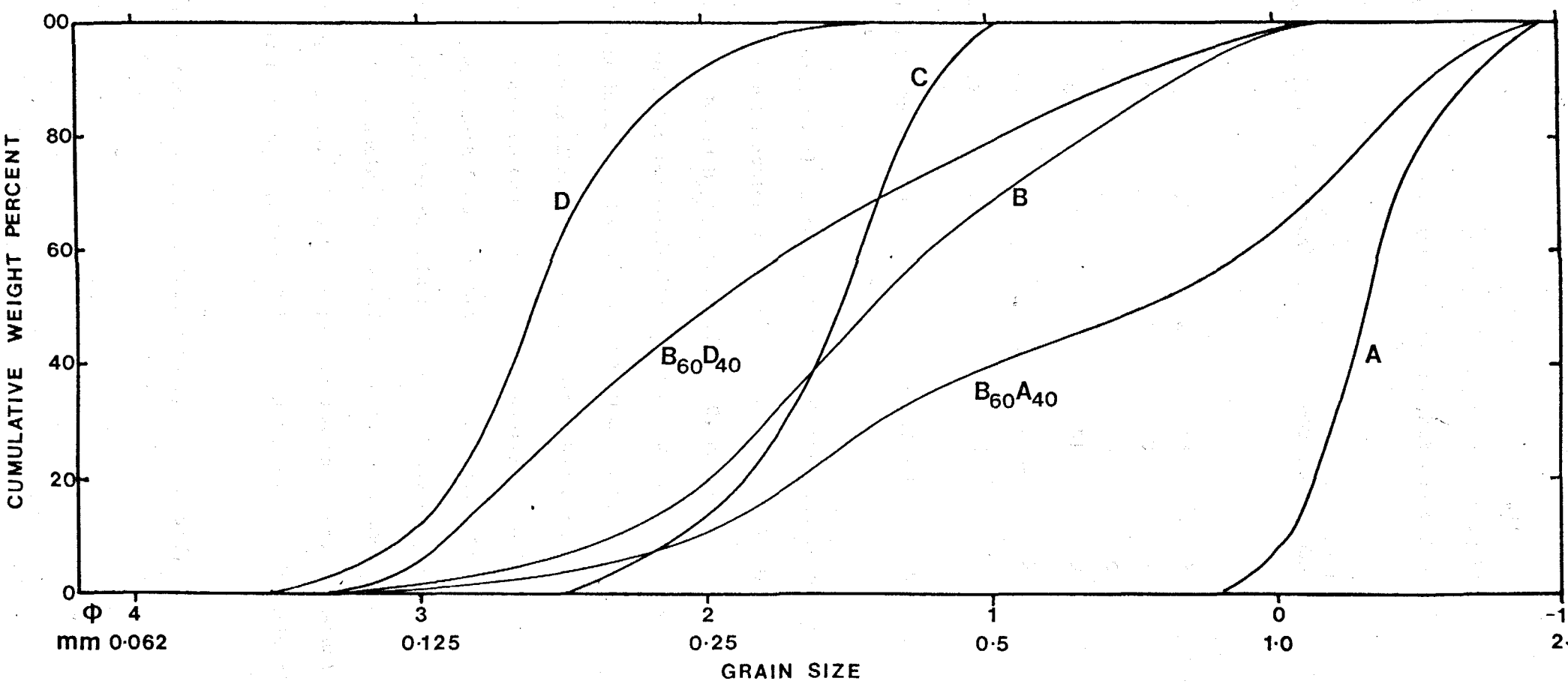

FIGURE 4·1 Grain Size distributions for the ARL sands

are presented in Table 4.2. In Figure 4.2 these results have been plotted as a cumulative roundness distribution so that the difference

	VERY ANGULAR %	ANGULAR %	SUB-ANGULAR %	SUB-ROUNDED %	ROUNDED %	WELL-ROUNDED %
A	6	20	38	21	13	2
B	12	28	30	20	8	2
C	13	66	19	2	0	0
D	0	0	12	28	51	9
$B_{60}A_{40}$	10	24	32	22	10	2
$B_{60}D_{40}$	7	17	22	24	26	4

TABLE 4.2 - RESULTS OF THE ROUNDNESS ANALYSES FOR THE ARL SANDS TESTED

between each sample becomes clearer. Using the 50 per cent level, a mean roundness class can be assigned to each sample: D, rounded; $B_{60}D_{40}$, subrounded; A, B and $B_{60}A_{40}$ subangular; C, angular.

Porosities and relative porosities of the sands were determined using the following technique. Experiments on 20 different sands, using a variable amplitude vibratory feeder, showed that a height of two metres was high enough to ensure a minimum porosity for all the sands, when fed at the lowest feasible rate from a funnel. This height (two metres) was used for the six sands tested and the rate of pouring was adjusted by reducing the funnel aperture to as small as was possible. A vibratory feeder, which provides a constant, adjustable rate of pouring, has been found more suitable than funnels for experiments of this kind.

From the weight (800 gms) and mineral density of the sand, the

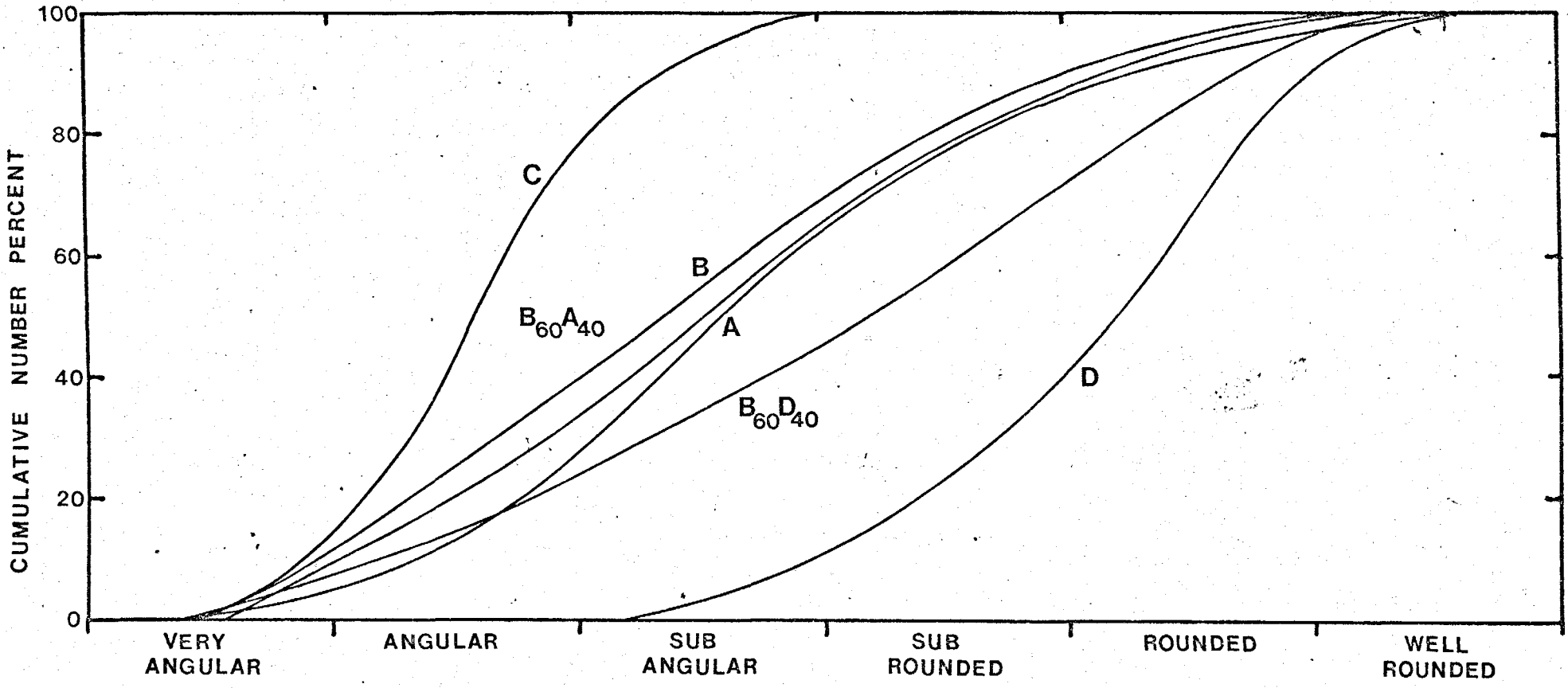

FIGURE 4.2 Grain Roundness Distributions for the ARL sands

porosity (n_{min}) of the structure in the measuring cylinder was calculated. To obtain the maximum porosity the measuring cylinder was sealed and slowly rotated three times in a vertical plane. This technique produces a consistently loose structure with a high porosity (n_{max}). The average of three measurements was used for both n_{min} and n_{max}. Variations using this technique were less than 1% in porosity. The procedure outlined above for determining the limiting porosities of a granular material does not involve specialised equipment (such as vibratory hammers) and can easily be performed in any laboratory. It would prove valuable if limiting porosities were more frequently reported alongside fractional porosity measurements as a further sediment descriptor.

Slow saturated deposition, into the measuring cylinder, of a known weight of sand, gave the initial value of porosity for the sand deposited in a similar manner in the wave measuring tank. This initial porosity was always found to be less than n_{max}. The cylinder was then partially buried in the sand in the tank and vibrated until the volume had reduced to a minimum. From the reduced volume the porosity was calculated and assumed to be equal to the final porosity of the same sand in the tank, having undergone the same vibration procedure. For two of the sands (B and D) this technique of assessing the porosities was confirmed by marking the level of sand in the tank and laboriously digging it out. By drying and weighing the sand and measuring the volume occupied in the tank (found by filling to the mark with water) the porosities were calculated. They agreed with measuring cylinder readings to better than ½% porosity. Results of fractional and relative porosities for all the sands are presented in Table 4.3.

	A	B	C	D	$B_{60}D_{40}$	$B_{60}A_{40}$
n_{max}	0.471	0.451	0.430	0.414	0.419	0.430
n_r%	0	0	0	0	0	0
n(initial)	0.449	0.441	0.420	0.404	0.413	0.396
n_r%	26.4	9.9	12.5	13.9	7.9	36.2
n(final	0.410	0.377	0.360	0.342	0.350	0.346
n_r%	63.2	73.3	87.5	100	90.8	89.4
n_{min}	0.371	0.350	0.350	0.342	0.343	0.336
n_r%	100	100	100	100	100	100

TABLE 4.3 - FRACTIONAL AND RELATIVE POROSITIES OF THE ARL SANDS TESTED

4.1.3 Experimental procedures

Each of the six sands were subjected to the following routine in order to assess the variation in their elastic wave propagation characteristics over a range of packing conditions, controlled by the maximum and minimum obtainable porosity. All the sands were tested in the fully-saturated state; temperatures and pressures were those of the laboratory. Fluctuations in temperature were, however, continuously recorded as the dependence of compressional wave velocity on this parameter is substantial and corrections to a standard temperature can easily be applied.

Initially the measuring tank (Figures 3.5 and 3.8) was filled with tap water and allowed to stabilise at room temperature by leaving it overnight. The compressional wave velocity of the water was determined from a series of time interval measurements made at varying transducer separations. Actual transducer separation need not be known using

this technique, as the velocity is determined from the gradient of a linear plot of time interval against change in distance, which is measured from the protruding back of one transducer from the tank wall to an accuracy of 0.5 mm. The final time interval measurement was taken with the transducer faces flush with the inside of the tank. They were clamped in this position to prevent any accidental movement as the time interval was subsequently used in a ratio to determine velocities in the sediment.

Adjacent to the compressional transducers, the two shear wave probes were positioned in such a way that they were rigidly suspended, using a slotted spacer and clamps from an overhead framework. It was essential that the probes were not in contact with the tank walls because of the problems of compressional waves radiating from the bimorphs through the tank and interfering with the received shear wave.

Preparation of the sand to be tested began with washing. An upward flow of water through the sand, using a pipe in a bucket, maintaining a fluidised state, had three purposes. Firstly, it dissolved and removed by the overflow, any soluble salts from the sand. Secondly, by maintaining the sand in a fluidised state light inorganic matter rose to the surface and was washed away. Thirdly, it removed entrapped air from the sand. Bubbles of gas in a sediment can have a profound effect on its acoustic properties (Anderson, A., 1974). To ensure complete saturation, the bucket and sand was then placed in a chamber under vacuum. A rotary pump enabled the pressure to be maintained at the water vapour pressure; it was then left overnight.

With the shear and compressional wave transducers in place, the sand was deposited in the tank using a small beaker. The beaker was immersed in the bucket and filled with sand covered by a layer of water.

It was then transferred and immersed in the water-filled tank before being slowly and evenly deposited. This procedure was repeated, transferring a beaker of water from the tank to the bucket each time to keep the water levels constant, until the sand level was 4 cm from the top of the tank. At no time during this operation did the sand come in contact with air. A very loose saturated sand structure is obtained using this method, it was important, therefore, that the tank was not accidentally knocked or vibrated as the high porosity sand is easily disturbed.

The transmitter compressional wave transducer was then set at its resonant frequency. To obtain this, both the voltage and current waveforms were monitored on the dual channel oscilloscope, Figure 4.3a. The input voltage was set to 30v and the current waveform on the second channel was adjusted to the same amplitude, Figure 4.3b. By inverting one of the waveforms and adjusting the frequency until the two pulses cancelled each other out (i.e. when the two wave forms were exactly in phase) the resonant frequency was found and read on the digital counter/timer, accurate to 1 Hz. The voltage pulse, after having travelled through the sand, was then displayed as shown in Figure 4.4. The interval and amplitude were measured using a square pulse as a cursor on the second channel, Figure 4.5.

To obtain the shear wave measurements the probes were first disconnected from the support framework and the slotted spacers were removed. This left the probes held in position by the sand. Cables from the transducers were supported so that the probes were not stressed and, therefore, would not move from their original positions. A single cycle 400v peak-to-peak pulse was used as an input signal. Figure 4.6 shows clearly the late arrival of a shear wave. The initial part of the trace consists of noise from compressional waves

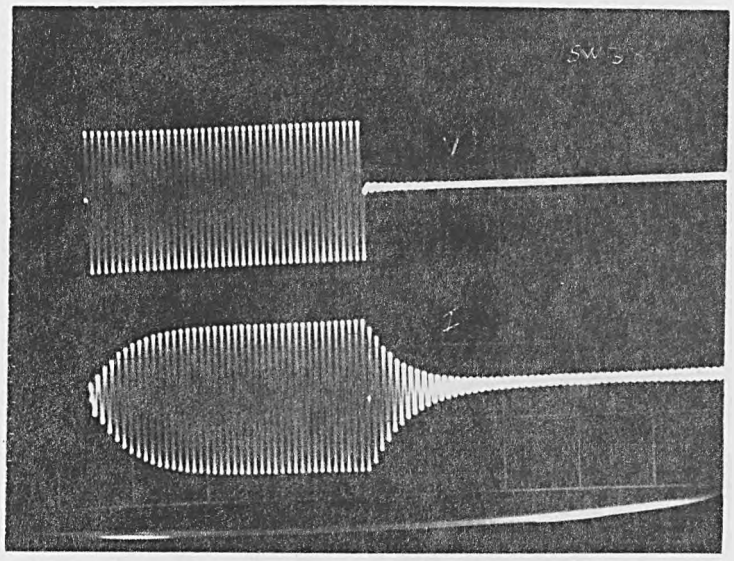

(a) The complete waveforms

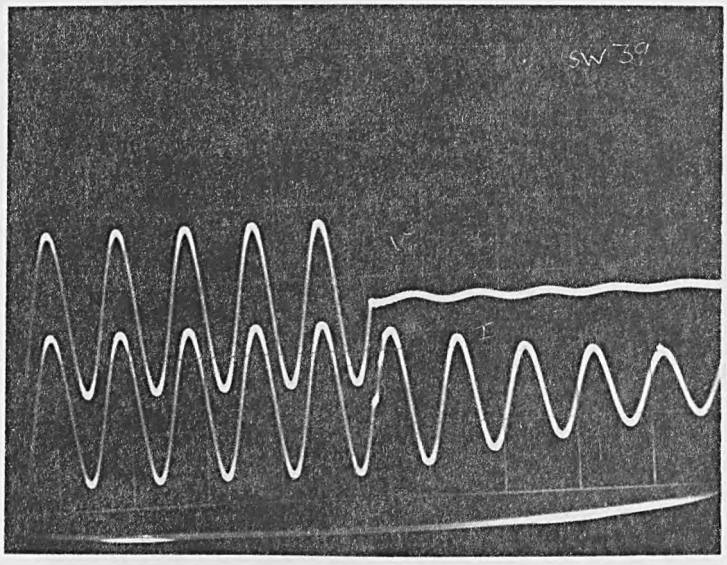

(b) The waveforms in phase, therefore at the crystal's resonant frequency

FIGURE 4.3 INPUT PULSED WAVEFOMS OF THE ARL COMPRESSIONAL WAVE TRANSDUCER, the upper channel is the voltage pulse and the lower channel is the current pulse.

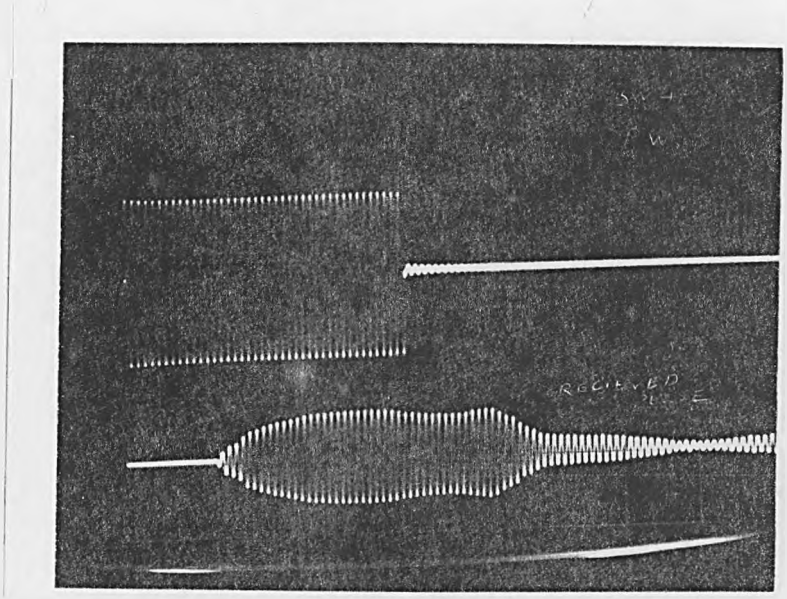

FIGURE 4.4 INPUT AND RECEIVED VOLTAGE PULSE OF THE COMPRESSIONAL TRANSDUCERS (ARL)

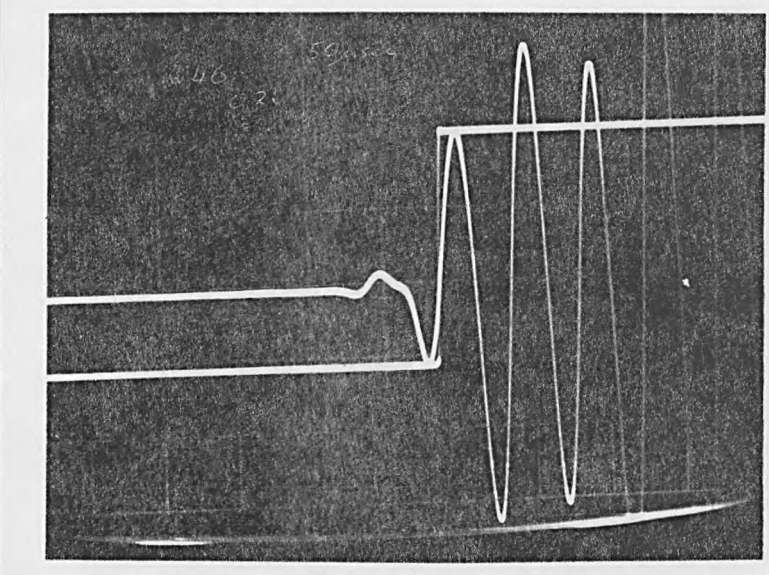

FIGURE 4.5 INITIAL PORTION OF RECEIVED ARL COMPRESSIONAL WAVE PULSE AND SQUARE PULSE, the square pulse length was used as a cursor for measuring time intervals.

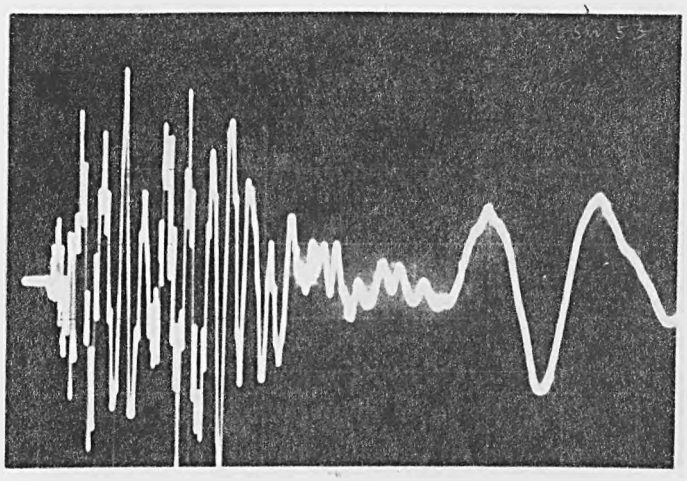

FIGURE 4.6 Typical unfiltered signal from the ARL shear wave transducer through sand

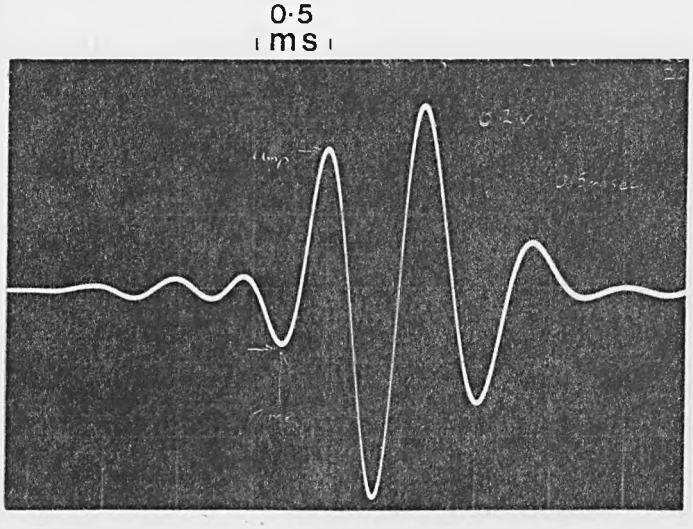

FIGURE 4.7 Typical filtered signal from the ARL shear wave transducer through sand

originating from the transmitter and travelling along a variety of paths to the receiver. Much of this noise was eliminated by band-pass filtering. A typical example of the trace after filtering is shown in Figure 4.7. The onset of the shear wave is difficult to identify hence the square pulse was superimposed on an identifiable feature (the first trough was used) and the time interval recorded. Amplitude measurements were also made; however, the scatter in the results were too large to draw firm conclusions.

After having reclamped the slotted spacer to the shear wave probes the sand was vibrated, reducing the porosity. Compaction of sand using a dynamic technique, such as vibration, is complex in its mechanics. The densities obtained are dependent on direction and time of vibration, frequency, maximum acceleration (found from frequency and amplitude) mould size and grain characteristics. Brand (1973) testing dry material, found that a maximum density was achieved irrespective of grain size at an acceleration of 1.5g, after 30 minutes. He cautions, however, that the relative density obtained is unlikely to reach a value of 100 per cent. With the electromagnetic vibrator available such control over the various parameters was impossible. When the sand was in its initial high-porosity state then only a small amount of vibration caused a reduction in porosity. Both compressional and shear wave measurements were made as previously, as the porosity was decreased in stages by vibration. Although during the vibration the shear wave could not be monitored (because of the supporting framework and vibration causing interference with the received pulse) the high frequency compressional wave ($\cong$112 kHz) could still be monitored. During vibration the time interval of the compressional wave could be seen to decrease. This phenomenon was

used as a qualitative indicator of decreasing porosity in the sand.

From a series of trial experiments on different sands, a procedure for obtaining a maximum density using the vibrator was established. It was found that a maximum density was always achieved after 15 minutes vibration at the maximum amplitude, with a further 15 minutes vibration during which the amplitude was gradually reduced to a minimum. If the gradual reduction in amplitude procedure was not observed, lower wave velocities resulted, indicating higher porosities. Evaluation of the porosities from this technique were described previously. After vibration the sand was left for 10 minutes to stabilise. This procedure was adopted after having noted that small changes in the wave form occurred during the first few minutes after vibration. Time intervals invariably increased slightly during this period and amplitudes decreased. It is difficult to formulate an explanation for this relaxation phenomenon!

After the maximum density had been reached, further compressional wave measurements were made at decreasing transducer separations. Trial experiments proved that moving the transducers during vibration, followed by a further period of vibration in which the amplitude was gradually reduced to a minimum, resulted in the maximum density being maintained throughout these readings. Shear wave time intervals and amplitude readings were also recorded at decreasing probe separations along the length of the tank. The probes were inserted during vibration, clamped in position, and left during the decreasing vibration period as before. Removal of the clamps then allowed each of the shear wave measurements to be made. During this procedure, the disturbance to the sand structure is possibly at its maximum and the porosity may not have reached the minimum value obtained previously.

Despite this, the method of velocity calculation only assumed that the porosity is constant during this procedure and not necessarily identical to the minimum porosity obtained when the transducers were in their original positions.

It should be noted here that the porosity along the paths between the two transducers is assumed to be the same as the average porosity for all the sediment in the tank. Brand (1973), among others, has pointed out that inhomogeneities within sand bodies, especially those subjected to vibratory compaction, do exist. In Brand's experiments on a split sample he found variations in porosity of up to two per cent and there is no reason why such variations should not also have occurred in these experiments. It is apparent that because porosity is an important parameter, in any assessment of granular materials, not only should techniques be employed to find porosity accurately, but techniques to look at inhomogeneities in porosity throughout a sample should be investigated.

4.1.4 Compressional wave data

The experimental procedures detailed in section 3 yield parameters that have to undergo several operations and corrections before useful acoustic and elastic values are obtained. One sample ($B_{60}A_{40}$) has been used to illustrate the method by which raw data yielded by all six sand samples has been processed.

Before the sediment was deposited in the tank, time interval (t_1) and transducer separation (d) were measured in water, enabling the velocity to be calculated. These experimental values for sand $B_{60}A_{40}$ are shown in Table 4.4.

RELATIVE TRANSDUCER SEPARATION, d mm	TIME INTERVAL t_1 msec	
63.0	0.1120	
57.0	0.1080	Sand $B_{60}A_{40}$
51.0	0.1040	Temperature 20.8°C
46.0	0.1010	Resonant Frequency
41.0	0.0975	108.678 kHz
33.5	0.0930	Water Velocity
28.0	0.0890	(V_{w1}) 1486 m sec^{-1}
21.5	0.0840	
12.5	0.0780	
5.5	0.0735	
22.0	0.0850	
41.5	0.0975	

TABLE 4.4 - DISTANCE AND TIME MEASUREMENTS FOR COMPRESSIONAL WAVES IN WATER

The distances (d) are not actual transducer separations but relative distances (the measurement made was that of the protruding transducer housing from the outside of the tank to the nearest 0.5 mm). As water temperature influences velocity it was constantly monitored and an average reading was recorded. Figure 4.8 shows a linear plot of these results; a straight line has been fitted using a least-squares method, the slope of which is the water velocity at 20.8°C (V_{w2}). A correlation coefficient (r^2) indicates the 'degree of fit' of the experimental points to the straight line.

In the final position the adjustable transducer was 'set' by tightening the clamp. The transducer's position, therefore, remained secure until after the sand had been deposited and the vibration programme completed. From Figure 4.8 the time interval (t_2) for

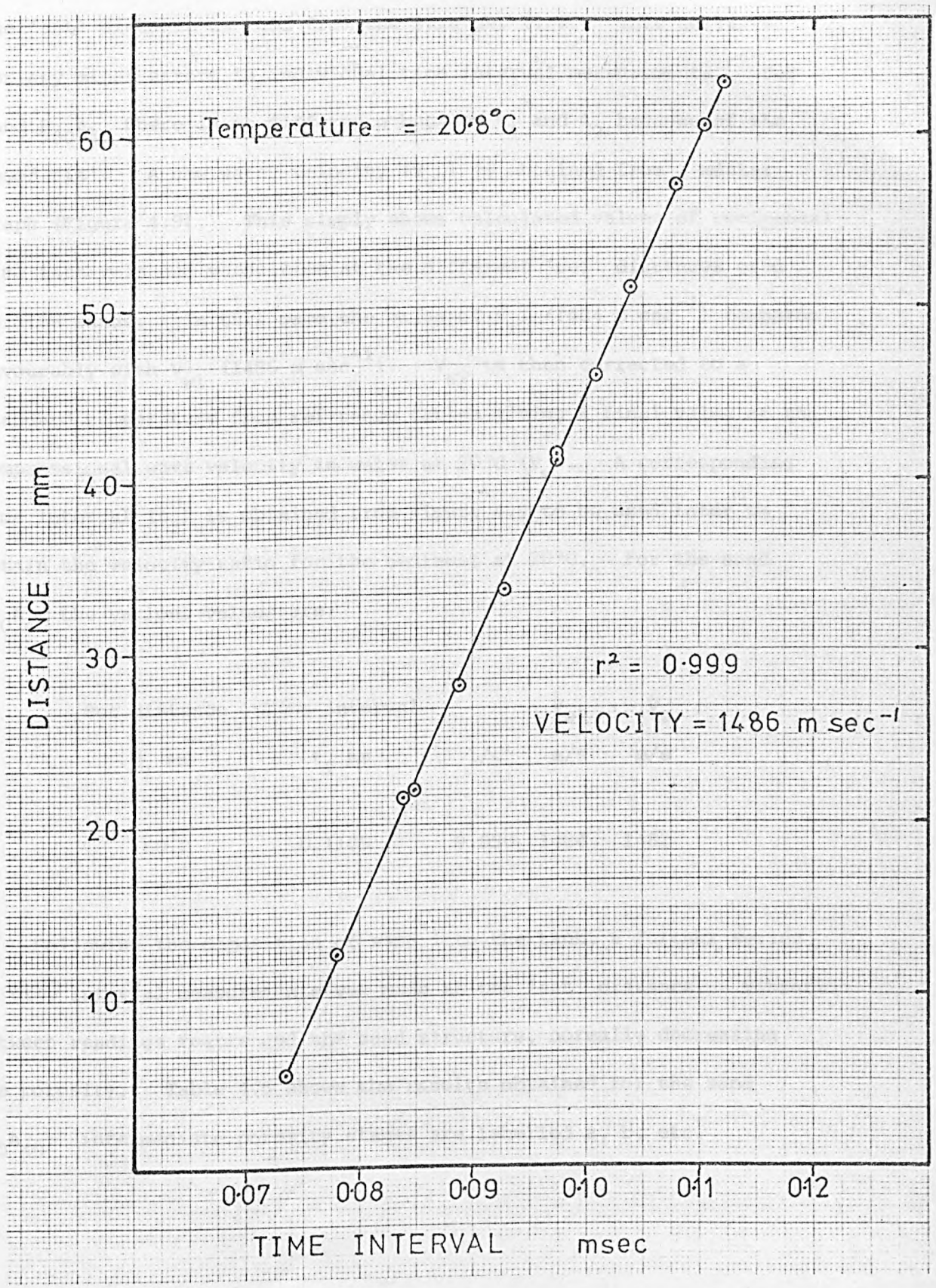

FIGURE 4.8 Distance vs Time Interval for compressional waves through water in the ARL tank

the 'set' distance is read from the straight line. This corrects for any minor errors in individual time interval measurements. For sand $B_{60}A_{40}$ there is no difference between t_1 and t_2 because of the 'good fit'. A new water velocity (V_{w2}) is obtained from a master graph (Figure 4.9). This simply shows calculated values of reciprocal time intervals and velocities at the different 'set' distances used for the sands. In this case the value of V_{w2} (1484 m sec^{-1}) compares favourably with V_{w1} (1486 m sec^{-1}). V_{w2} is then corrected to a standard temperature from reference tables giving a final value of the compressional wave velocity in water at 20°C (V_w). A corresponding time interval (t_3) is obtained from Figure 4.9 to be used later to obtain the velocity ratio for the sediment at 20°C. For the sand $B_{60}A_{40}$ the various values are:

Set distance d_1 mm	Time interval t_2 ms	$1/t^2$	V_{w2} m/s	V_w m/s
60.0	0.1105	9.050	1484	1482

Following the deposition of sand into the tank, a further series of time interval measurements was made at the 'set' distance. Vibration between readings rearranged the sand structure, normally decreasing the porosity. Table 4.5 shows the results obtained for the sand $B_{60}A_{40}$; intermediate porosity stages are labelled a, b, etc.

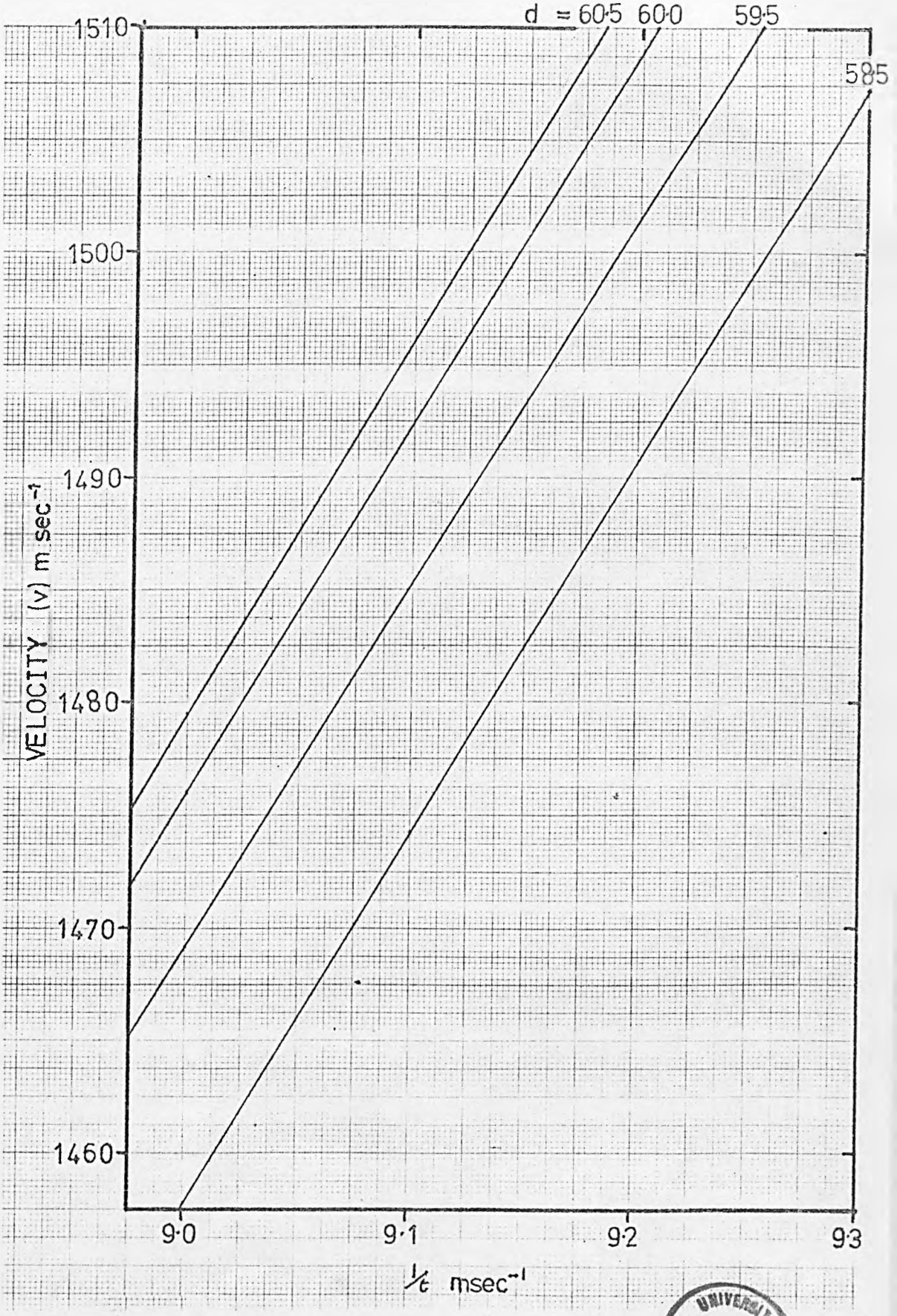

FIGURE 4.9 Velocity vs $1/t$ at different set distances in the ARL tank

	FRACTIONAL POROSITY n	TIME INTERVAL t_4 ms	
a	0.396	0.0950	Sand $B_{60}A_{40}$
b	-	0.0945	Temperature 20.6°C
c	-	0.0935	Resonant Frequency
d	-	0.0920	112.821 kHz
e	0.346	0.0915	'Set' distance 60.0 mm

TABLE 4.5 - COMPRESSIONAL WAVE TIME INTERVALS AT THE SET DISTANCE FOR SAND $B_{60}A_{40}$ AT DIFFERENT POROSITIES

Porosity 'a' is the highest porosity obtainable using the slow deposition technique, its value is calculated from the procedure described earlier. The most compact packing state, porosity 'e', is reached when the time interval reaches a minimum after long vibration times. Although numerical values of porosity for intermediate packing states are not available using this technique, the observation of a steadily decreasing time interval (i.e. increasing velocity) indicates that the sand structure is decreasing in porosity without exhibiting any irregular behaviour.

Limiting time intervals (t_4), those at porosity 'a' and 'e', have been used with the 'set' distance to read the velocity (V_{p1}) from a graph similar to Figure 4.9 in the appropriate velocity range. This was corrected to 20°C (V_{p2}) and a new time interval (t_5) obtained. The velocity ratio (VR) between water and sand at 20°C then becomes t_3/t_5. Finally, the compressional wave velocity (V_p) for the sand at the given porosity is calculated from

$$V_p = VR \times V_w$$

For the sand $B_{60}A_{40}$

V_w ms^{-1}	t_3 ms	n	t_4 ms	V_{p1} ms^{-1}	V_{p2} ms^{-1}	t_5 ms	VR	V_p ms^{-1}
		0.396	0.0950	1726	1724	0.0951	1.164	1725
1482	0.1107							
		0.346	0.0910	1802	1800	0.0911	1.215	1801

A second method for evaluating the velocity in sand was used after the above measurements were completed. Time interval and distance measurements were taken as the transducers were moved closer together. Primarily, the purpose of the set of readings was to obtain amplitude values so that the wave attenuation could be evaluated, but time intervals were also recorded so that a second value of the velocity in sand was obtained. Movement of the transducer between readings inevitably led to a structural disturbance in and around the wave path. In an attempt to retain the minimum porosity obtained previously by vibration, the tank was vibrated during and after each movement of the transducer. Table 4.6 shows the results of this set of measurements for the sand $B_{60}A_{40}$ which are shown graphically in Figure 4.10.

RELATIVE TRANSDUCER SEPARATION, d mm	TIME INTERVAL ms	
60.0	0.0910	Sand $B_{60}A_{40}$
56.0	0.0885	Temperature 20.8°C
51.0	0.0860	Resonant Frequency
46.0	0.0830	112.821 kHz
41.5	0.0800	Velocity 1831 ms^{-1}
35.5	0.0755	Velocity corrected
31.5	0.0750	to 20°C 1829 ms^{-1}
26.5	0.0725	
20.5	0.0690	
14.5	0.0660	

TABLE 4.6 - DISTANCE AND TIME MEASUREMENTS FOR COMPRESSIONAL WAVES IN SAND $B_{60}A_{40}$

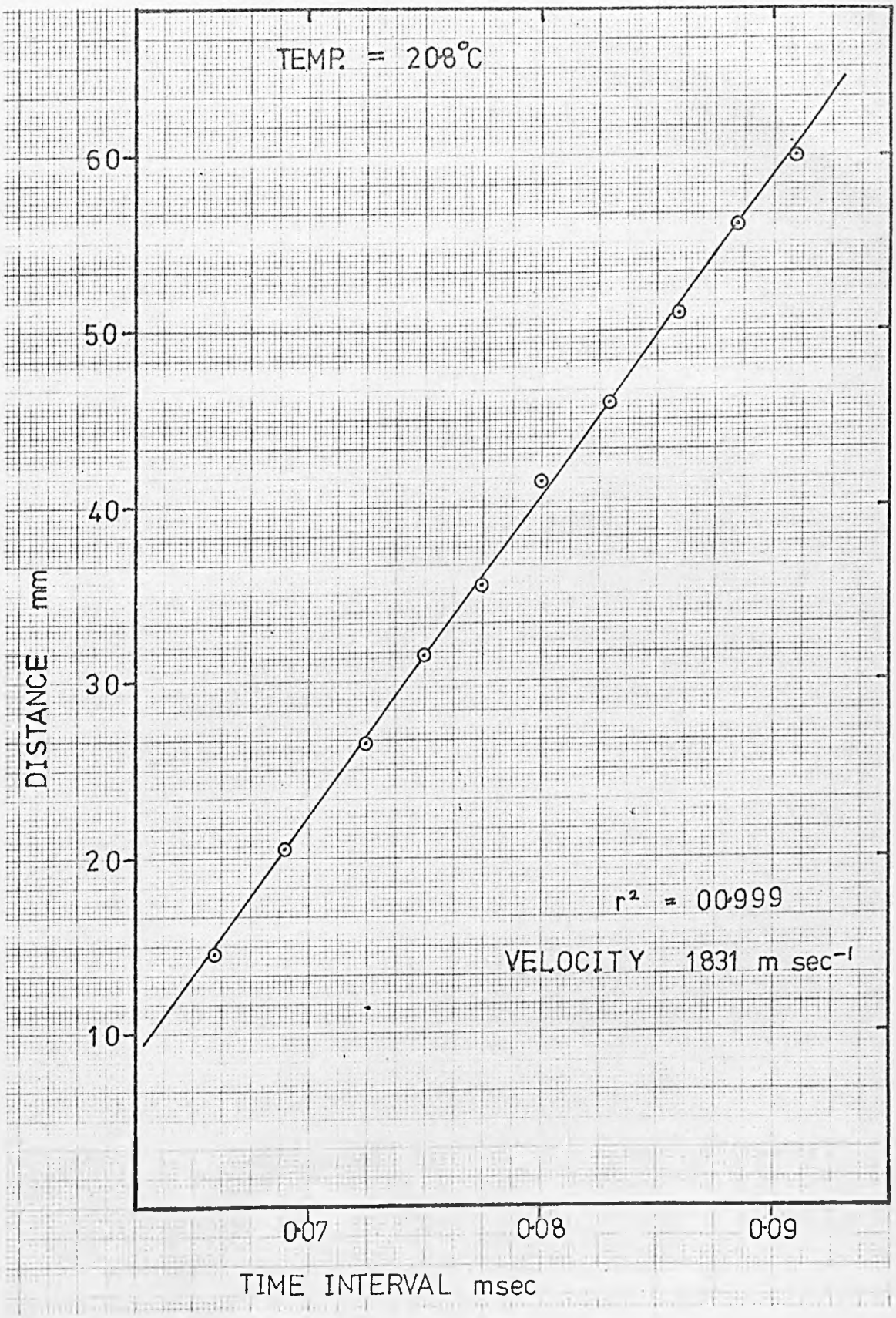

FIGURE 4.10 Distance vs Time Interval for compressional waves in sand $B_{60}A_{40}$

Differences between the two velocities (1801 and 1829 ms^{-1}) are attributed to the structural disturbance caused by the second method. The higher velocity resulting because the action of pushing the transducers closer together further decreases the porosity in the vicinity of the transducers. To ascertain the importance of the transducer movement on the sand structure and velocity, an experiment was performed on sand A. Two sets of distance-time interval measurements were recorded; one with the transducers moving together with vibration, the other without vibration and with the transducers moving apart. In the first case a velocity of 1758 ms^{-1} was obtained with a correlation coefficient (r^2) of 0.999. In the second case, a velocity of 1696 ms^{-1} was obtained with a correlation coefficient of 0.994. The difference in velocity (3.5%) and the lower correlation coefficient with the second method illustrates the care that must be exercised when interpreting results of this kind. In the light of this evidence the compressional wave velocities used are those obtained from the velocity ratio method.

Final values for all the sands tested are presented in Table 4.7 and graphically in Figure 4.11.

In Figure 4.11 the broken lines are linear extrapolations to the minimum and maximum porosities. Table 4.8 presents the complete set of values (both experimental and extrapolated) of compressional wave velocities and porosities. Figure 4.12 is a plot of relative porosity again compressional wave velocity using values from Table 4.8.

Amplitude measurements on the received wave form at varying transducer separations has enabled attenuation coefficients to be calculated. Table 4.9 shows both the raw data and computations used to evaluate the attenuation coefficient (α) for the sand $B_{60}A_{40}$. The measured distance (d) is converted into the true separation between the transducer faces (D).

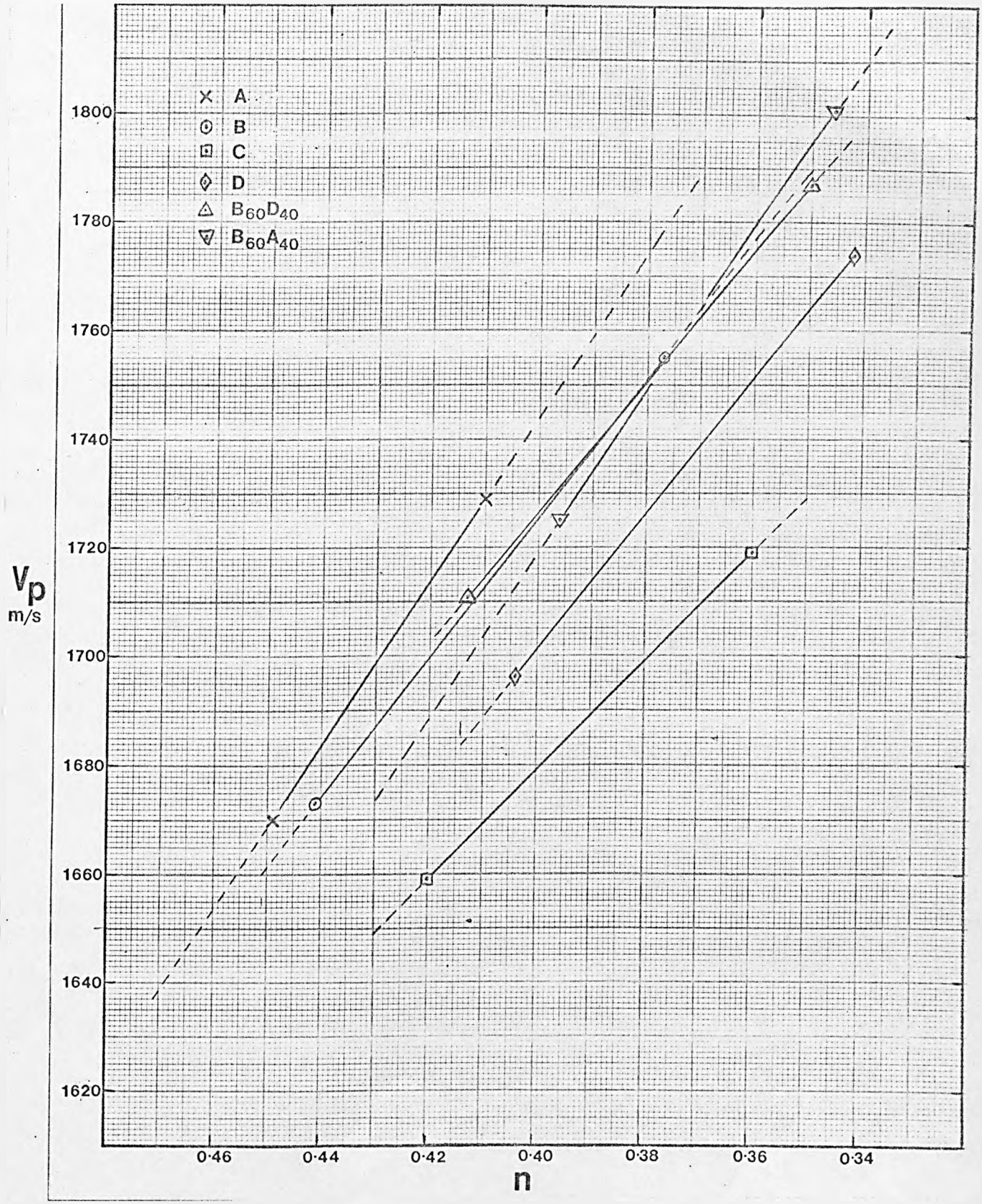

FIGURE 4.11 Compressional Wave Velocity vs Porosity for the ARL sands

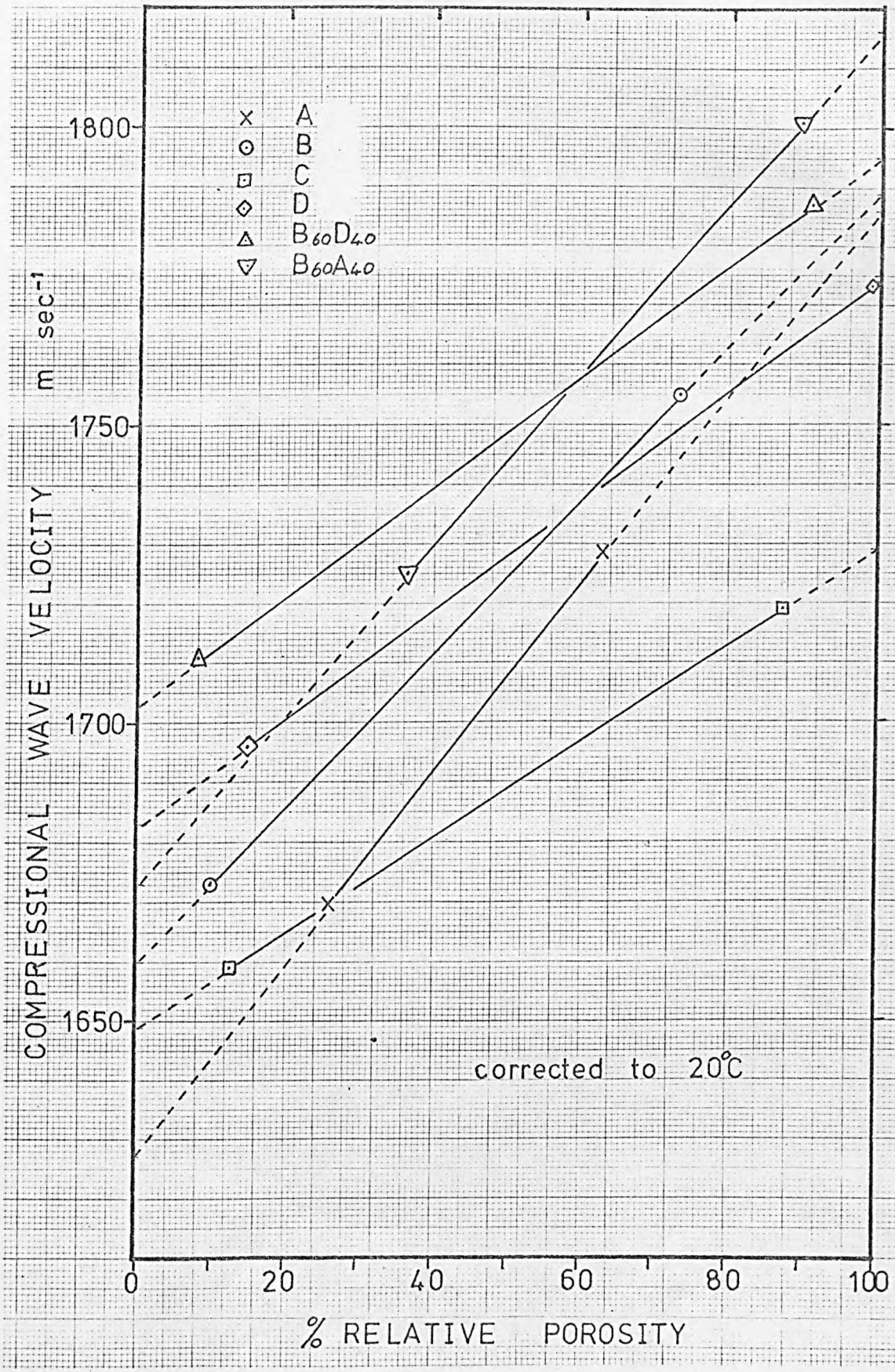

FIGURE 4.12 Compressional Wave Velocity vs Relative Porosity for the ARL sands

Amplitude (A) was measured in volts directly off the oscilloscope from the chosen part of the received wave-form. The largest separation has been used as a reference distance so that the voltages can be converted into relative decibel values (A_1) using:

$$A_1 = 20 \log \frac{A}{0.43} \text{ dB}$$

Spherical spreading losses (SL) of the wave are calculated from:

$$SL = 20 \log \frac{D}{0.1560} \text{ dB}$$

The difference between A_1 and SL represents the energy loss caused by the sand body after correcting for spreading.

SAND	POROSITY n	VELOCITY V_p ms^{-1}	
A	0.449	1670	Temperature 20°C
	0.410	1729	Frequency 112 kHz
B	0.441	1673	
	0.377	1755	
C	0.420	1659	
	0.360	1719	
D	0.404	1696	
	0.342	1774	
$B_{60}D_{40}$	0.413	1711	
	0.350	1787	
$'B_{60}D_{40}$	0.396	1725	
	0.346	1801	

TABLE 4.7 - COMPRESSIONAL WAVE MEASUREMENTS FOR THE ARL SANDS TESTED

SAND	POROSITY n	RELATIVE POROSITY %	VELOCITY V_p ms^{-1}
A	0.477	0.0	1627
	0.449	26.4	1670
	0.410	63.2	1729
	0.371	100.0	1786
B	0.451	0.0	1660
	0.441	9.9	1673
	0.377	73.3	1755
	0.350	100.0	1789
C	0.430	0.0	1649
	0.420	12.5	1659
	0.360	87.5	1719
	0.350	100.0	1729
D	0.410	0.0	1683
	0.404	13.9	1696
	0.342	100.0	1774
	0.342	100.0	1774
$B_{60}D_{40}$	0.419	0.0	1703
	0.413	7.9	1711
	0.350	90.8	1787
	0.343	100.0	1795
$B_{60}A_{40}$	0.430	0.0	1673
	0.396	36.2	1725
	0.346	89.4	1801
	0.336	100.0	1816

TABLE 4.8 - MEASURED AND EXTRAPOLATED VALUES OF COMPRESSIONAL WAVE VELOCITY, POROSITY AND RELATIVE POROSITY FOR ALL THE SANDS TESTED IN THE ARL TANK

d	D	A	A_1	SL	A_1 - SL
mm	m	volts	dB	dB	dB
60.0	0.156	0.43	0.00	0.00	0.00
56.0	0.152	0.43	0.00	0.25	-0.25
51.0	0.147	0.46	0.59	0.53	0.06
46.0	0.142	0.47	0.77	0.84	-0.07
41.5	0.137	0.48	0.96	1.13	-0.17
35.5	0.132	0.52	1.65	1.49	0.16
31.5	0.127	0.55	2.14	1.79	0.35
26.5	0.122	0.60	2.89	2.12	0.77
20.5	0.116	0.68	3.98	2.55	1.43
14.5	0.110	0.76	4.95	3.04	1.91

TABLE 4.9 - AMPLITUDE MEASUREMENTS AND CONVERSION TO dB VALUES CORRECTED FOR SPREADING LOSS IN THE SAND $B_{60}A_{40}$

To obtain the attenuation coefficient (α) a linear plot of distance (D) against amplitude minus spreading loss (A_1 - SL) was plotted; Figure 4.13 shows this graph for the sand $B_{60}A_{40}$. A straight line was 'fitted' to the experimental points using the least squares method; the slope of this line being the attenuation coefficient, α dB m^{-1}. The spread of results in Figure 4.13 is not typical of the sands tested so the results from sand $B_{60}D_{40}$ are also plotted (Figure 4.14). In an attempt to establish how the attenuation varies with changes in porosity, the amplitude recorded when the sand was initially deposited has been used (this value was not recorded for the sands A and B). For the sand $B_{60}A_{40}$ this amplitude was 0.39 volts = 0.848 dB, dividing by the 'set' distance (0.156m) produces an extra 5.4 dB m^{-1}. Results for all the sands tested are presented in Table 4.10 and plotted against porosity in Figure 4.15.

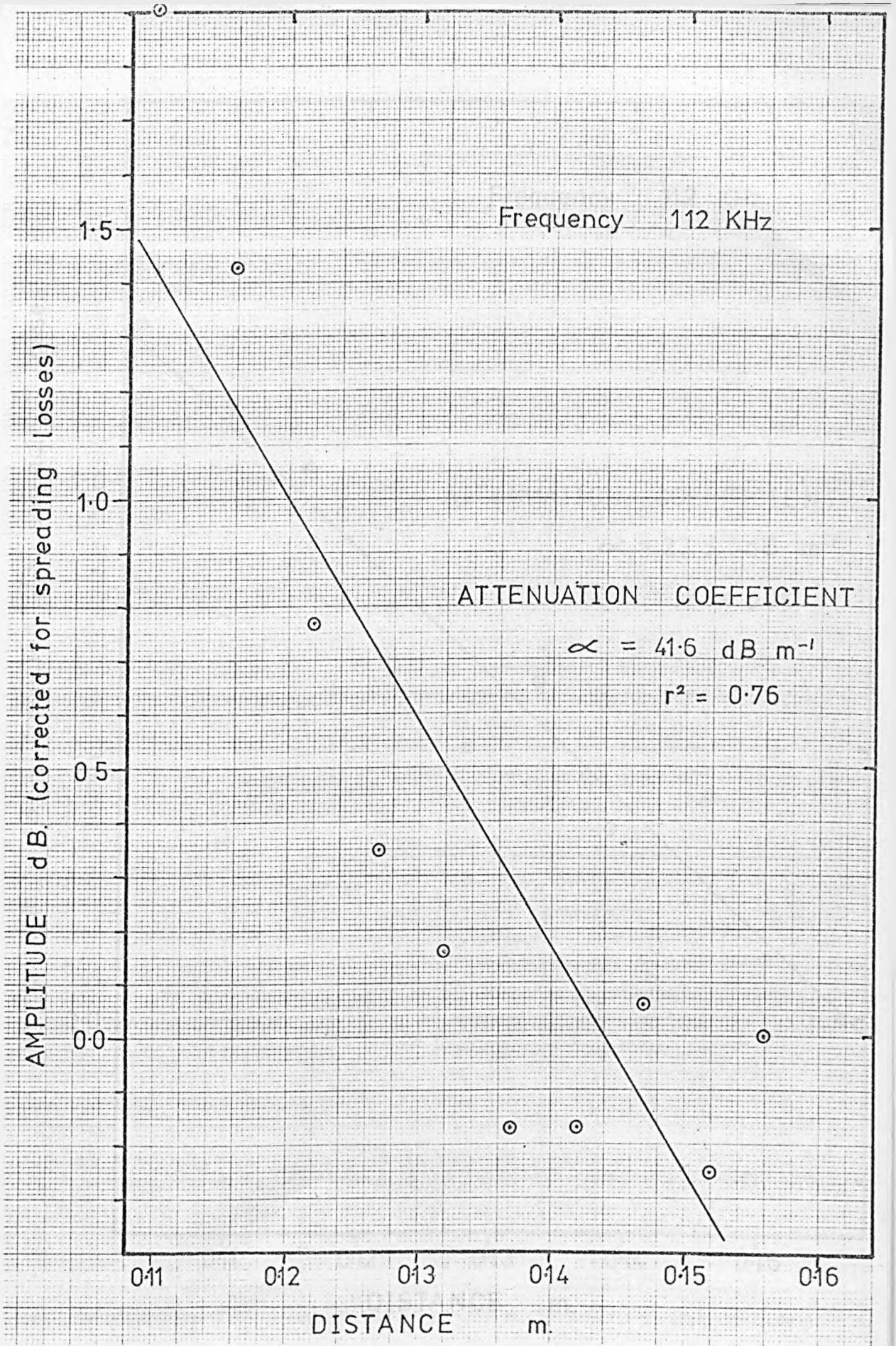

FIGURE 4.13 Compressional Wave Amplitude vs Distance for sand $B_{60}A_{40}$

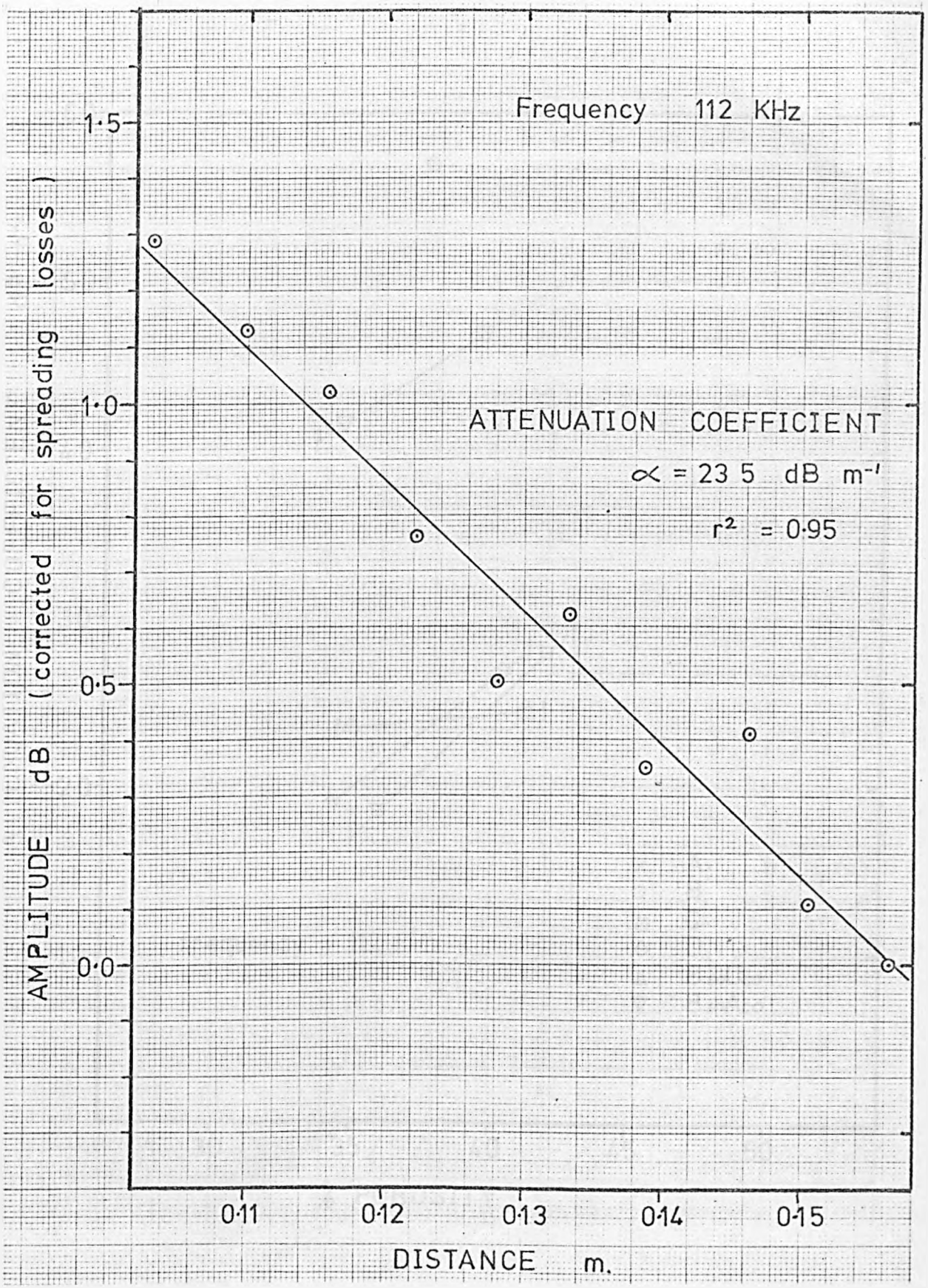

FIGURE 4.14 Compressional Wave Amplitude vs Distance for sand $B_{60}D_{40}$

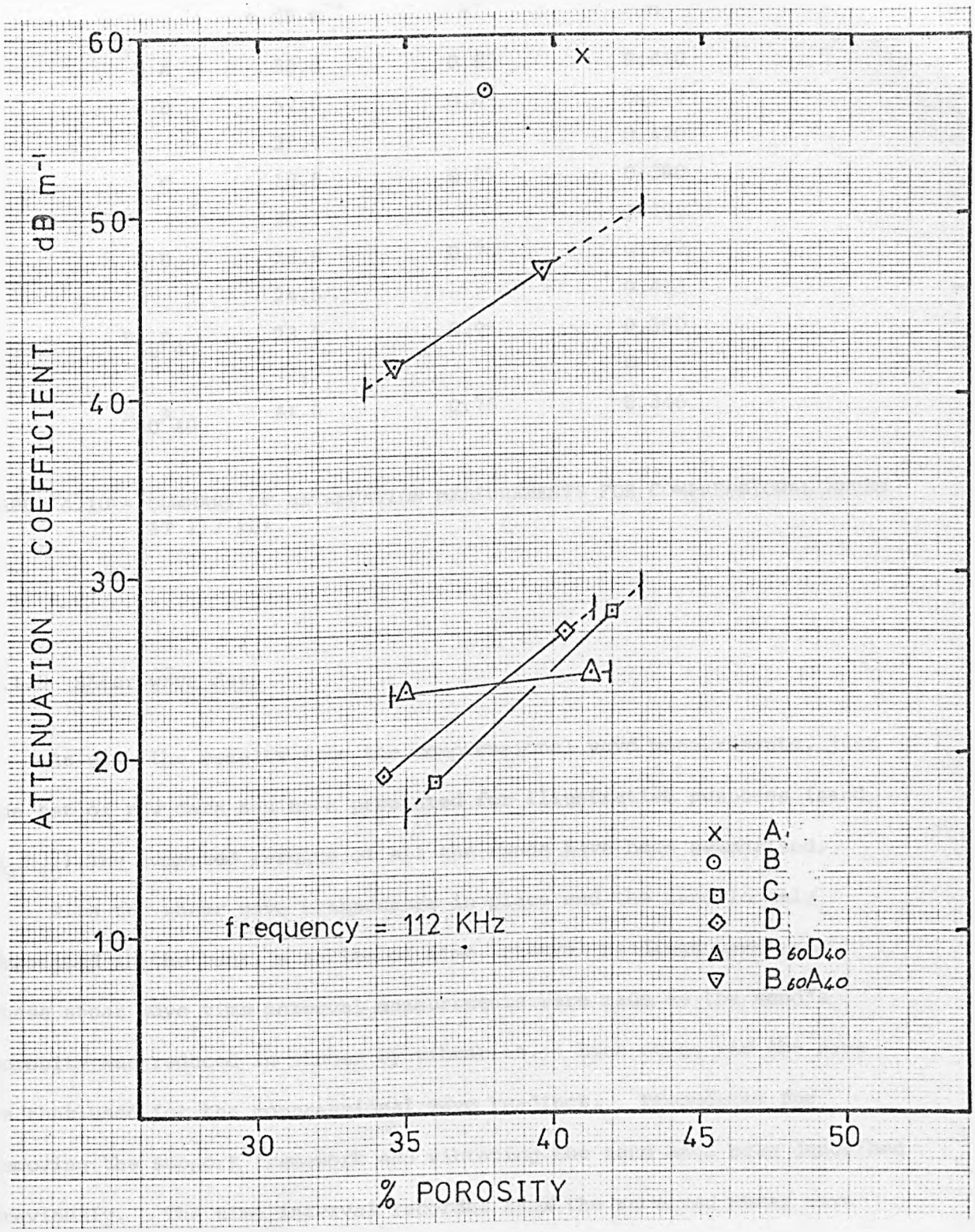

FIGURE 4.15 Attenuation Coefficient vs Porosity for the ARL sands

SAND	ATTENUATION COEFFICIENT α dB m^{-1}	CORRELATION COEFFICIENT r^2	FRACTIONAL POROSITY n
A	58.8	0.80	0.410
B	57.0	0.69	0.377
	27.7		0.420
C	18.5	0.87	0.360
	26.7		0.404
D	18.9	0.75	0.342
	24.5		0.413
$B_{60}D_{40}$	23.5	0.95	0.350
	47.0		0.396
$B_{60}A_{40}$	41.6	0.76	0.346

TABLE 4.10 - SUMMARY OF ATTENUATION MEASUREMENTS FOR COMPRESSIONAL WAVES AT 112 kHz.

4.1.5 Shear wave data

As with the results from the compressional wave measurements, just one set of raw data has been presented for illustrative purposes (sand $B_{60}A_{40}$). The computed results of all the sands have been summarised.

With the shear wave transducers in place and the sand loosely deposited in the tank, a series of time interval readings were made. These shear wave time interval measurements were made as the sand's porosity was reduced in stages by vibration. Each stage was the same as that used for the compressional wave readings. Procedures for removing the support framework and vibrating the sand have been described previously. The time interval recorded from the received shear wave was longer than the real time taken for the pulse onset; a consistently recognisable feature had to be used (see Figure 4.7). Table 4.11 shows the measured time intervals for shear waves in the sand $B_{60}A_{40}$ at

different porosity stages.

	FRACTIONAL POROSITY n	TIME INTERVAL msec	
a	0.396	2.543	
b	-	2.389	Temperature 20.6°C
c	-	2.187	Frequency 1600 Hz
d	-	1.979	
e	0.346	1.636	

TABLE 4.11 - SHEAR WAVE TIME INTERVALS AT THE SET DISTANCE FOR SAND $B_{60}A_{40}$ AT DIFFERENT POROSITIES.

As with the compressional wave measurements, only the first and last porosity stages have numerical values but the regular behaviour (decreasing time interval) between each period of vibration once again indicated that the vibration caused a steady reduction in porosity.

Unlike the compressional waves, which propagate through water, no simple reference for obtaining a shear wave velocity ratio is available. Consequently, a series of time interval measurements at varying transducer distances had to be performed. These measurements were made, along the length of the tank, after the vibration programme had been completed. These results for the sand $B_{60}A_{40}$ are shown in Table 4.12 and plotted in Figure 4.16. Changes in distance between the two probes was controlled by the slotted spacer which had slots machined at half-inch intervals.

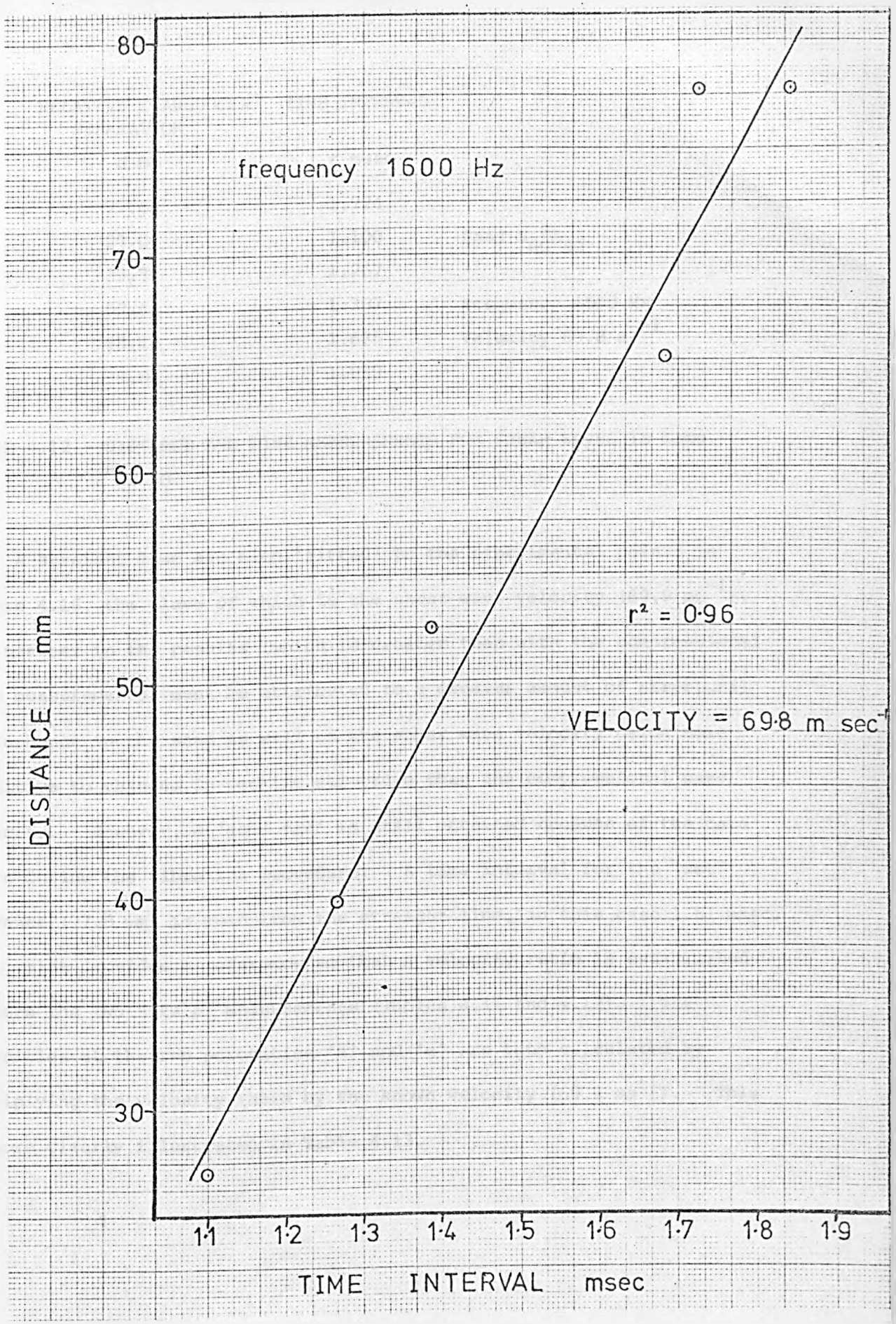

FIGURE 4.16 Distance vs Time Interval for shear waves in sand $B_{60}A_{40}$

RELATIVE TRANSDUCER SEPARATION d mm	TIME INTERVAL t msec	
77.8	1.724	
27.0	1.100	Sand $B_{60}A_{40}$
39.7	1.267	
52.4	1.387	Frequency 1600 Hz
65.1	1.685	Velocity 69.8 ms^{-1}
77.8	1.839	

TABLE 4.12 - DISTANCE AND TIME MEASUREMENTS FOR SHEAR WAVES IN SAND $B_{60}A_{40}$.

A straight line has been 'fitted' to the experimental points in Figure 4.16, the slope of which is the shear wave velocity (69.8 ms^{-1}). The scatter in the results (which is greater than with the compressional wave measurements) must be attributed to a greater amount of structural disturbance in the sand as well as the shear wave velocity being more sensitive to changes in packing structure than the compressional wave velocity. However, a 'good fit' is still obtained because of the care taken during the vibration procedure. A time interval for the 'set' distance (77.8 mm) is read from the straight line, in this case 1.81 msec. This value provides a reference so that a velocity ratio is established between the two sets of measurements (Tables 4.11 and 4.12). The velocities at the two porosities 'a' and 'e' are then calculated by multiplying the velocity ratio by the known velocity (69.8 ms^{-1}). This is more clearly illustrated in Table 4.13.

	FRACTIONAL POROSITY n	VELOCITY RATIO VR	SHEAR WAVE VELOCITY VR x 69.8 ms^{-1}
a	0.396	$\frac{1.81}{2.543} = 0.712$	49.7
e	0.346	$\frac{1.81}{1.636} = 1.107$	77.2

TABLE 4.13 - CALCULATION OF SHEAR WAVE VELOCITY FOR DIFFERENT POROSITIES IN SAND $B_{60}A_{40}$.

Shear wave velocities have been calculated in a similar way at the limiting porosities obtained by vibration in the tank. These values have been plotted against porosity in Figure 4.17 and linear extrapolations, to the maximum and minimum porosities, are shown by the broken lines. Table 4.14 summarises both the experimental and extrapolated shear wave velocities for all the sands tested. In Figure 4.18 a linear plot of shear wave velocity against relative porosity is shown for each sand; the broken line again indicates the extrapolated regions.

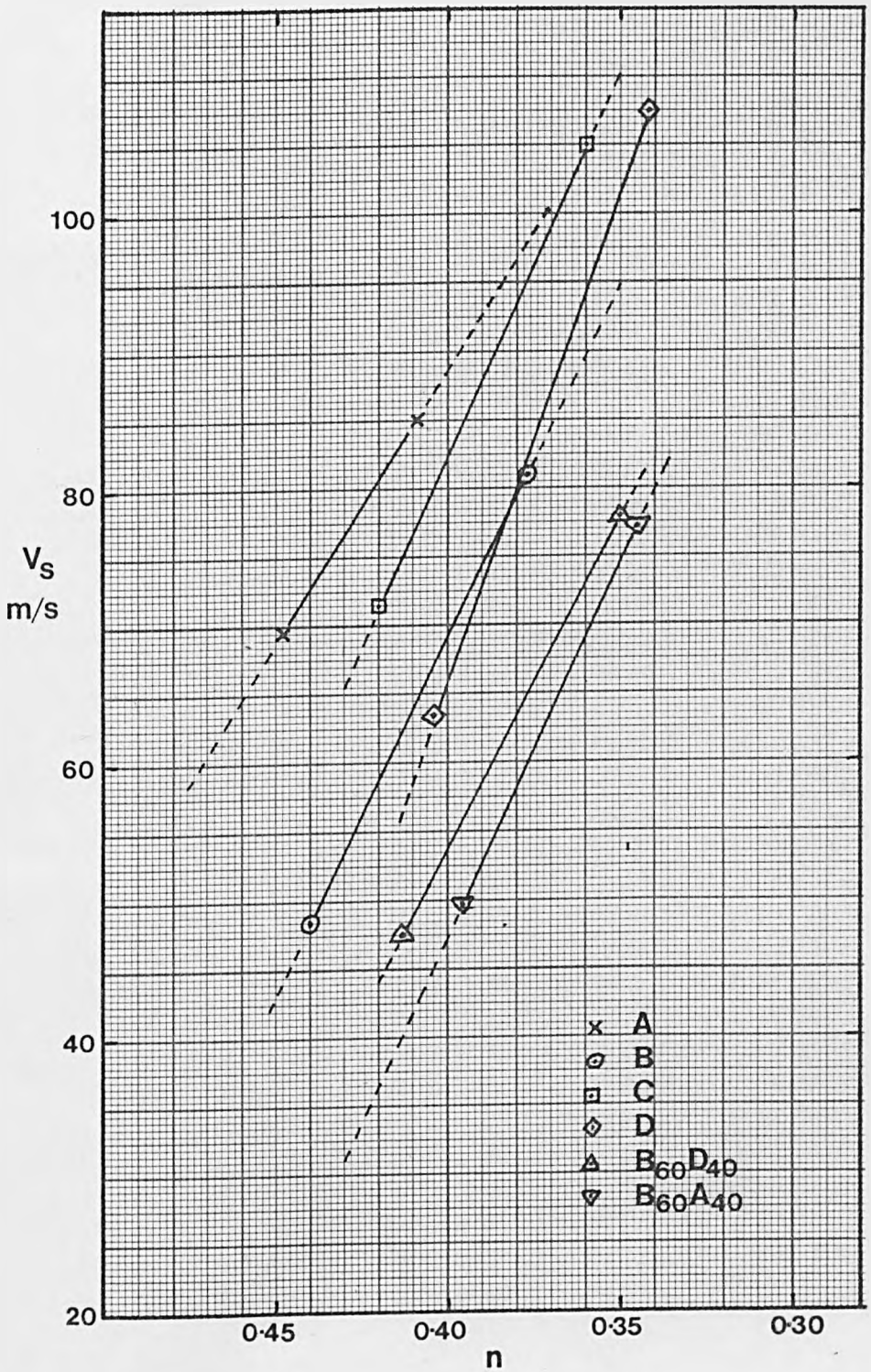

FIGURE 4·17 Shear Wave Velocity vs Porosity for the ARL sands

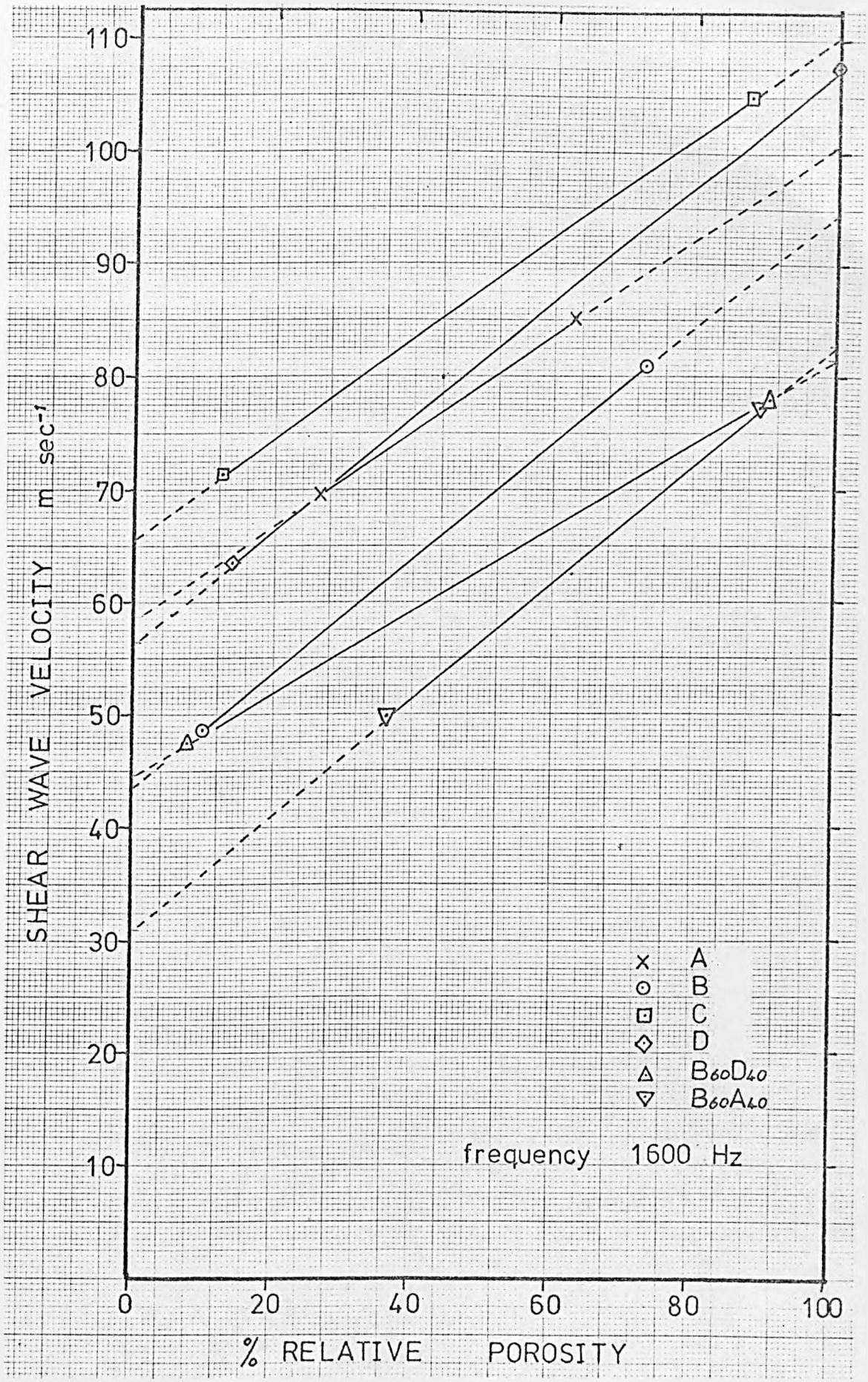

FIGURE 4.18 Shear Wave Velocity vs Relative Porosity for the ARL sands

SAND	POROSITY n	RELATIVE POROSITY %	VELOCITY V_s ms^{-1}
A	0.477	0.0	58.6
	0.449	26.4	69.7
	0.410	63.2	85.1
	0.371	100.0	100.5
B	0.451	0.0	43.7
	0.441	9.9	48.7
	0.377	73.3	80.9
	0.350	100.0	94.5
C	0.430	0.0	65.5
	0.420	12.5	71.3
	0.360	87.5	105.0
	0.350	100.0	110.5
D	0.410	0.0	56.4
	0.404	13.9	63.5
	0.342	100.0	107.4
	0.342	100.0	107.4
$B_{60}D_{40}$	0.419	0.0	44.6
	0.413	7.9	47.5
	0.350	90.8	78.0
	0.343	100.0	81.4
$B_{60}A_{40}$	0.430	0.0	31.0
	0.396	36.2	49.7
	0.346	89.4	77.2
	0.336	100.0	82.7

TABLE 4.14 - MEASURED AND EXTRAPOLATED VALUES OF SHEAR WAVE VELOCITY, POROSITY AND RELATIVE POROSITY FOR ALL THE SANDS TESTED IN THE ARL TANK.

4.2 Jackson's Porosity Cell

4.2.1 Introduction

The ARL experiments, while providing an interesting initial data base for the behaviour of shear waves in unconsolidated sands, had several undesirable features.

(a) The ARL tank and vibration unit were not specifically designed for the purpose for which they were used. Consequently, the vibration modes established probably caused significant porosity variations throughout the sample which could explain some of the scatter in the data. It also meant that the 'setting up' procedure was extremely laborious and not well controlled.

(b) As a consequence of (a), only the limiting porosities could be ascertained.

(c) The shear wave transducers were designed with imposed constraints which were not relevant to these experiments.. A flat radiating surface for the active face of the transducers was the primary irrelevant constraint which was imposed. It has been shown that this constraint, compared with later designs, must severely limit the shear strain energy transmitted to the sediment as well as drastically reducing the sensitivity of the receiver.

(d) As a result of (c) the received shear wave signal is not as well defined as it might be and has an extremely low amplitude. Close band pass filtering and isolation from the container provided an acceptable solution at the time that was, however, neither elegant nor convenient.

(e) The number of sands tested was small.

Despite the practical difficulties of using the ARL systems, the

initial set of data was considered to be reliable and valid but its limitations have already been described. Developments in transducers designed specifically for this application, together with the control and instrumentation of Jackson's Porosity Cell, offered the opportunity of extending these variable porosity tests on a wider range of sands.

4.2.2 Sediment description

In the porosity cell 19 artificial sediments were tested. All were obtained from sieve fractions except sands L and N which were naturally occurring beach deposits. Sands E, F, G, H, J, K, L, M and N were nearly pure (>98%) quartz sands. Sands $N_{80}F_{20}$, $N_{60}F_{40}$, $N_{50}F_{50}$, $N_{40}F_{60}$, $N_{20}F_{80}$ and $N_{20}K_{80}$ were mixtures of sands N, F and K where the subscripts indicate the respective weight of the component sand in per cent. Sands S1, S3.5 and S4 consist of commercially available solid glass spheres taken from 1ϕ, 3.5ϕ and 4ϕ sieves. The final sample consists of sieved, crushed shell fragments (-1—0ϕ). Cumulative grain size distributions for all these samples are plotted in Figures 4.19 and 4.20. In Table 4.15 the statistical grain size parameters defined previously are given.

Grain shape was estimated using a binocular microscope from a sample of 100 grains for each of the primary samples (i.e. excluding the composite sands). The roundness distributions for these samples are plotted in Figure 4.21. Since a larger number of samples was used in these tests than compared with the ARL tank (6), the roundess is plotted on a linear basis using the roundess scale of Powers 1953. This enables small differences in mean roundness (R_{50}) to be distinguished by assigning a roundness value to each sand. These values are shown in Table 4.16.

Unlike the ARL sands there is a large variation in the sphericity

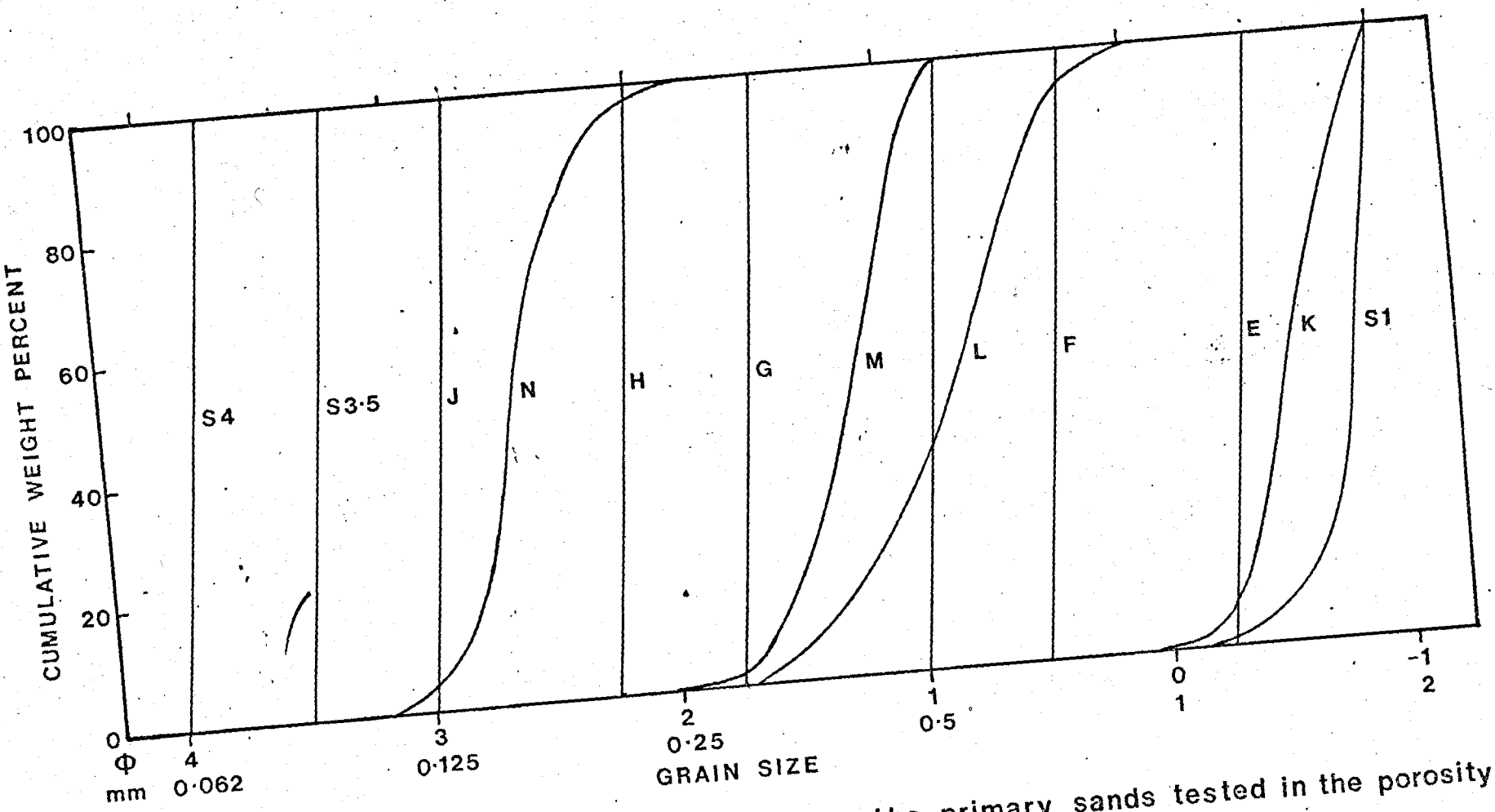

FIGURE 4·19 Grain Size distributions for the primary sands tested in the porosity cell

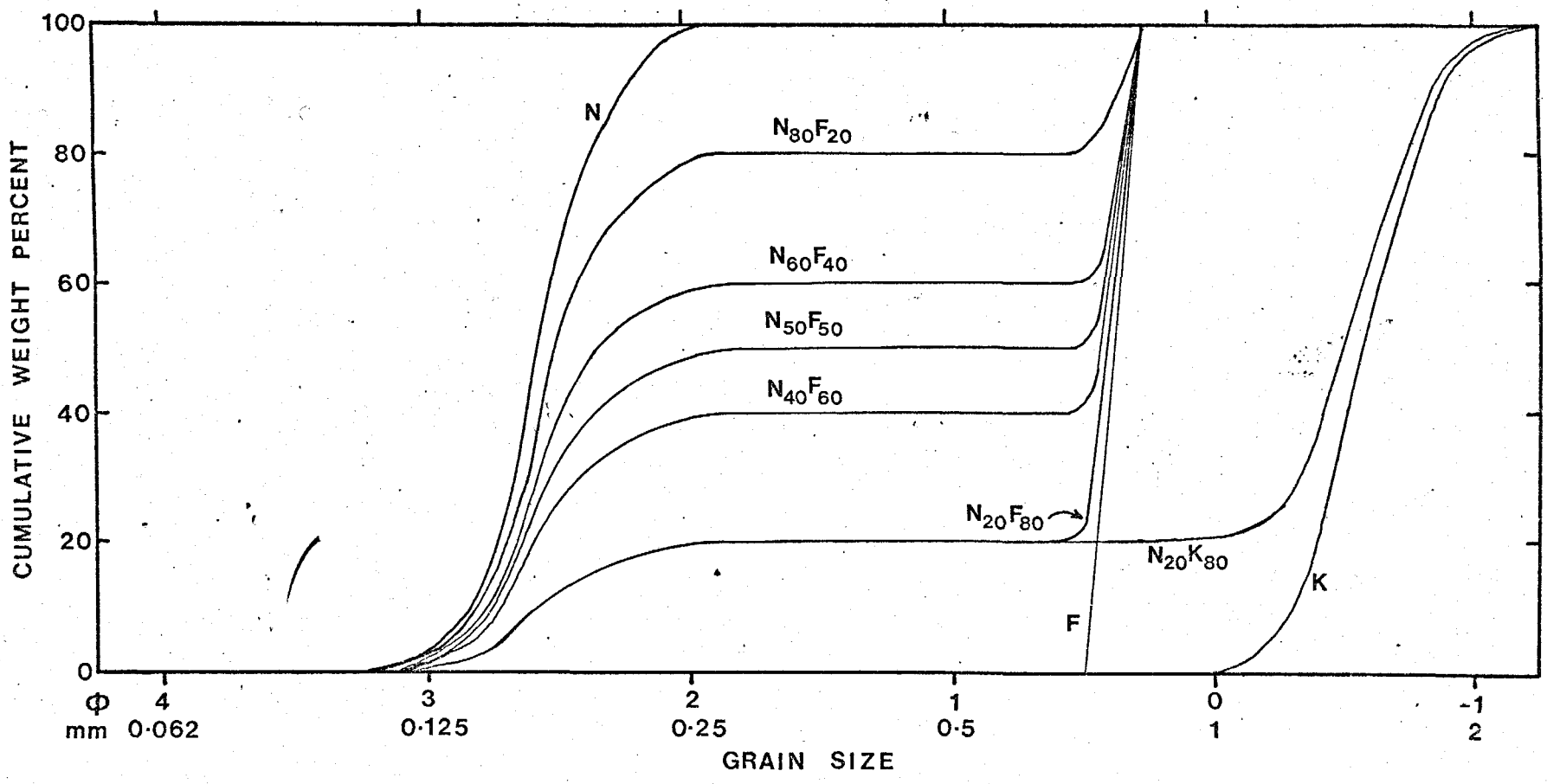

FIGURE 4·20 Grain Size distributions for the mixed sands tested in the porosity cell

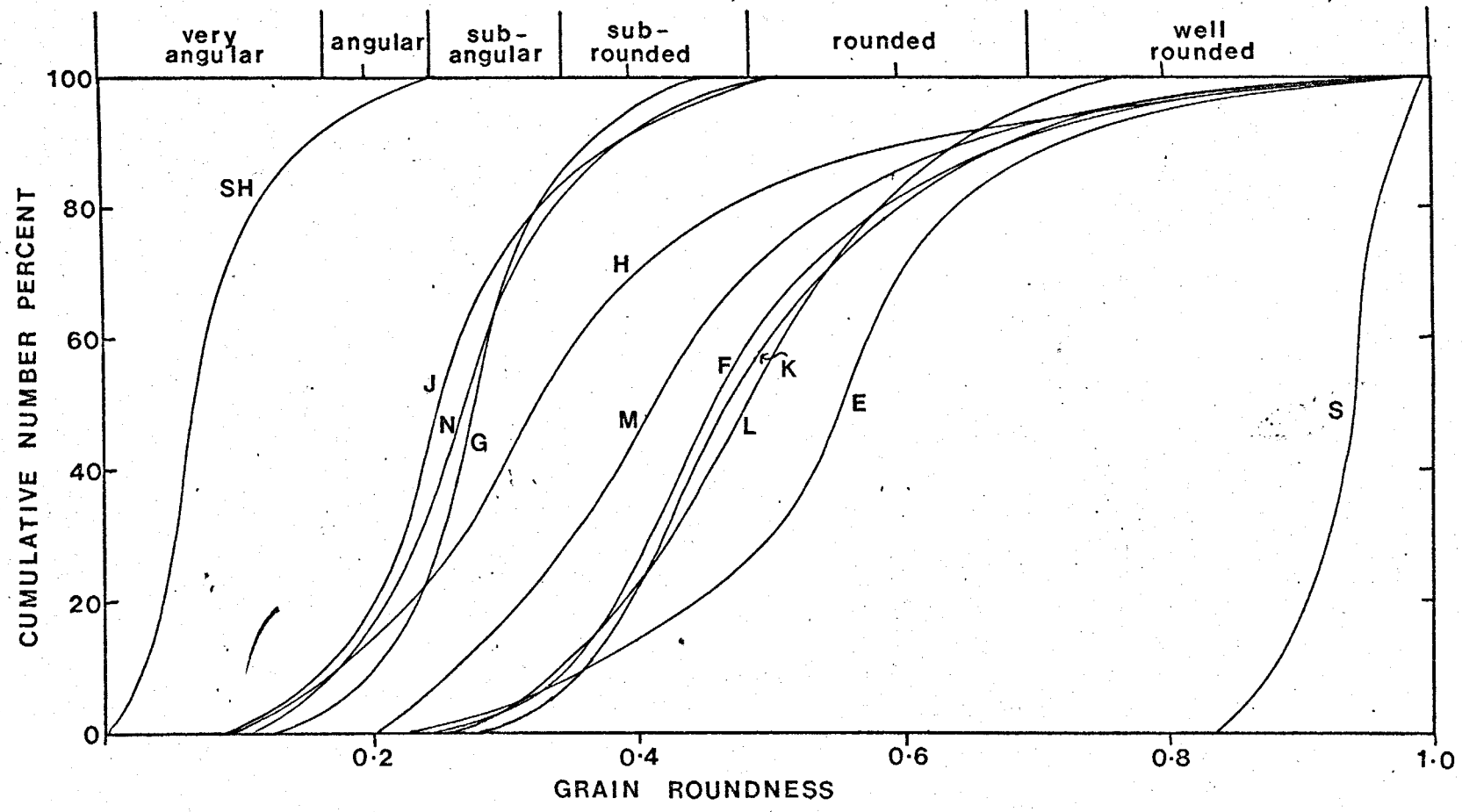

FIGURE 4·21 Grain Roundness distributions for the primary sands tested in the porosity cell

of these samples. While most of the samples would be described as roughly equidimensional or nearly spherical the glass spheres (S1, S3.5 and S4) were almost completely spherical whereas the shell fragments consisted of a variety of shapes of very low sphericities. In fact, most of the shell fragments would be best described as 'plate-like'.

Unlike the ARL procedures, separate techniques were not required to measure the seismic velocities and to ascertain maximum and minimum porosities for each sample. The porosity cell and vibration table allows the maximum porosity to be determined at the beginning of each test (by very slow deposition in water) and the minimum porosity to be determined at the end of each test (by the vibration procedure). The maximum and minimum porosities for each sample and their differences are summarised in Table 4.16.

SAND	D_M	S_p	Sk_p	K_p
E	-0.375	-0.077	0.000	0.857
F	0.375	-0.077	0.000	0.857
G	1.625	-0.077	0.000	0.857
H	2.125	-0.077	0.000	0.857
J	2.875	-0.077	0.000	0.857
K	-0.588	-0.225	0.078	0.978
L	0.797	-0.386	-0.177	0.906
M	1.202	-0.255	-0.162	0.922
N	2.552	-0.238	0.125	1.071
S1	-0.875	-0.077	0.000	0.857
S3.5	3.375	-0.077	0.000	0.857
S4	3.875	-0.077	0.000	0.857
$N_{80}F_{20}$	1.887	-0.980	0.758	2.164
$N_{60}F_{40}$	1.782	-0.993	0.638	0.473
$N_{50}F_{50}$	1.390	-0.983	-0.360	0.421
$N_{40}F_{60}$	1.118	-0.969	-0.882	0.541
$N_{20}F_{80}$	1.012	-0.893	-0.904	7.260
$N_{20}K_{80}$	0.357	-1.344	-0.791	3.342
SH				

TABLE 4.15 - STATISTICAL MEASURES FROM THE GRAIN SIZE ANALYSES FOR THE SANDS TESTED IN THE POROSITY CELL.

SAND	R_{50}	n_{max}	n_{min}	$n_{max} - n_{min}$
E	0.56	0.452	0.344	0.108
F	0.46	0.448	0.350	0.098
G	0.28	0.473	0.379	0.094
H	0.33	0.478	0.386	0.092
J	0.25	0.481	0.399	0.082
K	0.47	0.444	0.337	0.107
L	0.48	0.446	0.344	0.102
M	0.41	0.443	0.336	0.107
N	0.28	0.466	0.370	0.096
S1	0.95	0.362	0.311	0.051
S3.5	0.95	0.380	0.308	0.072
S4	0.95	0.407	0.326	0.081
$N_{80}F_{20}$	0.31	0.425	0.356	0.069
$N_{60}F_{40}$	0.35	0.394	0.307	0.087
$N_{50}F_{50}$	0.37	0.387	0.303	0.084
$N_{40}F_{60}$	0.38	0.390	0.289	0.101
$N_{20}F_{80}$	0.42	0.411	0.306	0.105
$N_{20}K_{80}$	0.43	0.395	0.261	0.134
SH	0.08	0.709	0.592	0.117

TABLE 4.16 - MEAN ROUNDNESS VALUES AND MAXIMUM AND MINIMUM POROSITIES FOR THE POROSITY CELL SAMPLES.

4.2.3 Experimental procedures

Before the samples were tested the porosity cell graduation marks were calibrated. This was achieved by pouring one litre of distilled water into the cell with the acoustic transducers in their final position. A reading of 1024 meant that all volume measurements had to have 24 subtracted to obtain a true value.

Calibration of the compressional wave transducers (from a distance-time plot in water) showed that a 1.75μsec delay occurs from all sources (this

includes both the effect of the quarter-wavelength epoxy resin facing on the transducers and any electronic delays in the system). The set distances used for the acoustic measurements were just less than the internal dimension of the cell (76.1 mm). For the compressional waves this was 65.6 mm and for the shear waves 49.6 mm (shorter due to the protrusion of the shear wave elements.

Prior to testing, a known dry weight of each sand was fully saturated in slightly salted tap water which was left overnight to equilibriate to room temperature. The cell was filled with this water and the voltage drop across both sets of electrodes and the compressional wave time interval recorded.

The cell was filled with the sand using a slow underwater deposition technique. A rubber bung was fitted to the top of the cell through which passes a large polythene funnel and a return pipe with an adjustable flow valve. Saturated sand was transferred underwater to the funnel using a small beaker. Deposition rate was controlled using the valve on the return pipe such that a slow steady 'rainfall' occurred without any turbulence. All the known weight of sand was deposited in this way taking care not to produce any accidental knocks or vibrations which would cause the high porosity structure to settle.

Time intervals for both the compressional and shear wave pulses were recorded directly from the oscilloscope to accuracies of 0.1 and 1 μsec respectively. Voltage differences across both sets of electrodes were recorded to accuracies of 1 mV and the volume of saturated sand recorded to the nearest 1 cm^3. Temperature was recorded to the nearest 0.1°C.

The porosity of the sand structure was reduced in stages using the variable amplitude vibrating table. Initially only minimum amplitudes

for short time periods (<5 sec) were needed to create porosity changes of ≅ 0.01. As the porosity decreased progressively larger amplitudes and time periods were required for similar porosity changes. The minimum porosity was found to be obtained by a long period (10 minutes) of intermittent maximum amplitude vibrations followed by a slow reduction in amplitude for a period of about five minutes. This technique is similar to that found necessary for the ARL tank. After each vibration stage the temperature, voltage, time delays and volume reading were recorded.

Following the first set of data (Run 1) the cell was unclamped from the vibrating table and inverted allowing the sand to settle in the porosity cell's graduation column. Subsequent reinversion produced a very rapidly deposited structure that, in general, had a higher porosity than the slow deposition technique. After the cell was reclamped to the vibrating table the measurement sequence was repeated. This inversion was repeated twice for each sample (Runs 2 and 3). Although the fast deposition technique normally produced slightly higher initial porosities the final porosities were generally lower, after maximum vibration, for the slow deposition technique employed for the first set of data. Maximum and minimum porosities shown in Table 4.16 are taken from whichever technique provided the highest or lowest porosity.

As part of the ongoing programme to investigate the performance of the shear wave transducers and their self-monitoring elements, the transient recorder was used interfaced to the desk-top computer to analyse the frequency response characteristics.

4.2.4 Results

Data obtained from the nineteen sediment samples tested, following the

experimental procedure described in the previous section, is presented in the following manner. Raw data for a typical example is presented with suitable graphical illustrations. Pertinent points typical of all of the data is discussed using this data set but, where significant variations occur for other samples, these are presented and also discussed. The whole data set is summarised with suitable tables and graphs which will be examined in more detail in the following discussion section.

Sediment sample M is used to illustrate the raw data collected. It is chosen, not because it exhibits any unique features, but because it represents the 'middle-of-the-range' in terms of size and shape distributions and has features typical of most of the other sediments tested.

Data for sample M is shown in Table 4.17

where T = temperature

Vol. = volume reading from the graduations on the cell

t_p = measured transit time for the compressional wave pulse

t_s = measured transit time for the shear wave pulse

n = porosity

$$n = \frac{(Vol - 24) - W/\rho_m}{Vol - 24}$$

W = weight of dry sediment used in test

ρ_m = density of sediment minerals

V_p = compressional wave velocity corrected to 20°C

$$V_p = \frac{65600}{t_p - 1.75} + 2.9(20-T)$$

T	Vol.	t_p	t_s	n	V_p	V_s	FF_s	FF_1	
C		μsec	msec		m/s	m/s			
17.7	----	46.3	-----	-----	1479	--	1.000	1.000	RUN 1
17.7	1238	40.7	1.027	0.438	1691	48	3.283	3.293	
18.6	1238	40.7	1.085	0.438	1688	46	3.332	3.349	
18.6	1235	40.7	1.017	0.437	1688	49	3.342	3.359	
18.6	1230	40.6	0.958	0.434	1693	52	3.356	-----	
18.6	1220	40.6	0.870	0.430	1693	57	3.393	3.406	
18.6	1210	40.5	0.832	0.425	1697	60	3.435	3.443	
18.6	1200	40.5	0.821	0.420	1697	60	3.482	3.489	
18.6	1189	40.4	0.768	0.414	1701	65	3.556	3.560	
18.6	1180	40.3	0.737	0.410	1706	67	3.612	3.610	
18.6	1170	40.2	0.717	0.405	1710	69	3.687	3.677	
18.6	1160	40.1	0.695	0.399	1715	71	3.766	3.747	
18.6	1150	39.9	0.655	0.394	1724	76	3.860	3.831	
18.6	1140	39.7	0.644	0.389	1733	77	3.939	3.905	
18.6	1130	39.5	0.640	0.383	1742	78	4.023	3.985	
18.6	1118	39.3	0.610	0.376	1751	81	4.149	4.058	
18.7	1110	39.2	0.608	0.372	1755	82	4.229	4.174	
18.7	1100	39.0	0.612	0.366	1765	81	4.332	4.276	
18.7	1090	38.9	0.595	0.360	1770	83	4.430	4.382	
18.7	1080	38.7	0.577	0.354	1779	86	4.529	4.481	
18.7	1068	38.5	0.545	0.346	1789	91	4.603	4.593	
18.7	1058	38.4	0.545	0.340	1794	91	4.711	4.706	
18.7	1051	38.3	0.522	0.336	1799	95	4.725	4.753	
18.7	1051	38.3	0.537	0.336	1799	92	4.720	4.751	
18.7	1051	38.3	0.519	0.336	1799	95	4.720	4.751	
18.8	1248	40.8	0.933	0.443	1683	53	3.302	3.385	RUN 2
18.8	1240	40.7	0.963	0.439	1688	51	3.320	3.406	
18.8	1220	40.6	0.895	0.430	1692	55	3.405	3.491	
18.9	1200	40.5	0.755	0.420	1696	66	3.512	3.592	
18.9	1180	40.3	0.646	0.410	1705	77	3.615	3.692	
18.9	1160	40.0	0 580	0.399	1718	86	3.756	3.814	
19.0	1140	39.9	0.690	0.389	1722	72	3.921	3.990	
19.0	1120	39.6	0.642	0.377	1736	77	4.105	4.175	
19.1	1100	39.3	0.607	0.366	1750	82	4.303	4.371	
19.1	1073	38.8	0.582	0.350	1773	85	4.577	4.622	
19.4	1063	38.5	0.580	0.343	1787	86	4.706	4.739	
19.4	1062	38.5	0.566	0.343	1787	88	4.711	4.745	
19.1	1244	40.9	1.004	0.441	1678	49	3.302	3.396	RUN 3
19.1	1241	40.9	0.986	0.439	1678	50	3.307	3.400	
19.1	1230	40.8	0.963	0.434	1683	51	3.354	3.451	
19.1	1210	40.7	0.888	0.425	1687	56	3.439	3.540	
19.3	1190	40.4	0.827	0.415	1699	60	3.584	3.688	
19.4	1169	40.2	0.752	0.404	1708	66	3.740	3.838	
19.4	1149	39.9	0.679	0.394	1721	73	3.902	3.991	
19.5	1130	39.6	0.638	0.383	1735	78	4.083	4.157	
19.5	1110	39.4	0.624	0.372	1744	79	4.255	4.330	
19.7	1086	39.0	0.597	0.358	1762	83	4.486	4.553	
19.7	1070	38.7	0.573	0.348	1776	86	4.635	4.632	

TABLE 4.17 Typical example (sand M) of data obtained from the porosity cell.

V_s = shear wave velocity

$$V_s = \frac{49.6}{t_s}$$

FF_s = formation factor using small electrodes

FF_l = formation factor using large electrodes

These values of formation factor are corrected to 20°C and were provided by P. Jackson.

The three vibration procedures are designated RUN 1, 2 and 3. In RUN 1 the first set of readings is for the water which was added prior to the sediment.

Data for sample M given in Table 4.17 is shown graphically in the following figures: V_p versus n in Figure 4.22, V_s versus n in Figure 4.23, FF_s and FF_l versus n for RUN 1 in Figure 4.24 and FF_s and FF_l versus n for RUN 2 and 3 in Figure 4.25. V_p versus n (Figure 4.22) illustrates that the scatter can be as much as 15 m/s at a given porosity or n can vary by up to 0.1 at a given velocity. These values are well outside the expected experimental errors (V_p ± 3.8 m/s and n ± 0.001).. V_s versus n (Figure 4.23) while again illustrating a definite trend has scatter larger than that expected from experimental errors (V_s ± 2.5 - 10 m/s). The potential problem with the porosity cell is that porosity inhomogeneities may exist throughout the sand body. The reason for the two sets of resistivity electrodes was to ascertain whether any consistent differences between the central part of the cell (using FF_s) and the whole of the base section (using FF_l) could be detected. In Figure 4.24 it can be seen that while at the start and finish of RUN 1 FF_s and FF_l are the same they diverge during the middle of the vibration procedure indicating

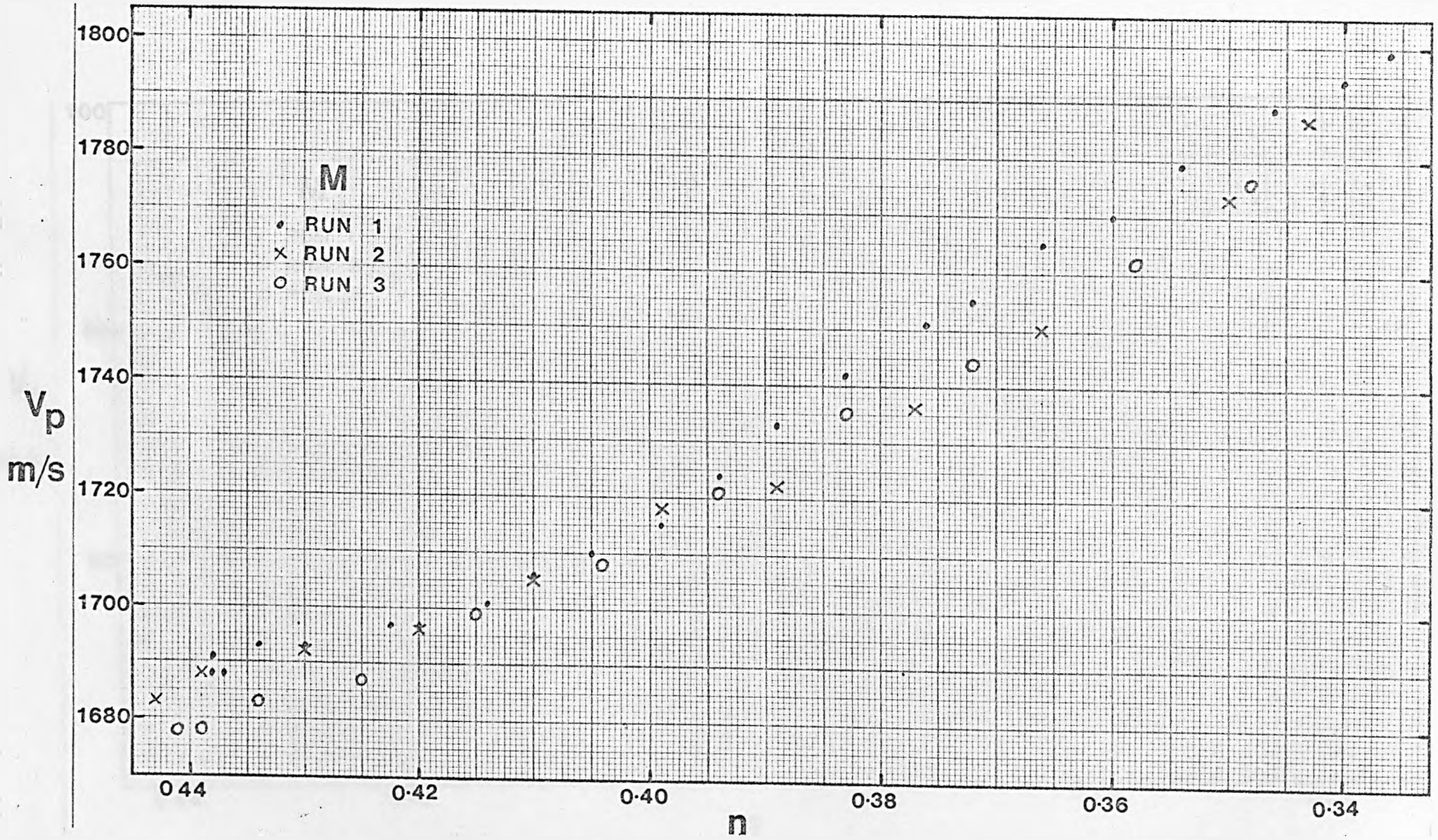

FIGURE 4.22 Compressional Wave Velocity vs Porosity for sand M

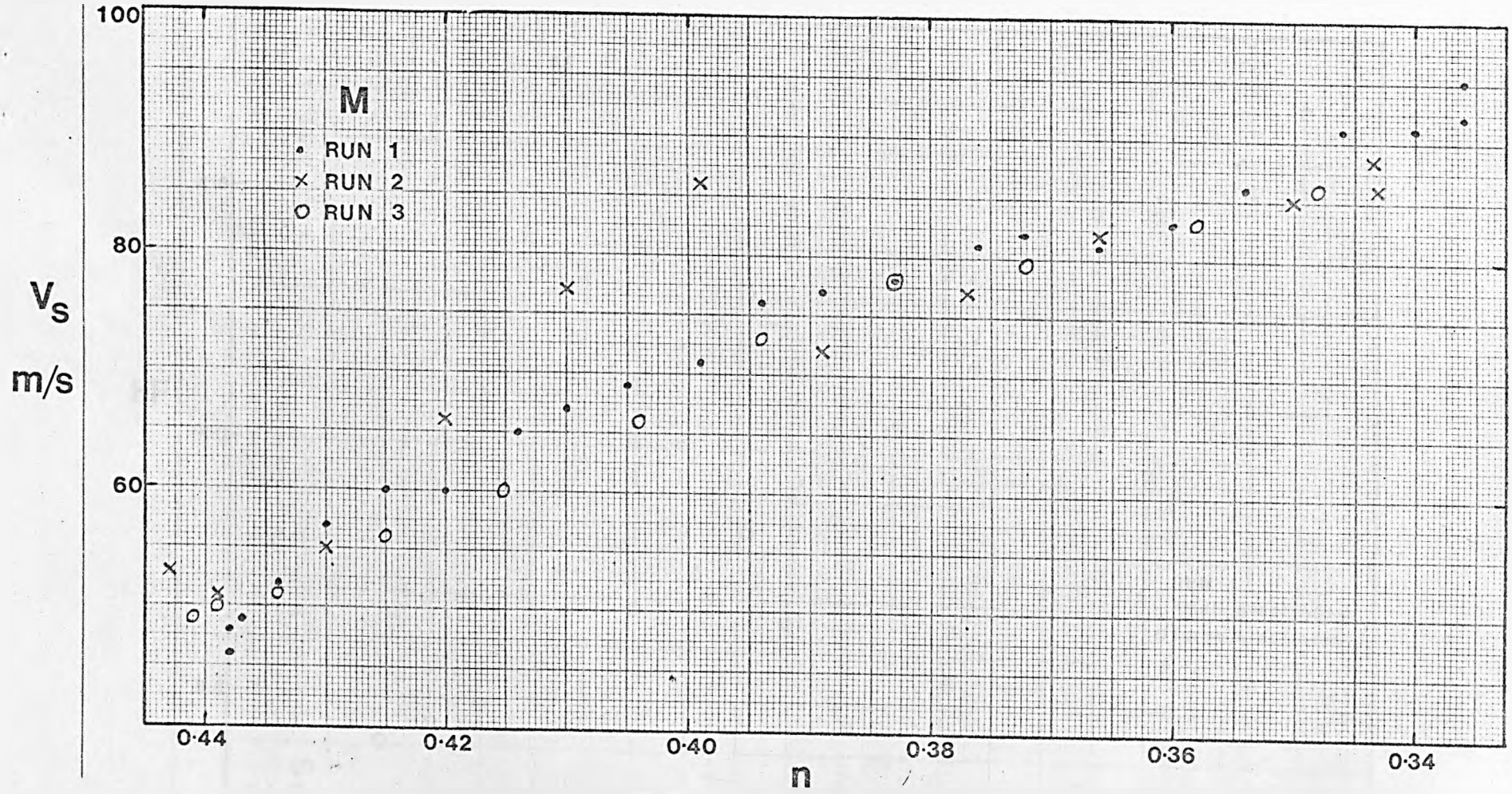

FIGURE 4.23 Shear Wave Velocity vs Porosity for sand M

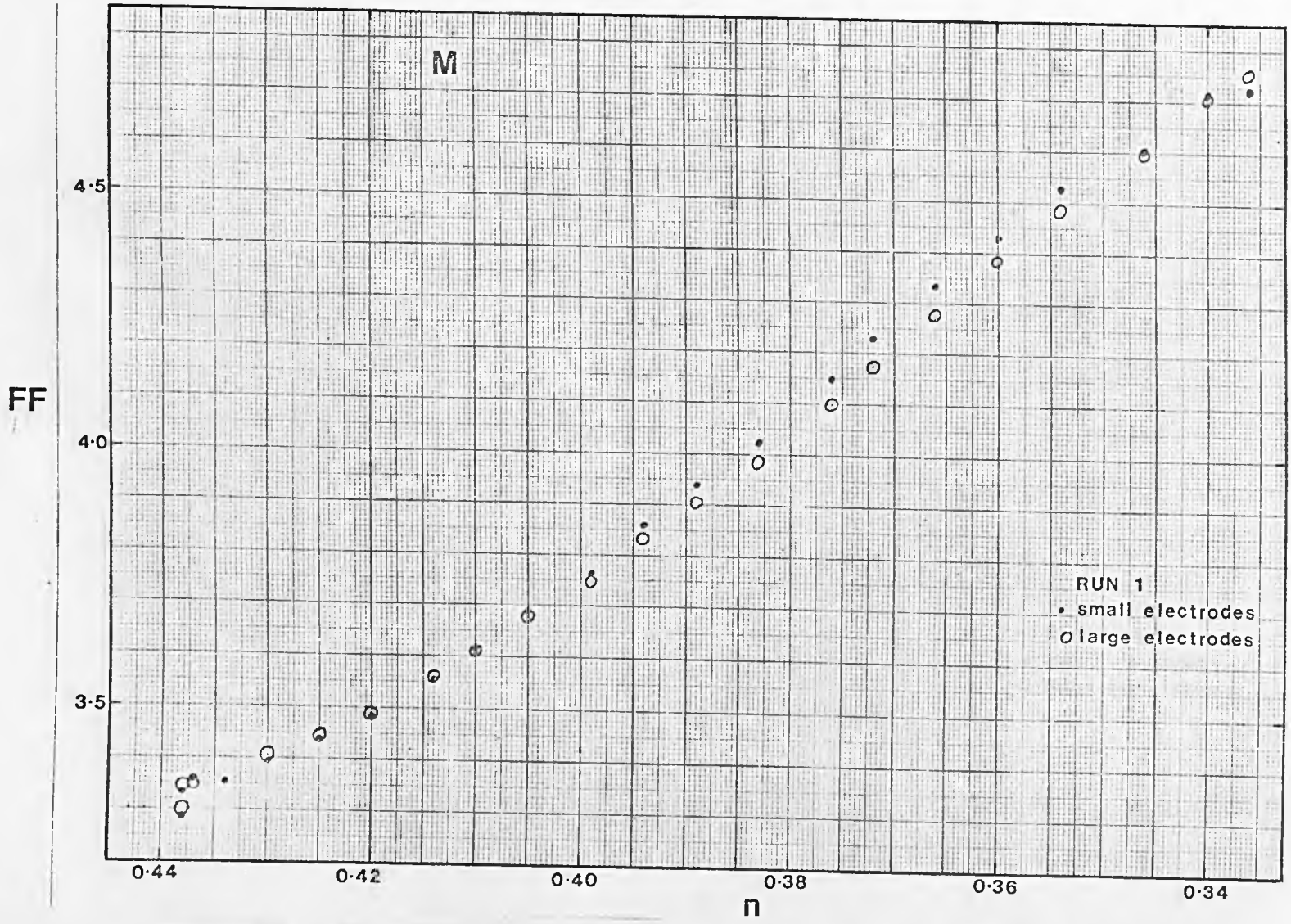

FIGURE 4.24 Formation Factor vs Porosity for sand M, RUN 1

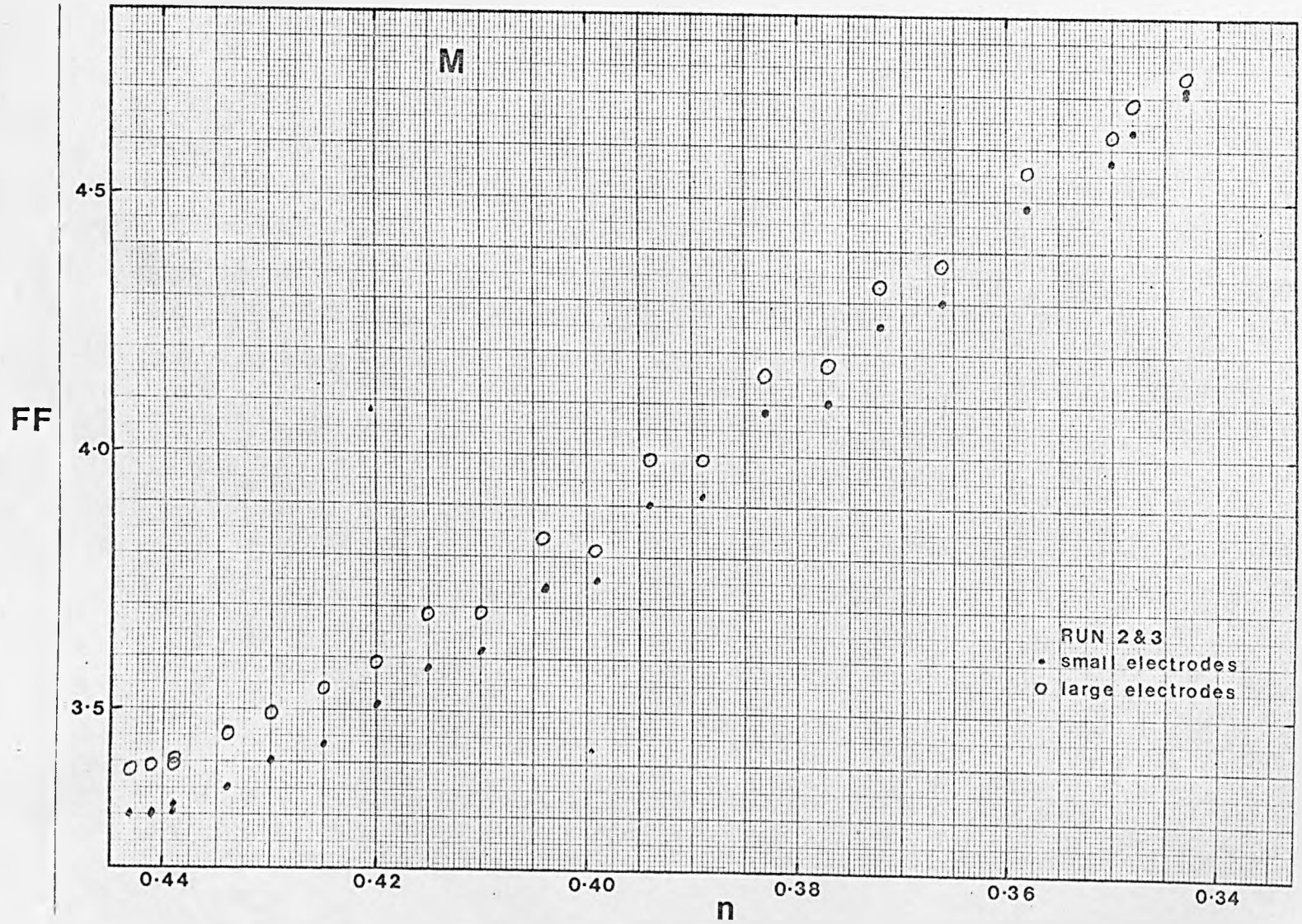

FIGURE 4.25 Formation Factor vs Porosity for sand M, RUN 2&3

higher porosities in the middle of the cell than round the outside. It can be estimated that this difference in porosity is only 0.002 at a maximum during RUN 1 but for RUN 2 and 3 may increase to 0.008. It can also be seen that FF for RUN 2 and 3 is generally higher (especially FF_1) than during RUN 1. Figures 4.26 and 4.27 show plots of FF_s against V_p and V_s respectively illustrating that using FF_s rather than n does not significantly reduce the amount of scatter. It must be assumed, therefore, that most of the differences in V_p and V_s at any given porosity are real. For the purposes of this study the differences in the porosity obtained directly from the volume reading and from a calibration procedure, using the electrical resistivity formation factor, FF are too small to be of any significance. Hence the porosity values used for all the data is that obtained directly from the volume readings.

Plots of V_p and V_s versus n, for all the sediments tested, are used to summarise the complete data set in Figures 4.28, 4.29, 4.30, 4.31, 4.32 and 4.33. Table 4.10 summarises the maximum and minimum values of n, V_s and V_p.

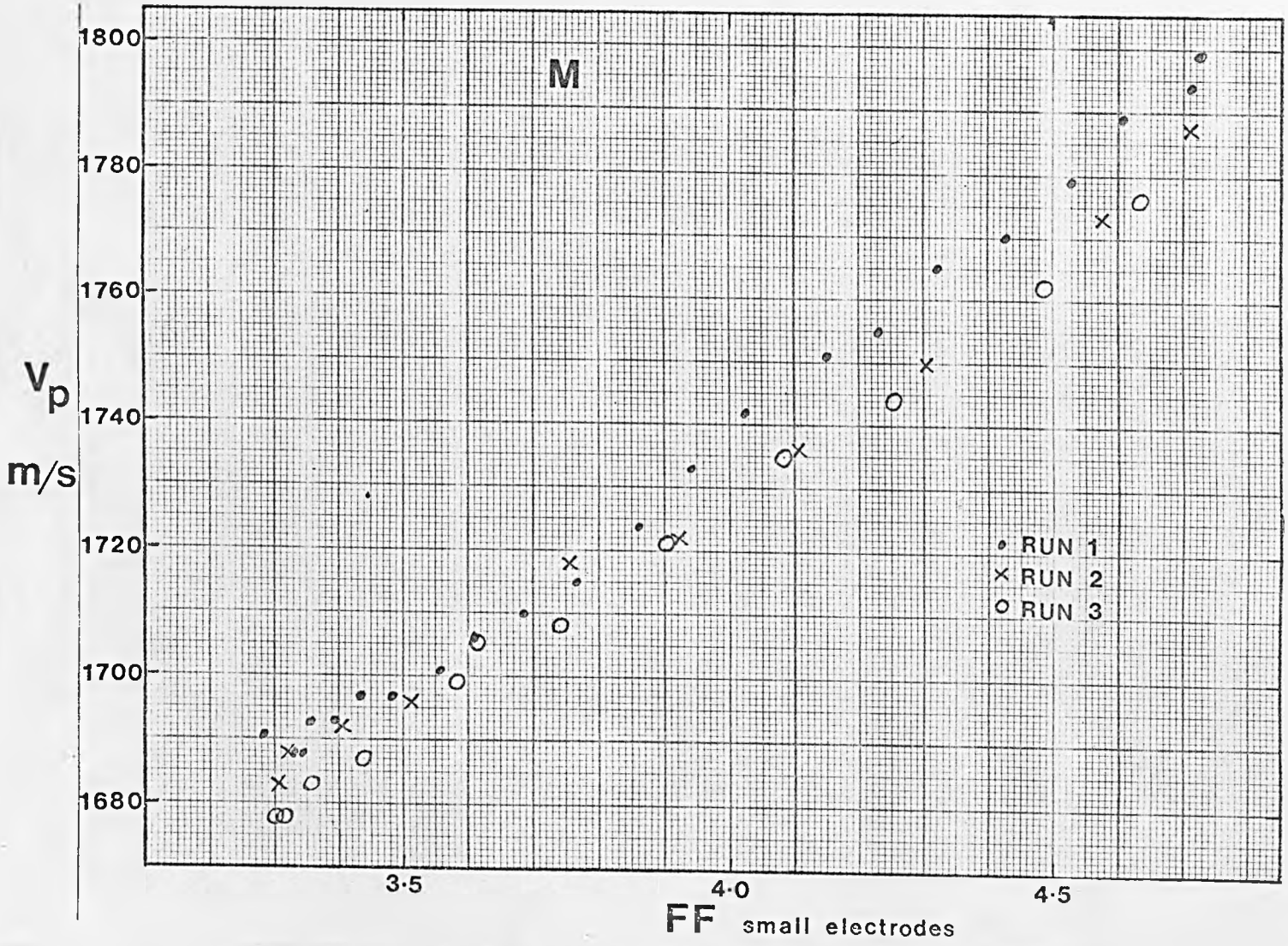

FIGURE 4.26 Compressional Wave Velocity vs Formation Factor (small electrodes) for sand M

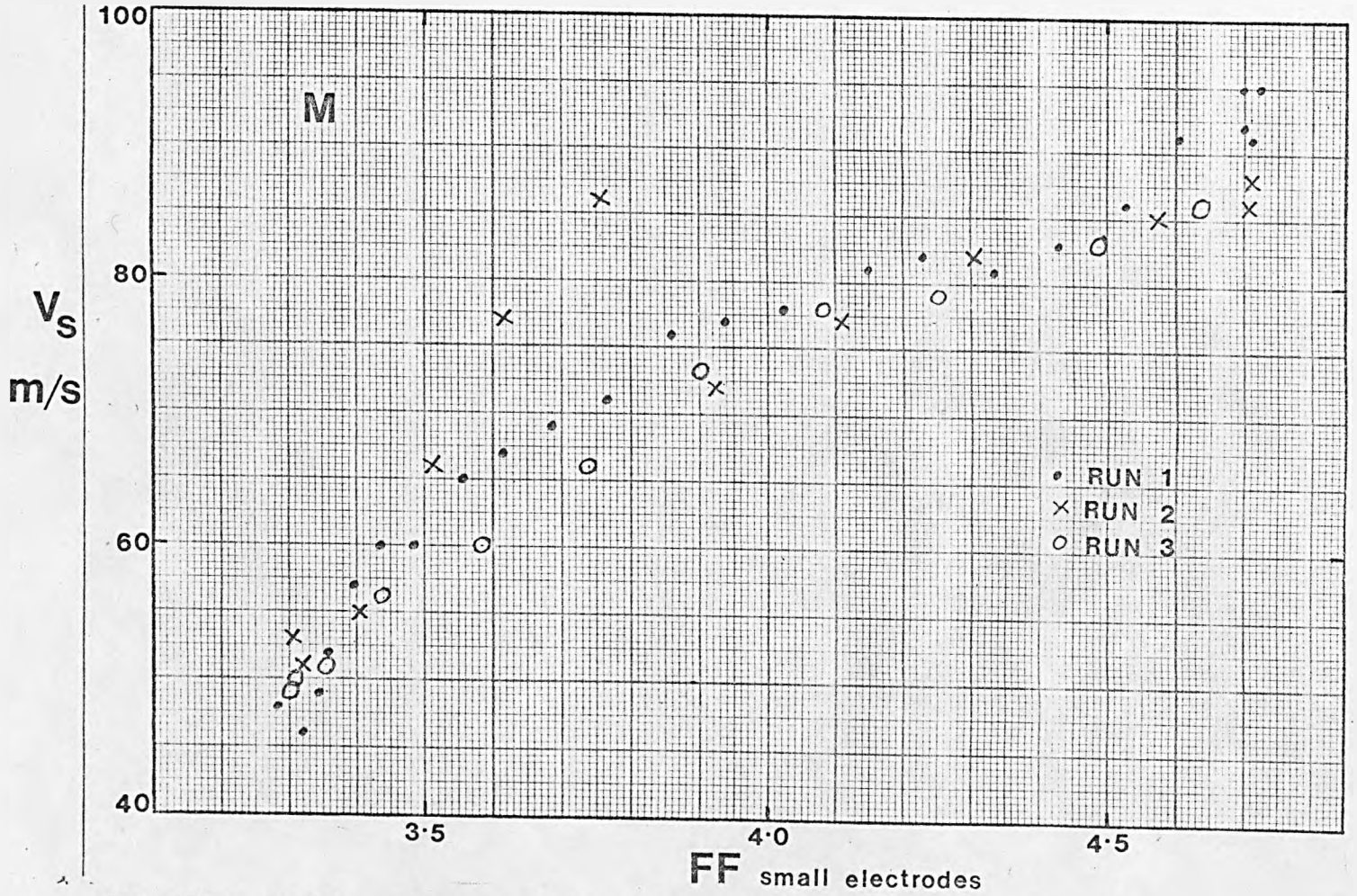

FIGURE 4.27 Shear Wave Velocity vs Formation Factor (small electrodes) for sand M

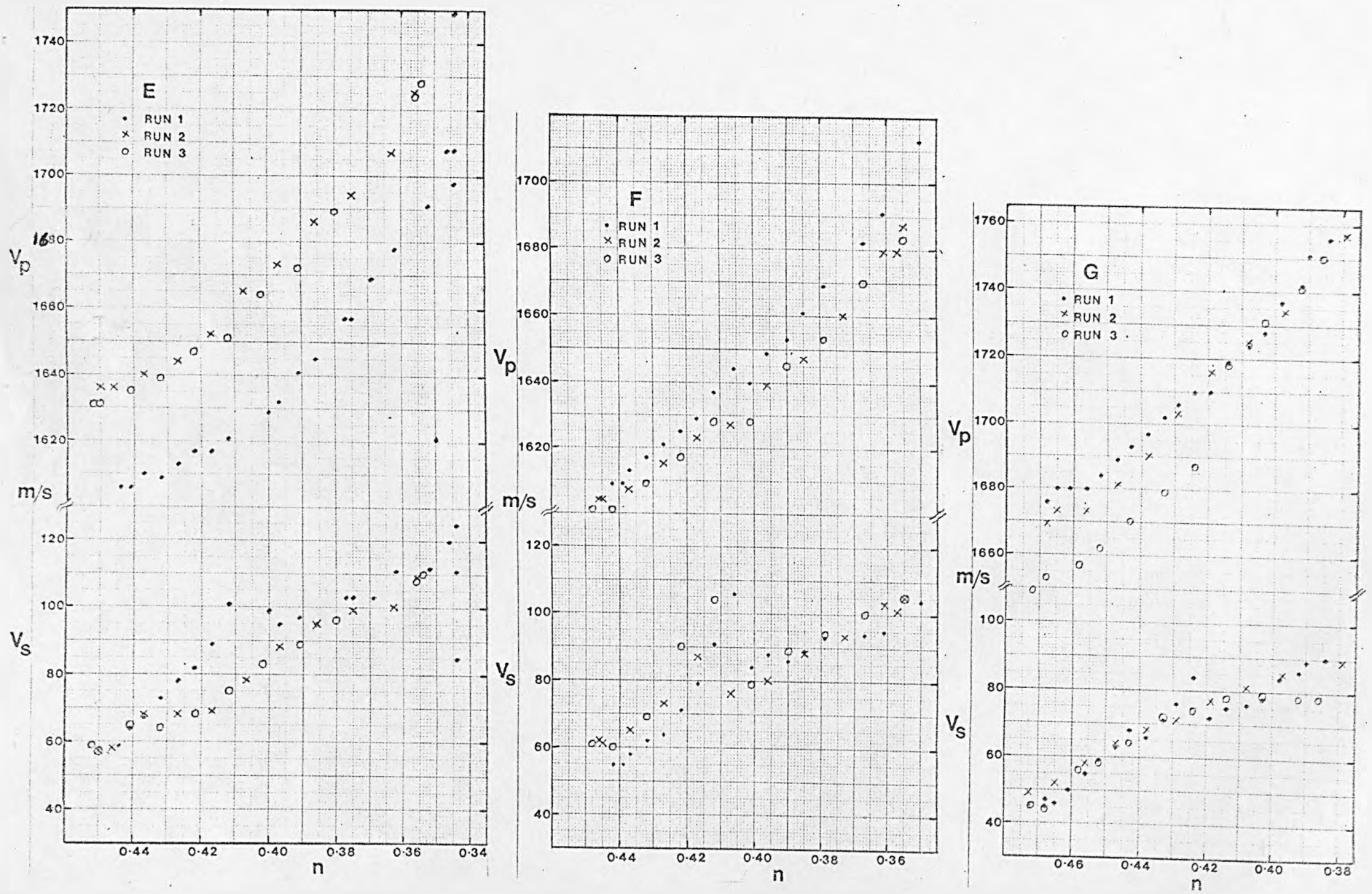

FIGURE 4.28 V_p & V_s vs Porosity for sands E, F and G

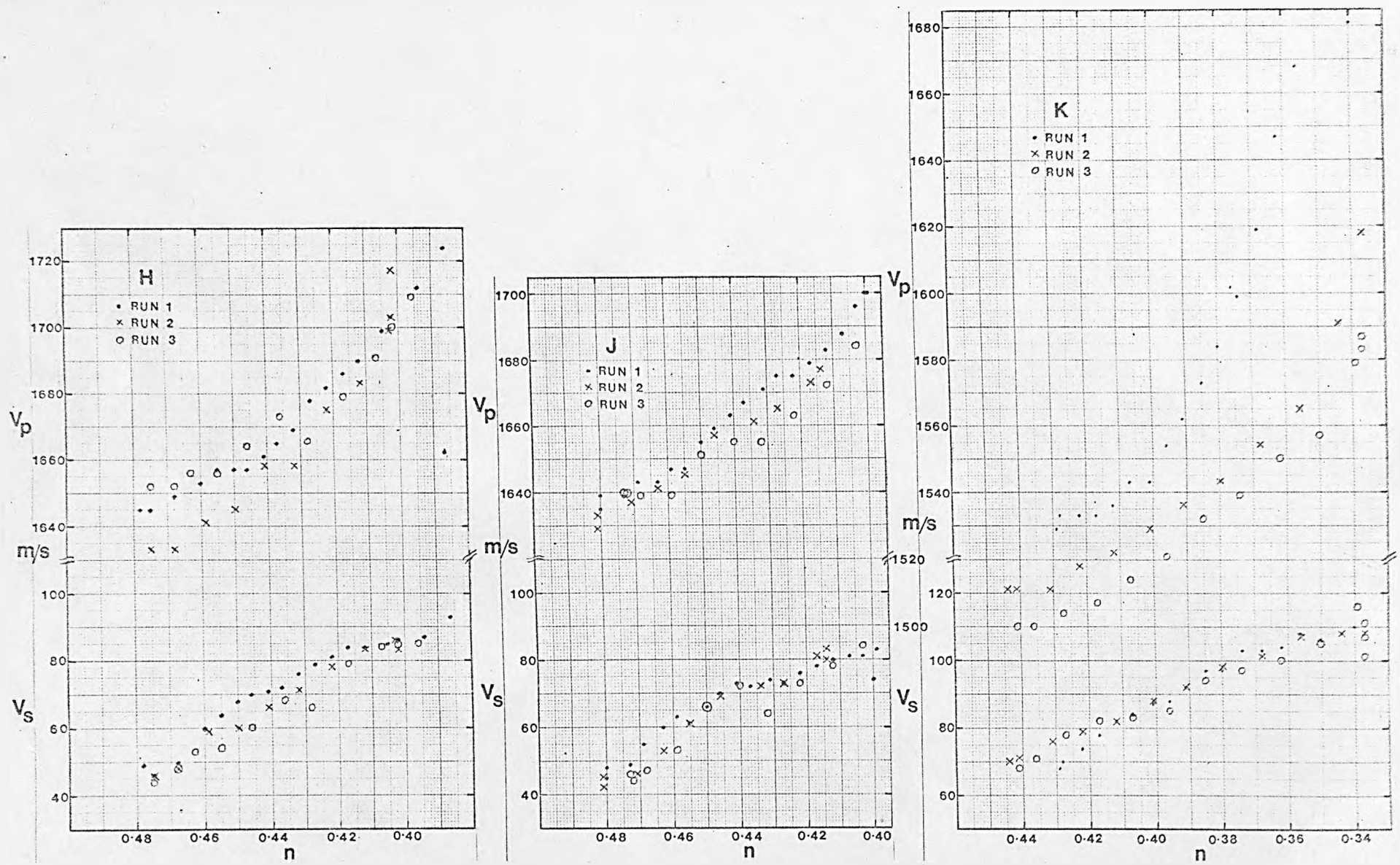

FIGURE 4.29 V_p & V_s vs Porosity for sands H,J and K

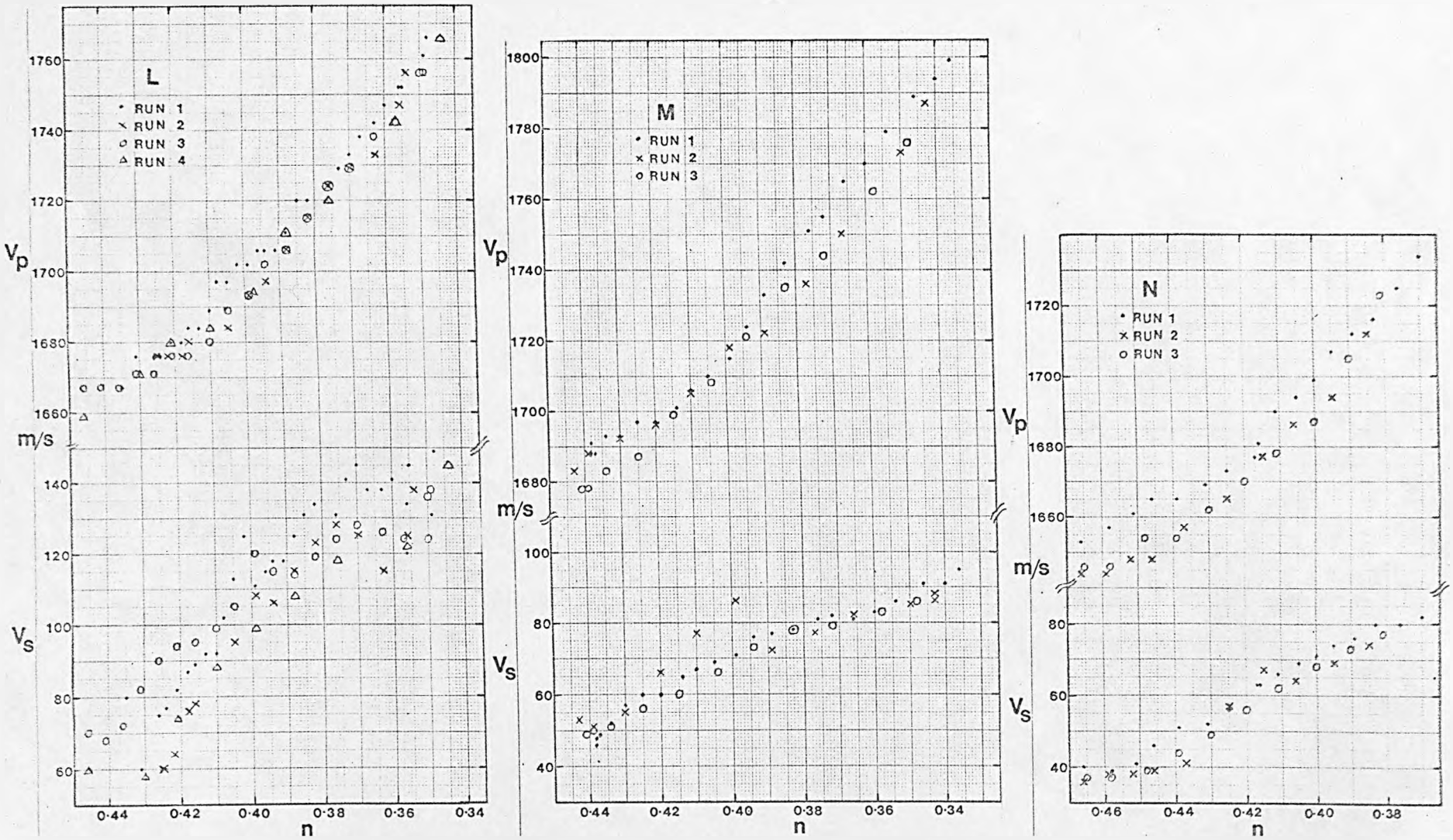

FIGURE 4.30 V_p & V_s vs Porosity for sands L, M and N

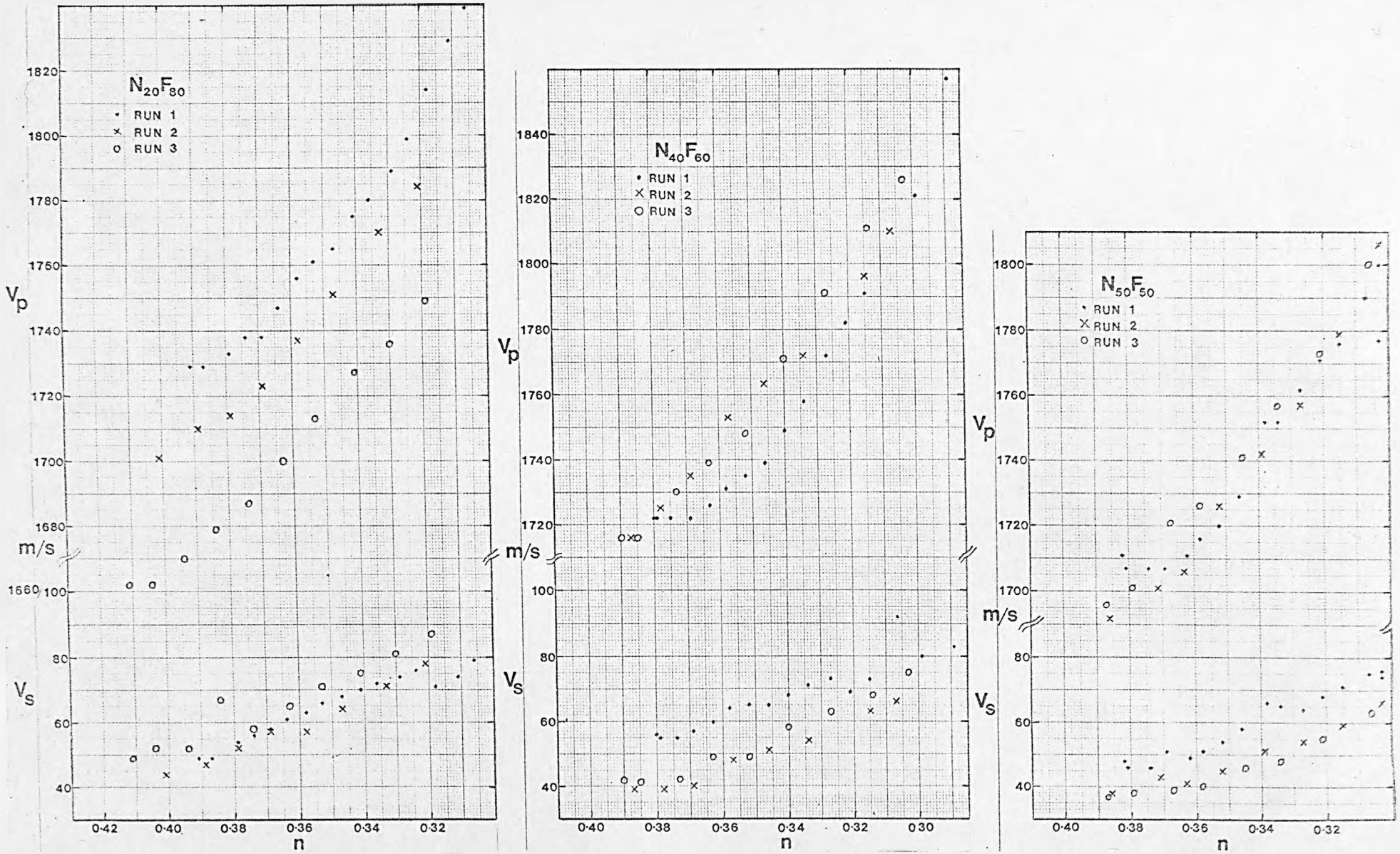

FIGURE 4.31 V_p & V_s vs Porosity for sands $N_{20}F_{80}$, $N_{40}F_{60}$ and $N_{50}F_{50}$

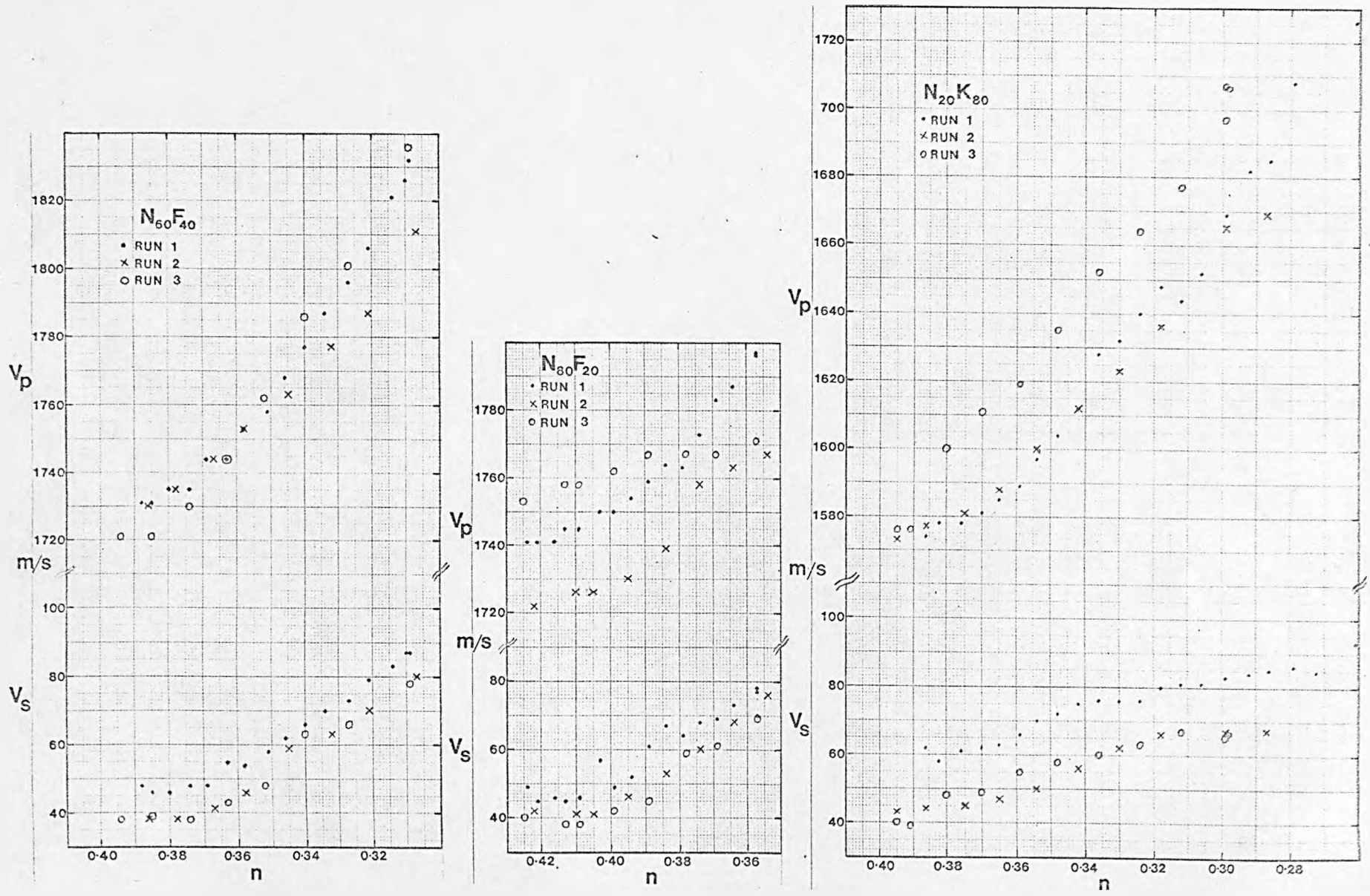

FIGURE 4.32 V_p & V_s vs Porosity for sands $N_{60}F_{40}$, $N_{80}F_{20}$ and $N_{20}K_{80}$

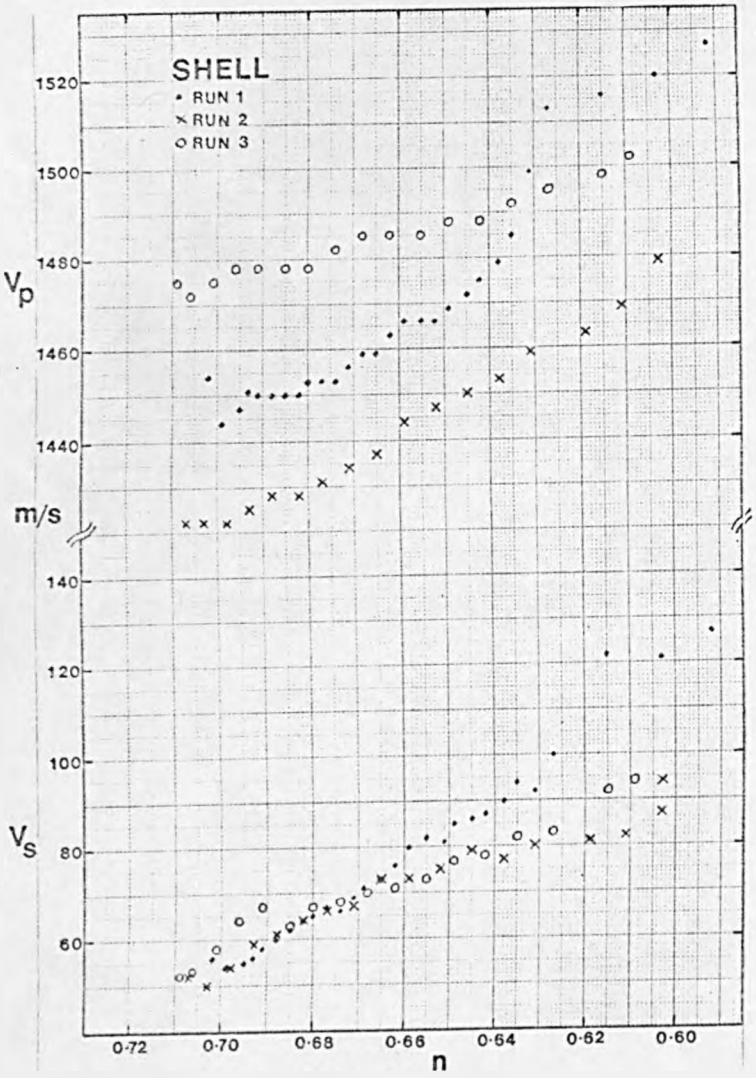
SHELL
RUN 1
RUN 2
RUN 3
1520
1500
1480
1460
1440
m/s
140
120
100
80
60
V_p
V_s
0·72
0·70
0·68
0·66
0·64
0·62
0·60
n

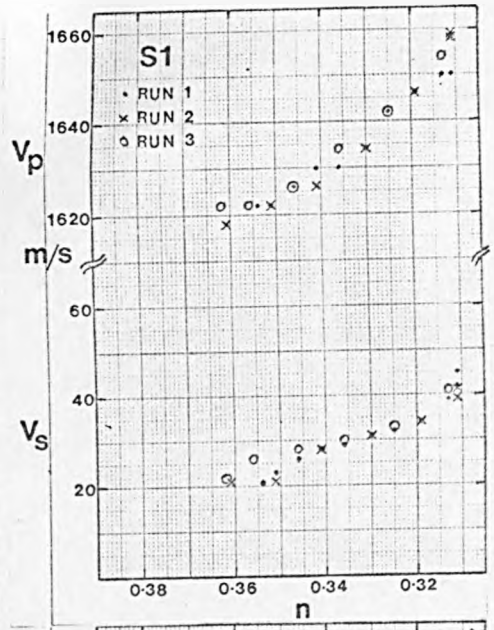
S1
RUN 1
RUN 2
RUN 3
1660
1640
1620
m/s
60
40
20
V_p
V_s
0·38
0·36
0·34
0·32
n

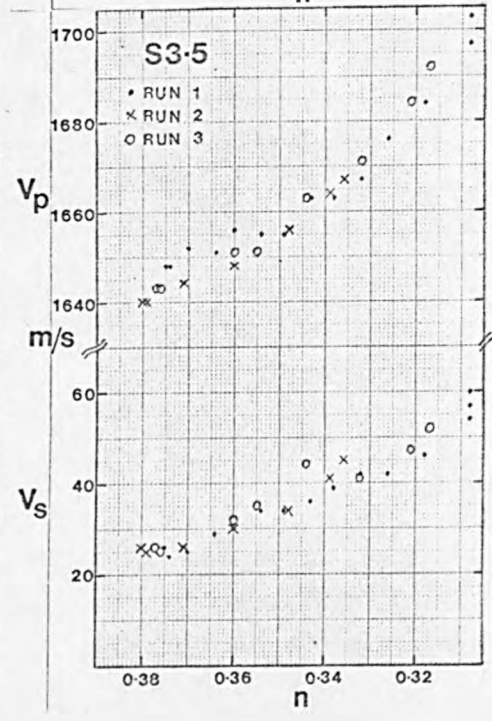
S3·5
RUN 1
RUN 2
RUN 3
1700
1680
1660
1640
m/s
60
40
20
V_p
V_s
0·38
0·36
0·34
0·32
n

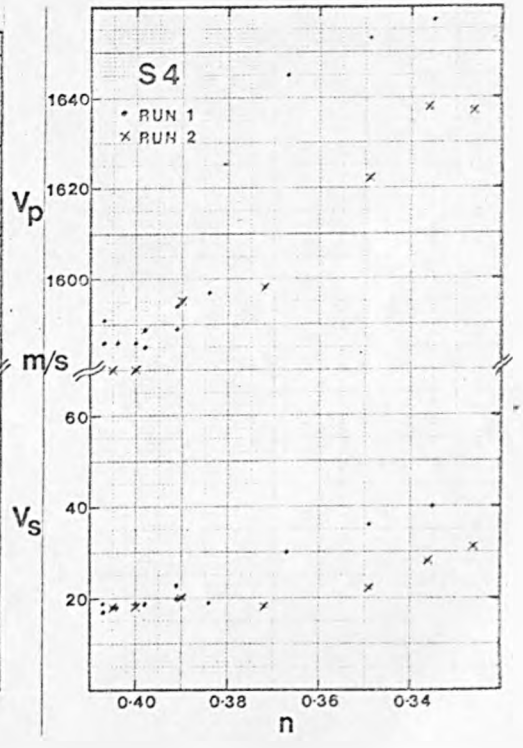
S4
RUN 1
RUN 2
1640
1620
1600
m/s
60
40
20
V_p
V_s
0·40
0·38
0·36
0·34
n

SAND	n_{max}	n_{min}	$n_{max} - n_{min}$	V_{pmax} m/s	V_{pmin} m/s	$V_{pmax} - V_{pmin}$ m/s	V_{smax} m/s	V_{smin} m/s	$V_{smax} - V_{smin}$ m/s
E	0.452	0.344	0.108	1749	1606	143	120	57	63
F	0.448	0.350	0.098	1713	1601	112	105	55	50
G	0.473	0.379	0.094	1757	1649	108	90	44	46
H	0.478	0.386	0.092	1724	1633	91	93	44	49
J	0.481	0.399	0.082	1700	1629	71	84	42	42
K	0.444	0.337	0.107	1681	1500	181	116	68	48
L	0.446	0.344	0.102	1766	1659	107	149	58	91
M	0.443	0.336	0.107	1799	1678	121	95	46	49
N	0.466	0.370	0.096	1734	1644	90	82	36	46
S1	0.362	0.311	0.051	1659	1618	41	45	21	24
S3.5	0.380	0.308	0.072	1703	1640	63	60	24	36
S4	0.407	0.326	0.081	1657	1580	77	40	17	23
$N_{80}F_{20}$	0.425	0.356	0.069	1797	1722	75	78	38	40
$N_{60}F_{40}$	0.394	0.307	0.087	1836	1721	115	87	38	49
$N_{50}F_{50}$	0.387	0.303	0.084	1806	1692	114	76	37	39
$N_{40}F_{60}$	0.390	0.289	0.101	1857	1716	141	83	39	44
$N_{20}F_{80}$	0.411	0.306	0.105	1839	1662	177	87	44	43
$N_{20}K_{80}$	0.395	0.261	0.134	1726	1573	153	86	39	47
SH	0.709	0.592	0.117	1527	1422	105	127	50	77

TABLE 4.18 Summary of porosity and elastic wave velocity measurements for the sands tested in the porosity cell.

4.3 Discussion

4.3.1 Porosity measurements

The evaluation of porosity, and consequently bulk density, in these experiments is central to the theme of 'packing structure'. It is necessary, therefore, to briefly discuss the techniques used for measuring porosity in both sets of experiments before the wave velocities are considered. In the ARL tank only the initial and end porosities could be calculated whereas in the porosity cell a total volume reading provided a continuous measurement of average porosity. It cannot be assumed, however, that in either sets of experiments the porosity is uniform throughout the whole sample. In the ARL tank there was no way of investigating possible porosity irregularities but the resistivity electrodes in Jackson's porosity cell did allow some estimate of porosity variations to be made. In Figure 4.34 the difference in formation factor (FF small electrodes - FF large electrodes) is plotted versus porosity, n, for the sand M. On run 1 the graph illustrates that while at the beginning of the test the porosity is lower in the centre of the cell, the vibration procedure causes it to become higher and then lower again at the end of the test. For runs 2 and 3 the porosity in the centre is always lower than the average porosity but the difference generally decreases as the test proceeds, finally reaching a similarly low value as for run 1. This effect can also be seen in Figures 4.24 and 4.25, although not as clearly. These figures indicate that the maximum difference in porosity across the central part of the cell compared to the whole cell is given by a difference in formation factor of approximately 0.12. The corresponding change in porosity is approximately 0.015.

It is clear from the above discussion that the two types of deposition

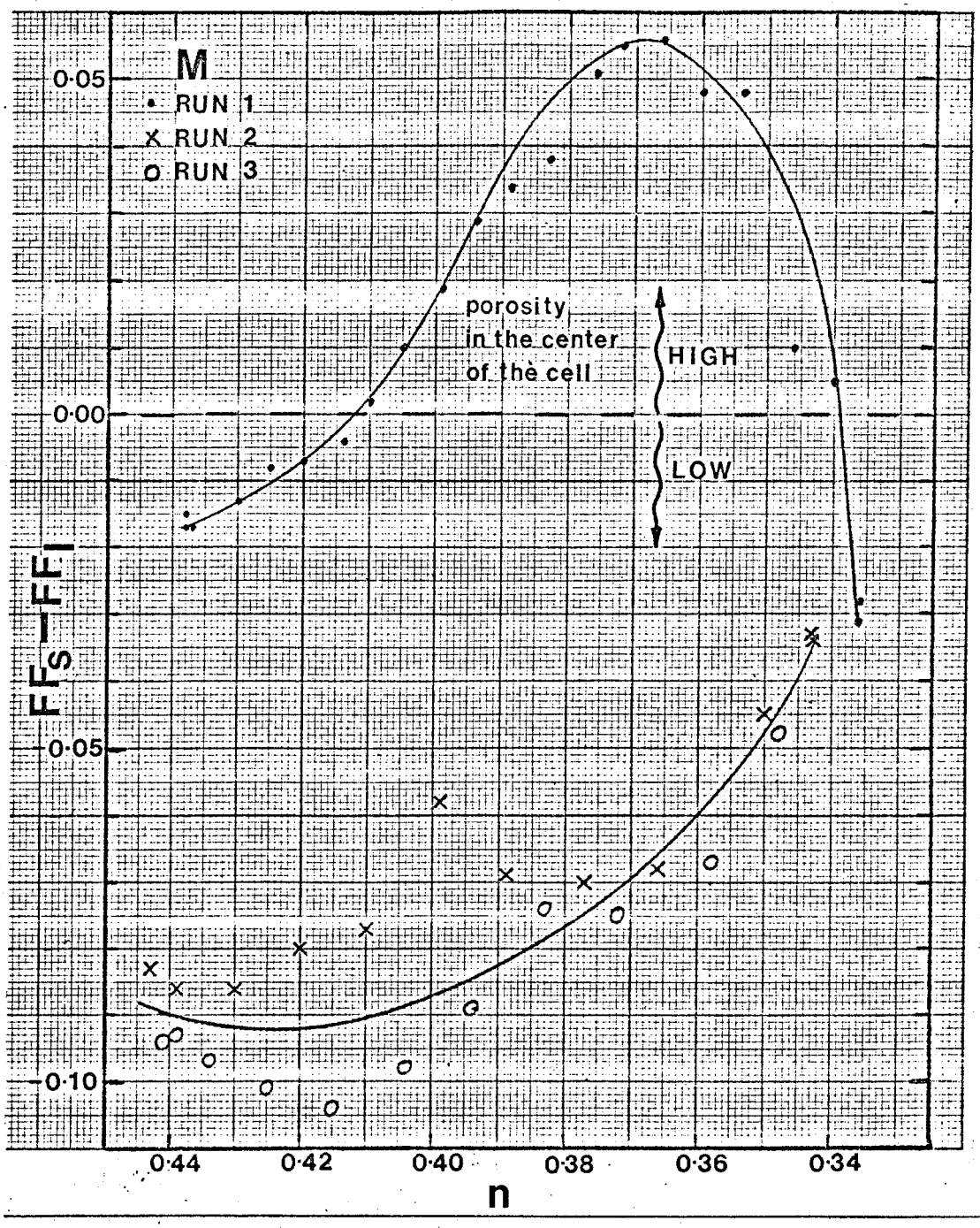

FIGURE 4.34 Difference in Formation Factor ($FF_S - FF_I$) vs Porosity for sand M

used in the porosity cell, that used for run 1 and that used for runs 2 and 3, cause measurable differences in packing structure. However, these differences are only small when compared with much of the scatter found in the velocity measurements. It should be stressed that while the magnitude of the porosity variations in the illustrated sand, M, is typical of all the sands, the character of the graphs changes from one sand to another. Therefore, it must be concluded that sediment characteristics, the type of sedimentation procedure, the design of the cell and the vibration parameters, all contribute to the small packing irregularities observed.

4.3.2 Compressional wave measurements

Before examining the overall trends of compressional wave data in detail the accuracy of the measurements will be examined. In both systems the velocity measurement in the sand is calculated from the travel time of a pulse after a calibration procedure in water. Time intervals in the ARL system were accurate to ± 0.25 μsec and ± 0.1 -sec in the porosity cell. It is not easy to estimate the accuracy of the set distance measurement but if ± 0.5 mm is taken to be the worst possible case then the overall accuracy for the two systems are:

	time interval	transducer separation
ARL tank	$\pm \frac{0.25}{95} \times 100 = \pm 0.263\%$	$\pm \frac{0.5}{150} \times 100 = \pm 0.333\%$
	$= \pm 4.5$ m/s	$= \pm 5.7$ m/s
porosity cell	$\pm \frac{0.1}{45} \times 100 = \pm 0.222\%$	$\pm \frac{0.5}{65} \times 100 = \pm 0.769\%$
	$= \pm 3.8$ m/s	$= \pm 13.1$ m/s

The errors caused by the timing inaccuracies are random whereas the transducer separation error was systematic for a given test because the transducer position was unaltered. A glance through the V_p versus n plots for the porosity cell (Figures 4.28-4.33) shows that the actual random error for any given run is usually well within the calculated ± 3.8 m/s. The systematic error of ± 13.1 m/s is not revealed by the experimental results. However, this systematic error, caused by the transducer separation, will be constant for all the porosity cell samples.

Another potential source of systematic error could occur by not identifying the correct onset of the received signal. In this case the timing would be in error by $\frac{N}{F}$ where F is the resonant frequency of the transducer N is any integer. For the ARL system F = 112 kHz and for the porosity cell F = 250 kHz. Therefore, if N = 1 the minimum error from this cause would be:

	$\frac{1}{F}$	% error	velocity error
ARL tank	9μs	$\equiv \frac{9}{95} \times 100 = 9.5\%$	$\equiv$ 161 m/s
porosity cell	4μs	$\equiv \frac{4}{45} \times 100 = 8.9\%$	$\equiv$ 151 m/s

This type of error is much too large to account for the differences observed in different test runs for the same sand in the porosity cell. The largest difference observed between different runs is for sand $N_{20}F_{40}$ and for SHELL where differences of up to 70 m/sec were observed at similar porosities. It must be concluded, therefore, that the differences observed in V_p during different runs must be real and are attributed to subtle changes in the packing structure. Two sands, K and $N_{20}K_{80}$ exhibited a very poor received waveform and it is thought possible that this data may be suspect and that the onset may be in error by $\frac{1}{F}$. If this was the

case then V_p for these sands should be increased by approximately 150 m/s.

Compressional wave velocity is frequently plotted against porosity, for example, Figure 4.35 (after Akal, 1972) illustrates the scatter from in-situ measurements. Assuming that the data is accurate, then the variation in sound speed (typically at least 150 m/s) must be attributed to inherent grain characteristics. Figure 4.11 summarises the laboratory data for the ARL tank and Figure 4.36 summarises the data for the porosity cell apart from the tests on the shell fragments (see Figure 4.33). These plots are, of course, slightly different from Figure 4.35 in that they show the variation in V_p when the sand structure is changed from very loose to very compact rather than individual points for a large number of sands. In the case of the ARL results the linear extrapolations to maximum and minimum porosities is intended to show the likely extent of velocity variations had the system been capable of producing the complete porosity range.

It is readily apparent from Figure 4.36 that the data from sand K and $N_{20}K_{80}$ looks suspect as discussed earlier in this section and is not included in the following discussion. Apart from these sands, the shell and the glass spheres (S1, S3.4 and S4) the data lies in a relatively narrow band within the range of published values. Of primary interest in this investigation was the range of velocities exhibited by saturated sand-size sediments over their complete range of packing structures. $V_p max - V_p min$ varies from 71 m/s for sand J to 177 m/s for sand $N_{20}F_{80}$ with an average value of 114 m/s taken from Tables 4.8 and 4.10, excluding SH, K, $N_{20}K_{80}$, S1, S3.5 and S4. $V_p max - V_p min$ for SH was 105m/s and the average for the glass ballotini (S1, S3.5 and S4) was 60 m/s.

The variation in V_p with n for the 25 samples investigated in this study are in broad agreement with the data on four samples obtained by

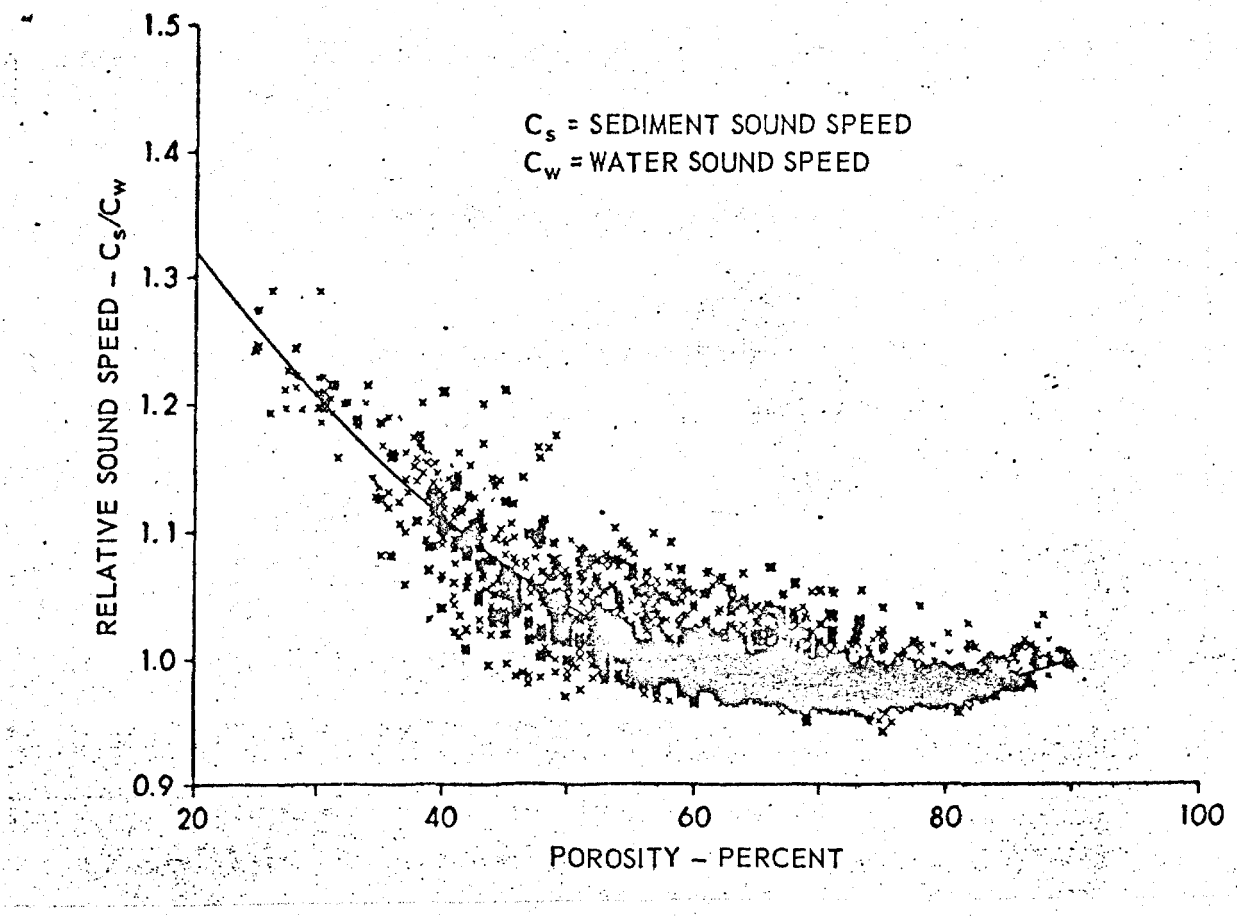

FIGURE 4.35 Relative Sound Speed vs Sediment Porosity
[after Akal, 1972]

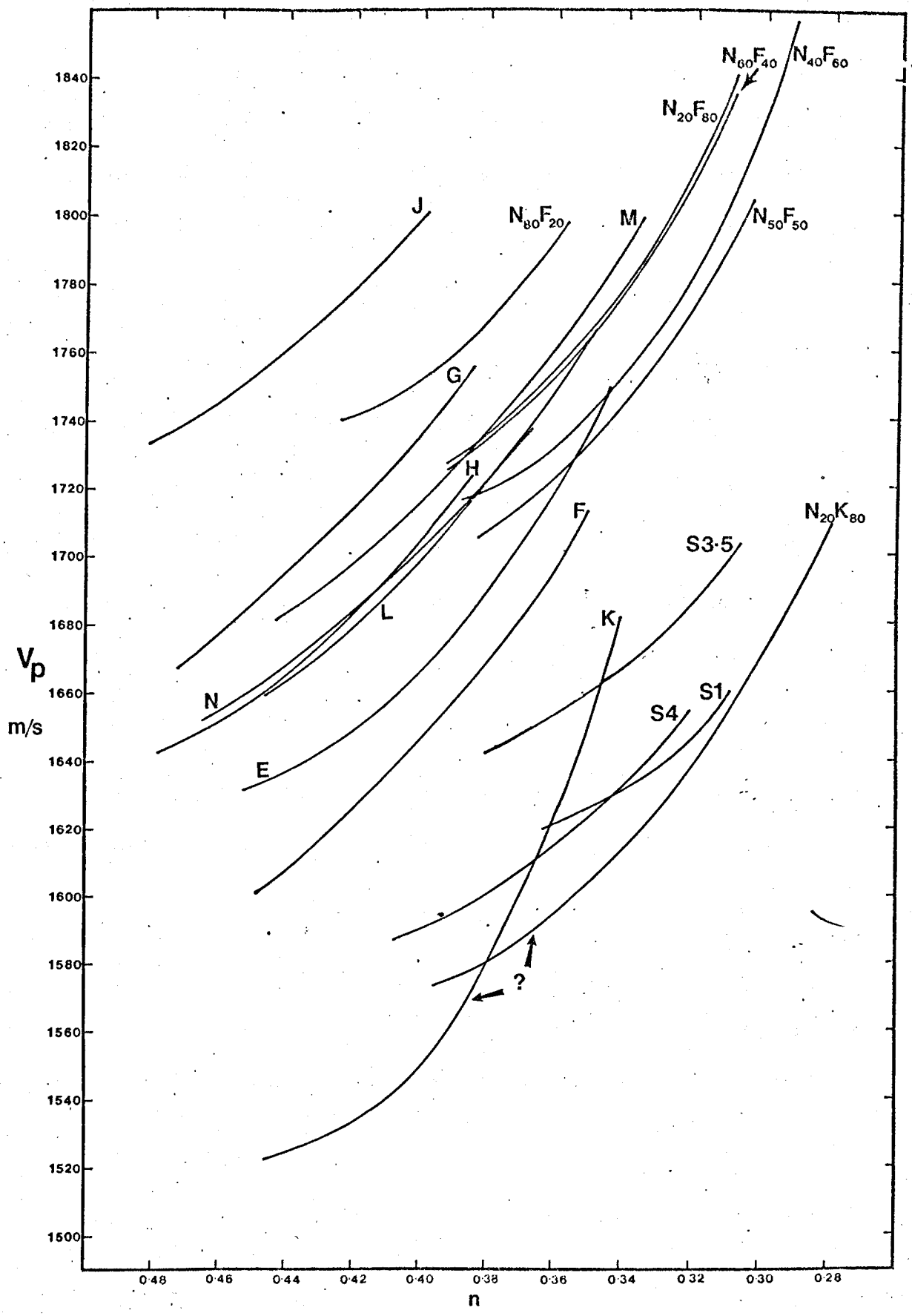

FIGURE 4.36 V_p vs Porosity for the sands tested in the porosity cell

Simpkin(1974) using a similar experimental procedure. Simpkin(1974) also notes that the gradient $\frac{\Delta V_p}{\Delta n}$ tends to increase as n decreases. This is a common feature of all the sediments tested in the porosity cell. Also reported are variations in V_p for different runs of the same sediment of up to ± 15 m/s which is very similar to the data presented here. He also concludes that these differences cannot be accounted for by experimental error and must be caused by variations in packing caused by both random elements and slight changes in the deposition and vibration programmes of each run.

An examination of the relationship between V_p and the relative porosity reveals that the band of results is as wide as when n is used. Therefore, although relative porosity is an important parameter for describing the state of a sand structure it does not contribute to an understanding of the variation of V_p with n. It is interesting to note here the problems of determining relative porosity with accuracy. Caution should always prevail when using relative porosity as a structural parameter because of the large errors than can result from its determination (Tavenas et al., 1973). Porosity by itself can be a difficult parameter to ascertain with confidence (especially in saturated sands in situ). A small error in the determination of maximum porosity, minimum porosity and actual porosity can accumulate a large error when the relative porosity is determined (equation 2.29). Table 4.19 illustrates this point with a simple example. Real and measured values of n, n_{max} and n_{min} vary by only ± 0.01, however, the computed values of relative porosity (n_r) differ by ± 20%.

	REAL VALUE	MEASURED VALUE (1)	MEASURED VALUE (2)
n	0.41	0.40	0.42
n_{max}	0.46	0.47	0.45
n_{min}	0.36	0.37	0.35
n_r%	50	70	30

TABLE 4.19 - EXAMPLE OF HOW ERRORS IN POROSITY MEASUREMENTS INFLUENCE THE CALCULATED RELATIVE POROSITY

Despite the narrow band within which the results lie, an attempt has been made to investigate whether the inherent grain characteristics can account for the differences that exist between each sand. Figure 4.37 is a plot of compressional wave velocity against mean grain size (D_M). Not only is the range of velocities for each sand clearly illustrated but the velocity at a common porosity (37.5%) is shown (read from Figures 4.11 and 4.36. Where the sand did not pass through this porosity an extrapolated value has been plotted. Published data collected in situ undoubtedly shows that a scattered correlation exists between mean grain size and sound velocity over the whole spectrum of marine sediments (e.g. Taylor Smith, 1974, p. 43, Fig. 1). The scatter is particularly apparent in sizes above 0.1 mm (i.e. in the sand range). Although, theoretically, grain size has no influence on the porosity of a non-cohesive granular material, in natural sands smaller grain sizes generally exhibit higher porosities than larger grain sizes (see Figure 4.38). As the sand size decreases, friction, adhesion and structural bridging become important because of the increasing ratio of surface area to volume. This, together with more variation in grain shape as the size decreases, leads to higher porosities. Coarser sediments, when naturally deposited,

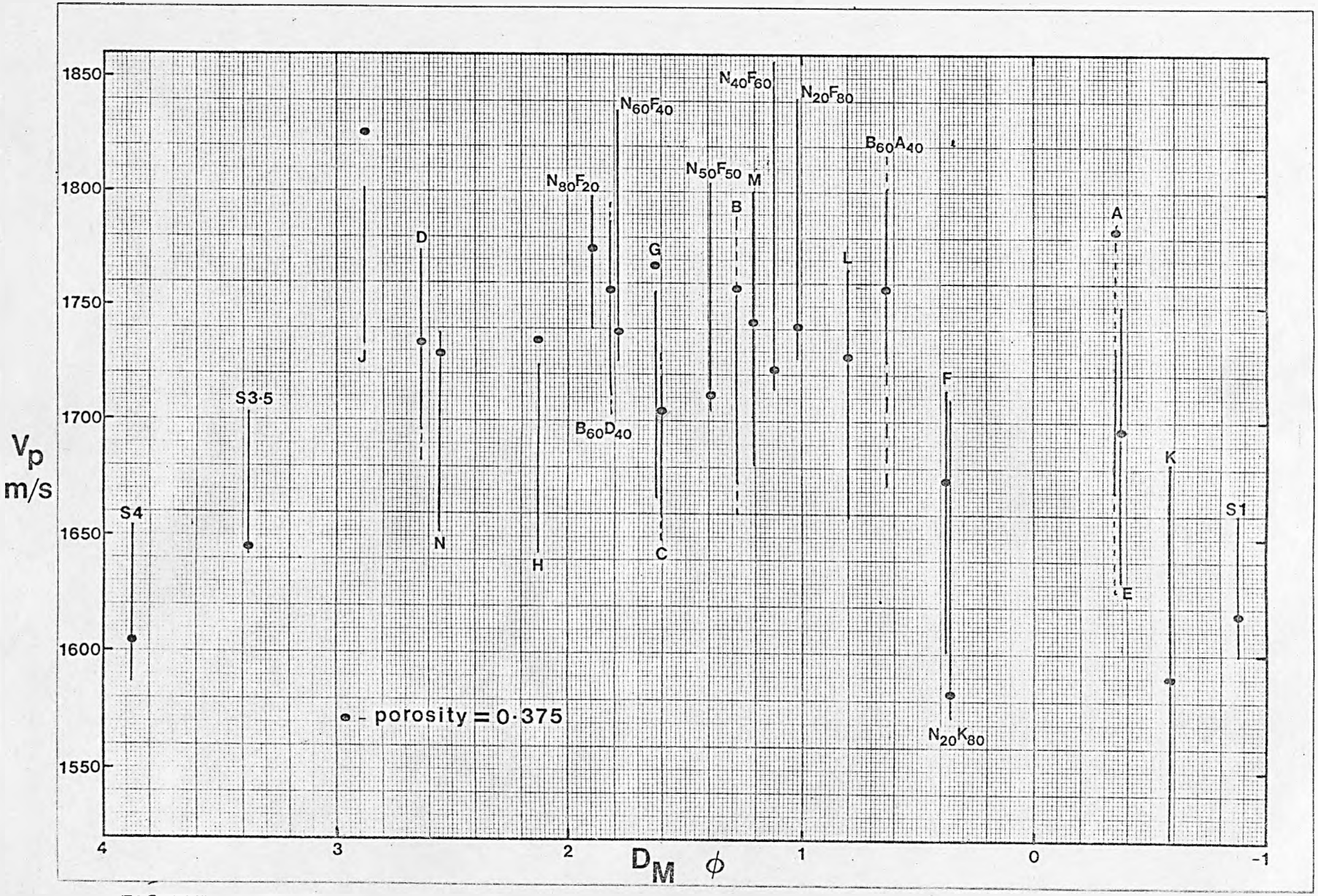

FIGURE 4.37 Compressional Wave Velocity vs Mean Grain Size for all the sands tested

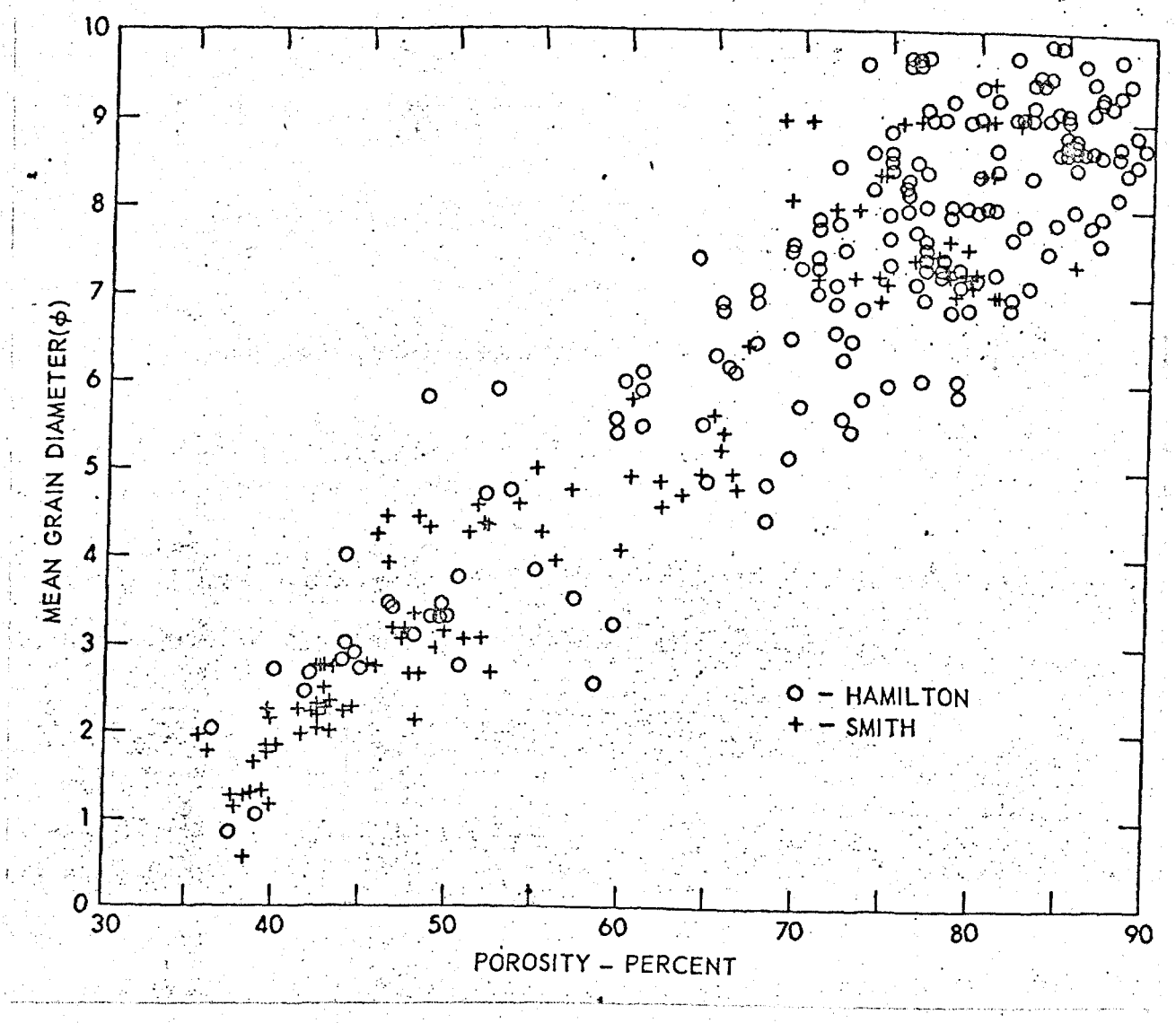

FIGURE 4.38 Mean Grain Diameter vs Porosity
[after Anderson, 1974]

will, therefore, have higher sound speeds purely as a function of porosity. It has not conclusively been determined if grain size along influences sound speed.

In Figure 4.37 there is no obvious correlation between D_M and V_p. However, apart from S4 and S3.5 (and ignoring K and $N_{20}K_{80}$) there is a definite trend of increasing V_p as the grain size decreases.

A better correlation exists between the mean roundness R_{50} (obtained from Figures 4.2 and Table 4.16) and V_p as shown in Figure 4.39. This shows a definite increase in V_p with increasing angularity. The tentative trend seen in Figure 4.37 can, therefore, be accounted for by the fact that, apart from the small glass spheres S4 and S3.4, the angularity of the grains generally increases as the grain size decreases. On this evidence it is concluded that V_p is unaffected by grain size alone but does seem to be affected by the grain shape. A linear regression analysis on this data produces the equation $V_p = -199.5R_{50} + 1814.4$.

On the basis of the above arguments a complex situation exists where the in-situ V_p increases with increasing grain size as a result of lower porosities but at constant porosity V_p increases with decreasing grain size as a result of increasing angularity. V_p increases with increasing angularity as a result of the increasing rigidity component $\frac{4G}{3}$ in the equation 2.4.

$$V_p = \left(\frac{K}{\rho} + \frac{4G}{3\rho}\right)^{\frac{1}{2}}$$

which is obtained from the shear wave velocity, V_s.

The other sorting characteristics showed no correlation with the compressional wave velocity.

Attenuation measurements were made concurrently with those of velocity in the ARL tank and this data is summarised in Figure 4.15. Clearly there

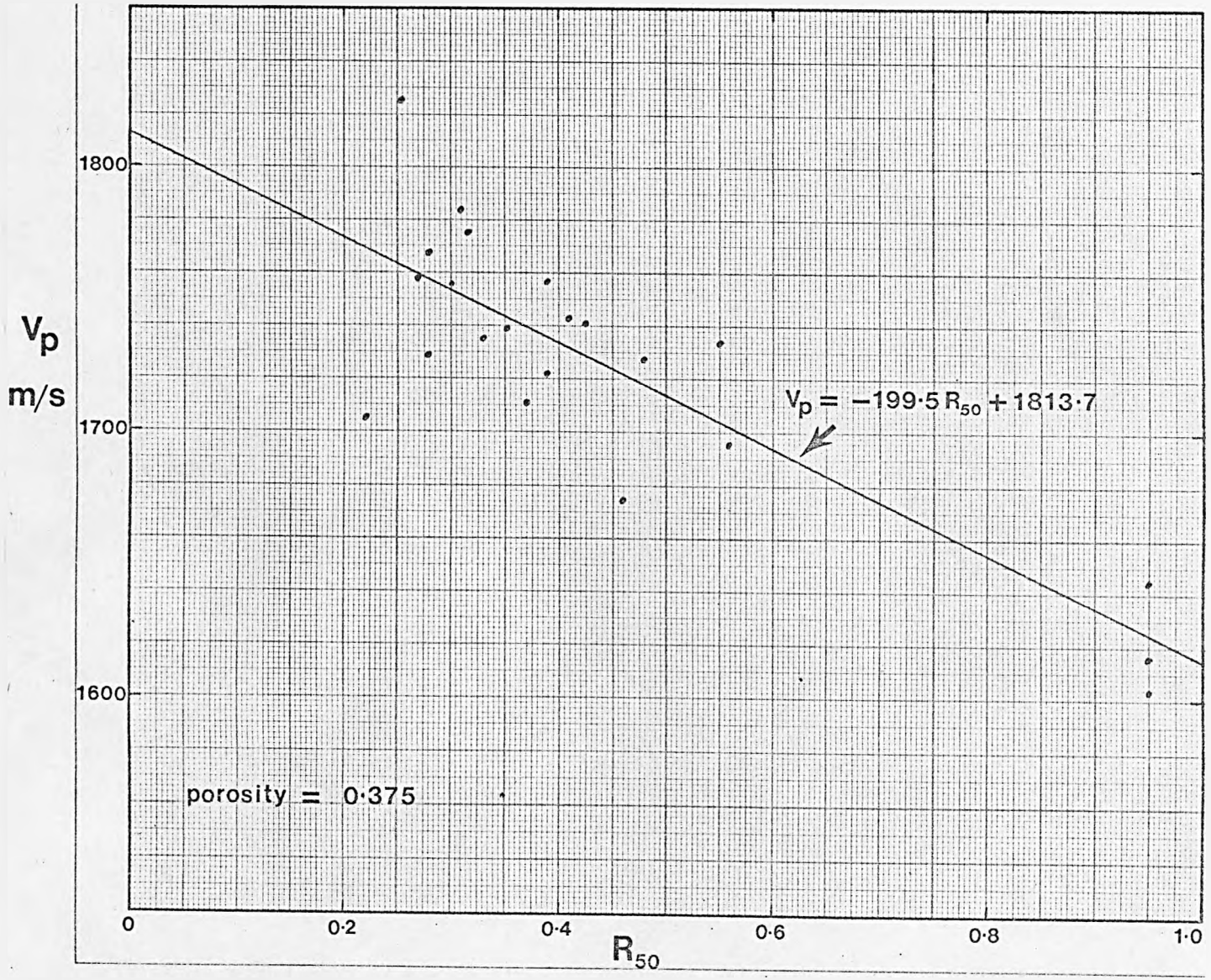

FIGURE 4.39 Compressional Wave Velocity vs Mean Grain Roundness

is a noticeable effect caused by a change in porosity for a given sand. Up to 10 dB m^{-1} has been recorded for a change in porosity from a maximum to a minimum (i.e. $\cong$ 1 dB m^{-1} for a 1% change in porosity). It is evident that the variation in attenuation coefficients for the different sands is several times greater than the changes caused by porosity. Figure 4.40 shows a plot of attenuation coefficient against mean grain size at a common porosity ($\cong$ 37.5%). Figure 4.41 summarises most of the published attenuation data in pure sand. Results from this study at 112 kHz lie within these published values. However, an increase in attenuation with increasing mean grain size is found agreeing with the data of Busby and Richardson (1957) but disagreeing with the data of Hampton (1967) and Nolle (1963). In-situ data of Hamilton and Taylor Smith have been combined by Anderson, A. (1974) (Figure 4.42) showing a maximum attenuation in fine sand size sediments. This data, especially in the sand range, is very scattered. No useful conclusions can be made from the few results obtained, only the inconsistencies in attenuation values with mean grain size from different sources, are worth noting.

4.3.3 Shear wave data

The accuracy of the shear wave velocity is difficult to estimate with any degree of certainty but a worse case will be considered. Calibration procedures in a large tank of dry sand of the cantilever mounted shear wave elements used in the porosity cell clearly demonstrated that by identifying the onset and using the distance between the outer edges of the element a straight line, distance versus time graph, is obtained which passes through the origin. The distance between the transducers remained constant throughout the test and hence a systematic error of $\frac{0.5}{49.6} \times 100 = 1\%$ is the largest that could occur. This would

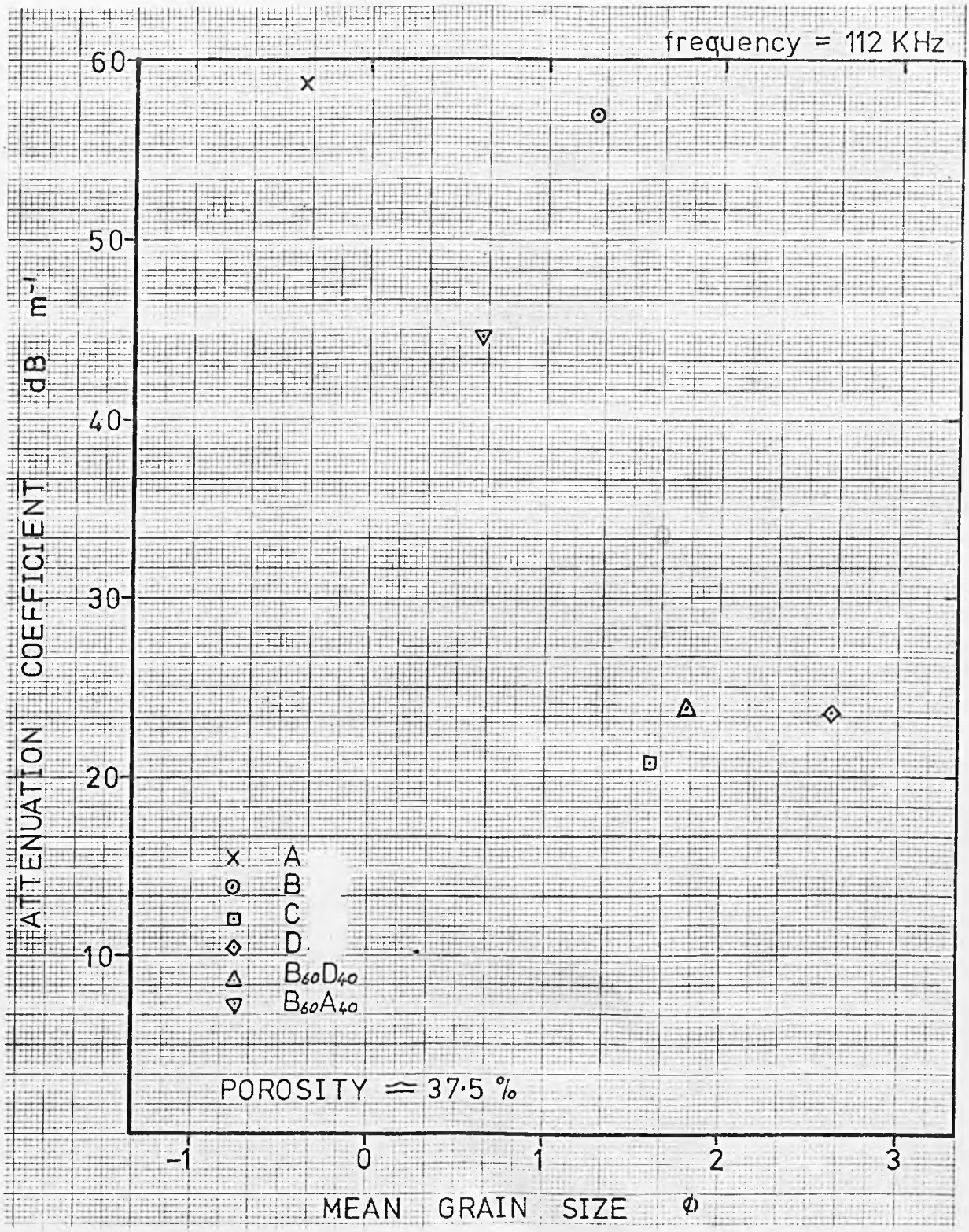

FIGURE 4.40 Compressional Wave Attenuation Coefficient vs Mean Grain Size for the ARL sands

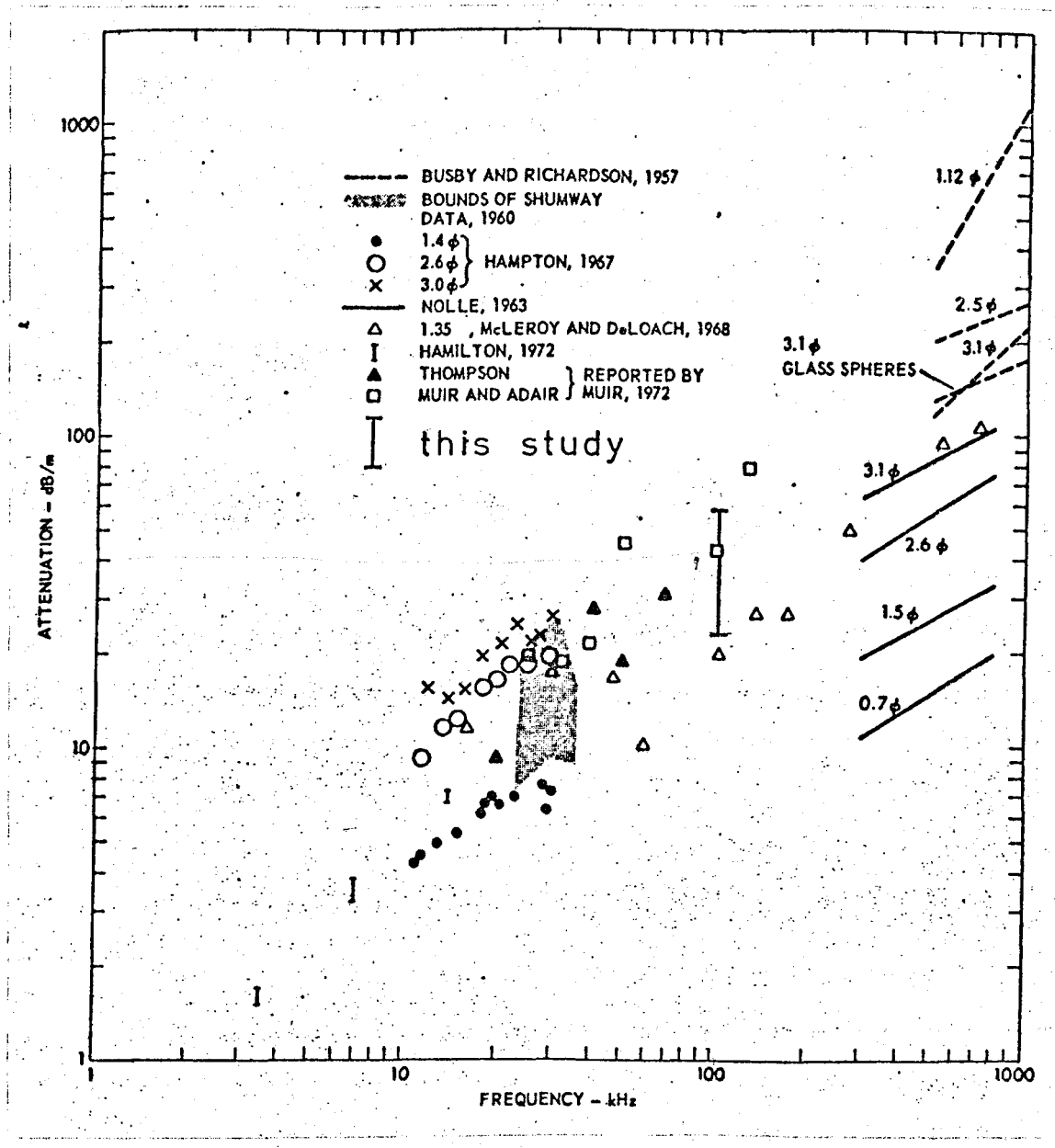

FIGURE 4.41 Compressional Wave Attenuation vs Frequency for sands [after Anderson 1974]

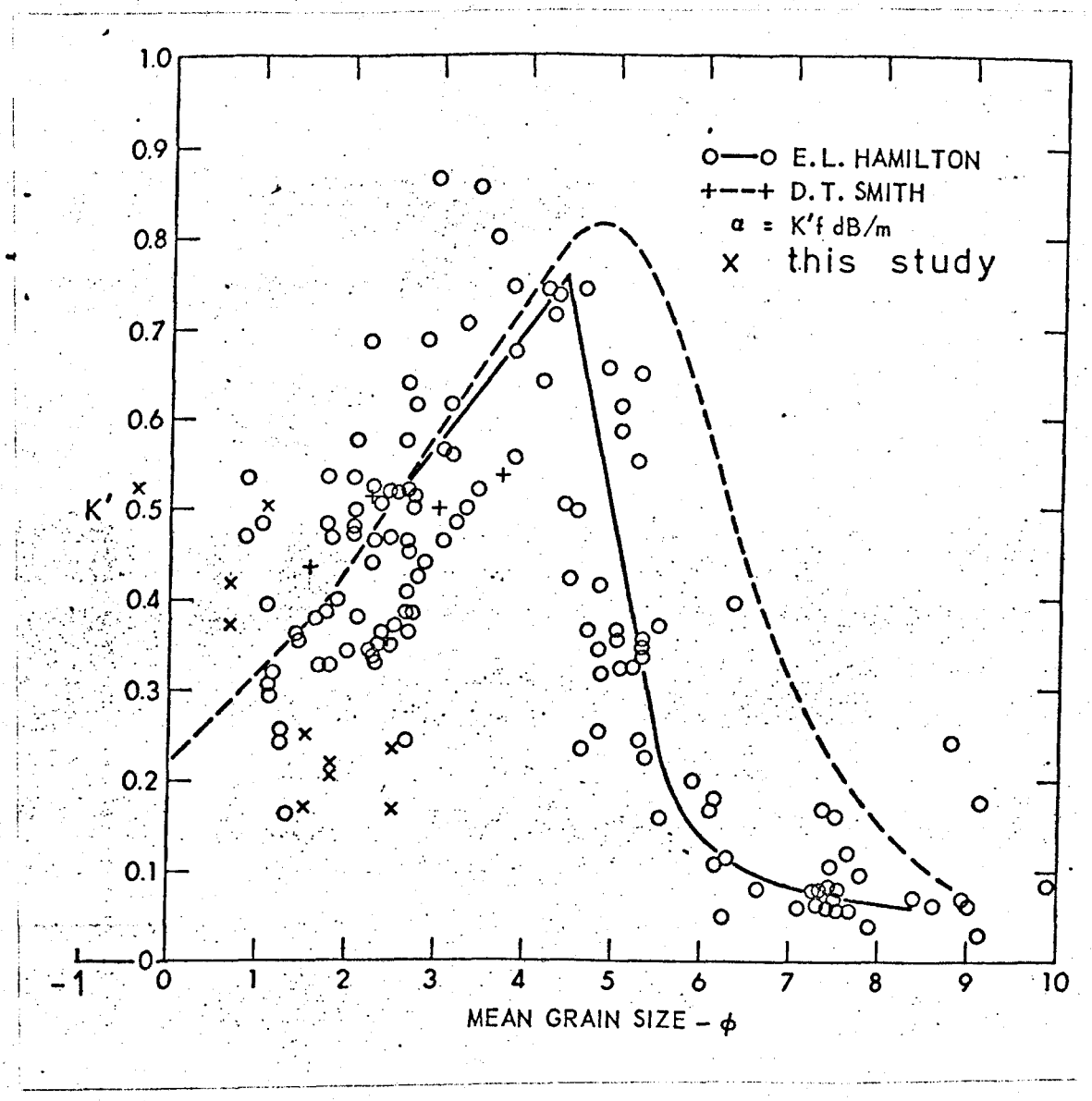

FIGURE 4.42 Mean Grain Size vs Compressional Wave Attenuation Constant K'
[after Anderson, 1974]

result in a ± 0.2 m/s error when V_s = 20 m/s or ± 1.4 m/s when V_s = 140 m/s.

Timing errors constitute the main source of random error and while the time intervals were measured to 1μsec the more likely accuracy is only ± 50 μsec. This produces errors ranging from ± 10% or ± 10 m/s when V_s = 100 m/s to ± 5% or ± 2.5 m/s when V_s = 50 m/s. These values are consistent with much of the random scatter of data in Figures 4.28 to 4.33. It does not, however, explain all the differences between the different runs for each sand tested.

Figures 4.17 and 4.43 summarise the V_s versus n data for the ARL tank and the porosity cell respectively. Linear plots are drawn in Figure 4.17 because of the sparse data and the broken lines shown are extrapolations to maximum and minimum porosities. It is clear from Figure 4.43 that the trends are not linear but have a slightly increasing gradient with increasing porosity for most of the samples. Velocities measured range from 17 m/s to 149 m/s and the ranges of velocity for each sample vary from 23 m/s to 91 m/s with an average of 48 m/s.

Shear waves in marine sediments have been studied much less than have compressional waves, despite their potential value, because of the difficulties of propagating such a stress wave. Hamilton (1975) reviewed what little information existed on saturated marine sediments. Results from Cunny and Fry (1973) form the bulk of the sand data used. Velocities varied from 53 m/s to 287 m/s in the depth range 0.1m to 7.2m. Higher values, up to 567 m/s , are reported in Hamilton's review, but near-surface velocities (less than 0.5m) only vary between 53 m/s and 140 m/s. Effective pressure, from over-burden, is a critical factor causing large increases in shear wave velocity. Therefore, only the near-surface data can be compared with the results of this study.

The overall results from this present study are in general agreement

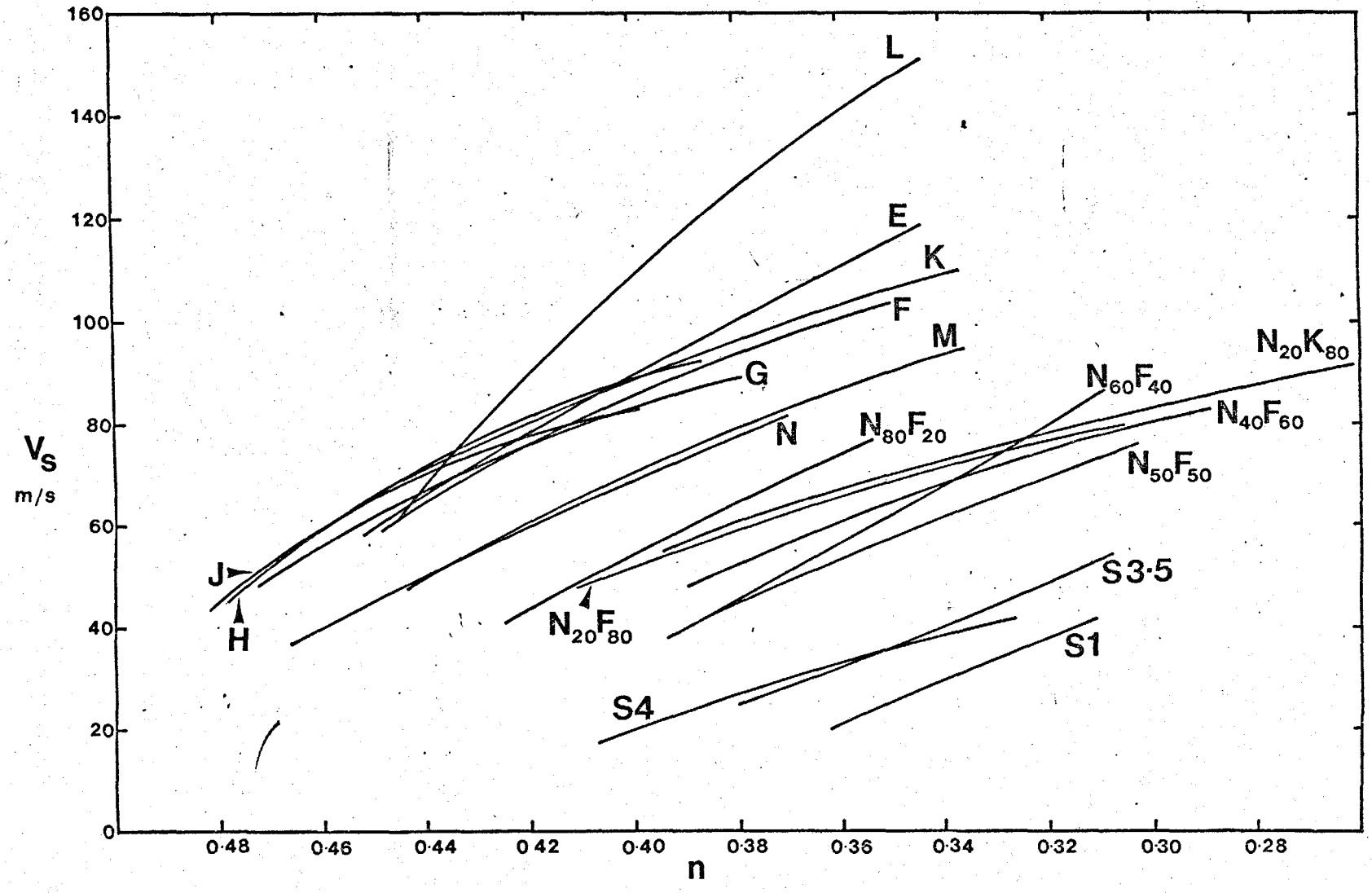

FIGURE 4.43 Shear Wave Velocity vs Porosity for the sands tested

with those of Cunny and Fry (1973). Values lower than 53 m/s are attributed to very loose packing structures, which are unlikely to exist in-situ and artificial sediments (glass spheres).

Shear wave velocity is plotted versus the mean grain size in Figure 4.44 with values at a common porosity (n = 0.375) shown for comparison. There is clearly no obvious correlation between V_s and D_M even at a constant porosity. Figure 4.45 plots V_s at the 0.375 porosity level versus the mean roundness R_{50}. The extrapolation of the shell sample to this porosity is not a real attempt to predict the velocity at a porosity of 0.375 but to illustrate the trend of increasing velocity with increasing angularity. Using all the points on the graph the following equation was found by a linear regression analysis

$$V_s = -90.5R_{50} + 114.8$$

Apart from the samples SH, L, S4, S3.5 and S1, another group stands out for special mention. The group labelled 'mixtures' contains all the samples composed of two sand types. They form a closely grouped set below the main body of data. The remaining sands over the small range of R_{50} from 0.22 to 0.56 show no obvious correlation with V_s. Sand L has a high value of V_s which may be attributed to the large sorting coefficient. However, sand B has an even larger sorting coefficient and does not have an abnormally high value of V_s. There is in general no correlations between any of the sorting characteristics measured and V_s.

The group of sands labelled 'mixtures' are artificial distributions composed of two other sands. It is readily apparent that these 'mixtures' exhibit lower shear wave velocities and hence a lower elastic shear modulus. In a non-cohesive sand this shear modulus results from frictional forces at grain contacts and from geometrical 'interlocking' of grains. It is no surprise, therefore, to find large increases in

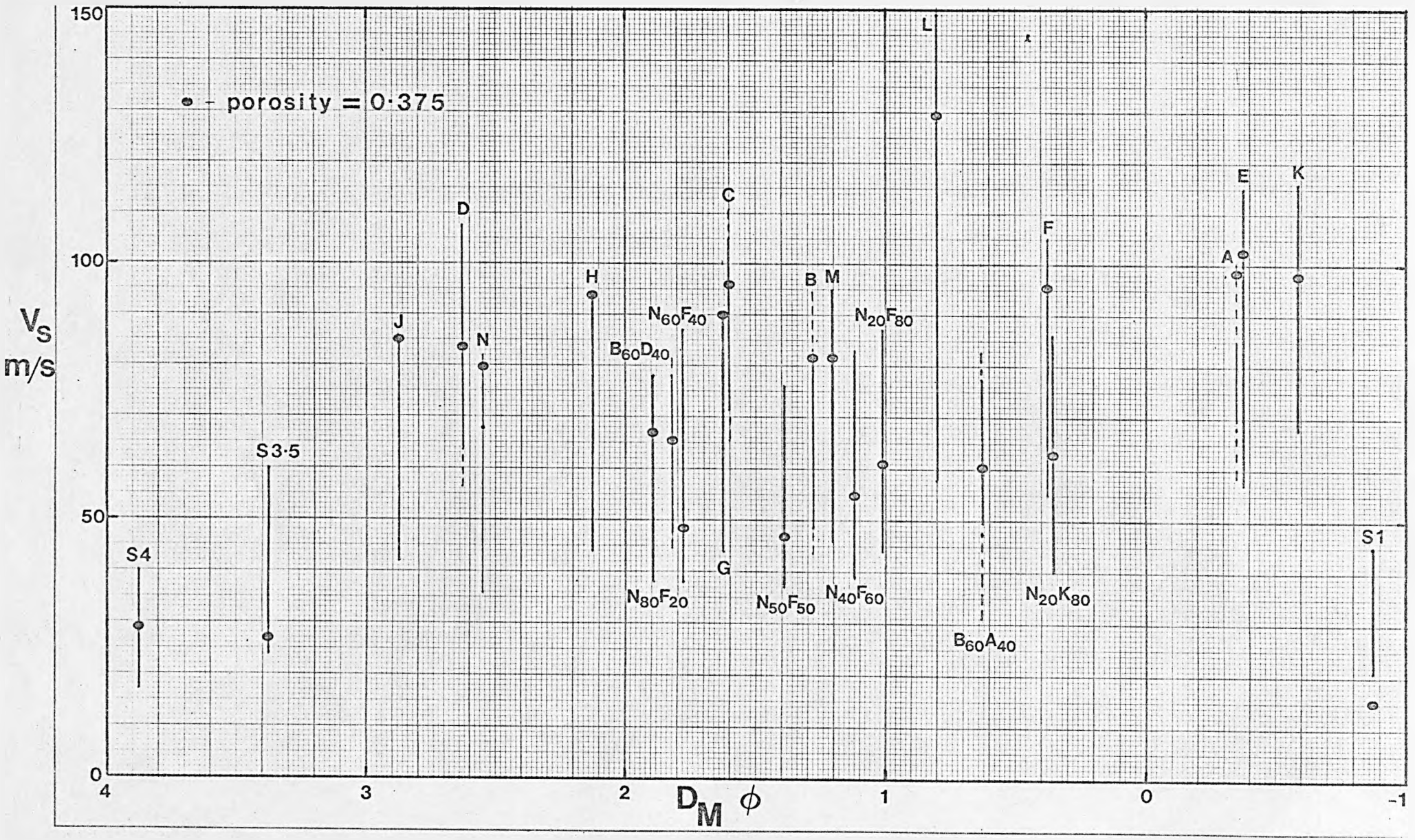

FIGURE 4.44 Shear Wave Velocity vs Mean Grain Size for all the sands tested

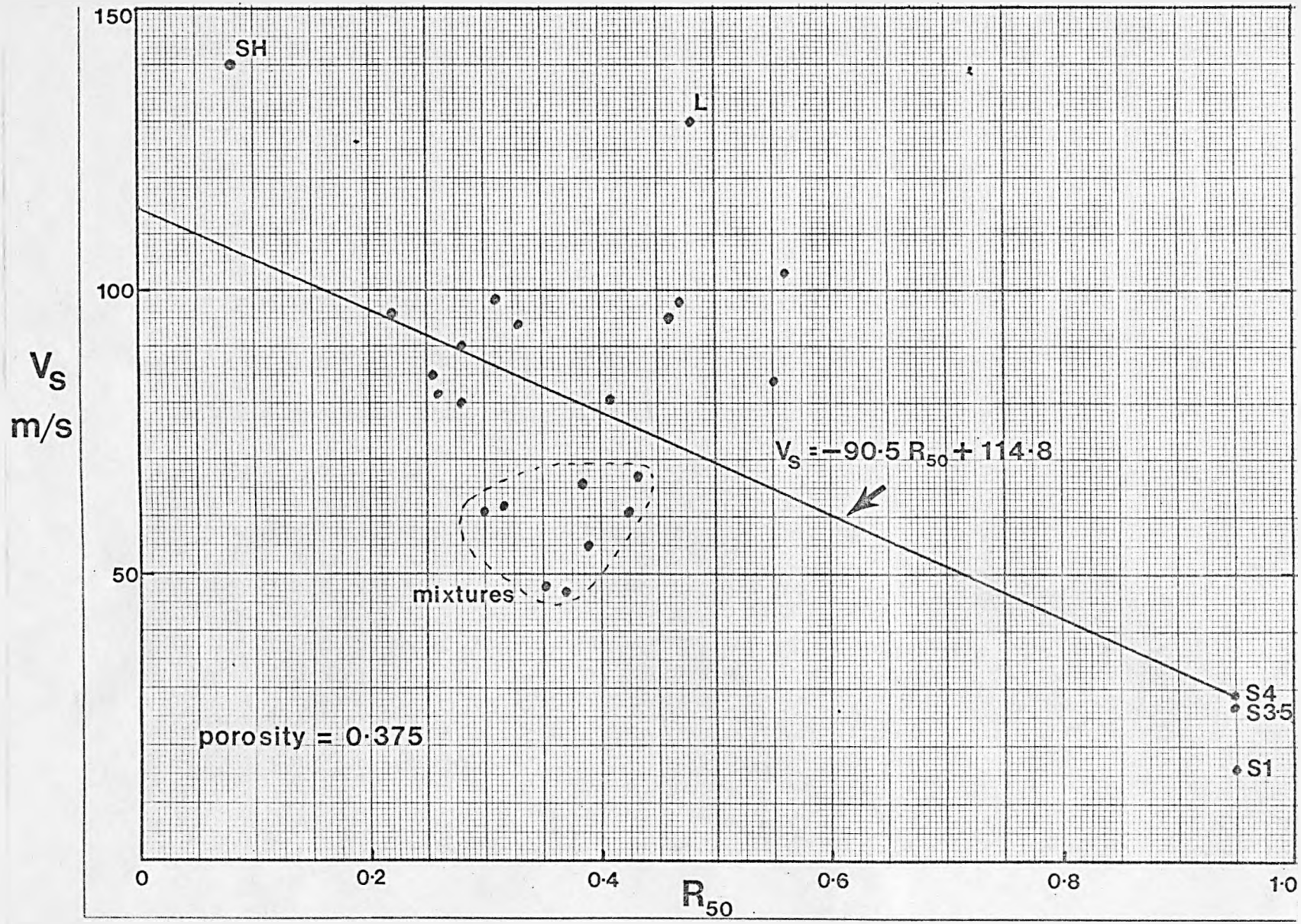

FIGURE 4.45 Shear Wave Velocity vs Mean Grain Roundness for all the sands tested

shear wave velocity as the packing structure decreases in porosity. Grain size is essentially a geometrical factor and the lack of correlation with shear wave velocity is consistent with this idea. At any given porosity the distribution of grain sizes will have a marked effect on geometrical configurations and hence possibly the shear modulus. From the data of these experiments it is found that the velocity is lower for the samples composed of a mix of two other sands. This may seem to contradict some ideas on natural packing suggesting that wide ranges of particle size produce structures with increased rigidity. A conceptual model that fits the data of this study is one whereby in wider grain size distribution sands the larger grains form the rigid framework in which the smaller grains lie. In this case the smaller grains (or some of them) do not contribute to the overall rigidity of the structure. This would account for the lower shear wave velocities. This model does not contradict the idea that wide ranges of particle sizes have higher natural rigidities, this could be a result of a lower overall porosity being attained compared with a uniform grain size structure. Only at equal porosities would the more uniformly sized sand exhibit higher velocities. The sand with a wider range of grain size would be able to exhibit both lower porosities and higher rigidities.

A situation may also exist where the geometrical packing arrangements of the grains in this study (using the vibrating technique) are substantially different from natural packing structures with the same grains and at the same porosity. It could also be argued that the distributions themselves may cause effects not found in natural distributions. The mixtures were artificially prepared to increase the spread of grain sizes. They have the lower velocities which may be a consequence of their artificial preparation rather than a result of their grading. If this

were the case then a natural sand with the same grain sorting coefficients as the 'mixtures' may have much higher shear wave velocities. It is also to be expected from purely geometrical considerations that certain distributions of grain size (whether natural or artificial) will maximise 'intergrain locking' and hence shear wave velocity.

There is one trend in the V_s data for the mixtures of sand N and F. That is, while all the mixtures have values of V_s, when n = 0.375, lower than either N or F, a minimum value of V_s occurs when there is roughly equal amounts by weight of each sand. This is illustrated in Figure 4.46. It would seem from this data that a mixture of these two sands in any proportion is unlikely to exceed the V_s value for sand F.

While discussing the effect a sand structure can have on the shear wave velocity, it is interesting to note an effect observed during some runs using the porosity cell. With reference to Figure 4.28 for sand E, run 1 shows a distinct break in the V_s versus n trend when n = 0.412. It suggests that during the vibration process a structure was forming that had a rigidity that, although it was high, was unstable. The trend is not observed in runs 2 and 3. This type of behaviour can also be clearly observed for sands F (runs 1, 2 and 3), G (run 1), J (run 3), L (runs 2 and 3) and M (run 1). In sand F,where the sudden drop in velocity occurs for all three runs, a discontinuity can be clearly seen at the same time in the V_p data, indicating that the effect is not due to any experimental errors. It must be remembered that the vibration procedure (e.g. switching off suddenly from maximum vibration) could produce very erratic data.

Finally, one other observation is worth noting. The value of V_s invariably increased over long periods of time (overnight) typically by a factor of up to 2 or 3. This was conclusively proved to be a function

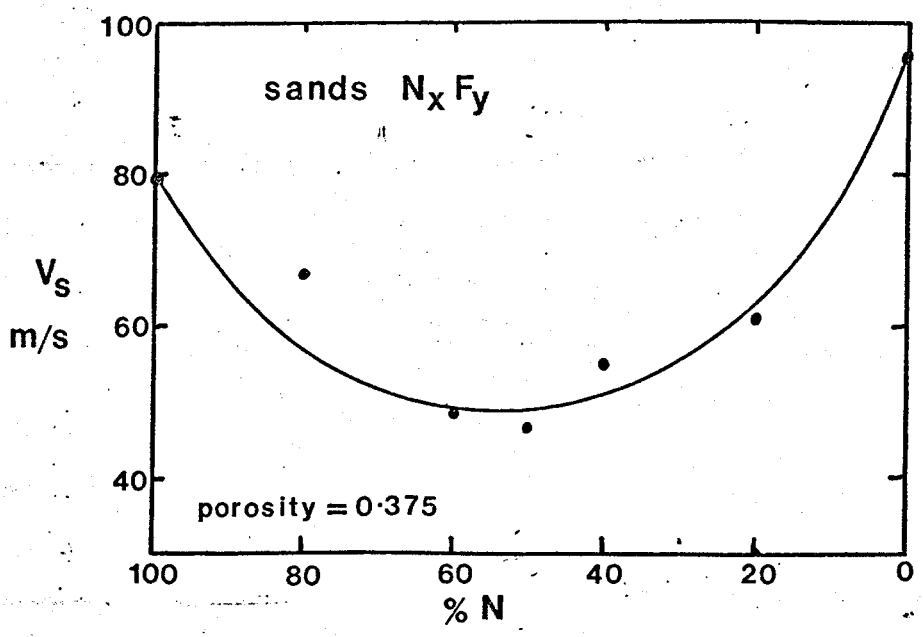

FIGURE 4·46 Shear Wave Velocity vs % N for the sand mixtures $N_X F_y$

of temperature variation causing stresses to be applied to the sand structure by contraction of the cell. A minimal amount of vibration caused V_s to return very close to its original value.

4.3.4 Elastic moduli

In this section the values of V_s, V_p and n are used to investigate how the data, for all the sands tested, influences the moduli computed using elastic theory.

The V_p and V_s data summarised in Figures 4.11, 4.17, 4.36, 4.43 and for the shell sample in Figure 4.33 can be divided into groups. For V_s four main groups are assigned; SH for the shell sample because the porosities are not comparable with any other sample, S for the glass spheres, MIX for the mixtures of different sands and X for the remaining samples. Using these divisions four V_s versus n graphs are produced in Figure 4.47a representing generalised trends for the different types of sand. The same procedure has been used for V_p in Figure 4.47b except that X and MIX are represented by the same curve. The following equations summarise the simplified data produced in Figure 4.47 where V_s and V_p are in m/s and n is the fractional porosity.

X:- $V_s = 172.9 + 46.4n - 654.8n^2$,
MIX:- $V_s = 48.4 + 480.4n - 1220.2n^2$, } $V_p = 2913.1 - 4998.8n + 4916.1n^2$

S:- $V_s = 67.0 + 223.6n - 892.9n^2$, $V_p = 2390.1 - 3412.7n + 3616n^2$

SH:- $V_s = -199.8 + 1341.1n - 1398.8n^2$, $V_p = 2686.3 - 3205.4n + 2053n^2$

From these equations it is possible to show how the calculated elastic moduli vary with porosity for these types of sediments. In Figure 4.48 the values of G and K have been plotted using equations 2.9 and 2.10 and E is plotted using equations 2.3 and 2.6 together with the

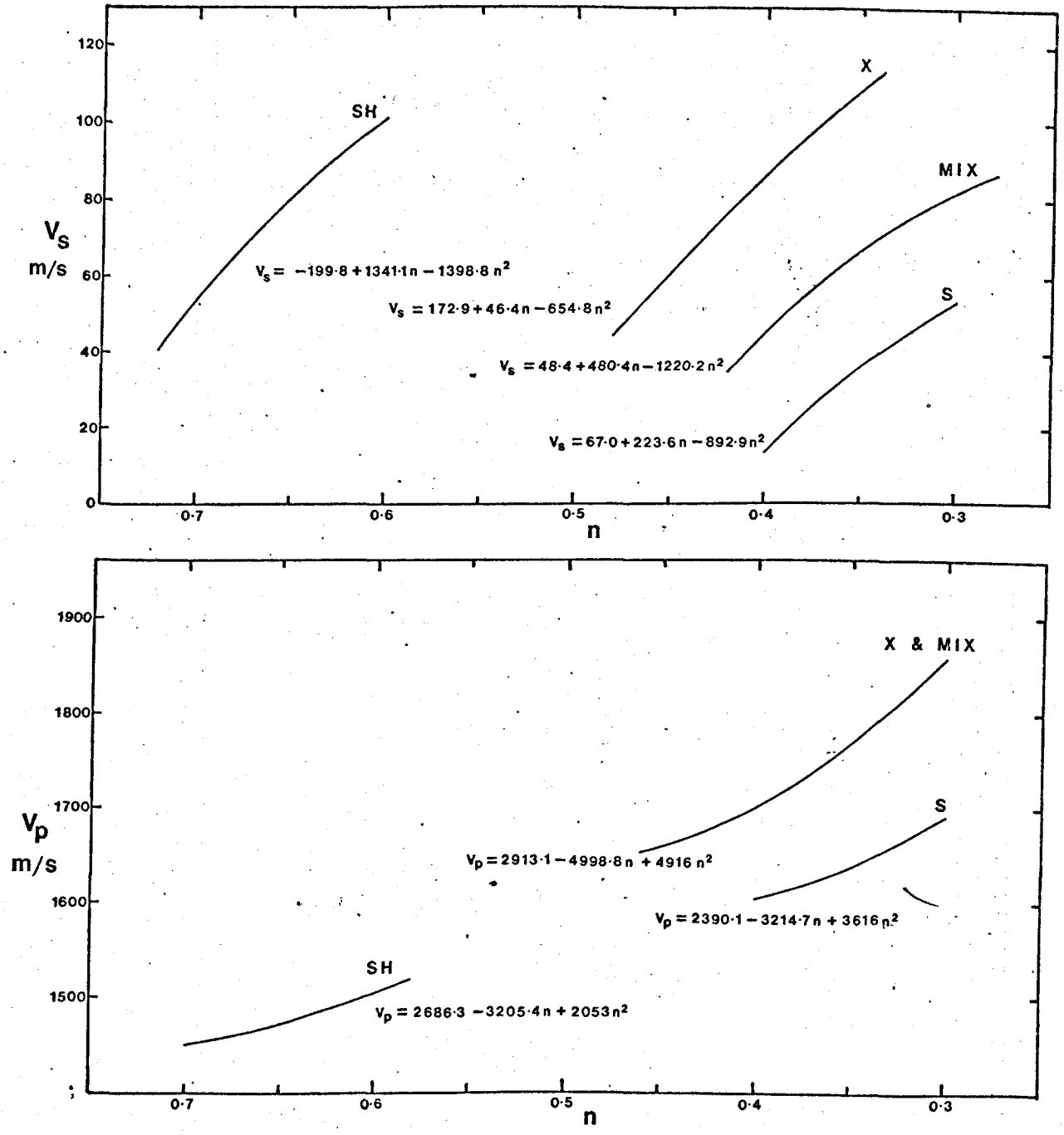

FIGURE 4.47 Compressional and Shear Wave Velocity vs Porosity for the simplified groups of sands X, MIX, S & SH

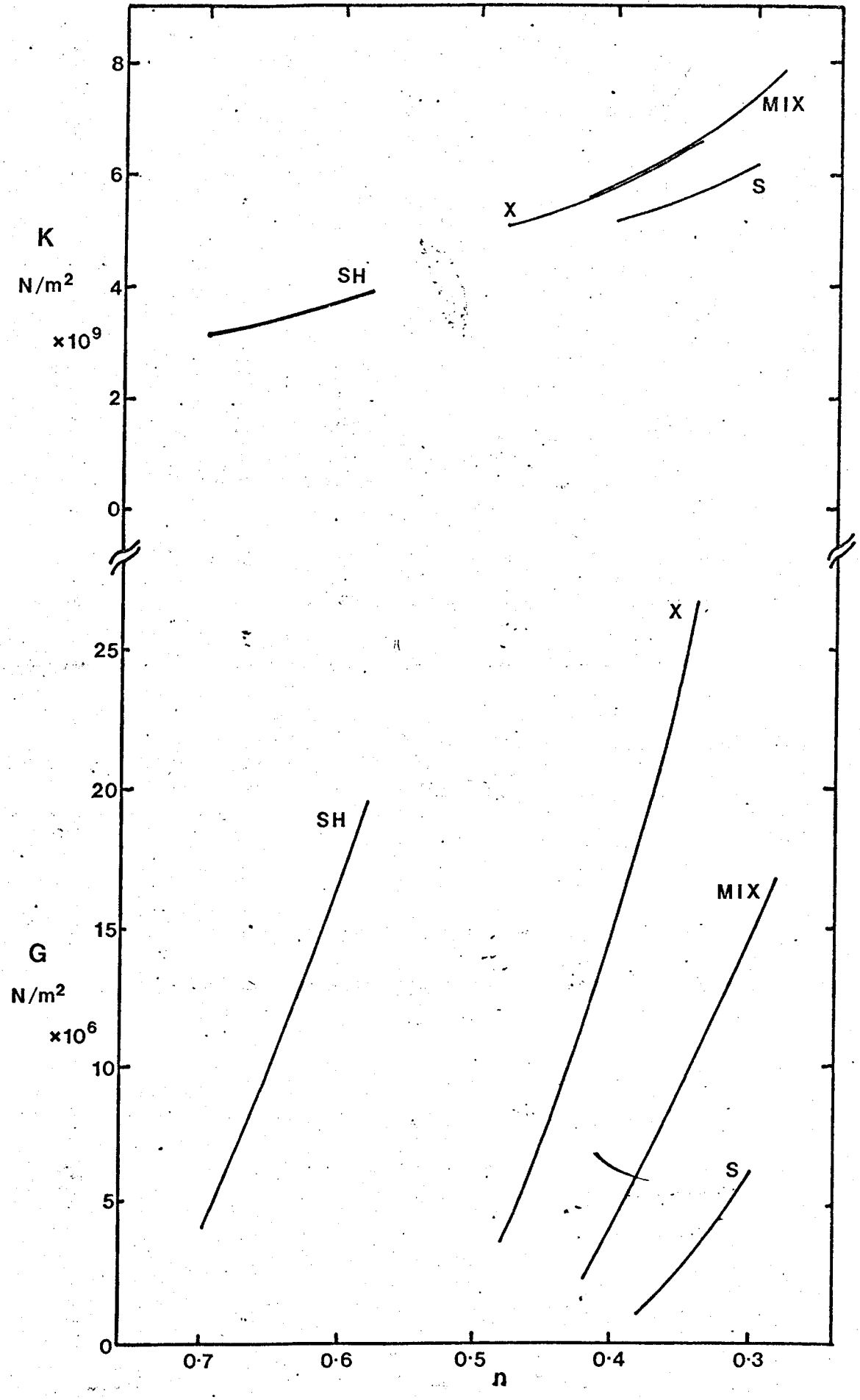

FIGURE 4.48 Bulk and Shear Modulus vs Porosity for sands X, MIX, S & SH

velocity ratio V_p/V_s in Figure 4.49. Apart from the bulk modulus K, this data clearly demonstrates the large variation in these parameters for different sediment types. Using a constant value of porosity of 0.375 the following table illustrates the variation in the elastic moduli for sands X, MIX and S.

	X	MIX	S	
K	6.01	6.03	5.31	$N/m^2 \times 10^9$
G	19.4	6.6	1.3	$N/m^2 \times 10^6$
E	59.0	19.6	4.0	$N/m^2 \times 10^6$
V_p/V_s	17.8	30.6	65.0	

Poisson's ratio, ν, varies very little at these large V_p/V_s ratios. The actual variation is from 0.4962 for SH when n = 0.58 to 0.4999 for S when n = 0.40. Bulk modulus, K, changes very little for different types of sediments at similar porosities. In contrast to K, the shear modulus, G, containing the V_s^2 term, produces very marked changes as a result of differences in grain shape and size distribution. The effect of G is also similar in the expression for Young's modulus, E. While the generalised values of these moduli for sands have been known before it is now possible to estimate the likely effect caused by changes in porosity and grain characteristics.

Anderson (1974) summarised data of Hamilton and Taylor Smith showing that over a wide variety of sediment types the shear modulus reaches a maximum in the fine sand grade. No such trend is observed on the sands tested in this study. However, a large variation in moduli has been found to occur for small changes in porosity. The high rigidities reported for sediments in the fine sand range are probably attributable to a combination of both non-cohesive grain-to-grain contacts, with the resulting frictional forces and cohesive mechanisms in the

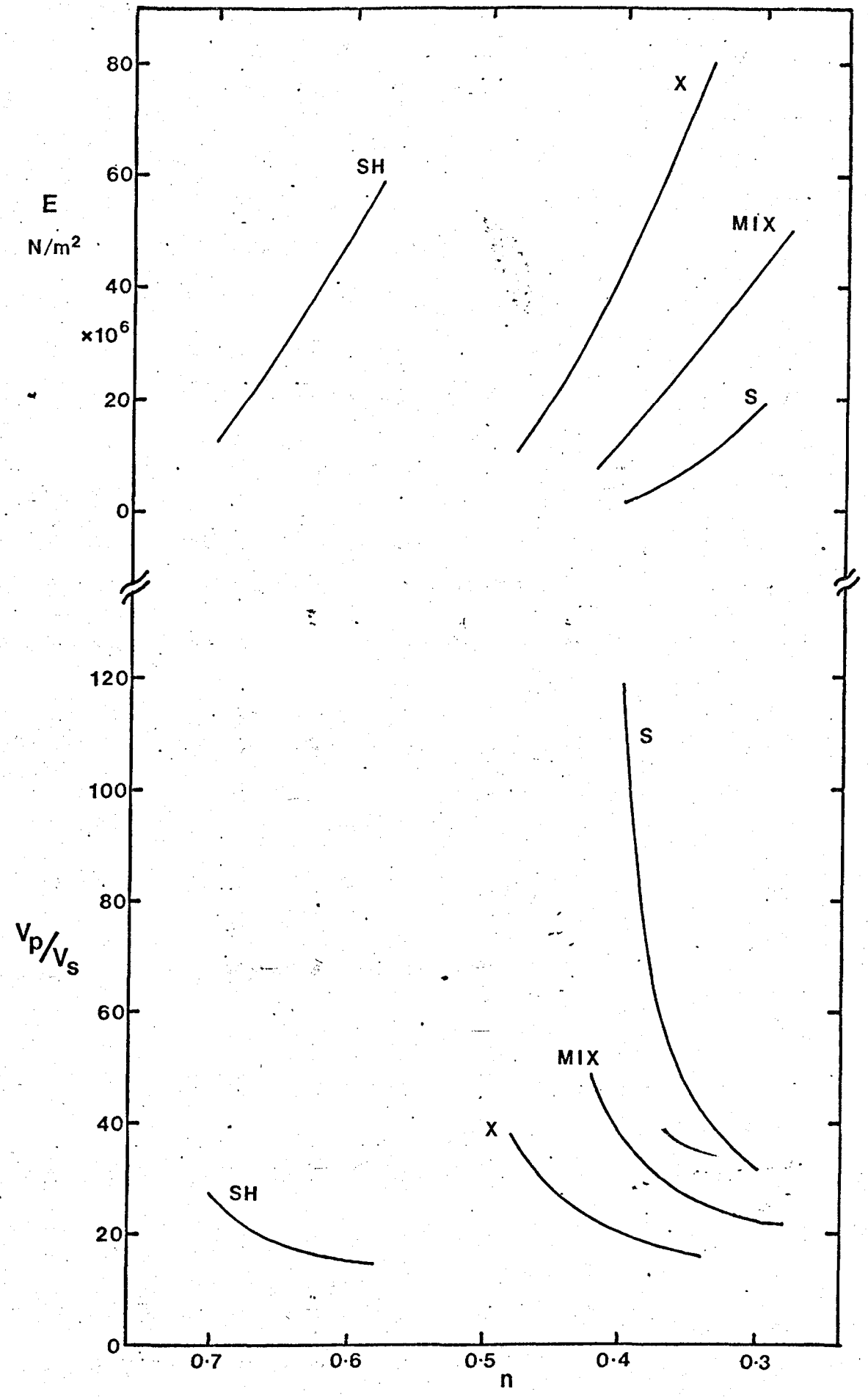

FIGURE 4·49 Young's Modulus and V_p/V_s vs Porosity for sands X, MIX, S & SH

finer particles. Sediments with mean grain sizes of around 4ϕ are particularly liable to exhibit a large range of properties purely as a result of the changes in grain size distribution. Narrow distributions will provide shear moduli based entirely on frictional forces whereas for wider distributions a combination of cohesive and frictional forces will be in operation which could maximise their cumulative effects.

5. OEDOMETER TESTS

5.1 Introduction

In chapter 3.2.4 the modified oedometer cell was described with reference to Figure 3.12. Compressional and shear wave transducers were mounted in the top and bottom porous stones either side of the sediment sample. In this chapter the details and results of some experiments using this modified oedometer are described.

Chapter 4 dealt exclusively with non-cohesive sediments under no confining pressures (apart from their own weight). It demonstrated the variability of seismic velocities with changing sediment type and packing structure. In particular, the velocity of shear waves (V_s) was shown to be highly dependent on both the porosity of the sand and its grain characteristics (grading and shape). This large variation in V_s has a profound influence on the calculated elastic moduli as shown by Figures 4.4.8 and 4.4.9.

In natural soils the moduli will, to a large extent, be influenced by factors other than grain size, shape and porosity. The most dominant parameter is undoubtedly the effective stress. For this reason alone, any understanding of the relationships which exist between the acoustic and mechanical properties of sediments can only be fully appreciated if effective stress is considered. Incorporating both compressional and shear wave transducers into laboratory soil testing cells enables the effective stress relationships to be examined. At the same time the more normally measured soil mechanics parameters can be obtained.

In this chapter some of the oedometer data is not presented in a standard format, although some of the tests were performed according to British Standard BS 1377. The purpose of these tests was to establish

that shear waves could be measured using bender elements in soils through a range of effective stresses and to investigate whether any simple correlations exist between the moduli derived from the wave velocity data (dynamic) and the moduli derived from the stress strain data (static). Much of the work in this chapter has previously been reported, (Schultheiss,1981).

5.2 Consolidation tests

Three sediments, a silt, a silty clay and a potter's clay were prepared in a water-saturated state and tested normally in the oedometer (Figure 3.12) to examine the differences in their acoustic and mechanical behaviour. The grain size distributions for these sediments are given in Figure 5.1. Each sample was loaded incrementally as in a normal consolidation test where each load is twice the previous load. Initially, when a sample is loaded, the stress is borne almost entirely by the pore water in the form of an excess pore pressure. The hydraulic gradient created drives pore water out of the sample, at a rate that depends on the soil permeability, causing a reduction in the volume of the sample. As the excess pore pressure is dissipated the load is gradually transferred to the mineral structure. The process is termed primary consolidation and is complete when the excess pore pressure is zero. Further consolidation also occurs (secondary consolidation) due to creeping of the mineral structure. In the normal consolidation test the incremental loading takes place after 100% primary consolidation has occurred. This is normally indicated by a change of slope on a strain-log time curve which for nearly all soils takes place in the first 24 hours. Stress-strain curves for the three specimens are shown in Figure 5.2 where the strain is that measured for 100% primary consolidation. The horizontal bars show the range of strain measured at each stress increment. The behaviour of the different sediments

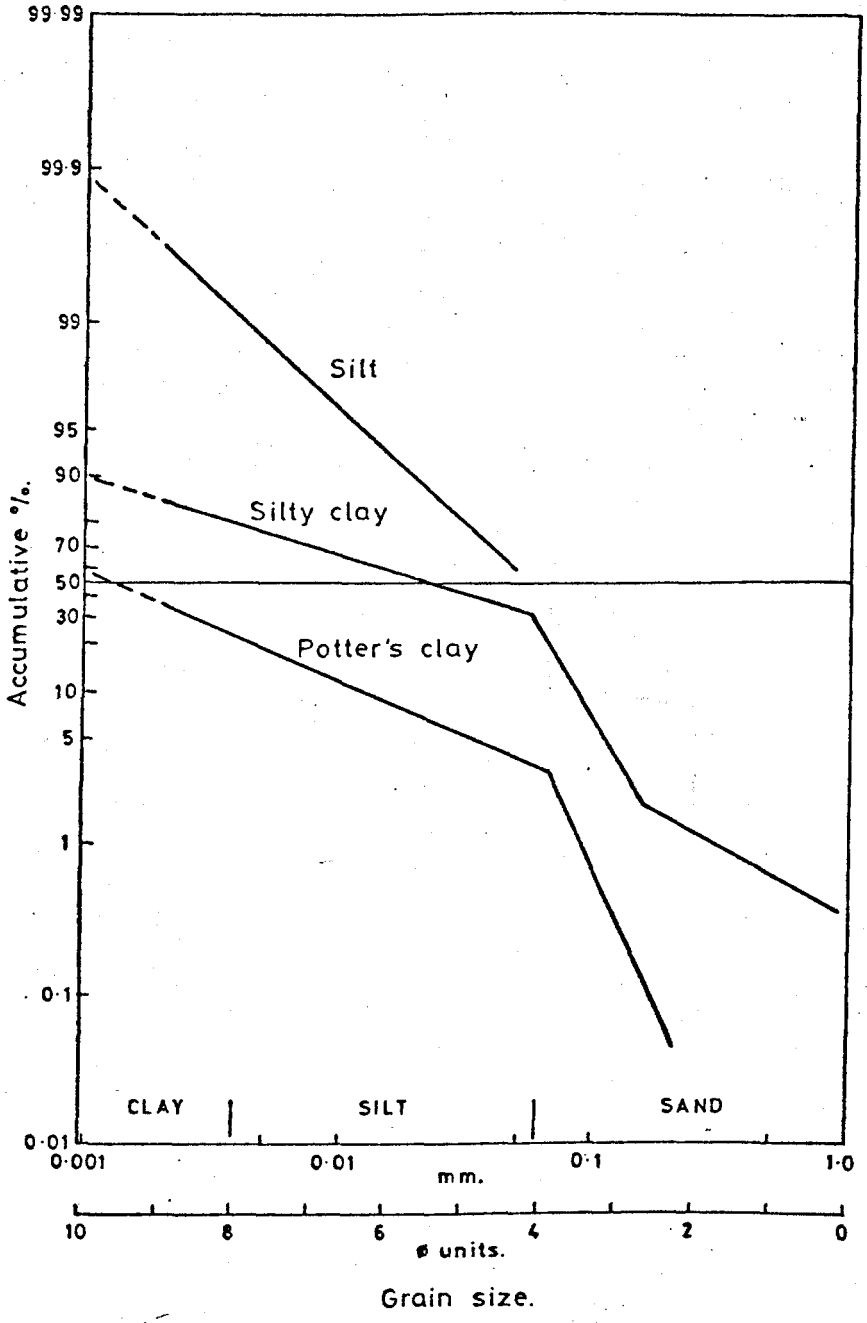

FIGURE 5.1 Grain size distributions for the samples tested in the oedometer cell

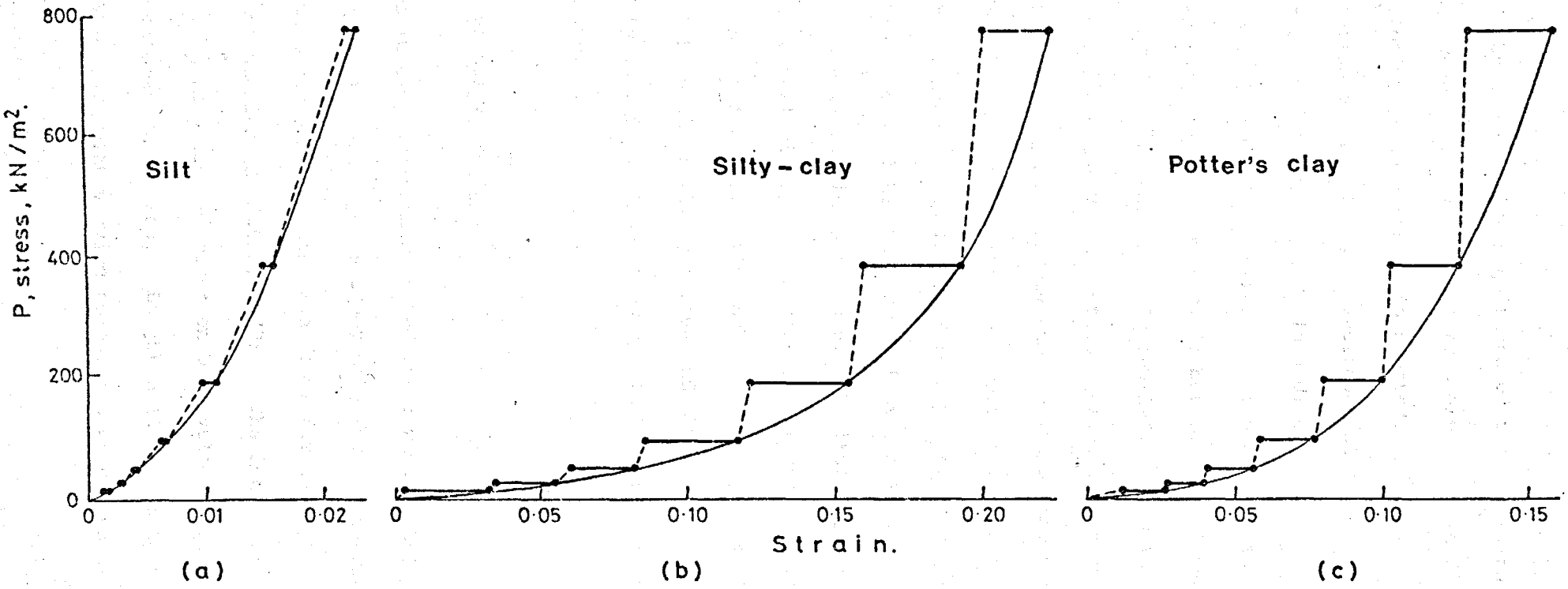

FIGURE 5.2 Stress – strain consolidation plots for the samples tested in the oedometer cell

is clearly depicted by the relative magnitudes of these strains. Corresponding shear wave velocity-stress curves are given in Figure 5.3 where the final velocity at each stress is plotted.

On the application of each load, V_s increases at a rate which depends on the permeability. The increase in V_s is a direct consequence, and perfect illustration, of the load transfer from the pore fluid to the mineral frame. In the potter's clay a small but consistent decrease in V_s occurs immediately after each load is applied. This is illustrated graphically in Figure 5.4 where V_s is plotted against strain for the complete test. Probably the most likely explanation of the phenomenon is that a build up of excesss pore pressure occurs in the vicinity of the transducers when a load is applied. This may occur because the transducers, which are mounted in the porous stones, must cause a significant disturbance in the drainage path. Control tests on the same material, but using a cell without transducers, have shown no measurable differences in the overall consolidation behaviour. However, this explanation has not been conclusively proven and the possibility that the loss of rigidity on initial loading occurs in the standard oedometer must still be considered.

5.3 Shear wave velocity gradients

The variation in compressional wave and shear wave velocity with depth (velocity gradients) are important not only for engineering applications but also for modelling the sea floor for geophysical and underwater acoustics studies (Hamilton, 1979). The introduction of P and S wave transducers into the oedometer enables velocity gradients to be predicted from laboratory samples. Laughton (1957) also measured the variation in V_p and V_s with varying compacting pressures which greatly

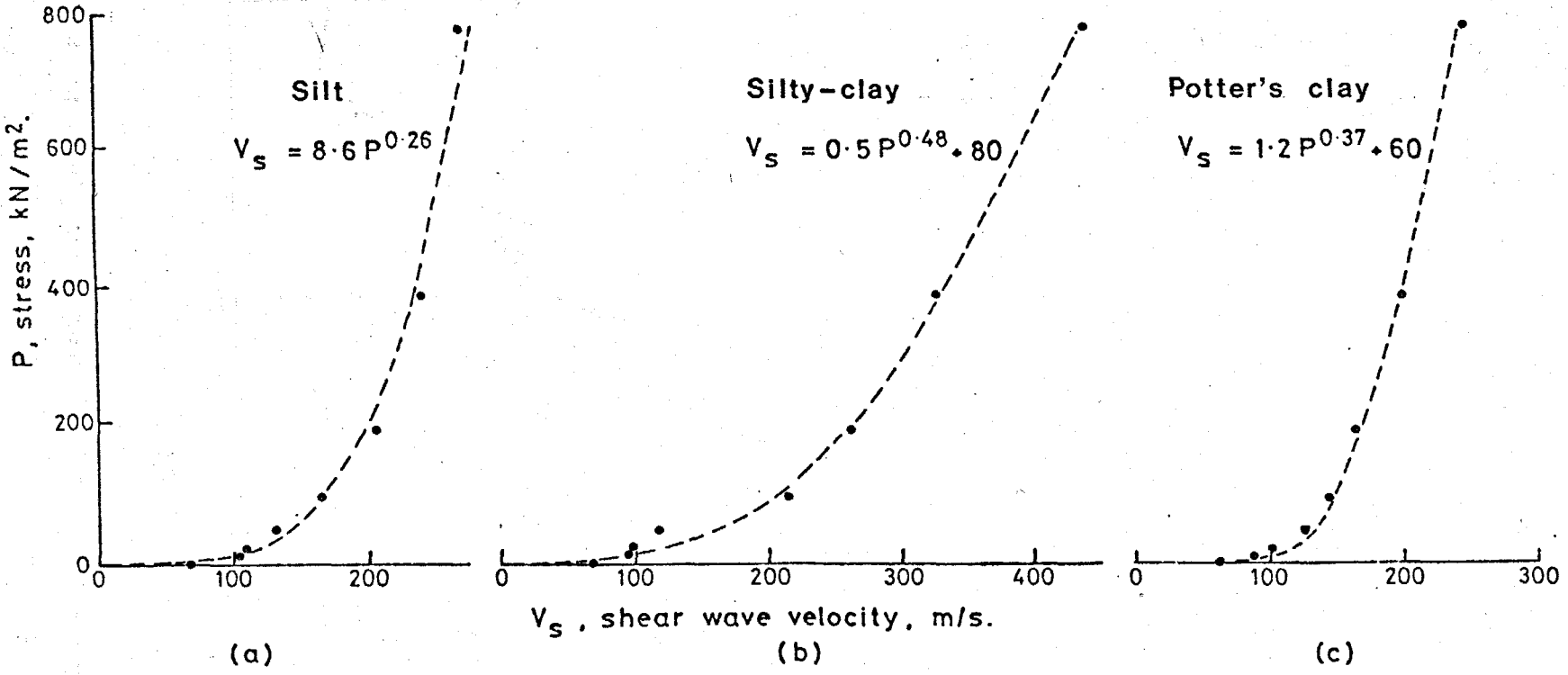

FIGURE 5.3 Stress – V_S consolidation plots. Power equations $P = K V_s^n + C$ are fitted to the final compression curve. Units of P and V_s are kN/m^2 and m/s respectively.

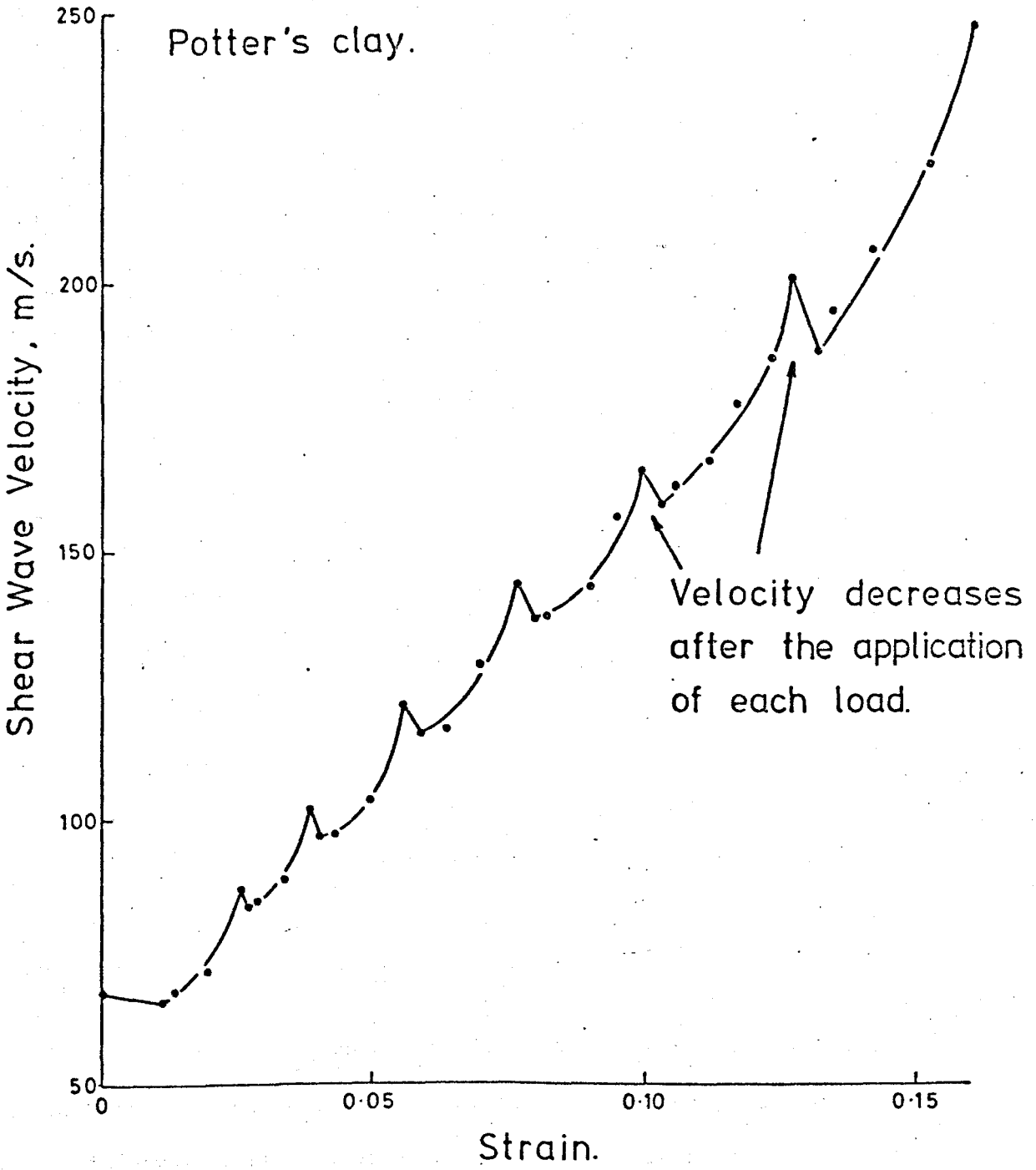

FIGURE 5.4 Strain – V_S consolidation plot for potter's clay.

exceeded those used in these experiments (up to 100MPa). However, shear waves could only be detected at compacting pressures exceeding 49MPa where the velocity is over 1 km/sec. In these experiments shear waves could be detected from zero up to the maximum compacting pressure of 800 kPa.

A review of shear wave velocity gradients by Hamilton (1976) concluded that for natural sand bodies the equation $V_s = KP^n$, where K and n are constants and P is the compacting pressure, gave a pressure exponent, n, lying between 0.25 and 0.33. He found the available data to be too sparse for silt clays to use power equations and instead used linear equations for different depth ranges.

In this study, power equations have been fitted to the curves in Figure 5.3. A pressure exponent of 0.26 is indicated for silt sample ($V_s = 8.6P^{0.26}$) which lies in the range for sand bodies quoted above. Power equations also describe the data for the silty clay and potter's clay in the form $V_s = KP^n + C$, where the pressure exponents are 0.48 and 0.37 respectively. The highest exponent is in the silty clay sample which may be indicative of two mechanisms operating together to maximise the rate of increase in rigidity with increasing compaction pressure:

(i) Frictional forces from grain-to-grain contacts

(ii) Electrochemical forces operating between the finer grains.

5.4 Static and dynamic moduli

Static moduli are computed from stress-strain relationships obtained in a given test. However, because the modulus for any given soil in any test is highly variable, other factors have to be considered. Primarily, these are: the magnitude and sign of the stress increment, the time for which it is applied, and the previous stress history.

In a normal consolidation test, for example, drainage is allowed and the modulus is calculated when a quasi equilibrium position is reached (100% primary consolidation, no excess pore water pressure). This produces a relatively low modulus used for estimating settlements. Even lower values of this modulus would be obtained if the sample were allowed to creep further due to secondary consolidation.

Dynamic moduli are calculated from the stress-strain relationships of elastic stress waves as given by the velocities V_p and V_s (see Chapter 2.1). The strain levels generated by the transducers are small enough to be considered elastic and, apart from measurements at very low frequencies, there are probably no time effects and, hence, little or no drainage.

As certain static moduli are required for design purposes, any attempt to determine these by seismic techniques must answer the following questions:

(a) Do the same controlling parameters (e.g. mineralogy, void ratio, permeability, particle size, shape and morphology) similarly influence both the static and the dynamic moduli calculated from seismic velocities?

(b) If so, what is the resulting correlation between what moduli and how accurately can it be predicted?

5.5 A preconsolidation test on silt

From normal consolidation tests, such as those depicted in Figure 5.2, the primary static constrained modulus D is given by the gradient of the curve. D increases smoothly as a function of increasing stress as do the seismic velocities V_p and V_s. Consequently, any dynamic moduli calculated from V_p and V_s will increase smoothly and, hence, broadly

speaking, correlate with the static moduli despite differences in the order of magnitude. In order to test for a more fundamental correlation between the different moduli a sediment that exhibits a more irregular behaviour was thought likely to prove more informative.

A pre-consolidated soil will exhibit an inflexion in the stress-strain plot around the pre-consolidation pressure P_p (Stamatopoulos and Kotzias, 1978); it follows that D will be a minimum at this point. This stress-strain curve is not dissimilar to that described by Whitman et al. (1964). They concluded that, starting from some initial axial stress P_o, the stress-strain curve for a sand in confined compression is S-shaped. Initially, at small stresses, the sand exhibits yielding behaviour (Figure 5.5a). This is interpreted on a physical basis as being primarily the deformation and yielding at the grain contacts caused by the high contact stresses. As the applied stress is increased, the grain contacts fail and slip occurs; the grains reach a more compact geometrical arrangement and the resistance to further straining increases, resulting in the characteristic locking behaviour (Figure 5.5a) of the confined compression test. Yielding is not normally observed because the yielding range is small, less than $\frac{1}{2}P_o$.

When a sand is pre-consolidated, as described by Stamatopoulos and Kotzias (1978), to some given axial stress P_p then allowed to rebound at a lower stress P_1, the major component of the non-elastic strain due to grain slippage has already taken place during this first cycle. Consequently, this allows the yielding nature to be fully revealed during the second application of load. This is succeeded by the locking behaviour which occurs once the grain slip has occurred and the sample has recompacted. The yielding followed by the locking behaviour under these conditions produces the S-shaped curve, as illustrated in Figure 5.5.

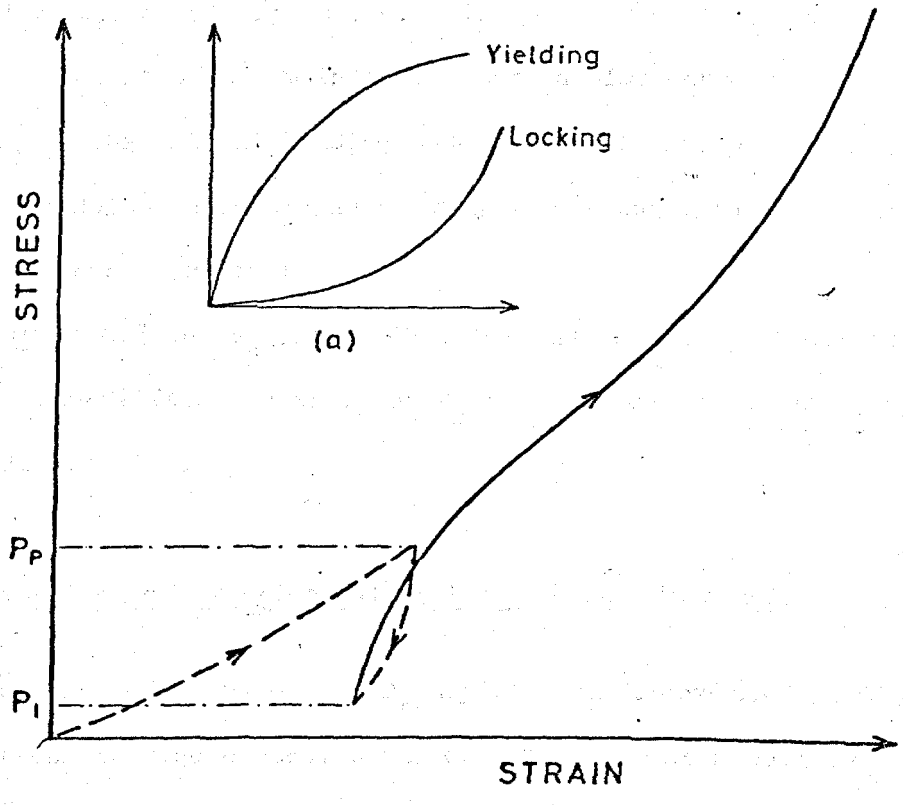

FIGURE 5.5 The yielding and locking behaviour of a sand in confined compression

The stress-strain relationship for a test on pre-consolidated silt is shown in Figure 5.6. A silt sample was pre-stressed to 108 kPa and then allowed to rebound under a 12 kPa stress. Incremental loading, using smaller stress increments than in a normal test, was supplemented by a low level (ΔP) cyclic loading at each load, P, where $\Delta P = 0.045$. One such loading procedure at $P = 386$ kPa is shown in detail within an expanded section of Figure 5.6. The primary constrained static modulus, D, is the gradient of the main stress-strain plot between two successive loads; D_l is the initial loading modulus from ΔP and D_r is the final relaxation modulus on unloading ΔP when a constant value is obtained (typically after 10 cycles).

In Figure 5.7 the V_s and V_p data for the test at each stress level is shown. No differences in V_p or V_s could be detected during the low level cyclic testing.

5.6 Comparison of experimental static and dynamic moduli

The static moduli D, D_l and D_r depicted in Figure 5.6 are plotted against stress in Figure 5.8a, b and c. The dynamic moduli ρV_p^2 and B_f, calculated using values of V_p and V_s as shown in Figure 5.7, are plotted against stress in Figure 5.8d and e. Yielding and locking behaviour, as discussed earlier, is clearly seen in the S-shaped curve (Figure 5.6) with the inflexion above P_p; this shows up more distinctly as a minimum value of D in Figure 5.8a. The cause of the initially very low values of D which produces a maximum value of D close to P_p is still unclear.

D_l exhibits a similar behaviour to D except with a more pronounced turning point and values higher by a factor of about 2 (Figure 5.8b). It is interesting to note that, even at the small stress increments ΔP,

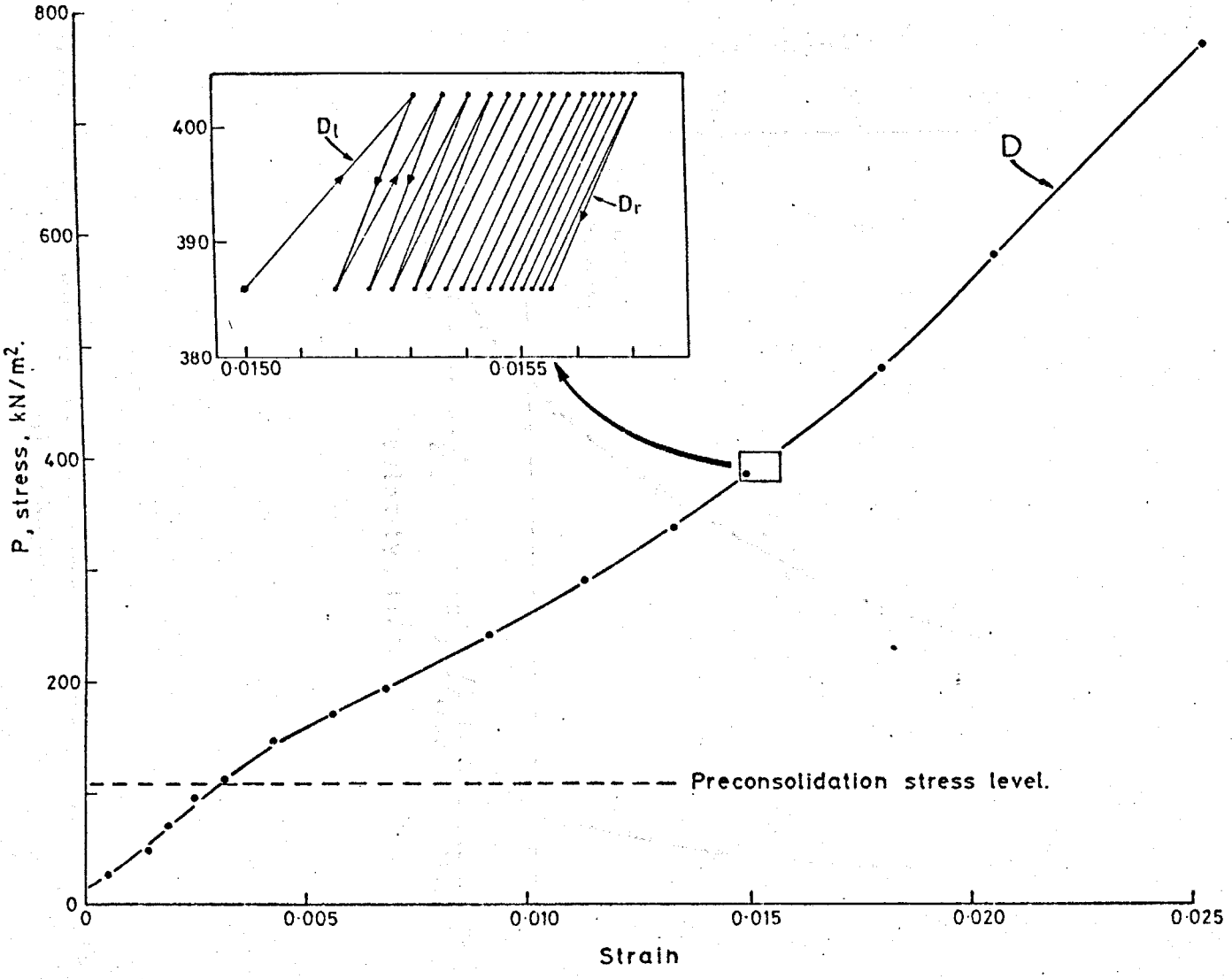

FIGURE 5.6 Stress-strain consolidation plot for a silt preconsolidated to 108 kN/m². The inserted figure shows an enlargement of the cyclic relaxation test, which was performed at each stage.

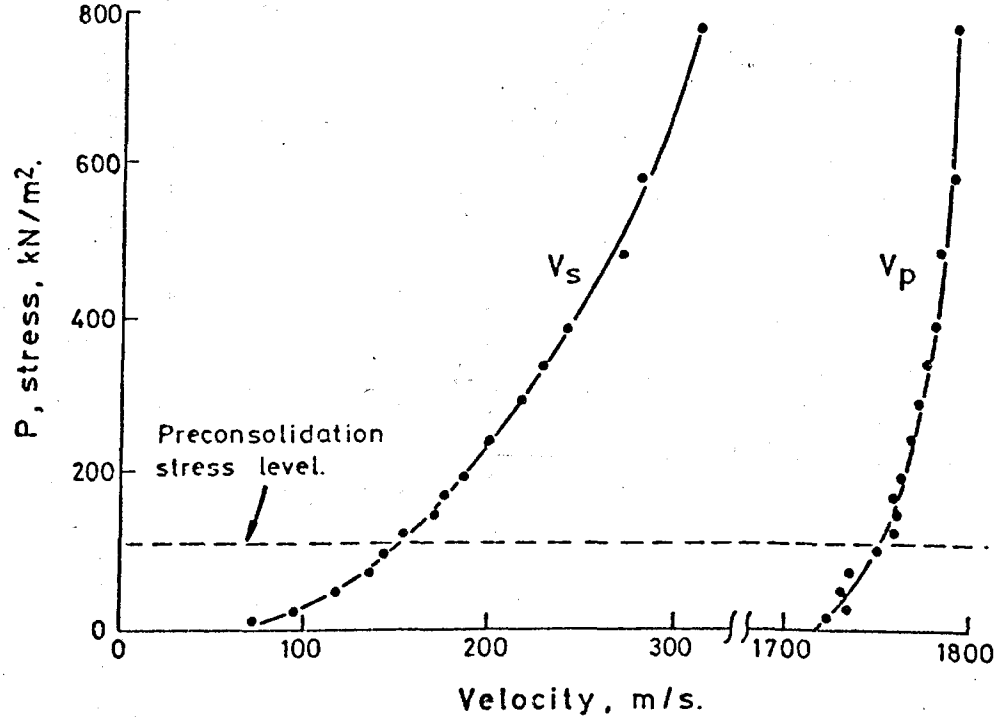

FIGURE 5.7 V_s and V_p versus stress for the preconsolidated silt sample.

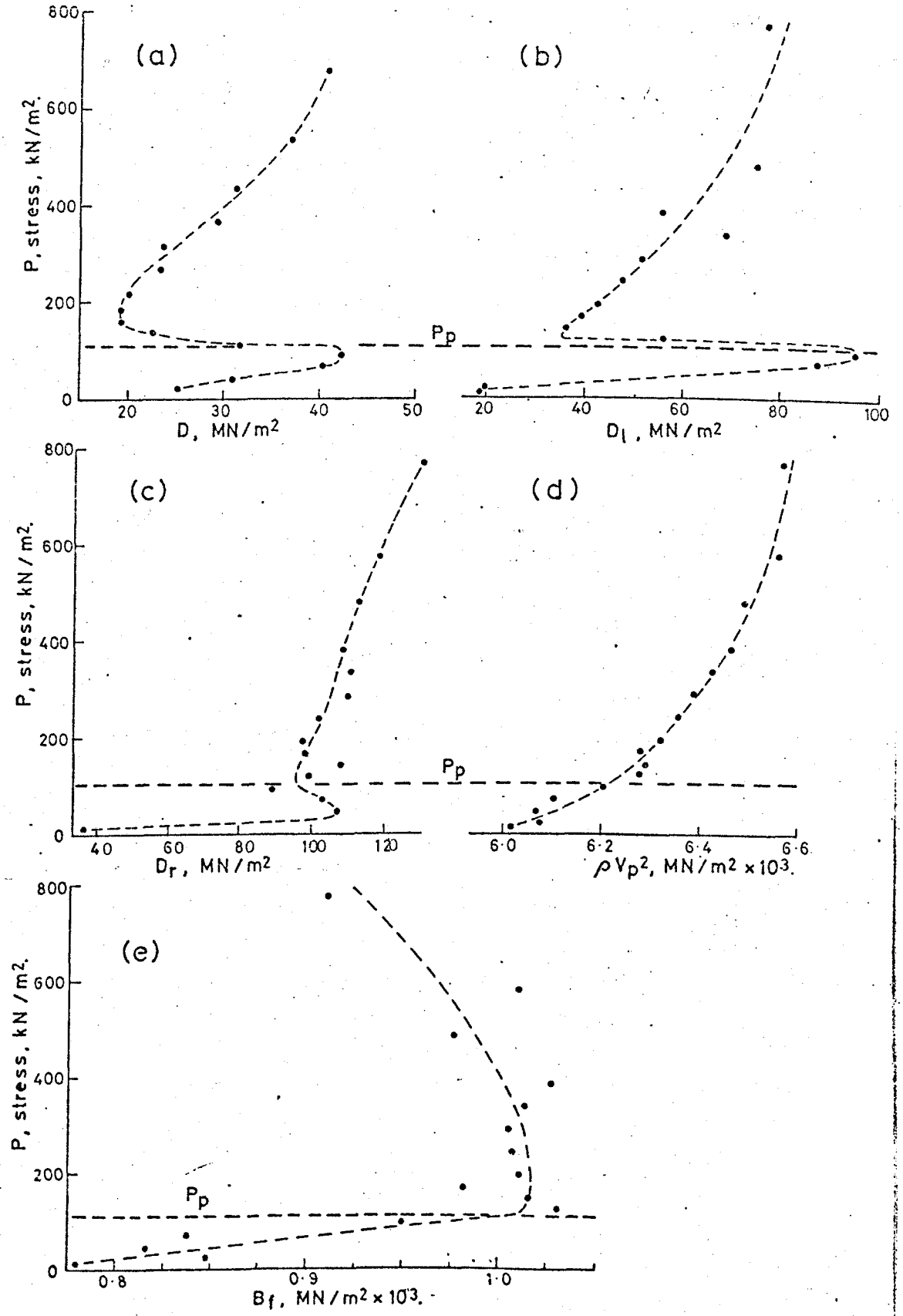

FIGURE 5.8 Static and dynamic moduli versus stress for the preconsolidated silt sample: [a] primary static constrained modulus, D, [b] initial ΔP loading modulus, D_I, [c] final ΔP relaxation modulus, D_r, [d] dynamic constrained modulus, ρV_p^2, [e] frame bulk modulus, B_f.

the effects of the preconsolidation are still apparent and the yielding or locking states are manifested by this low stress modulus. This is not the case for the final relaxation modulus, D_r (Figure 5.8c). Although there is vague discontinuity around P_p there is no minimum value as for D and D_1. It appears, therefore, that the cyclic loading stress history erases the effects of preconsolidation. Maximum values of D_r are a factor of about 1.5 higher than D_1.

From elastic theory, Taylor Smith (1974) has shown that the dynamic constrained modulus is given by ρV_p^2; this is plotted against the applied stress, P, in Figure 5.8d. The relatively smooth increase in the dynamic constrained modulus is in direct contrast with the variation of the static modulus D, with the former being larger by a factor greater than 10^2.

It is thought likely that the difference in nature between ρV_p^2 and D is primarily caused by the different drainage conditions and strain levels. In the elastic formulation of ρV_p^2, drainage is not accounted for yet the drainage of pore fluid plays the predominant role in the determination of D. In the case of a saturated material tested in a drained condition, the dynamic moduli calculated using V_p, which is governed mainly by the water, may be ill-founded. For such a drained condition a frame component of the total bulk modulus such as B_f, defined in Chapter 2.1, may be more applicable. B_f as a function of stress is shown in Figure 5.8c and, although it is not a constrained modulus and does not exhibit a minimum value comparable with that shown by D, it does exhibit, despite some scatter in the data, a discontinuity around P_p. This behaviour is more in line with that found for D_r in Figure 5.8c. Despite some tentative similarities between the two types of moduli, it seems that the large inelastic strains, caused by grain-to-grain rolling and sliding (characterised by D) are not revealed by V_p and V_s.

However, the small moduli measured with small cyclic loads may be related to some form of frame component which would constitute a part of the total dynamic moduli.

6. SMALL TRIAXIAL CELL

6.1 Results of an Initial Study

In Chapter 3.2.5 the modifications to a small triaxial cell were described. These were intended to enable compressional and shear wave velocities to be monitored during triaxial tests on soils without interfering with the normal test procedures.

Only a very limited amount of data was obtained from the experiments using this apparatus, for two reasons:

(1) It was intended originally as a feasibility exercise which, if successful, would indicate whether the modifications could similarly be made to a larger cell.

(2) The problems of noise generated by the mechanical parts of the system precluded, at that time, a more detailed study.

The only material tested in the small triaxial cell was a saturated quartz sand. Easy control of the confining and pore pressures in this type of system enabled the relationship between effective stress and the seismic wave velocities to be readily examined. Such a test was performed on the saturated sand for different values of both the confining and pore pressures. Data obtained for this test is presented in Figure 6.1 as a graph of shear wave velocity versus effective stress. It is interesting to note that the pressure exponent n in the equation

$$V_s = KP^n$$

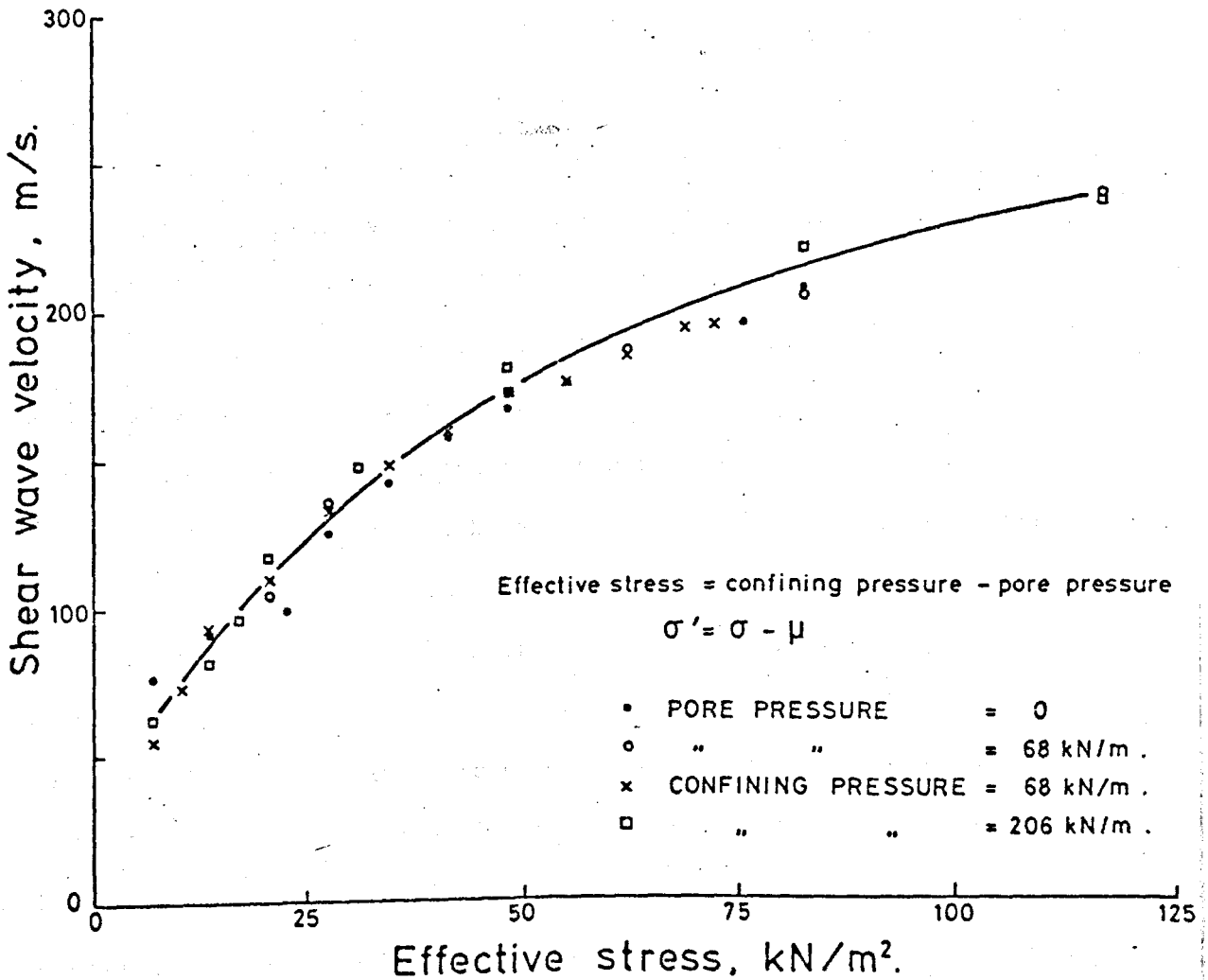

FIGURE 6.1 V_S versus effective stress for a medium sand in the small triaxial cell.

as used in Chapter 5.3 varies at these low values of P. As P varies from 10 kPa to 120 kPa the corresponding variation in n is from 0.54 to 0.3.

Although no other velocity gradient experiments have been performed on other sediments this modified cell offers a quick and reliable technique for obtaining this type of data on a large range of unconsolidated materials.

To test the feasibility of monitoring seismic wave velocities during a normal triaxial test the saturated sand was again used. On initial tests, where the electric motor was used to provide the constant strain rate, noise tended to obscure the shear wave signal which was displayed without any signal processing directly on an oscilloscope. With the bender elements very sensitive to vibrations below 5 kHz this problem will persist in many laboratory and field situations. It is particularly desirable, therefore, to use some signal enhancement technique to alleviate this problem such as a simple signal averaging technique. This technique has been used successfully during the trials with the in-situ probes and allowed very 'noisy' signals to be enhanced. With the small triaxial cell the only available alternative was to run the test by hand which allowed the shear wave onset to be observed although still with some difficulty.

In Figure 6.2 the data from this hand-run test is shown as plots of the deviator stress and shear wave velocity versus the axial strain. The test was run in a drained condition (i.e. constant pore pressure) with a strain rate of 1.25%/min. Although this type of plot does not show anything unexpected it does demonstrate the feasibility of this type of testing. In Figure 6.2 a sharp decrease in V_s occurs when the sample failed. The oscilloscope showed a fast drop in V_s to a much lower value than that illustrated in Figure 6.2. However, it was only a

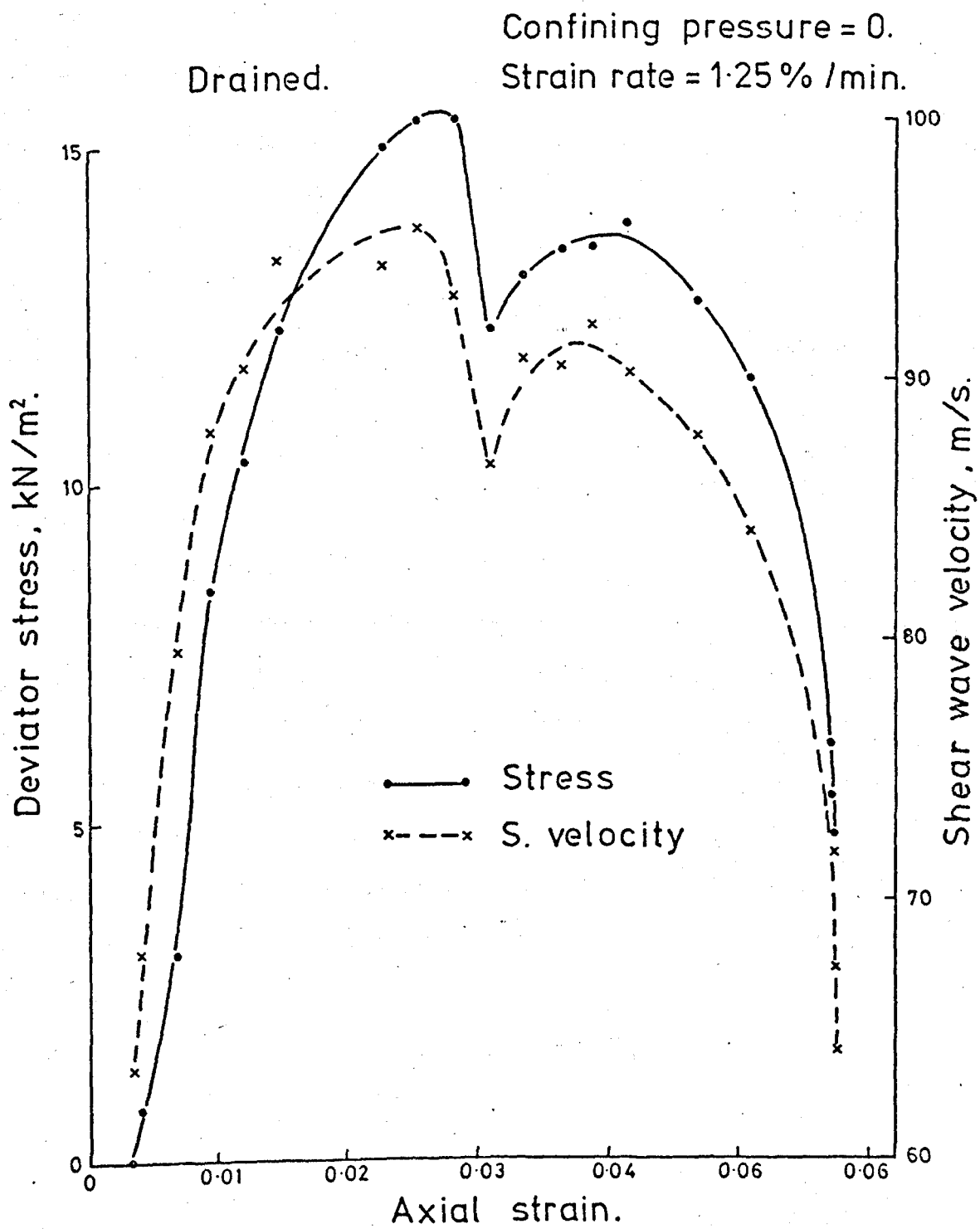

FIGURE 6.2 Deviator stress and V_s versus strain for a medium sand in the small triaxial cell.

momentary drop and occurred too quickly to be quantified without the necessary recording equipment.

6.2 Transducer performance

Oscillographs of the signals observed during the effective pressure test are shown in Figure 6.3. While this figure illustrates the general clarity of the shear wave signal obtained using the cantilevered bender elements, it shows a considerable change in signature at different pressures. For velocity measurements, using a pulse technique, only the shear wave onset is required to be recognised and this generally can easily be identified (start depicted by arrows). This test was performed with the bender elements in their raw state apart from a very thin layer of insulation. It was originally thought that the change in signal was caused by the effect of pressure on the highly-compliant elements. However, when the elements were potted in 'araldite' (reducing significantly their compliance) the effect was still much the same. This was confirmed later in the larger triaxial cell (see Chapter 7) where a similar behaviour was observed. It is concluded that the majority of the change in the signal is caused primarily by a change in the sediment's transfer function rather than by a change in the coupling characteristics of the transducer.

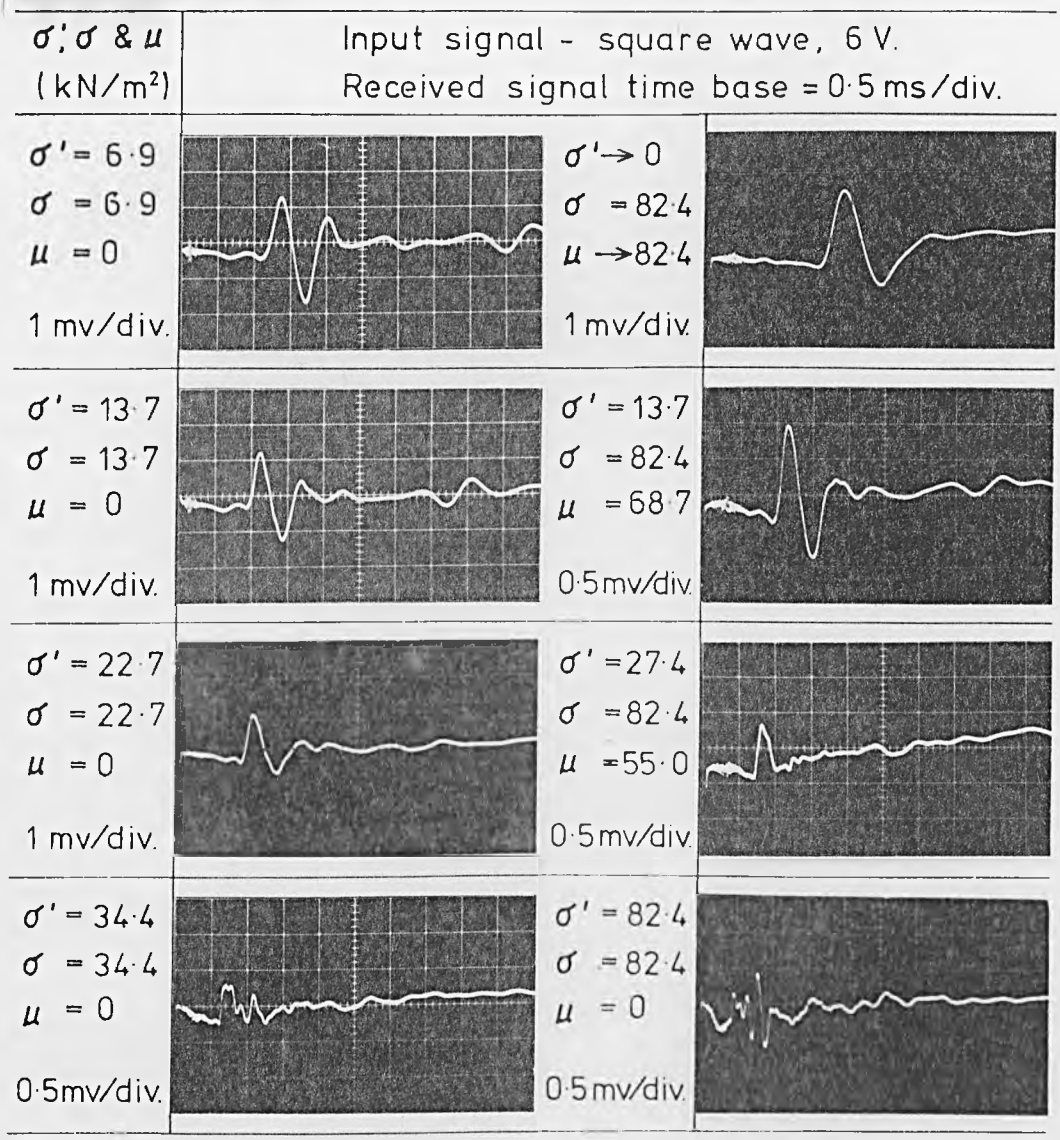

FIGURE 6.3 Received shear wave signals through sand in the small triaxial cell at different effective stress levels.

7. LARGE TRIAXIAL CELL

7.1 Background

In Chapter 3.2.6 the modifications made to a large triaxial cell were described which enabled both shear and compressional wave pulses, as well as electrical resistivity, to be monitored along the 200 mm length of the sample.

Tests performed in this cell were on a sand which was subjected to cyclic loading. The reason for this type of test was that an investigation into correlations between geophysical and geotechnical parameters, with particular emphasis on the liquefaction of sands, was taking place at Newcastle University. This afforded the opportunity to extend the range of application of the recently developed shear wave transducers.

Cyclic loading and liquefaction phenomena are important aspects of offshore foundation engineering, especially for gravity-type structures located on sand. The overall objectives of the Newcastle project were to obtain geophysical and cyclic loading data on a range of sands and to investigate whether any correlations exist between liquefaction potential and the geophysical parameters that could be used as a predictive tool in situ. The writer's shorter term objectives were to ensure that reliable measurements of shear wave velocity could be obtained and to investigate the behaviour of shear waves during some initial cyclic loading tests on sand.

7.2 Experimental Procedures

The sand used in the tests described in this chapter is Leighton Buzzard sand, a uniform medium grade (0.3-0.6 mm). The S.G. of the sand is 2.65 and the minimum and maximum void ratios are 0.515 and 0.801 respectively. The void ratio used in this test was 0.544 (relative density = 0.9).

Preparation of a sand sample subjected to cyclic loading is very important if consistent results are to be obtained (Mulilis et al., 1977).

In these initial tests the samples were prepared more rapidly than would ideally be desirable by pouring saturated sand into a water-filled mould. A small vacuum was applied to the sample which enabled the mould to be removed and the cell assembled and pressurised (Figure 3.18).

Cyclic loading was applied through the ram mechanically using a stress-controlled feedback loop from the output of the internal load transducer. The system allows an approximately sinusoidal loading to be applied to the undrained sample. A frequency of 0.1 Hz was used in these tests with no superimposed static shear stresses applied. The reversing shear stresses applied to the sample cause cyclic variations in the pore-water pressure and in the axial strain deformation (measured with a pore pressure transducer and a LVDT displacement transducer, respectively). This causes the effective stress to oscillate in phase with the pore pressure. As the number of cycles increases, the mean pore-water pressure experiences a steady increase and, hence, the effective stress is reduced. The point at which the pore water pressure first reaches the confining cell pressure, and the effective stress is zero, is termed 'initial liquefaction' and the rigidity of the sample is momentarily lost. This loss of rigidity occurs due to the stress transfer from the grain framework to the pore water while the overall porosity remains constant (Seedand Lee, 1966). The permanent and cyclic axial deformations are counteracted by corresponding variations in the lateral deformation which normally causes a barrelling of the sample. Non-uniform deformations can also occur, especially near to the top of the sample, and are normally attributed to density inhomogeneities caused during preparation.

In Figure 3.19 the block diagram shows the system used to make the seismic wave and resistivity measurements. Shear wave velocity was calculated as the ratio of the receiver separation and the time delay for a pulse to travel through the sample. Separation between the transducers is taken as the distance between the ends of the protruding elements.

A 10v d.c. step from a square wave was used to drive the transmitter at a 40 Hz repetition rate which was synchronised and delayed from the compressional wave and resistivity repetition frequency to overcome electrical feed-over effects. Received signals were recorded on an FM tape-recorder together with the stress, strain and pore pressure signals. Time delays and amplitudes of the shear wave signals were obtained from records obtained by replaying the tape into a recording oscilloscope operating in a raster mode. This data was entered into the micro-computer which calculated the velocity and other parameters after correction for strain effects.

Compressional wave velocity was calculated as the transmitter-receiver separation and the measured delay time (after calibration in water) of the pulse through the sample. A 300 kHz tone-burst with a 20v amplitude was used to drive the transmitter close to its resonant frequency. Under static or slowly-changing conditions (e.g. oedometer or porosity cell) the time interval is normally measured using a dual-trace delayed-timebase oscilloscope. For these cyclic loading tests using a 0.1 Hz frequency at least ten readings per cycle were required, i.e. one per second. This requirement was met by using a transient recorder plus desk-top micro-computer to acquire and process the compressional wave data. The computer was programmed to calculate the RMS value of the amplitude of four cycles of the received tone burst, and the position in time of one of the peaks, these two values being held in memeory in real-time and later stored on magnetic tape (Jackson et al., 1981). Corrected times were obtained to correspond to the onset of energy, assuming there was no dispersion and that time delays between readings did not vary by more than half of one wavelength.

Although the electrical resistivity of the sample and, hence, the

formation factor were also measured during these tests they are beyond the scope of this discussion but are presented by Jackson, et al., 1981.

7.3 Results and Discussion

Although several tests were performed using the procedures detailed in the previous section, it is only relevant for this study to examine some of the details. Consequently, the illustrations have been chosen to demonstrate the typical behaviour observed during the experiments.

Figures 7.1, 7.2 and 7.3 are illustrative examples of the behaviour of shear waves during two cyclic loading tests. The records are taken from a recording oscilloscope operating in the raster mode, hence time on the y-axis starts at the bottom of each record section. Time scales for each record vary and are shown separately on both x and y axes of each section. In Figure 7.1 the section A-B shows the results from a test where the shear wave velocity and amplitude dramatically decrease after about 7 cycles (70s) from the start of cyclic loading. Sections C-D and D-E are expanded sections (on both x and y axes) of section A-B as shown. The hand-written numbers on the y-axis are tape references. Although the repetition rate producing shear wave pulses was 40 Hz which was recorded on tape, the playback facility enabled the pulses to be variably gated to produce these records. For example, in section A-B the repetition rate has been divided by 16 so only 1 in 16 pulses is shown (2.5 Hz) whereas 1 in 8 are shown in sections C-D and D-E (5 Hz). Figure 7.2 illustrates in section F-H the small-scale shear wave velocity during the first few stress cycles which very rapidly increase in section G-H with a sudden total loss of rigidity at point X. This section is shown with a different x-axis scale as section I-J as section I-J and is continued in Figure 7.3 as section J-K where the

FIGURE 7.1 SHEAR WAVE SIGNALS RECORDED DURING A CYCLIC LOADING TEST ON SAND. SECTIONS C-D AND D-E ARE EXPANDED FROM A-B SECTION.

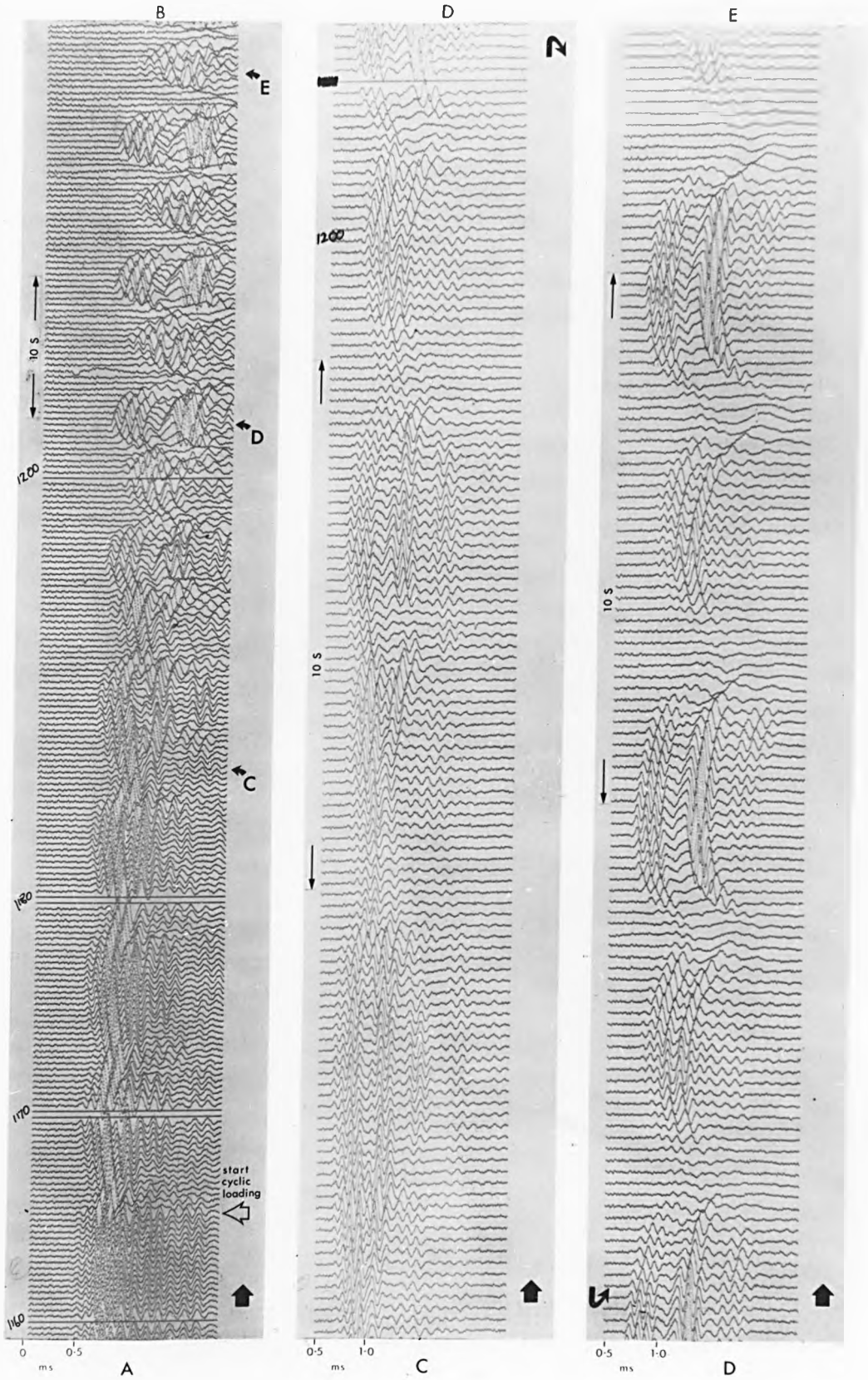
B
D
E
E
D
C
10 S
1200
1120
1170
1160
start
cyclic
loading
0
0·5
ms
A
10 S
1200
0·5
1·0
ms
C
10 S
0·5
1·0
ms
D

FIGURE 7.2 RECEIVED SHEAR WAVE SIGNALS DURING CYCLIC LOADING TESTS ON SAND ILLUSTRATING THE LIQUEFACTION AT X.

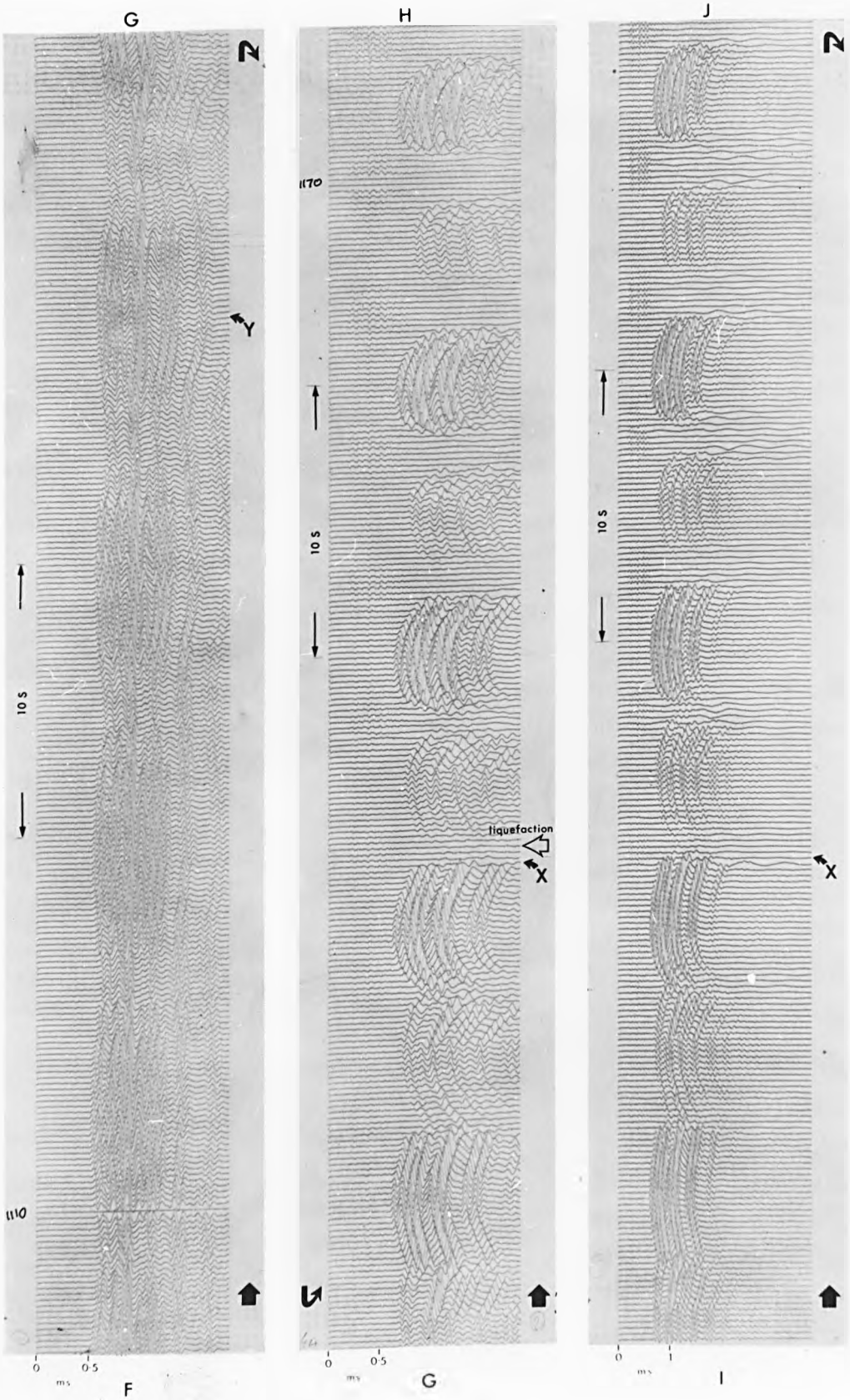
G
H
J
N
Y
X
10 S
1110
1170
liquefaction
0
0·5
1
ms
F
G
I

FIGURE 7.3 SHEAR AND COMPRESSIONAL WAVE SIGNALS OBTAINED DURING A CYCLIC LOADING TEST ON SAND. SECTION J-K ILLUSTRATES THE AMPLITUDE VARIATION OF P AND S WAVES AT THE END OF A TEST. SECTION L-M AND M-N ARE EXPANDED AND DELAYED RECORDS OF SECTIONS F-G AND G-H (FIGURE 7.2).

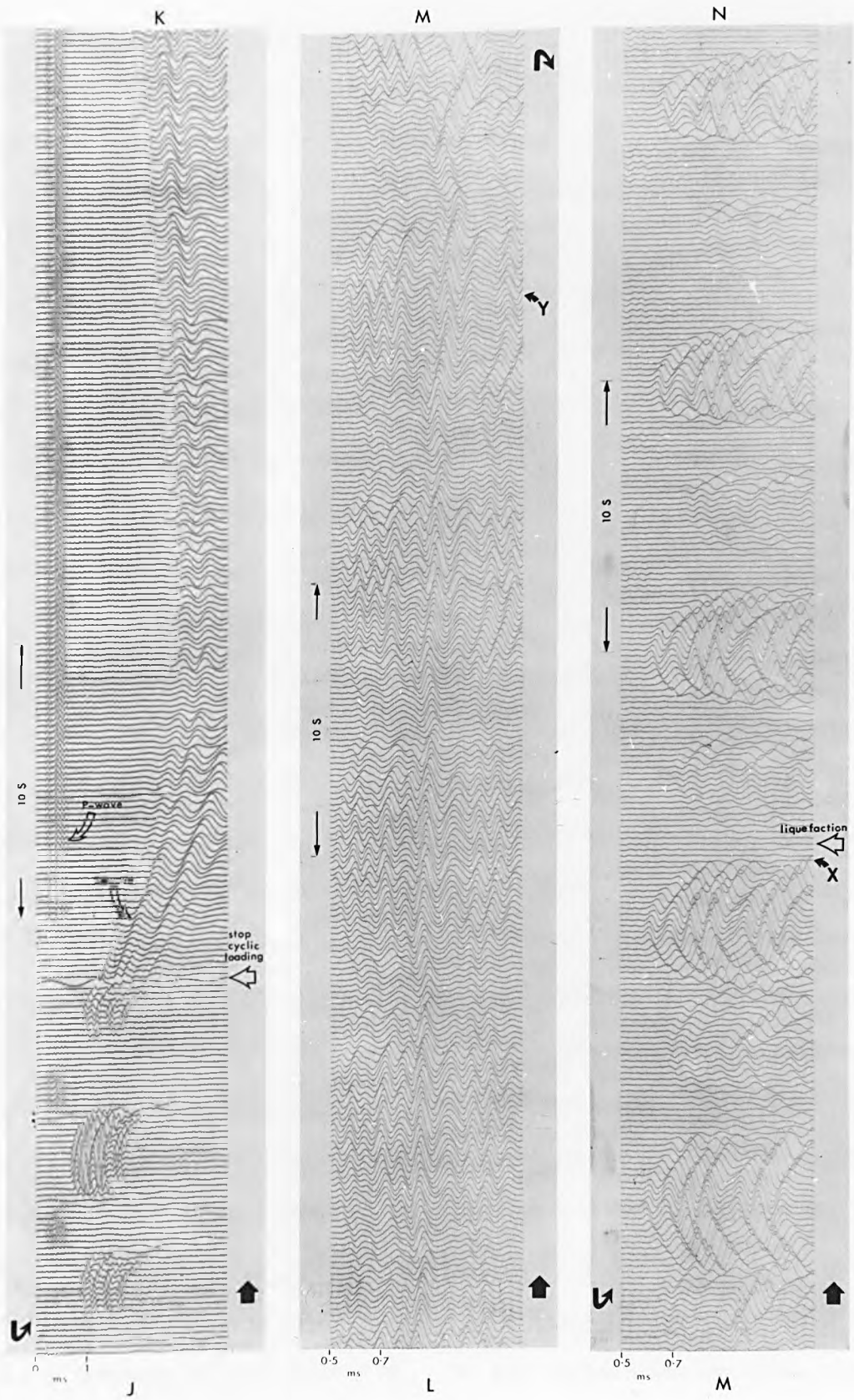
K
M
N
10 S
10 S
10 S
P-wave
stop
cyclic
loading
liquefaction
X
Y
Z
0
1
ms
0·5
0·7
ms
0·5
0·7
ms
J
L
M

cyclic loading has stopped.

In sections I-J and J-K not only is the shear wave behaviour perfectly illustrated but a small compressional wave can also be observed. This is not the compressional wave that was being monitored, this exhibited a strong signal at all times during the test, but it is a pulse being transmitted and received by the bender elements. While on the scale of these records it shows no deviation in velocity compared to the shear wave, the amplitude variation is clearly recorded, showing a marked decrease in attenuation during the periods when the sand had lost its rigidity. Undrained cyclic loading is essentially a constant porosity process, hence, the increased attenuation from zero effective stress to some positive value can probably be attributed to the losses caused by interparticle frictional forces.

Sections L-M and M-N are the same as sections F-G and G-H respectively except with the x-axes expanded and delayed. This provides a particularly clear illustration of the shear wave signature and its variation during cyclic loading. The extremely rapid reduction in velocity and amplitude at point X proved to be a more positive identification of initial liquefaction than the stress and pore-water pressure measurements.

To illustrate the relationships between the shear wave velocity and the other parameters measured, the test depicted in Figure 7.1 has been used. Shear wave velocity was calculated from the time intervals taken from enlarged records of sections C-D and D-E. These were then used to calculate the velocity after correcting for the strain variations. The shear wave amplitude was taken directly from the recording oscilloscope operating in a normal mode and its value is only a relative one. These profiles are shown in conjunction with the applied stress, pore/effective pressure and strain in Figure 7.4. In the applied stress trace significant

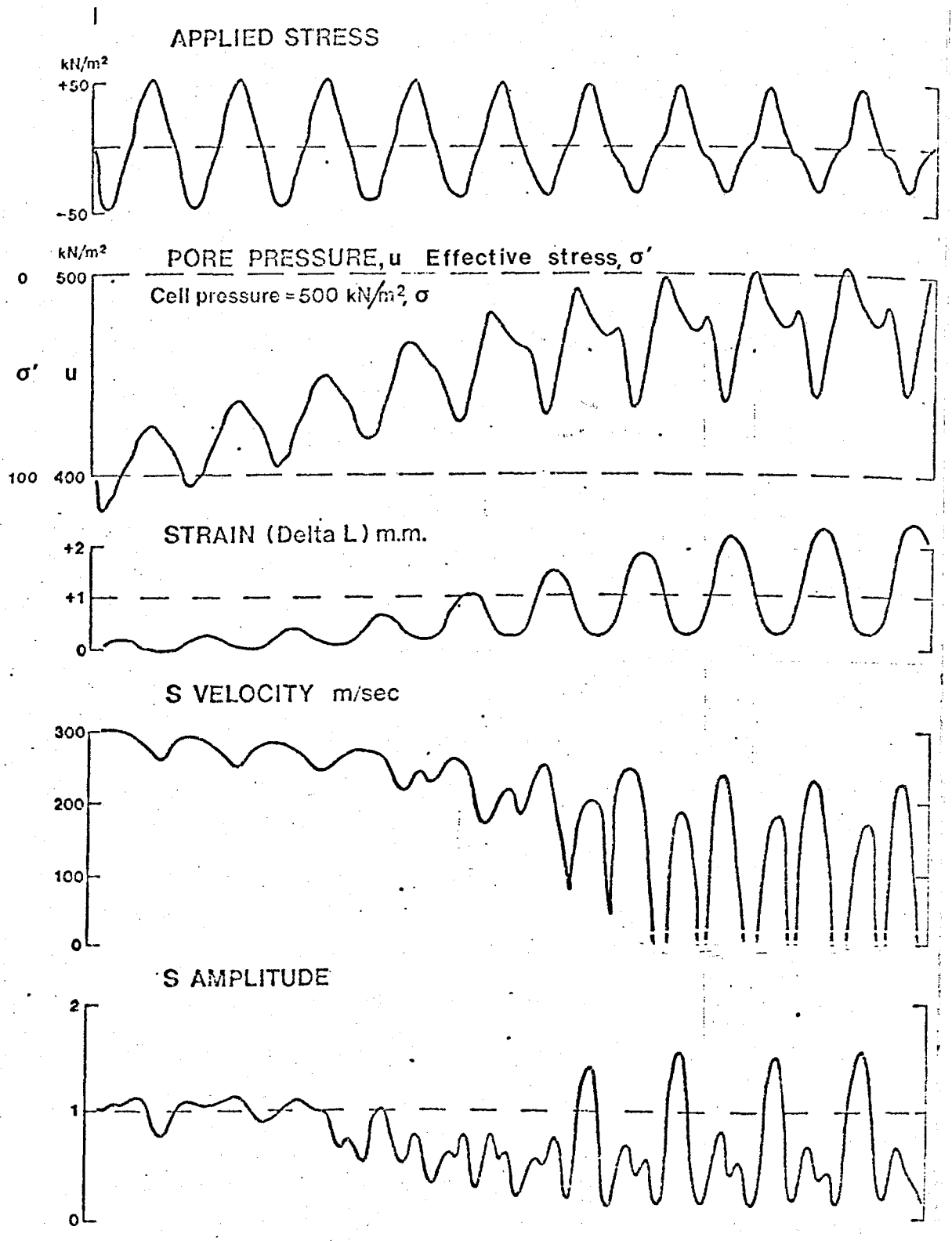

FIGURE 7.4 Stress, strain and shear wave data from a cyclic loading test (0·1 Hz) on sand in the large triaxial cell

deviations from the intended sinusoidal wave form can be observed even during the first few cycles. Deviations following liquefaction are inevitable as the sample no longer has the rigidity to support the full stress cycle. Cell pressure or total confining stress, σ, was kept constant at 500 kN/m^2 and the pore pressure, u, and effective stress, σ', are given by $\sigma' = \sigma - u$, therefore $\sigma' = 500 - u$. Non-sinusoidal behaviour in the stress causes large perturbations in the pore pressure trace. Initial liquefaction is normally assumed to have occurred when the effective stress first becomes zero. Strain can be seen to increase up to about +2.5 mm (increase in length) with a ± 1 mm of movement after liquefaction. The shear wave velocity and amplitude variations are quite dramatic around liquefaction. A velocity of 300 m/s was recorded for an effective stress of 100 kN/m^2 (slightly higher than that obtained in the small triaxial cell, Figure 6.1). The oscillations of shear wave velocity follow those of the effective stress with coinciding maxima and minima as would be expected. However, because of the relationship between V_s and σ' (Figure 6.1) changes in V_s when σ' approaches zero are very large. Initial liquefaction occurs during the seventh cycle, the effective stress and shear wave velocity become zero. It is interesting to note that, after liquefaction has first occurred, the effective stress trace indicates one point of liquefaction per cycle whereas the shear wave velocity is reduced to zero twice per stress cycle and these coincide with the non-sinusoidal stress perturbations. Clearly, there is a disparity between these two observations. On earlier cycles (5 and 6) the perturbations in the effective stress do not produce 2 maxima per cycle but only an extra inflexion. However, in the same cycles this extra inflexion manifests itself as an extra maxima in the shear wave velocity. This suggests that the pore pressure

response time is too slow to measure the true behaviour of effective stress during cyclic loading even on a very permeable sand. In a less permeable silt or clay this problem would become even more apparent whereas the shear wave velocity will provide an almost immediate response.

In the shear wave amplitude trace a similarly complex cyclic pattern is again observed. This trace shows maximum amplitudes at the maximum shear wave velocities caused by the non-sinusoidal irregularities in the effective stress cycle. A combination of factors is causing this effect but it is primarily due to the changing frequency content of the shear wave pulse at different values of σ'. Lower values of σ' cause the bimorph element to transmit lower frequency shear waves which have lower attenuation coefficients.

Figure 7.5 shows the same applied stress, pore pressure and strain plots in conjunction with the compressional wave time delay, velocity and amplitude. The variation in velocity only becomes apparent after the first few cycles. Near and after liquefaction maximum velocities correspond to maxima in the effective stress. Smaller maxima, similar in nature to those in the shear wave trace, are also observed to correlate with the non-sinusoidal irregularities of applied stress. It should be noted that the compessional velocity amplitude is only ± 6 m/s after liquefaction compared with ± 120 m/s for shear waves. The compressional wave amplitude is also related to the effective stress with lower effective stresses causing higher amplitudes. This phenomena has been discussed previously with reference to the observed compressional wave pulse in Figures 7.2 and 7.3, sections I-J and J-K.

The behaviour of the waveform generated by the bimorph element transducer in this apparatus during the cyclic loading tests is possibly the most convincing evidence that shear waves are being generated and

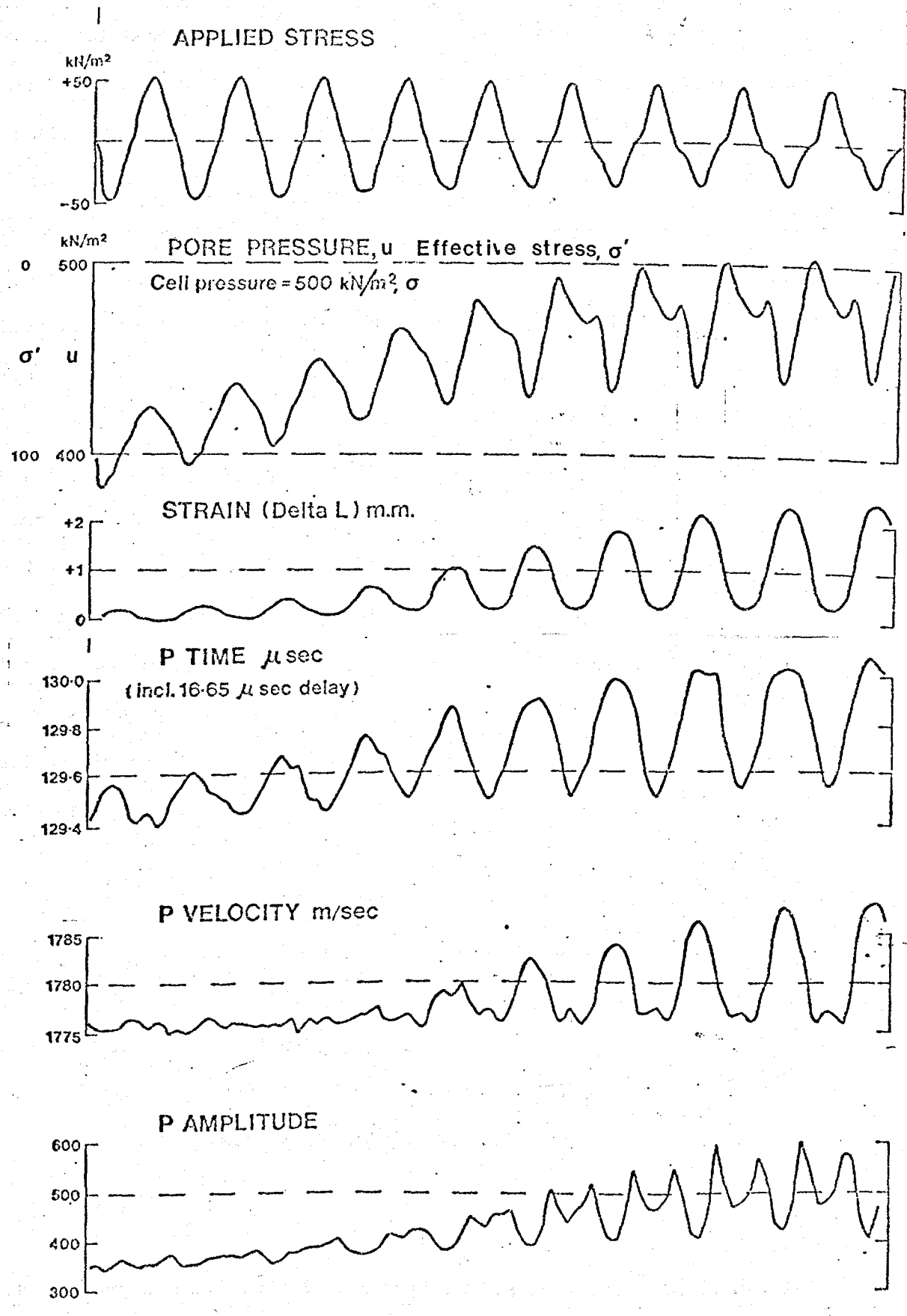

FIGURE 7.5 Stress, strain and compressional wave data from a cyclic loading test (0·1 Hz) on sand in the large triaxial cell

measured. Distance-time plots have previously demonstrated that the waveform was a body wave but these records provide the necessary evidence to demonstrate the loss of the waveform when a zero rigidity condition at constant porosity is reached. Horn (1980) reported that a vertical impulse to a sand body in porosity cell caused liquefaction of the sand. Evidence of this was given as the momentary (0.25s) disappearance of the shear wave trace (Horn, 1980, Figure 14). A close inspection of this figure reveals that, although the amplitude decreased, there was no change in velocity. Consequently, it should be concluded that the sand probably did not liquefy, but the sudden stress simply caused the shear motion of the transducer to decouple from the sand.

Undrained tests on sand in a triaxial cell are essentially a constant porosity process, hence, it is a useful technique for examining the relation between seismic velocities and effective stress. The following table summarises the extreme values of velocity at the end of the test (taken from Figures 7.3 and 7.5) in order to examine the change in the bulk modulus K.

	$\sigma' = 60$ kN/m^2	$\sigma' = 0$
V_p	1788 m/s	1776 m/s
V_s	230 m/s	0
n	0.35	0.35
ρ	2072.5 kg/m^3	2072.5 kg/m^3
K	6.48 x 10^9 N/m^2	6.54 x 10^9 N/m^2
V_p (Wood)	-	1675

The bulk modulus is calculated from equations 2.2 and 2.4. An increase in K for a reduction in effective stress is not a sensible result.

In the case where $\sigma' = 0$ Wood's equation (2.14) for a suspension could be considered applicable. Using values of 2650 kg/m^3 for ρ_m, 1.95×10^{-11} for β_m and 4.55×10^{-1} for β_w, V_f then equals 1675 m/s which is 101 m/s less than the observed value. When this value is used to calculate K, it becomes 5.81×10^9 N/m^2 which is less than for the case where $\sigma' = 60$ kN/m^2 amd is now a sensible result. However, the value 1776 m/s for V_p when $\sigma' = 0$ has a calculated error of only ± 4 m/s. The most likely explanation of these conflicting arguments is that only a small part of the sample actually lost all its rigidity. If we assume that this happened (an observed 'necking' at the top of the sample after failure supports this idea) then a situation would exist in which the compressional wave would only be low for a short distance. Consequently, the measured value does not represent the liquefied portion but is an average value through the whole sample. The shear wave velocity, however, is not an averaged velocity because it will not propagate through the liquefied portion. If this is the case, then the measurement of seismic wave velocities in tests such as these provides information on the performance of the test that would be difficult to obtain in any other way.

It is concluded that measurement of shear and compressional wave velocities and amplitudes using the above techniques, in this type of experiment, is possible both before and during the test procedure. While the objective of the Newcastle project is to correlate the initial shear and compressional wave parameters with liquefaction it is now clear that these parameters can provide far more information about the test procedure itself.

8. IN SITU MEASUREMENTS

8.1 Introduction

In chapter 3.3 the design and development of shear wave probes, suitable for use in unconsolidated sediments, was described. Two probe designs resulted from this work, Mk I (figure 3.23) and Mk II (figure 3.26) which were tested in a variety of laboratory sediments. The specific aim of this part of the project was to develop a shear wave technique that would augment other geophysical measurements in the upper layers of sea bed sediments. In particular it was intended to combine this technique with compressional wave and electrical resistivity techniques which had previously been developed at the Marine Sciece Laboratories (Simpkin, 1975 and Jackson, 1975), and to produce an instrument which would measure all the parameters simultaneously (figure 3.27).

Shear wave velocities in the upper few tens of centimetres do not lend themselves to measurement by refraction techniques due to the rapid rise in V_s with depth (even if efficient mode conversion from P to S waves could be obtained at the water-sediment interface). Consequently, it is inevitable that V_s in this region will have to be measured using probe techniques. Furthermore it is difficult to imagine an underway development that would enable rapid V_s surveys to be performed. In contrast to this situation, underway techniques for measuring compressional wave velocity and electrical resistivity in the uppermost sediment layers have proven viable (Bennell et al. 1982; Jackson et al. 1980).

The mark I and II shear wave probes were tested on cruises aboard RV Prince Madog along the North Anglesey coast (December 1979) and in Camarthen Bay (May 1980) respectively. A limited amount of data was

collected on these two cruises which is presented in the next two sections. Some of these data are also reported in Bennell et al. (1982).

8.2 RV prince Madog Cruise, December 1979.

The combined geophysical probe (Figure 3.27) was deployed at a number of stations in Red Wharf Bay, off the North East coast of Anglesey during December 1979. The station locations are shown in Figure 8.1. Table 8.1 lists the Decca co-ordinates of the stations and the shear wave velocities measured at each site. Compressional wave velocity ratios and electrical resistivity values, expressed as an apparent formation factor, AFF, are also shown. The compressional wave sediment/sea water velocity ratios were obtained from the measured ratio of the delay times with the probes in the sea water, just above the bottom, and with them embedded in the sediment. The shear wave velocities were clculated from the difference in arrival times of the pulse at the two receivers (3 and 8 cm). During these experiments one of the receivers was damaged on deck which meant that some of the V_s data was obtained using the time and distance between the sour-e and a single receiver. It is estimated that most of the V_s data is accurate to within ± 5m/s, with the main source of error being the accuracy of which the onset of the pulse could be determined.

The relatively narrow range of AFF's obtained indicates that a small range of sediment porosities was investigated. The shear wave velocities, however, exhibited considerable variation. This indicates that even for adjacent stations significant lateral changes may be occuring, presumably caused by subtle differences in packing structure which do not necessarily correlate with porosity as indicated by the electrical resistivity. A Shipek grab sample which was taken at each site did not always recover similar sediment to that which was often found

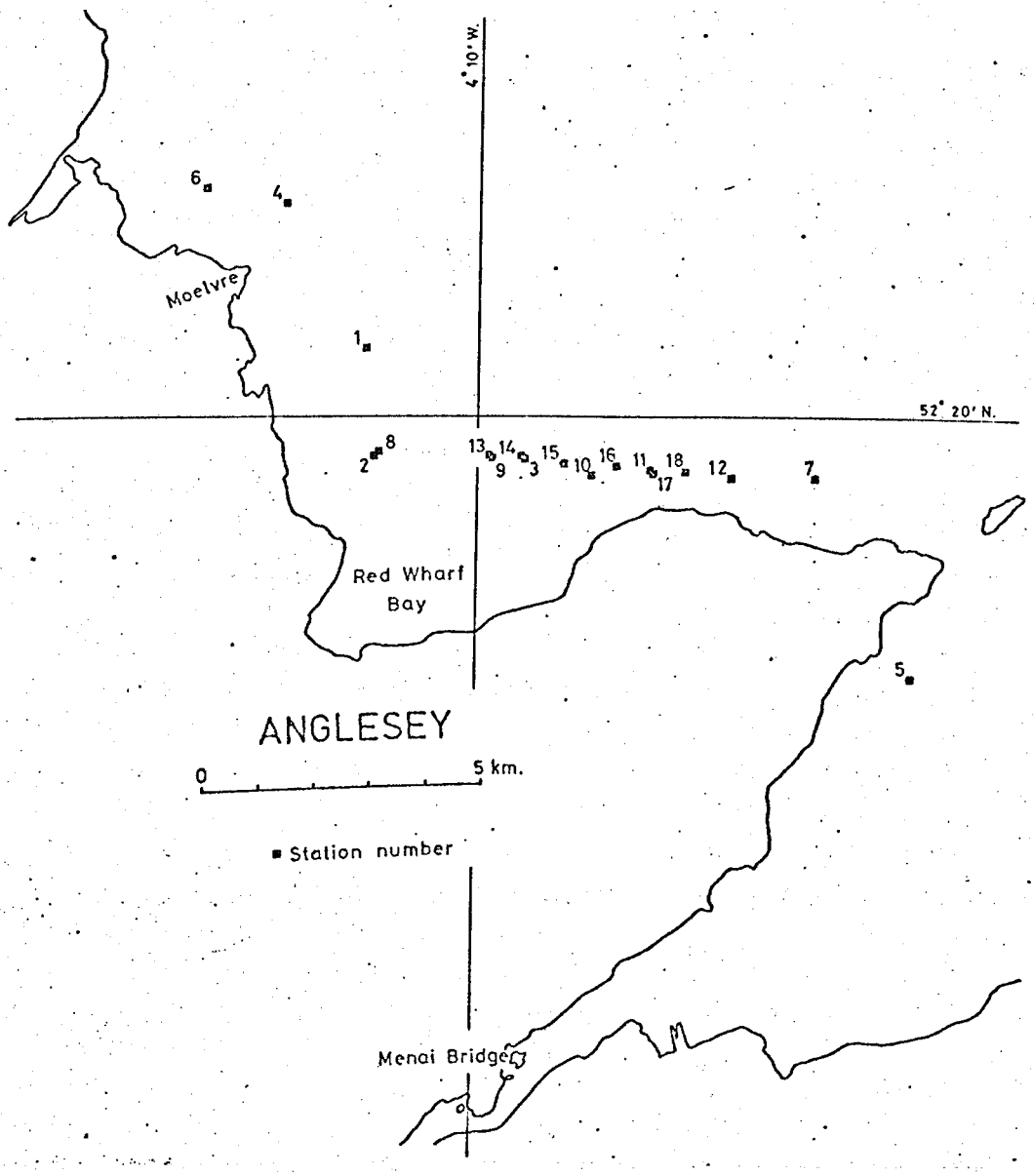

FIGURE 8.1 Site Location Map for RV Prince Madog cruise, December 1979

Station Number	Decca Co-ordinates Red	Green	Sediment Description	Velocity Ratio	Shear Wave Velocity m/s	Focussed AFF
1	E 2.9	C32.2		-	27	-
2	E 3.4	C33.9	muddy sand	1.037	120	-
3	E 1.5	C37.0	Sandy mud	1.028	71	3.1
4	E 3.0	B46.3	muddy sand	1.076	69	3.7
5	D22.2	C47.0	fine sand & shells	1.151	58	3.7
6	E 4.0	B45.0	med. sand & shells	1.120	44	4.0
7	D22.1	C42.0	fine shelly sand	1.138	44	3.8
8	E 3.3	C34.0	muddy fine sand	1.076	97	4.1
9	E 2.0	C36.1	v. muddy fine sand	1.071	-	3.7
10	E 0.9	C38.0	muddy sand	1.025	-	3.9
11	E 0.0	C39.0	muddy sand	1.048	-	3.7
12	D23.0	C41.0	shelly sand	1.071	65	3.9
13	E 2.0	C36.0	sand mud	1.042	48	3.5
14	E 1.5	C36.8	sand mud	1.101	47	3.5
15	E 1.0	C37.6	sand mud	1.079	52	4.1
16	E 0.4	C38.4	sand mud	1.084	58	4.05
17	E 0.0	C39.2	muddy sand	1.037	61	3.9
18	D23.3	C40.1	med. sand & shells	1.075	-	4.3

TABLE 8.1 Data obtained from the combined geophysical probe in Red Wharf Bay, December 1979, using the the Mk I shear wave probes.

adhering to the probes. This indicates that the lateral variability of sediment type in this area makes it essential to have a sampling device on the probe itself.

The main objective that has been achieved is that it was demonstrated that snall scale penetrating transducers can measure shear wave properties of surficial sediments in-situ.

8.3 RV Prince Madog Cruise, May 1980.

The combined geophysical probe was deployed in Camarthen Bay, off the South Wales coast during May 1980. Several modifications to the overall probe were made to improve its stability in the water and to reduce the number of individual cables comprising the umbilical cord.

The design of the shear wave probes was altered to make them far more rugged in order that they could penetrate hard sand without suffering any damage. This design is described in Chapter 3 and illustrated in Figure 3.26.

Table 8.2 lists the Decca co-ordinates of the stations, the shear wave velocities, compressional wave velocity ratio's and apparent formation factors (AFF's) for the sites occupied. The improvements in the ruggedness of the shear wave transducers enabled the probe to be handled with much less caution without suffering any damage. At the same time the signal quality was retained and slightly improved, but still giving an estimated accuracy of ± 5m/s. Using the same transducers, but surrounded by a noise insulating pneumatic bag, measurements in soft mud in Holyhead harbour have been made at transducer seperations of up to 17cm, giving a velocity of only 10m/s (Bennell et al. 1982).

The shear wave data from this cruise (and those data discussed in the previous section) cannot satisfactorily be examined with respect to changes in sediment type or correlated with compressional wave

Station Number	Decca Co-Ordinates Green	Purple	Sediment Description	Velocity Ratio	Shear Wave Velocity m/s	Focussed AFF
157	G32.0	J57.9	coarse sand	1.21	75	4.2
158	F47.8	J58.0	muddy sand	1.14	54	4.1
159	F46.0	J57.9	"	1.21	--	4.1
160	F44.0	J58.0	medium sand	1.16	67	3.9
161	F42.0	J58.2	muddy sand	1.18	75	4.4
162	F39.9	J58.1	medium sand	1.16	58	3.3
163	F37.7	J58.1	"	1.17	69	4.0
164	F35.8	J58.4	"	1.18	76	3.6
165	F34.0	J58.2	"	1.16	71	4.0
SW1	E43.5	A58.6	coarse sand	1.16	66	4.0
SW2	E44.2	A59.6	medium sand	1.17	66	4.2
SW3	E44.3	A59.4	sandy mud	1.17	57	4.2
SW4	E44.1	A59.5	"	1.16	54	3.8

TABLE 8.2 Data obtained from the combined geophysicl probe in Camarthen Bay, May 1980, using the Mk II shear wave probes.

velocity ratio's and apparent formation factors. Although the variations in the measured V_s values may be a direct result of subtle changes in porosity and packing structure, the only significant conclusion is that the shear wave velocities in surficial sediments are similar to those measured in the laboratory at low effective stresses (Chapter 4).

9. WHICH COMPRESSIONAL WAVE ?

In theories of seismic wave propagation in porous media, where the solid and fluid components are considered to be imperfectly coupled, (Biot, 1956, 1962; Ishihara, 1968; Stoll, 1974,1977) two dilatational waves (compressional) and one rotational wave (shear) are predicted. The shear wave velocity is governed by the rigidity of the sediment framework, which is affected only slightly by the presence of the pore fluid. One compressional wave velocity ($^{1}V_{p}$) is governed essentially by an aggregate bulk modulus of the solid and fluid components (equation 2.13). The second compressional wave ($^{f}V_{p}$) is transmitted through the sediment framework. The relative magnitudes of these two velocities cannot be readily calculated since the parameter which describes the interaction between the solid and fluid phases is unknown (Yew and Jogi, 1976). Whilst both waves are coupled together through the stiffnesses and relative motions of both solid and fluid components, it is clear that $^{1}V_{p}$ will be governed by the elastic moduli of the sediment framework.

Similarity in the values obtained from calculations based on Wood's equation (2.14) and those derived experimentally, indicate that the normally measured compressional wave velocity in saturated unconsolidated sediments is the first (faster, $^{1}V_{p}$) kind. Consequently elastic moduli are calculated from $^{1}V_{p}$ and V_{s} , primarily because they are the only velocities available. However, for moduli which relate to the granular framework of the sediment, it would seem to be far more appropriate to use $^{f}V_{p}$ and v_{s} in the calculation. Two sets of elastic moduli can be considered to exist (apart from the rigidity modulus which is only dependent on V_{s}) based on either v_{s} and $^{1}V_{p}$ or V_{s} and $^{f}V_{p}$.

For many applications in soil mechanics and foundation engineering the drained soil moduli,that can be determined from oedometer and triaxial tests, are required. These can be used as input parameters

for analytical techniques used to determine the response of soils to loadings. Dynamic loadings caused by foundation vibrations, earthquakes and wave action on offshore structures are of particular importance. The analytical techniques used for these problems have generally advanced ahead of the development of methods for evaluating the pertinent soil moduli (Hardin and Drnevich, 1972). These moduli are frame dominated in the sense that the interstitial pore fluid only introduces a time factor which depends on the permeability of the soil. Consequently, if soil moduli are to be ascertained from seismic techniques,which are of value to soil engineers, then they should be determined from measured values of $^{f}V_{p}$ as opposed to $^{1}V_{p}$ as is presently the case. The problem is,of course, that the existence of the second bulk compressional wave is not apparent on normal seismic records; this may be partially attributed to the fact that it is not being looked for. The potential correlation between seismic moduli, calculated from V_s and $^{f}V_{p}$, and conventional drained soil mechanics moduli can be illustrated by the following examples. Whitman et al. (1964) found in their experiments that the static modulus of dry sand, measured using small stress increments, roughly agreed with the dynamic modulus ρV_p^2. However, in the experiment on saturated silt (described in Chapter 5.5) the dynamic moduli are greater by approximately a factor of 10^2. It is conceivable that the V_p measured in the dry sand by Whitman et al. (1964) is in fact $^{f}V_{p}$,or $^{f}V_{p}$ may be very similar to $^{1}V_{p}$ in this case where the pores are filled with air; whereas in the saturated silt $^{1}V_{p}$ was measured which is much faster than in dry sand because of the high bulk modulus of water. Paterson (1956) designated $^{1}V_{p}$ and $^{f}V_{p}$ by the terms 'liquid wave' and 'frame wave respectively. In his acoustic measurements on sands, lower frequency waves were observed on the oscillographs which he interpreted as being the predicted 'frame wave'. Paterson's (1956) $^{f}V_{p}$ measurements on a

saturated beach sand varied from approximately 100 to 200 m/s under axial loads of 2 to 106 kPa. The data below denonstrates how the value of V_p changes the calculated dynamic modulus ρV_p^2.

	Density ρ kgm/m^3	Velocity V_p m/s	Dynamic modulus ρV_p^2 MPa	Static modulus D_r MPa
σ'=106 kPa (saturated) (silt)	2000	1750 (^1V_p)	6.125×10^3	0.09×10^3
	2000	200 (^fV_p)	0.08×10^3	

The first line is taken from the preconsolidated silt test (Chapter 5.5, Figure 5.8) showing a discrepancy in the static and dynamic moduli of a factor of 60. However, if it is assumed that the velocity measured was the 'liquid wave', ^1V_p, and in the second line this is replaced by a suitable value for the 'frame wave', ^fV_p, taken from Paterson's (1956) data, then the difference in the calculated dynamic and static moduli becomes comparitively negligible (11%).

Plona (1980), using a mode conversion technique, reports the experimental observation of the 'frame wave' in water-saturated, sintered glass spheres. Porosities ranged from 18.5% to 28.3% with corresponding changes in ^1V_p and ^fV_p of 4.84 km/s to 4.05 km/s and 0.82 km/s to 1.04 km/s respectively. Although the experimental details are convicing, the decrease in ^fV_p with decreasing porosity is not consistent with an increasing frame bulk modulus as the porosity decreases. Furthermore, the calculated bulk moduli, using the values of V_s and ^fV_p, are negative.

During the cyclic loading tests of sands reported in Chapter 7, waveforms of the type illustrated in Figure 9.1 were observed using the bender element transducers. They consist of three distinct frequency components which is illustrated by the different filter settings. It can be assumed that the fast, high frequency signal (Figure 9.1b) is ^1V_p. However, if it is postulated that Figures 9.1c and 9.1d are ^fV_p and V_s then there is no way of telling

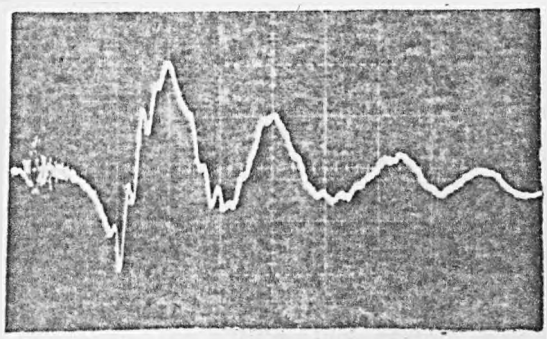

(a) No filter
0·2 v/div.

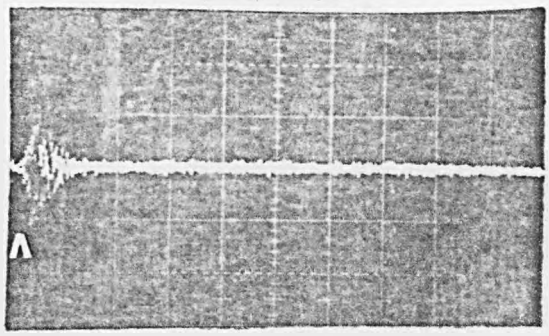

(b) High pass filter >25kHz.
0·1 v/div.

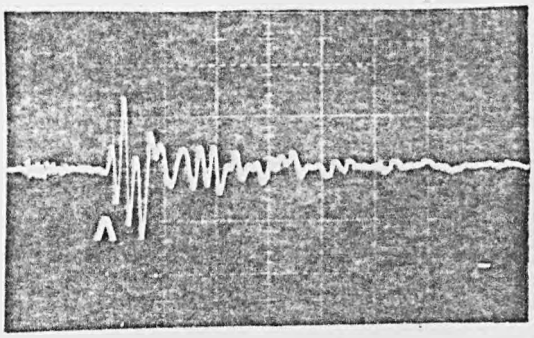

(c) Band pass filter
2·5 - 25 kHz.
0·1 v/div.

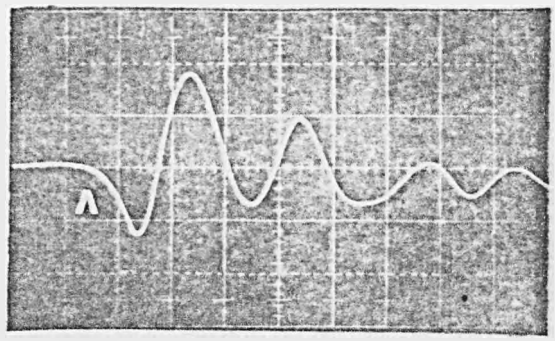

(d) Low pass filter <2·5kHz
0·2 v/div.

Received signal time base = 0·5 ms/div.

FIGURE 9.1 A RECEIVED SIGNAL THROUGH A SATURATED SAND SHOWING THE POSSIBLE EXISTENCE OF THREE TYPES OF BODY WAVES: (a) COMPLETE SIGNAL, (b) 'LIQUID WAVE', (c) 'FRAME WAVE', (d) SHEAR WAVE.

from the limited data which one is which. Both have similarly low velocities which could represent known shear wave velocities or approximately agree with the $^{f}V_{p}$ velocity reported by Patterson (1956).

From the above discussion it is evident that the existence of a second bulk compressional wave has yet to be conclusively proven. However, there are tentative signs that it does exist and the possible implications in terms of being able to remotely assess soil moduli in situ should generate the impetus for further study. It should be recollected that shear wave measurements in unconsolidated sediments have only recently become reliable because of their relatively slow velocity and high attenuation coefficients. A potentially similar problem now exists for identifying the second compressional wave. This problem is compounded by the envisaged difficulty of designing transducers with generating and detecting characteristics which will minimise the effect of the first compressional wave whilst maximising the effect of the second compressional wave. The high compliance of the bender element may prove a useful starting point especially if coupled with the self monitoring techniques to enable feed-back systems to simplify the received waveforms.

Page missing in original

10. CONCLUSIONS

(1) Shear wave transducers based on the piezo-electric bender element are suitable for measuring the shear wave velocity (Vs) over short distances (at least up to 20 cm) in a wide range of sediment types under varying effective stresses.

(2) The mechanical response of a bender element to an electrical driving signal can be measured by monitoring the electrical output from either a 'multimorph' element rigidly bonded to the transmitter or an electrically isolated section of the bender itself (self monitoring technique). This second technique should be equally applicable to other configurations of piezo-electric transmitters. These techniques provide valuable information on transducer performance as well as enabling electrical feed-back systems to improve the shape of the received waveform.

(3) For confined laboratory sediment samples bender elements potted in epoxy resin and mounted in a cantilever mode, where they protrude into the sediment, is the best configuration for generating and clearly detecting shear waves. This technique together with compressional wave transducers has been successfully used in Jackson's porosity cell, and oedometer and two triaxial cells. Parallel and series connected elements are used to maximise the sensitivity of the system.

(4) Without the use of feed-back electronics, the d.c. step of a square wave has been found to be the most successful and convenient driving signal for these types of transducers if Vs is being measured using the pulse technique.

(5) Shear wave pulse techniques using bender elements are limited in terms of path length. The primary limiting factor is the strain energy that can be imparted into the sediment before decoupling with the transmitter occurs. Signal averaging, single pulse techniques with transient recorder and cross-correlation using a random noise driving signal show the most promise for extending the usable path length.

(6) The most efficient transmitter/receiver configuration for rectangular bender elements generating and detecting shear waves is with both longer edges equidistant and parallel.

(7) Shear wave bender element transducer probes can be used to measure V_s in situ. The design used (Mk-II) incorporates a rugged steel casing suitable for shipboard use whilst maintaining shear wave sensitivity.

(8) Compressional wave velocity (V_p) in water saturated sands at 20°C are functions of porosity (n) as defined by the following generalised equations.

$V_p = 2913 - 4999n + 4916n^2$ for both well sorted and poorly sorted, sub-angular - rounded sands

$V_p = 2390 - 3215n + 3616n^2$ for well sorted glass spheres

$V_p = 2686 - 3205n + 2053n^2$ for very angular, well sorted shell fragments

(9) Shear wave velocity in water saturated sands at 20°C are functions of porosity as defined by the following generalised equations.

$V_s = 173 + 46n - 655n^2$ for well-sorted, sub-angular - rounded sands.

$V_s = 48 + 480n - 1220n^2$ for bimodal poorly-sorted, sub-angular - rounded sands.

$V_s = -200 + 1341n - 1399n^2$ for very angular, well-sorted shell fragments.

(10) There is no correlation between V_p, V_s and grain size. A poor correlation exists between velocity and mean grain roundness (R_{50}) defined by

$$V_p = -199R_{50} + 1814$$

$$V_s = -90R_{50} + 115$$

(11) The bimodal, poorly-sorted sands artificially prepared from two samples (mixtures) exhibited shear wave velocities lower than the component sands. It is argued that naturally occurring poorly-sorted sands may exhibit shear wave velocities higher than those found in these experiments.

(12) Differences in vibration procedures can produce sand structures with significantly different rigidities at the same porosity.

(13) The dynamic elastic moduli calculated from the above equations (9, 10) define them as functions of porosity for different sands (Figures 4.48 and 4.49). Large differences, particularly in Young's modulus and the shear modulus (G) occur with changing porosity and sediment type. For example, for well-sorted sands (X) G changes by a factor of 7 for a change in porosity of 0.48 to 0.35. The effect of grain shape is illustrated by the following example when n = 0.375.

$G = 1.3 \times 10^6$ N/m² for glass spheres

$G = 19.4 \times 10^6$ N/m² for sands X.

(14) In the oedometer cell the V_s-effective stress (P) relationships for different sediment types has been determined;

$V_s = 8.6P^{0.26}$ - silt

$V_s = 0.5P^{0.48} + 80$ - silty-clay

$V_s = 1.2P^{0.37} + 60$ - potter's clay

(15) A small decrease in V_s occurs after each incremental load in the potter's clay sample, which indicates either a non-uniform effective stress profile across the sample or an effective stress decrease which is not accounted for in the theory of consolidation.

(16) The shear wave technique incorporated in both the triaxial and oedometer cell is ideal for ascertaining the V_s-depth profile for a wide range of sediments.

(17) Large differences occur between the static and dynamic moduli, for a pre-consolidated silt sample tested in the oedometer, both in magnitude and as a function of stress. This is primarily attributed to the difference in drainage conditions. There is, however, a tentative correlation between the small strain relaxation modulus and the dynamic frame modulus.

(18) V_s and V_p during cyclic loading tests on sands is viable. V_s profiles provide an accurate assessment of the onset of liquefaction, V_s varying between 0 and 300 m/s.

(19) The failure mode during liquefaction has been analysed from the dynamic bulk modulus calculated from V_s and V_p. This has shown that the sand probably only liquefied at failure over a small part of the sample.

(20) Shear wave velocities measured in situ in surficial sediments varied between 17 m/s and 120 m/s without any apparent correlation with

electrical formation factor, V_p or sediment type.

(21) The second, slower, bulk compressional wave, predicted by theory but rarely observed might be more appropriate for calculating soil moduli. The use of geophysical techniques in foundation engineering might be significantly advanced if this wave velocity could be routinely measured.

(22) Observation of received waveforms in the triaxial cell using bender elements has tentatively identified what may be this second, slower compressional wave.

REFERENCES

Akal, T., 1972. The relationship between the physical properties of underwater sediments that affect bottom reflection, Marine Geology, 13, 251-266.

Akal, T., 1974. Acoustical characteristics of the sea floor: Experimental techniques and some examples from the Mediterranean Sea, in: Physics of Sound in Marine Sediments, (ed. L. Hampton) Plenum, N.Y., 447-480.

Anderson, A.L., 1974. Acoustics of gas bearing sediments, Applied Research Laboratories Technical Report, ARL-TR-74-19, The University of Texas at Austin.

Anderson, A.L. and L.D. Hampton, 1974. A method for measuring in-situ acoustic properties during sediment coring, in: Physics of Sound in Marine Sediments, (ed. L. Hampton) Plenum, N.Y., 357-371.

Anderson, D.G. and K.H. Stokoe, 1978. Shear modulus: A time dependant soil property, in: Dynamic Geotechnical Testing, ASTM. STP 654, 66-90.

Anderson, R.S., 1974. Statistical correlation of physical properties and sound velocity in sediments, in: Physics of Sound in Marine Sediments, (ed. L. Hampton) Plenum, N.Y., 481-518.

Ballard, R.F. and F.G. McLean, 1975. Seismic field methods for in-situ moduli, in: Proc. Conf. on In-Situ Measurement of Soil Properties, ASCE. Raleigh, N.C., 1, 121-150.

Bennell, J.D., P.D. Jackson and P.J. Schultheiss, 1982. Further development of sea-floor geophysical probing. Oceanology International 82, 4.8, 32pp.

Biot, M.A., 1941. General theory of three-dimensional consolidation, J. Appl. Phys., 12, 155-164.

Biot, M.A., 1956. Theory of propagation of elastic waves in a fluid saturated porous solid. I. Low frequency range. II. higher frequency range, J Acoust. Soc. Am., 28, 168-191.

Biot, M.A., 1962a. Mechanics of deformation and acoustic propagation in porous media, J. Appl. Phys., 33, 1482-1498.

Biot, M.A., 1962b. Generalized theory of acoustic propagation in porous dissipative media, J. Appl. Phys., 33, 1254-1264.

Bishop, A.W. and D.W. Hight, 1977. The value of Poisson's ratio in saturated soils and rocks stressed under undrained conditions, Geotechnique, 27, 369-384.

Brand, E.W., 1973. Some observations on the control of density by vibration, in: Evaluation of Relative Density and its role in Geotechnical projects involving Cohesion less soils, (ed. E.T. Selig and R.S. Ladd), ASTM. STP 523, 121-132.

Brandt, H., 1960. Factors affecting compressional wave velocity in unconsolidated marine sand sediments, J. Acoust. Soc. Am., 32, 171-179.

Buchan, S., F.C.D. Dewes, D.M. McCann, and D. Taylor Smith, 1967. Measurements of the acoustic and geotechnical properties of marine sediment cores, in: Marine Geotechnique, (ed. A.F. Richards) Univ. of Illinois Press, 65-92.

Buchan, S., D.M. McCann, and D. Taylor Smith, 1972. Relations between the acoustic and geotechnical properties of marine sediments, Q.J.L. Engng. Geol., 5, 265-284.

Bucker, H.P., J.A. Whitney, and D.L. Keir, 1964. Use of Stoneley waves to determine the shear velocity in ocean sediments, J. Acoust. Soc. Am., 36, 1595-1596.

Busby, J., and E.G. Richardson, 1957. The absorption of sound in sediments, Geophysics, 22, 821-829.

Celikkol, B., and P.M. Vogel, 1973. A new shear wave velocity measurement technique in ocean bottom soil samples. Proc. 6th. Offshore Technology Conference, Houston, Texas, OTC 1794.

Chilingarian, G.V., and K.H. Wolf, (eds.), 1975. Compaction of coarse grained sediments, I. Developments in Sedimentology, 18A, Elsevier Scientific.

Cunny, R.W., and Z.B. Fry, 1973. Vibratory in-situ and laboratory soil moduli compared, J. Soil Mech. Found. Div., ASCE. 99, SM12, 1055-1076.

Davies, D., 1965. Dispersed Stoneley waves on the ocean bottom, Bull. Seismol. Soc. Amer., 55, 903-918.

Davies, A.M., and P.J. Schultheiss, 1980. Seismic signal processing in engineering site investigation - A case history, Ground Engng., Vol. 13, No.4, 44-48.

Drnevich, V.P., B.O. Hardin, and D.J. Shippy, 1978. Modulus and damping of soils by the resonant-column method, in: Dynamic Geotechnical Testing, ASTM. STP 654, 91-125.

Feldhausen, P.H., and M.L. Silver, 1971. Seismic techniques for dynamic testing and engineering studies of sea-bed sediments, Underwater Jour., Dec. 263-279.

Folk, R.L., and W.C. Ward, 1957. Brazos river bar: A study in the significance of grain size parameters, J. Sedim. Petrol., 27, 3-26.

Gassmann, F., 1951. Über die elastizität poröser medien, Vierteljahrsschr Naturforsh. ges., Zürich, 96, 1-23.

Graton, L.C., and J.H. Frazer, 1935. Systematic packing of spheres, with particular relation to porosity and permeability, J. Geol., 43, 785-909.

Hamdi, F.A.I., 1981. Variations of seismic velocity with depth in near surface marine sediments and their engineering significance, unpublished PhD. thesis, University of Wales.

Hamdi, F.A.I., and D. Taylor Smith, 1981. Soil consolidation behaviour assessed by seismic velocity measurements, Geophysical Prospecting, 29, 715-729.

Hamilton, E.L., 1956. Low sound velocities in high-porosity sediments, J. Acoust. Soc. Am., 28, 16-19.

Hamilton, E.L., 1963. Sediment sound velocity measured in-situ from TRIESTE, J. Geophys. Res., 68, 5991-5994.

Hamilton, E.L. 1970. Sound velocity and related properties of marine sediments, N. Pacific, J. Geophys. Res., 75, 4423-4446.

Hamilton, E.L., 1971a. Elastic properties of marine sediments, J. Geophys. Res., 76, 579-604.

Hamilton, E.L., 1971b. Prediction of insitu acoustic and elastic properties of marine sediments, Geophysics, 36, 266-284.

Hamilton, E.L., 1972. Compressional-wave attenuation in marine sediments, Geophysics, 37, 620-646.

Hamilton, E.L., 1974. Geoacoustic models of the sea floor, in: Physics of Sound in Marine Sediments, (ed. L. Hampton) Plenum, N.Y., 181-221.

Hamilton, E.L., 1975. Acoustic and related properties of the sea floor: Shear wave velocity profiles and gradients, Naval Undersea Center, (NUC-TP-472), San Diego, California.

Hamilton, E.L., 1976. Sound altenuation as a function of depth in the sea floor, J. Acoust. Soc. Am., 59, 528-535.

Hamilton, E.L., 1976a. Shear wave velocity versus depth: A review, Geophysics, 41, 985-996.

Hamilton, E.L., 1976b. Altenuation of shear waves in marine sediments, J. Acoust. Soc. Am., 60, 334-338.

Hamilton, E.L., 1979. Sound velocity gradients in marine sediments, J. Acoust. Soc. Am., 65, 4, pp. 909-922.

Hamilton, E.L., H.P. Bucker, D.L. Keir, and J.A. Whitney, 1970. Velocities of compressional and shear waves in marine sediments determined in-situ from a research submersible, J. Geophys. Res., 75, 4039-4049.

Hampton, L.D., 1967. Acoustic properties of sediments, J. Acoust. Soc. Am., 42, 882-890.

Hardin, B.O., and F.E. Richart, 1963. Elastic wave velocities in gramular soils, J. Soil Mech. Found. Div., ASCE. 89, SMI, 33-65.

Hardin, B.O., and J. Music, 1965. Apparatus for vibration during the triascial test, in: Instruments and apparatus for Soils and Rock Mechanics, ASTM. STP 392, 55-74.

Hardin, B.O., and W.L. Black, 1968. Vibration modulus of normally consolidated clay, J. Soil Mech. Found. Div., ASCE. 94, SM2, 353-369.

Hardin, B.O., and V.P. Drnevich, 1972a. Shear modulus and damping in soils: Measurement and parameter effects, J. Soil Mech. Found. Div., ASCF, 98, SM6, 603-624.

Hardin, B.O., and V.P. Drnevich, 1972b. Shear modulus and damping in soils: Design equations and curves, J. Soil. Mech. Found. Div., 98, SM7, 667-692.

Hoar, R.J., and K.H. Stokoe, 1978. Generation and measurement of shear waves in-situ, in: Dynamic Geotechnical Testing, ASTM. STP 654, 3-29.

Horn, D.R., B.M. Horn, and M.N. Delach, 1968. Correlation between acoustic and other physical properties of deep sea cores, J. Geophys. Res., 73, 1939-1957.

Horn, I.W., 1980. Some laboratory experiments on shear wave propagation in unconsolidated sands, Mar. Geotechnol. 4, 1, 31-54.

Hunter, A.N., R. Legg, and E. Matsukawa, 1961. Measurements of acoustic attenuation and velocity in sand, Acoustica, 11, 26-31.

Ishihara, K., 1968. Propagation of compressional waves in saturated soil, In: Wave Propagation and Dynamic Properties of Earth Materials, (ed. G.E. Frianda-filidas), University of New Mexico Press, 451-467.

Jackson, P.D., 1975. An electrical resistivity method for evaluating the in-situ prosity of clean marine sands, Marine Geotechnology, 1, 2, 91-115.

Jackson, P.D., D. Taylor Smith, and P.N. Stanford, 1978. Resistivity-porosity-particle shape relationships for marine sands, Geophysics, 43, 6, 1250-1268.

Jackson, P.D., R. Baria, and D.M. McCann, 1980. Geotechnical assessment of superficial marine sediments using in-situ geophysical probes, Oceanology Int., 80, 33-46.

Jackson,P.D., P.J. Schultheiss, and R. Baria, 1981. Feedback systems in geophysics, 43rd European Association of Exploration Geophysicists meeting, Venice, May 1981.

Jackson, P.D., P.J. Schultheiss, P. Strachan, and R. Baria, 1981. The use of geophysical transducers to monitor a cyclically loaded sand, Institute of Geological Sciences Report, EG 81/3.

Jones, R., 1958. In-situ measurement of the dynamic properties of soil by vibration methods, Geotechnique, 8, 1-21.

Kitsunezaki, 1971. Field-experimental study of shear waves and the related problems, Cont. of the Geophysical Inst., Kyoto Univ., No. 11, 103-177.

Kolbuszewski, J.J., 1948. An experimental study of the maximum and minimum porosities of sands, Proc. 2nd Int. Conf. Soil Mech. and Found. Eng., 1, Rotterdam, 158-165.

Lambe, T.W., and R.V. Whitman, 1979. Soil Mechanics, John Wiley, N.Y. 553pp.

Laughton, A.S., 1954. Laboratory measurements of seismic velocities in ocean sediments, Proc. Roy. Soc., ser.A., 222, 336-341.

Laughton, A.S., 1957. Sound propagation in compacted ocean sediments, Geophysics, 22, 233-260.

McCann, C., and D.M. McCann, 1969. The attenuation of compressional waves in Marine sediments, Geophysics, 34, 882-892.

McCann, D.M., 1972. Measurement of the acoustic properties of marine sediments, Acoustica, 26, 55-66.

McLamore, V.R., D.G. Anderson, and C. Espana, 1978. Crosshole testing using explosive and mechanical energy sources, in: Dynamic Geotechnical Testing, ASTM, STP 654, 30-55.

Miller, R.P., J.H. Troncoso, and F.R. Brown, 1975. In-situ impulse test for dynamic shear modulus of soils, in: Proc. Conf. on In-Situ Measurement of Soil Properties, ASCE. Raleigh, N.C. 1, 319-335.

Morgan, N.A., 1969. Physical properties of marine sediments as related to seismic velocities, Geophysics, 34, 529-545.

Mulilis, P.J., J.B. Seed, C.K. Chan, J.K. Mitchell, and K. Arulananadan, 1977. Effects of sample preparation on sand liquefaction, J. Geotech. Engng. Div., ASCE. 103, GT2, 91-108.

Nacci, V.A., M.C. Wang, and J. Gallagher, 1974. Influence of anisotropy and soil structure on elastic properties of sediments, in: Physics of Sound in Marine Sediments, (ed. L. Hampton), Plenum, N.Y., 63-87.

Nafe, J.E., and C.L. Drake, 1957. Variation with depth in shallow and deep water marine sediments of porosity density and the velocities of compressional and shear waves, Geophysics, 22, 523-552.

Nolle, A.W., W.A. Hoyer, J.F. Mitsud, W.R. Runyan, and W.M. Ward, 1963. Acoustical properties of water-filled sands, J. Acoust. Soc. Am., 35, 1394-1408.

Paterson, N.R., 1956. Seismic wave propagation in porous gramular media, Geophysics, 21, 691-714.

Plona, T.J., 1980. Observation of a second bulk compressional wave in a porous medium at ultrasonic frequencies. Appl. Phys. Lett., 36, 4, 259-261.

Powers, M.C., 1953. A new roundness scale for sedimentary particles. J. of Sed. Petrol., 23, 117-119.

Rittenhouse, G., 1943. A visual method of estimating two-dimensional sphericity, J. Sedim. Petrol., 13, 79-81.

Schreiber, B.C., 1968. Sound velocity in deep sea sediments, J. Geophys. Res., 73, 1259-68.

Schultheiss, P.J., 1981. Simultaneous measurement of P and S wave velocities during conventional laboratory soil testing procedures, Marine Geotechnology, 4, 4, 343-367.

Schwarz, S.D., and F.R. Conwell, 1974. A technique for the in-situ measurement of shear wave velocities (V_S) for deep marine foundations, Proc. sixth, Offshore Technology Conference, OTC 2014, 755-762.

Seed, H.B., and K.L. Lee, 1966. Liquefaction of sands during cyclic loading, J. Soil Mech. Found. Div., ASCE, 92, SM6, 105-134.

Selig, E.T., and R.S. Ladd, (eds.), 1973. Evaluation of Relative Density and its role in geotechnical projects involving cohesionless soils, ASTM. STP 523.

Sharp, W.E., and Pow-Foong Fan, 1963. A sorting index, J. Geol., 71, 76-84.

Shirley, D.J., 1977. Laboratory and in-situ sediment acoustics, Applied Research Laboratories Technical Report, ARL-TR-77-46, The University of Texas at Austin.

Shirley, D.J., 1978. An improved shear wave transducer, J. Acoust. Soc. Am., 63, 5, 1643-1645.

Shirley, D.J., A.L. Anderson, and L.D. Hampton, 1973. In-situ measurement of sediment sound speed during coring, Applied Research Laboratories Technical Report, ARL-TR-73-1, The University of Texas at Austin.

Shirley, D.J., and A.L. Anderson, 1975a. Studies of sediment shear waves, acoustical impedance and engineering properties, Applied Research Laboratories Technical Report, ARL-TR-75-23, The University of Texas at Austin.

Shirley, D.J., and A.L. Anderson, 1975b. Acoustical and engineering properties of sediments, Applied Research Laboratories Technical Report, ARL-TR-75-58, The University of Texas at Austin.

Shirley, D.J., and A.L. Anderson, 1975c. In-situ measurement of marine sediment acoustical properties during coring in deep water, I.E.E.E., trans. Geoscience Electronics, 13, 163-169.

Shirley, D.J., and D.W. Bell, 1978. Acoustics of in-situ and laboratory sediments, Applied Research Laboratories Technical Report, ARL-TR-78-36, The University of Texas at Austin.

Shirley, D.J., and L.D. Hampton, 1978. Shear wave measurements in laboratory sediments, J. Acoust. Soc. Am., 63, 2, 607-613.

Shirley, D.J., D.W. Bell, and J.M. Hovern, 1979. Laboratory and field studies of sediment acoustics, Applied Research Laboratories Technical Report, ARL-TR-79-26, The University of Texas at Austin.

Shirley, D.J., J.M. Hovern, G.D. Ingram, and D.W. Bell, 1980. Sediment acoustics, Applied Research Laboratories Technical Report, ARL-TR-80-17, The University of Texas at Austin.

Shumway, G., 1960. Sound speed and absorption studies on marine sediments by a resonance method, parts 1 and 2, Geophysics, 25, 451-467 and 659-682.

Simpkin, P.G., 1974. Sound speed versus porosity for non-cohesive sea-floor sediments. Marine Science Laboratories Report, University College of North Wales, 18pp.

Simpkin, P.G., 1975. Remote sensing of sediment properties on the sea-floor, Proc. Underwater Construction Technology Conference, University College, Cardiff, U.K., 25pp.

Skoglund, G.R., W.F. Marcuseu, and R.W. Cunny, 1976. Evaluation of resonant column test devices, J. Geotech. Eng. Div., ASCE. 102, GT11, 1147-1158.

Stamatopoulos, A.C., and P.C. Kotzias, 1978. Soil compressibility as measured in the oedometer. Geotechnique, 28, 363-375.

Statton, C.T., B. Auld, and A. Fritz, 1978. In-situ seismic shear wave velocity measurements and proposed procedures, in: Dynamic Geotechnical Testing, ASTM, STP 654, 56-65.

Stevenson, R.W., 1978. Ultrasonic testing for determining dynamic soil moduli, in: Dynamic Geotechnical Testing, ASTM, STP 654, 179-195.

Stokoe, K.H., and R.D. Woods, 1972. In-situ shear wave velocity by cross-hole method, J. Soil Mech. Found. Div., ASCE. 98, SM5, 443-460.

Stokoe, K.H., and K.G. Abdel-Razzak, 1975. Shear modulus of two compacted fills, in: Proc. Conf. on In-Situ Measurement of Soil Properties, ASCE. Raleigh, N.C., 422-449.

Stokoe, K.H., E.J. Arnold, R.J. Hoar, D.J. Shirley, and D.G. Anderson, 1978. Development of a bottom-hole device for offshore shear wave velocity measurement. Offshore Technology Conference, Preprints, 3, 1367-80.

Stoll, R.D., 1974. Acoustic waves in saturated sediments, in: Physics of Sound in Marine Sediments, (ed. L.D. Hampton), Plenum Press N.Y. 19-40.

Stoll, R.D., 1977. Acoustic waves in ocean sediments. Geophysics, 42, 715-725.

Stoll, R.D., and G.M. Bryan, 1970. Wave attenuation in saturated sediments, J. Acoust. Soc. Am., 47, 1440-1447.

Tavenas, F.A., R.S. Ladd, and P. LaRochelle, 1973. Accuracy of relative density measurements: Results of a comparative test program, in: Evaluation of Relative Density and its role in geotechnical projects involving cohesionless soils, (eds. E.T. Selig and R.S. Ladd), ASTM. STP 523, 18-60.

Taylor Smith, D., 1974. Acoustic and mechanical loading of marine sediments, in: Physics of Sound in Marine Sediments, (ed. L. Hampton) Plenum, N.Y. 41-61.

Taylor Smith, D., 1975. Geophysical assessment of sea-floor sediment properties, Oceanology International 75, 320-328.

Urick, R.J., 1947. A sound velocity method for determining the compressibility of finely divided substances, J. Appl. Phys., 18, 983-987.

Urick, R.J., 1948. The absorption of sound in suspensions of irregular particles, J. Acoust. Soc. Am., 20, 283-289.

Urick, R.J., and W.S. Amend, 1949. The propagation of sound in composite media, J. Acoust. Soc. Am., 21, 115-119.

Viskone, A., 1976. Evaluation of in-situ shear wave velocity measurement techniques, Engineering and Research Center Report, REC-ERC-76-6, Bureau of Reclamation, Denver, Colorado, 40pp.

Whitman, R.V., E.T. Miller, and P.J. Moore, 1964. Yielding and locking of confined sand, J. Soil Mech. Found. Div., ASCE., 90, SM4, 57-84.

Whitmarsh, R.B., and Lilwall, R.C., 1982. A new method for the determination of in-situ shear wave velocity in deep-sea sediments. Oceanology International 82, Brighton, England.

Wilson, S.D., F.R. Brown, and S.D. Schwarz, 1978. In-situ determination of dynamic soil properties, in: Dynamic Geotechnical Testing, ASTM. STP 654, 295-317.

Wood, A.B., 1930. A textbook of Sound, McGraw Hi.., N.Y.

Yew, C.H., and P.N. Jogi., 1976. Study of wave motions in fluid-saturated porous rocks, J. Acoust. Soc. Am., 60, 1, 2-8.